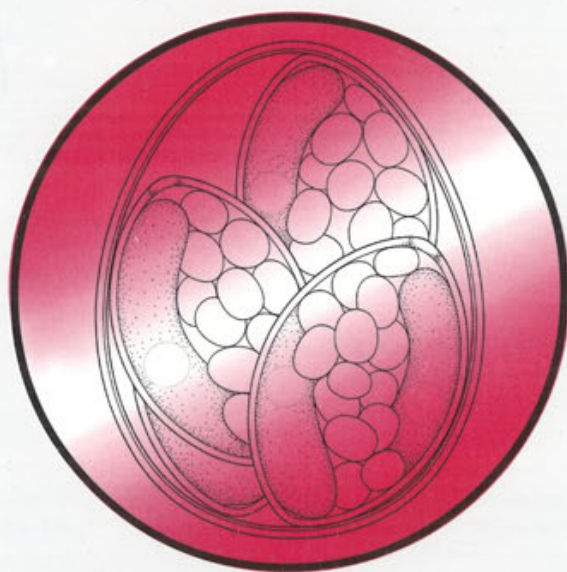


182

ACTA

PROTOZOOLOGICA



NENCKI INSTITUTE OF EXPERIMENTAL BIOLOGY

WARSAW, POLAND

<http://rcin.org.pl>

2006

VOLUME 45 NUMBER 4

ISSN 0065-1583

Polish Academy of Sciences
Nencki Institute of Experimental Biology
and
Polish Society of Cell Biology

ACTA PROTOZOOLOGICA
International Journal on Protistology

Editor in Chief Jerzy SIKORA

Editors Hanna FABCZAK and Anna WASIK

Managing Editor Małgorzata WORONOWICZ-RYMASZEWSKA

Editorial Board

Christian F. BARDELE, Tübingen	Donat-Peter HÄDER, Erlangen
Linda BASSON, Bloemfontein	Janina KACZANOWSKA, Warszawa
Louis BEYENS, Antwerpen	Stanisław L. KAZUBSKI, Warszawa
Helmut BERGER, Salzburg	Leszek KUŹNICKI, Warszawa, <i>Chairman</i>
Jean COHEN, Gif-Sur-Yvette	J. I. Ronny LARSSON, Lund
John O. CORLISS, Bala Cynwyd	John J. LEE, New York
György CSABA, Budapest	Jiří LOM, České Budějovice
Johan F. De JONCKHEERE, Brussels	Pierangelo LUPORINI, Camerino
Isabelle DESPORTES-LIVAGE, Paris	Kálmán MOLNÁR, Budapest
Genoveva F. ESTEBAN, Dorset	David J. S. MONTAGNES, Liverpool
Tom FENCHEL, Helsingør	Jytte R. NILSSON, Copenhagen
Wilhelm FOISSNER, Salzburg	Eduardo ORIAS, Santa Barbara
Jacek GAERTIG, Athens (USA)	Sarah L. POYNTON, Baltimore, Berlin
Vassil GOLEMANSKY, Sofia	Sergei O. SKARLATO, St. Petersburg
Andrzej GRĘBECKI, Warszawa, <i>Vice-Chairman</i>	Michael SLEIGH, Southampton
Lucyna GRĘBECKA, Warszawa	Jiří VÁVRA, Praha

ACTA PROTOZOOLOGICA appears quarterly.

The price (including Air Mail postage) of subscription to *Acta Protozoologica* at 2007 is: 200.- € by institutions and 120.- € by individual subscribers. For the matters regarding subscription of the *Acta Protozoologica*, please contact Editor Elect Dr Krzysztof WIACKOWSKI, Institute of Environmental Sciences, Jagiellonian University, Gronostajowa 7, 30-387 Kraków, Poland; E-mail: wiacko@eko.uj.edu.pl; phone: +48 12 664 51 21

Front cover: Jirků M. and Modrý D. (2005) *Eimeria fragilis* and *E. wambaensis*, two new species of *Eimeria* Schneider (Apicomplexa: Eimeriidae) from African anurans. *Acta Protozool.* **44**: 167-173

©Nencki Institute of Experimental Biology
Polish Academy of Sciences
This publication is supported by the Ministry of Science and
Higher Education

Desktop processing: Justyna Osmulka, Information Technology
Unit of the Nencki Institute
Printed at the MARBIS, ul. Poniatowskiego 1
05-070 Sulejówek, Poland

Acta Protozoologica 1963-2006

Jerzy SIKORA and Leszek KUŹNICKI

Department of Cell Biology, Nencki Institute of Experimental Biology, Polish Academy of Sciences, Warsaw, Poland

Summary. Note on the history of the international journal *Acta Protozoologica*, its establishment, colleagues involved in its management, and the main scientific events that were recorded and published.

Key words: *Acta Protozoologica*, congresses on protozoology, Jagiellonian University, journals on protistology, Nencki Institute of Experimental Biology, Protozoa, Warsaw University.

The first journal on Protozoa was *Archiv für Protistenkunde* (recently: *Protist*) edited by Fritz Schaudin and published by Gustav Fischer in 1902. The second one was *The Journal of Protozoology* (recently: *Journal of Eukaryotic Microbiology*) established by the Society of Protozoologists in 1954.

The journal *Acta Protozoologica* was founded in 1963 on the initiative of Zdzisław Raabe from Warsaw University and Stanisław Dryl from the Nencki Institute of Experimental Biology in Warsaw, Polish Academy of Sciences, Poland. The international Board of Editors was established and the Editorial Office was located at the Nencki Institute of Experimental Biology. PWN (State Polish Scientific Publishers) acted as the journal's publisher till 1989. In 1990, the Nencki Institute became the independent publisher of *Acta Protozoologica*, and the Polish Society for Cell Biology became its co-publisher in 1997.

Address for correspondence: Jerzy Sikora, Department of Cell Biology, Nencki Institute of Experimental Biology, Polish Academy of Sciences, ul. Pasteura 3, 02-093 Warszawa, Poland; Fax: (4822)8225342; E-mail: j.sikora@nencki.gov.pl

As announced in the previous issue of the *Acta Protozoologica*, the Nencki Institute of Experimental Biology of the Polish Academy of Sciences, the publisher of the journal *Acta Protozoologica* since 1963, informed all readers and authors that it would cease publishing the journal as of January 1, 2007. The Nencki Institute declared that all benefits and rights to the journal after January 1, 2007 shall be owned by the Department of Hydrobiology, Institute of Environmental Sciences, Jagiellonian University, Kraków, Poland. We hope that the new publisher and Editorial team receive a warm reception from authors and readers.

For the last 45 years the journal *Acta Protozoologica* was managed by four chief-editors: Zdzisław Raabe (1963-1971), Stanisław Dryl (1972-1977), Stanisław Dryl and Stanisław Kazubski (1978-1989), Stanisław Kazubski (1990-1992) and Jerzy Sikora (1993-2006).

Taking into account our involvement in running the journal for the past 16 years, we wish to present some remarks concerning its past and present.

Acta Protozoologica was fully peer-reviewed from the very beginning. Primarily, each volume consisted of

30-40 papers (fasciculi). From Volume 14 (1975) it became quarterly issued. Special issues published contributions of participants like: Volume 7 (1970) Symposium on "Physiology of Motor Response in Protozoa, Warsaw, 1968; Volume 11 (1972) International Symposium "Motile Systems of Cells" held in Cracow, Poland (1971); Volume 18 (1979) International Symposium on Cell Motility (1978); Special Congress Volume of *Acta Protozoologica*, Progress in Protozoology, Proceedings of VI International Congress of Protozoology, Warszawa, Poland, 1981 Part I (1982) and Part II (1984). For Post-Congress Volume II, as a special contribution for the celebration of the twentieth anniversary of protozoological congresses, L. Kuźnicki and B. Honigberg wrote an article "International collaboration among protozoologists during the years 1961-1981." Also, special supplements comprised: Cumulative Indexes of *Acta Protozoologica* volumes 1-40, Part I (*Acta Protozool. Suppl.* 40: 1-46, 2001), Subject Index of *Acta Protozoologica* volumes 1-40, Part II (*Acta Protozool. Suppl.* 41: 1-46, 2002).

Acta Protozoologica publishes comprehensive and updated basic, experimental, and theoretical contributions on the broad aspects of protistology and cell biology of lower Eukaryote, including: behaviour, biochemistry and molecular biology, development, ecology, genetics, parasitology, physiology, photobiology, systematics and phylogeny, and ultrastructure. It also covers topics, such as: various roles of protists as animal food resources and their control. The journal publishes original research reports, critical reviews of current important subjects written by invited experts in the field, rapid short communications, book reviews, and letters to the editor. The original research reports have standard contents: title, summary, key words, abbreviations used, introduction, materials and methods, results, discussion, acknowledgements, and references; the dates of manuscript submission and acceptance are specified. In every last issue of the year, the contents of the whole volume, the subject index, and the list of reviewers is provided. From Volume 30 (1991), a new, bigger and more convenient format was introduced, allowing us to publish high quality photographs.

Acta Protozoologica published obituary notices on famous scientists: Kazubski S., Kuźnicki L., Sikora J. (1992) Bronisław M. Honigberg - obituary notice. 31: 127-128; Wasik A. (1993) George I. Poljansky -

obituary notice. 32: 199-200; Kuźnicki L. (1996) Stanisław Dryl - obituary notice. 35: 1-2; Kazubski S. L. (1997) Witold Kasprzak - obituary notice. 36: 1-2; Grębecki A., Korohoda W. (1998) Karl-Ernst Wohlfarth-Bottermann - obituary notice. 37: 1-3; Beyer T. V., Skarlato S. O. (1999) Igor Borissovich Raikov - obituary notice. 38: 1-3.

We suppose that some data concerning authors and articles published in the last 16 years in *Acta Protozoologica* might be of interest. The journal has published the papers of above 1400 authors coming from all over the world. The nationalities of the authors who published their papers in *Acta Protozoologica* during last 16 years are presented in Table 1. Also the subjects of papers varied, however, the majority of papers concerned morphology and taxonomy, morphogenesis and physiology (especially motile events in ciliates, amoebae and flagellate). Varieties of taxa were studied however ciliates and apicomplexa were the predominant subjects.

Recent subscriptions by libraries and individual subjects from over 20 countries (as well as some orders for the complete collection of the journal since its very beginning in 1963) prove that the distribution of *Acta Protozoologica* is worldwide and multi-professional: beside specialists in cell biology of lower organisms, the audience comprises many researchers, educators, and students in biomedical, veterinarian, and environmental sciences.

We wish to express our sincere thanks to all Members of the Editorial Board, Editors: Hanna Fabczak, Anna Wasik and Małgorzata Woronowicz-Rymaszewska; and collaborating scientists all around the world who, over the years, have dedicated their valuable time and expertise to reviewing papers submitted for publication in *Acta Protozoologica*. The editors acknowledged in every forth number of the volume all colleagues who had served as voluntary reviewers for one or more manuscripts submitted to be published in that year. The position of the *Acta Protozoologica* as a one of the five leading journals in protistology we owe to our many friends and colleagues from institutions around the world, that have helped in reading papers submitted to be published in this journal.

We are sure *Acta Protozoologica*, from 2007 under a new Editorial team, will remain, as before, one of our leading journals, publishing original papers and reviews on lower Eukaryote cells.

Table 1. Nationality of authors who published their papers in *Acta Protozoologica* during last 16 years (1991-2006).

Countries	1991	1992	1993	1994	1995	1996	1997	1998	1999	2000	2001	2002	2003	2004	2005	2006	Total
Argentina				1								3	1	2			7
Australia	2			2		1	3				1	4	10	1	1		25
Austria			1		2	3	2	4			2		4	4	6	8	36
Belgium							2			4	1			1	7	8	23
Brazil				1		2		1					9	1	14	13	41
Bulgaria	3	2	3					2	2	2		3		2		2	21
Canada			1							4		2	1		1		9
Cuba																4	4
Czech Republic	1			1	2	1	2	1	1	7		4	2	9	10	9	50
Denmark		2	6				4				2		1		2		7
Egypt								1								3	4
Estonia										2							2
Finland	1								1	1			1				4
France	1	3	2	1			1	2		2		1	5	8	2	1	29
Germany	7	14	8	17	5	13	12	11	5	13	20	15	11	9	10	9	179
Hungary	3	2	2	2	3	2	1	3		6	4	11	5		6	5	55
India	6	6	9	2	18		4	7	10	3	9		2	10	8	6	100
Israel												2					2
Italy		9		1	2	14	3	4	6	2		7			4		52
Japan	1	2	3	3								3	6	4		3	25
Mexico				6	9												15
Netherlands	1												1	3	4	5	14
Nigeria												2					2
P. R. China			4		1	1	1			8	6	11	15	11	17	20	95
Poland	23	10	11	8	9	16	17	10	12	16	25	8	8	17	8	17	215
Portugal								2						1	3		6
Russia	5	6	6	2	6		7	5	4	5	3	1	5	3			58
Senegal				2	2				8		4						16
Slovakia	1													4			5
South Africa			10		6	2		6	6	2	3			4			39
Saudi Arabia								2	2		1	1				2	8
South Korea														5	1		6
Spain		4		9		9			2	4	11	4	6				49
Sweden					1		4	1	1		2			3	1		13
Switzerland													3	7	1		11
Trinidad and Tobago													1				1
Turkey										1		3	2				6
Ukraine															1		1
United Kingdom		1	1		3	5	3	3		4	1	5	2	3	10	9	50
USA	3	1	5	12	20	6	15	4	3	12	9	5	14	19	4	6	138
Venezuela											3						3
Yugoslavia-Serbia											2						2
Total	58	62	72	70	89	75	81	69	63	98	109	95	115	131	121	130	1438

The Unusual, Lepidosome-coated Resting Cyst of *Meseres corlissi* (Ciliophora: Oligotrichea): Encystment and Genesis and Release of the Lepidosomes

Wilhelm FOISSNER¹, Maria PICHLER², Kahled AL-RASHEID³, and Thomas WEISSE²

¹Universität Salzburg, FB Organismische Biologie, Salzburg, Austria; ²Institut für Limnologie der Österreichischen Akademie der Wissenschaften, Mondsee, Austria; ³King Saud University, Department of Zoology, Riyadh, Saudi Arabia

Summary. *Meseres corlissi* Petz and Foissner (1992) is an oligotrichine ciliate covering the resting cyst with epicortical scales called lepidosomes. We studied in detail encystment as well as the genesis and release of the lepidosomes, using live observation, morphometry, and transmission electron microscopy. Encystment is remarkable in changing body shape distinctly and showing two phases of intense rotation. When encysting, the conical body becomes globular and forms a discoidal "head" via a fibrous ligament. Then, the cell rotates rapidly about its main axis for a minute. We speculate that this rotation transports the lepidosomes and cyst wall precursors to the cell's cortex. When rotation stops, the lepidosomes are released within about 5 - 20 s. Then occurs a second, slow rotation phase lasting several minutes and possibly distributing the material released by the cyst wall precursors. The lepidosomes develop in Golgi vesicles. Maturation thus occurs in a membrane-bound vesicle and is a complex process with seven distinct stages. The central cavity of the lepidosome develops asymmetrically, and the large meshes of the lepidosome wall develop earlier than the small ones. Growth of the lepidosomes does not occur by vesicular transport processes. The lepidosomes are released by classical exocytosis. The lepidosome (vesicle) membrane closes the port and becomes part of the newly forming cortex. Detailed data on encystment and lepidosome genesis are rare. However, it turned out that both, encystment and lepidosome genesis are more complex in *M. corlissi* than in most other ciliates.

Key words: cystic ciliates, exocytosis, oligotrichine ciliates, *Strombidium oculatum*, transmission electron microscopy, vegetative ciliates, volume relationship.

INTRODUCTION

Lepidosomes are epicortical, organic structures of definite shape produced intracellularly by trophic and/or cystic ciliates (Foissner *et al.* 2005). They occur in a

variety of ciliates and often have nice shapes and structures. Lepidosomes were recognized only recently as a specific structure of ciliates (Foissner *et al.* 2005), likely because they have been described under a bewildering variety of names, e.g., Schleim, curieux éléments, gelatinous covering, foam, external scale layer, epicortical scales, "scales", chalice-like structures, and yellow or brownish globules. In *Meseres corlissi*, lepidosomes occur only in the cystic stage, where they are part of the pericyst (Foissner 2005, Foissner *et al.* 2005).

Address for correspondence: Wilhelm Foissner, Universität Salzburg, FB Organismische Biologie, Hellbrunnerstrasse 34, A-5020 Salzburg, Austria; E-mail: Wilhelm.Foissner@sbg.ac.at

Except of *Colpoda cucullus* (Kawakami and Yagiu 1963a, b), the genesis and release of the lepidosomes remained unknown. This contrasts other protist groups, especially algae, where external scale genesis and release have been studied in great detail (e.g. Hibberd 1980, Romanovicz 1981, Pienaar 1994). Thus, the lepidosome-coated resting cyst of *Meseres corlissi* provided an excellent opportunity to study scale genesis and release in a ciliate.

Our investigations showed that lepidosome and cyst wall genesis are complex processes connected with the production of four types of highly organized cyst wall precursors which produce, inter alia, the slime adhering the lepidosomes to the resting cyst. These data and cyst wall genesis will be described in a forthcoming paper (Foissner and Pichler 2006). Here, we concentrate on lepidosome genesis and release as well as on encystment which shows several peculiarities likely related to the lepidosomes and slime precursors.

We studied encystment previously (Foissner *et al.* 2005), but missed several important processes because the light of the microscope and the microaquaria disturbed encystment whose conditions can be only partially reproduced. Now, we used another method which provided epidemic encystment, and we could study the process in great detail in the light and electron microscope.

MATERIALS, METHODS AND TERMINOLOGY

Material and cultivation. The population studied was isolated from a meadow soil of Upper Austria, i.e., in the surroundings of the town of Kefermarkt, using the non-flooded Petri dish method (Foissner *et al.* 2002).

Cultures of *M. corlissi* were established with about 20 cells on Eau de Volvic (French table water) enriched with some squashed wheat grains and *Cryptomonas lucens* (UK Culture Collection of Algae and Protozoa, CCAP, Windermere).

Induction of encystment. The various encystment stages were obtained by transferring about 2000 specimens from an exponentially growing culture (about 10% dividers) into a Petri dish 5 cm across, together with 7 ml culture medium and the food contained therein. This isolated part of the culture was then controlled hourly with a dissecting microscope. Encysted specimens were recognized already after 5 h, but epidemic encystment occurred after 20 h when food was visibly reduced.

Encysting and non-encysting specimens were isolated with a fine pipette and transferred into micro-aquaria made of vaseline and a coverslip on a microscope slide. Microscopic observation was performed under dimmed light because ordinary light intensity greatly disturbs the encystment process; full light was used only for the micrographs.

Morphological and cytological methods. The methods described in Foissner (2005) and Foissner *et al.* (2005) were used.

Morphometry. We provide detailed morphometric data for most of the structures described. This is uncommon in cyst research and was criticized by both reviewers. The first reviewer suggested that it "would make much more sense to give round figures", and the second one even believes that the "tabulated values should be deleted". Thus, some comment is necessary.

In our opinion, a basic, descriptive statistics greatly improves the value and interpretation of the observations because of showing the variability of the data and the number of specimens and/or observations they are based. As concerns the present and a forthcoming study, morphometry was indispensable for discriminating between the about 35 developmental stages of five types of cyst wall precursors. Certainly, the measurements are influenced by, e.g., shrinkage or inflation during fixation and embedding, the magnetic hysteresis of the lenses of the electron microscope, and the uncertainty to know whether the section passes through the widest part of the structure (when globular, this can be checked by the membranes whose tripartite structure can be seen clearly only if the section is in or near to the mid). Accordingly, the data are less exact than they appear in Table 2. However, this applies to most measurements, and the more they are distorted by external factors the more statistics is required (Sachs 1984)! In any case, data with statistics are much more reliable than the frequently used "about". Today, international journals would not accept ciliate descriptions without appropriate statistics, though the data are influenced by the preparation procedures, the calibration error of the microscope, and other shortcomings. However, we know of these problems and thus can estimate their influence and, if appropriate, can test for differences with comparative statistics. Thus, more exact data should become the rule in cystology, too.

Terminology. General ciliate terminology follows Corliss (1979), cytological terminology is according to Alberts *et al.* (1994), and cyst terminology is according to Gutiérrez *et al.* (2003), Foissner (2005), and Foissner *et al.* (2005).

RESULTS

Trophic cell

The specimens from Upper Austria are highly similar to those from the Salzburg type locality (Petz and Foissner 1992) and the Dominican Republic (Foissner *et al.* 2005). Usually, cells are obconical or pot-shaped and have a size of about $70 \times 50 \mu\text{m}$ *in vivo* (Figs 2, 4). The somatic cortex is covered by an average of eight rows of about $15 \mu\text{m}$ long bristles. The anterior body end is occupied by about 16 collar and 15 ventral adoral membranelles. The whole cell, including somatic cilia and adoral membranelles, is covered by the so-called perilemma and a thin layer of mucus (Foissner *et al.* 2005). The perilemma is typical for some groups of spirotrich ciliates and consists of one to several tripartite

membranes lying upon the cell membrane of the ciliate (Foissner 2005; Fig. 57).

Encystment

Protargol impregnation and transmission electron microscopy showed that about one third of the specimens of exponentially growing cultures have lepidosomes and cyst wall precursors in various stages of development; 10% even contain few or many fully differentiated lepidosomes. Thus, encysting cells are found throughout the life cycle. We consider this as a specific survival strategy, details of which will be reported in a separate paper.

The above mentioned specimens look like ordinary cells, even if they contain many mature lepidosomes, while "truly" encysting specimens show a series of morphological and physiological changes described in the following paragraphs (Figs 1, 4-20). Although encystment is a continuous process, six distinct stages can be distinguished, each associated with certain morphological and/or physiological changes.

Stage (a): The first morphological changes recognizable are a considerable reduction of the cell volume and a slight elevation of the peristomial bottom, likely caused by some constriction of the peristomial collar (Figs 1a, 4, 5, 16, Table 1). The basic cell shape is maintained, and many developing and some mature lepidosomes are recognizable in the light- and electron microscope. The

somatic cilia become shorter gradually and swimming speed decreases.

Stage (b): Next, the cell becomes globular and develops a very distinct constriction anteriorly, i.e., reaches the "head stage" which is significantly shorter than the theront stage, while the volume remains the same (Figs 1b, 6, 7, 17, Table 1). The formation of the head is achieved by an about 200 nm thick ring of fibres (Fig. 18). Many mature or almost mature lepidosomes are now scattered throughout the cell and length reduction of the somatic cilia continues (Fig. 13).

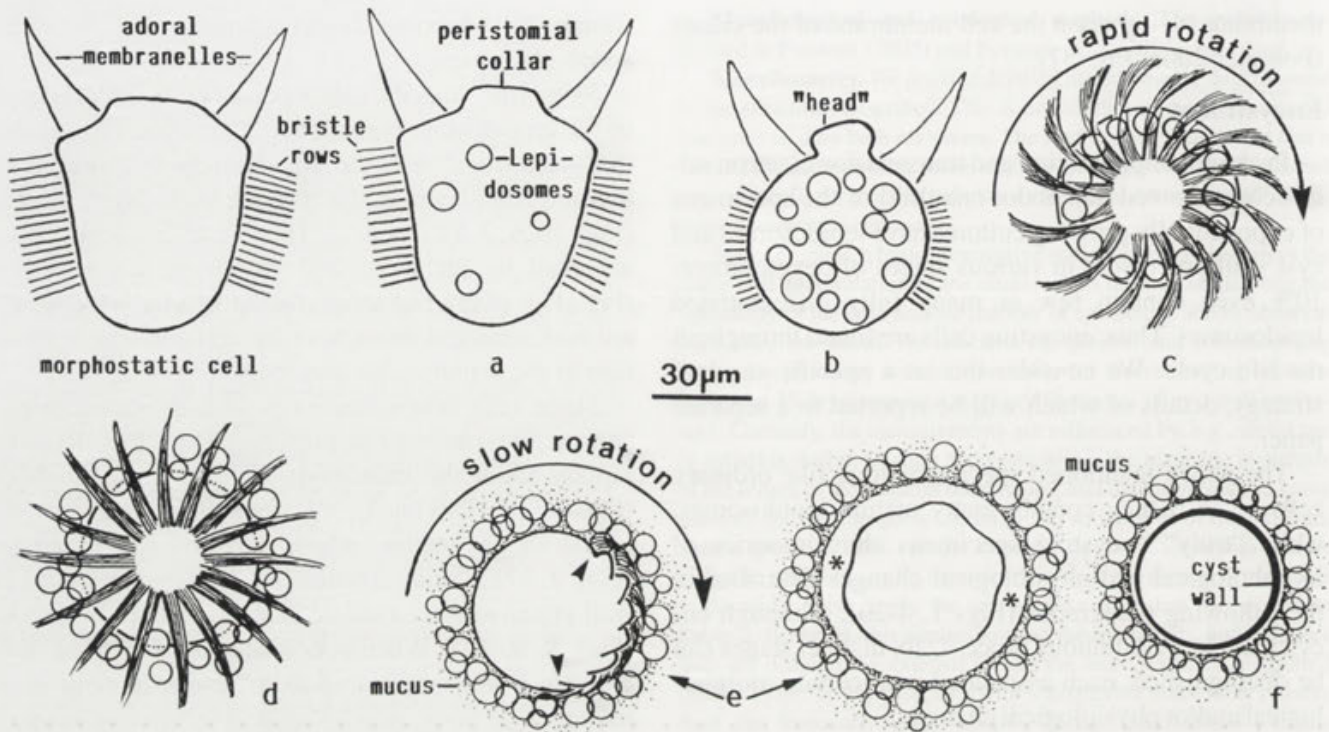
Stage (c): When stage (b) is fully developed, a conspicuous process commences, that is, the cell rotates rapidly about the main body axis for a minute or so (Figs 1c, 8). Obviously, this rotation is caused by the adoral membranelles, which are almost unshortened (Figs 9, 17). During rotation, the lepidosomes and cyst wall precursors accumulate in the periphery of the cell (Figs 8, 9, 17). When specimens are disturbed, they perform a few short, rapid jumps and then continue to rotate.

Stage (d): Then, the cell splays the adoral membranelles and the rotation stops abruptly (Fig. 9). The lepidosomes are now tightly underneath the cortex and are released immediately. The release of the lepidosomes occurs within 5 - 20 s, rarely within 60 s, as observed in 10 specimens (Figs 1d, 10, 19). Lepidosome release is spectacular, that is, they appear to glide through the

Table 1. Size and volume changes of *Meseres corlissi* during encystment. Data based on fixed, Epon-embedded specimens as used for transmission electron microscopy, except of trophont measurements which are from life. Measurements in μm . CV - coefficient of variation in %, M - median, Max - maximum, Min - minimum, n - number of specimens investigated, SD - standard deviation, SE - standard error of mean, \bar{X} - arithmetic mean.

Characteristics	\bar{X}	M	SD	SE	CV	Min	Max	n
Trophonts								
Length	72.7	76	15.2	3.5	21.0	60	88	19
Width	59.4	64	7.9	1.8	13.3	48	42	19
Volume (truncated cone) ^a	118 488 μm^3							19
Theronts ready to encyst								
Length	62.9	64	6.1	1.4	9.7	52	76	19
Width	48.4	48	2.8	0.6	5.8	44	55	19
Volume (truncated cone) ^a	66 367 μm^3							19
Encysting cell in "head" stage								
Length (with head)	55.9	56	5.3	1.2	9.4	44	64	19
Width	48.0	48	3.2	0.7	6.7	40	52	19
Volume (ellipsoid) ^a	67 523 μm^3							19
Early resting cysts								
Length	41.4	40	3.6	0.7	8.7	36	48	19
Width	38.8	40	4.4	1.0	11.4	28	44	19
Volume (sphere) ^a	33 493 μm^3							19

^a Geometric figure applied for volume calculation



Figs 1a-f. *Meseres corlissi*, encystment according to live observations and micrographs (Figs 4-15). **a** - early stage of encystment, where the peristomial collar narrows and some almost mature lepidosomes occur; **b** - "head" stage, where the cell becomes globular and has many mature lepidosomes; **c** - frontal view during the rapid rotation phase which lasts for about 1 min and possibly slings the lepidosomes to the periphery of the cell; **d** - then, the cell stops rotation and all lepidosomes are released within about 20 s; **e** - next, the cell rotates slowly for about 5 min, reducing the adoral membranelles and secreting mucous material. Two important processes occur during the slow rotation phase: cell size is reduced causing the wrinkled shape, and cyst wall material is secreted eventually appearing as an up to 10 μm wide, bright zone (asterisks); **f** - young resting cyst with lepidosome layer 0 - 3 μm distant from cyst wall.

cortex, whereby the cell becomes slightly but distinctly inflated, just like it would take a deep breath. For cytological details, see electron microscopy below.

Stage (e): Within the next two minutes, the shortening adoral membranelles attach to the cell which then commences to rotate slowly for about five minutes; likely, the rotation is caused by the shortened adoral membranelles, though no distinct movements of their cilia are recognizable (Figs 1e, 11). During rotation, the cell gets a slightly irregular outline and becomes smaller, that is, reaches a diameter of about 40 μm, likely due to the high activity of the contractile vacuole which expels water every 10 s. Further, the rotation is associated with the secretion of an up to 10 μm thick slime layer which pushes away the lepidosomes. The slime is very hyaline and recognizable mainly due to the adhering bacteria; it does not stain with uranyl acetate and lead citrate, and thus a wide, clear zone becomes recognizable between cell and lepidosome

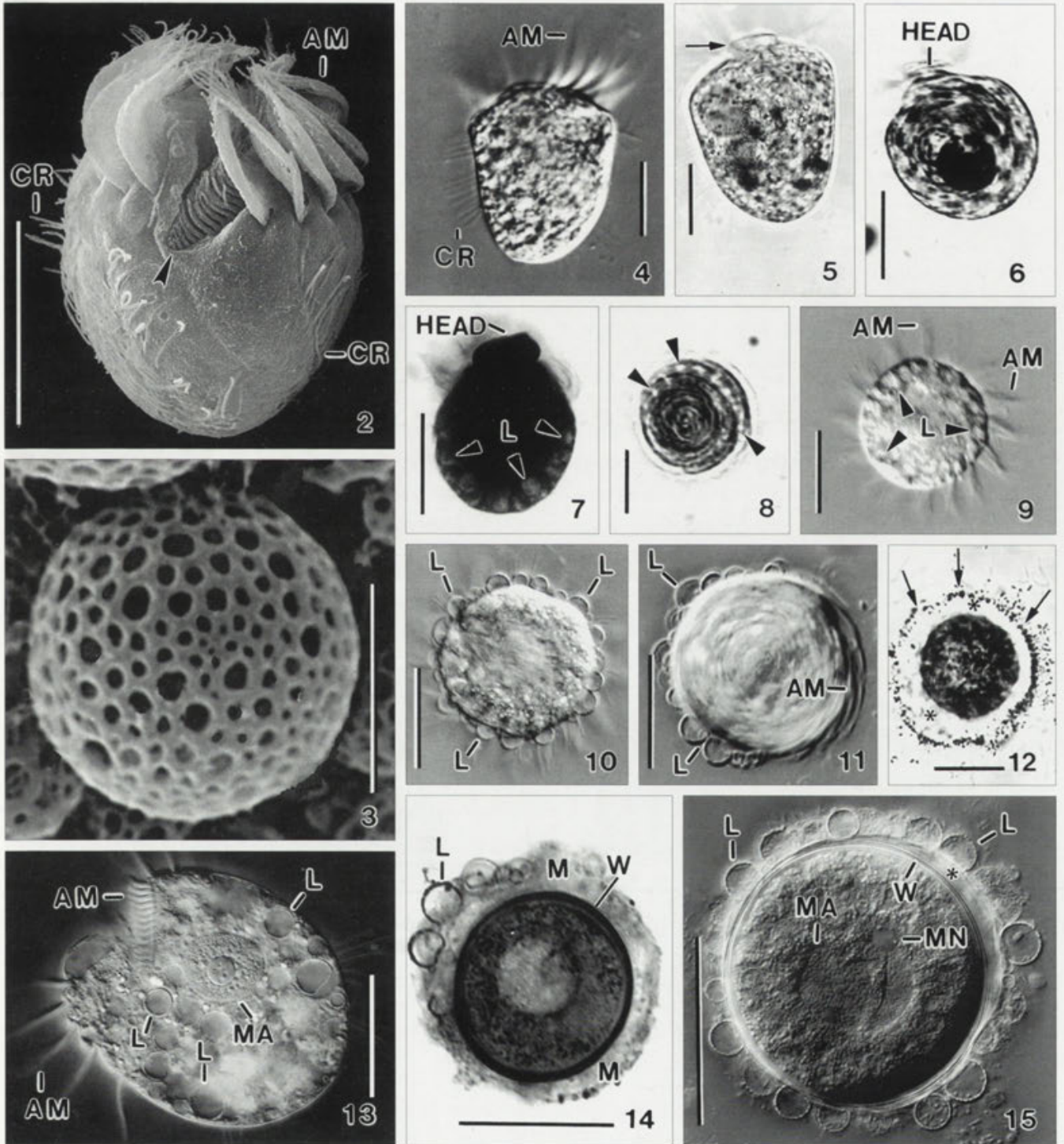
coat in the light- and electron microscope (Figs 12, 20).

Stage (f): When rotation ceases, the cyst wall *s. str.* is assembled and separated from the mucous coat by 1-3 μm (Figs 1f, 15). When such cysts are treated with alcian blue, the newly produced cyst wall and the mucous coat stain heavily (Fig. 14), showing the presence of acid mucopolysaccharides (Foissner *et al.* 2005). In mature cysts, the wall does not stain with alcian blue (see Foissner *et al.* 2005 for more detailed cytochemical data).

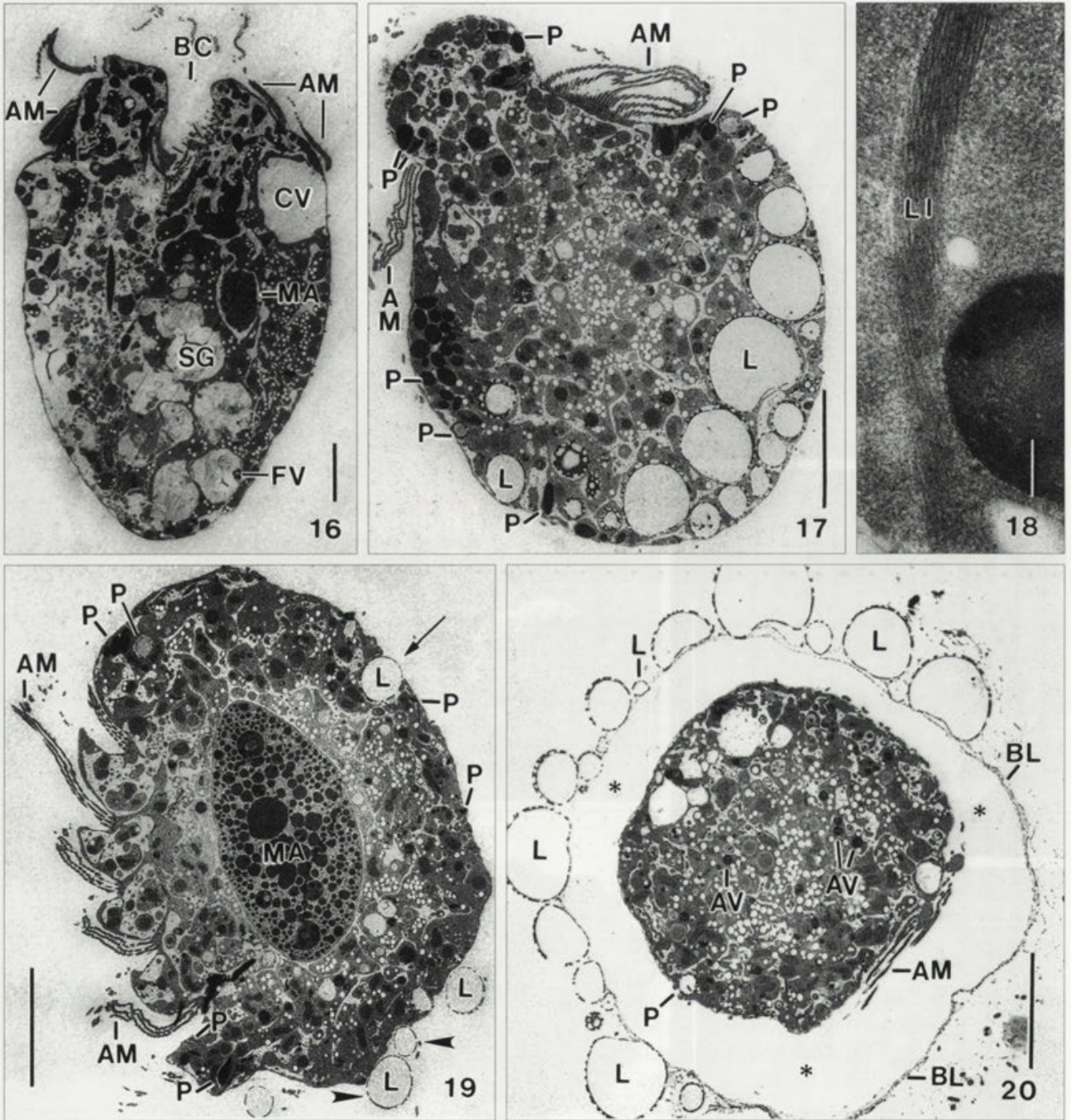
Mature resting cyst

The mature resting cyst of *M. corlissi* has been investigated by Foissner (2005) and Foissner *et al.* (2005). Thus, we provide only a very brief description needed for understanding the present paper.

Mature cysts of *M. corlissi* are globular and about 45 μm across (Fig. 15). They belong to the kinetosome-



Figs 2-15. *Meseres corlissi*, vegetative and encysting specimens in the scanning electron microscope (2, 3), *in vivo* in the bright field (5, 6, 8, 12) and interference contrast (4, 9-11, 13, 15) microscope, after fixation as used for transmission electron microscopy (7), and stained with alcian blue (14). 2, 4 - ventral views showing general organization and buccal vertex (arrowhead); 3 - a lepidosome; 5 - early encystment stage with narrowed peristomial collar (arrow); 6, 7, 13 - "head" stage with many lepidosomes (L). 8 - rapid rotation stage where the lepidosomes (arrowheads) accumulate in the cell's periphery; 9, 10 - after rapid rotation (8), the cell stops (9) and releases the lepidosomes (10) within about 20s; 11, 12, 14 - then the cell begins to rotate slowly, reduces the adoral membranelles (11), and releases cyst wall material which forms a thick, bright coat (12, asterisks) deeply staining with alcian blue (14). Arrows in figure (12) mark coat margin quickly colonized by bacteria; 15 - young cyst with narrow space (asterisk) between cyst wall and lepidosome coat. AM - adoral membranelles, CR - ciliary rows, L - lepidosomes, M - mucous layer, MA - macronucleus, MN - micronucleus, W - cyst wall. Scale bars: 5 μ m (3); 30 μ m (2, 4-15).



Figs 16-20. *Meseres corlissi*, overviews of a vegetative cell (16) and of encysting specimens (17-20) in the transmission electron microscope. 16 - (corresponds to specimens like those shown in Figures 2, 4) - longitudinal section showing the overall organization of a vegetative specimen; 17, 18 - (correspond to specimens like those shown in Figures 6, 7) - a "head stage" specimen at the end of the first rotation phase, as recognizable by the peripheral location of the lepidosomes (L) and cyst wall precursors (P). The specimen rounds up and constricts the oral area by a fibrous ligament (18), producing a highly characteristic knob, the "head"; 19 - (corresponds to specimens like that shown in Figure 10) - a globular specimen just extruding the lepidosomes (arrow); those marked with arrowheads have just left the cell and are shown at higher magnification in Figure 53. The adoral membranelles (AM) are still intact, and many cyst wall precursors (P) are recognizable; 20 - (corresponds to specimens like that shown in Figure 12) - the cell now commences to rotate slowly, reduces the adoral membranelles, and releases the cyst wall precursors which push away the lepidosomes, producing a thick, slimy, stainless zone around the cell (asterisks). AM - adoral membranelles, AV - autophagous vacuoles, BC - buccal cavity, BL - basal layer of lepidosome coat, CV - contractile vacuole, FV - food vacuole, L - lepidosomes, LI - ligament, MA - macronucleus, P - three types of cyst wall precursors described in a forthcoming paper, SG - starch grain. Scale bars: 200 nm (18); 10 μ m (16, 17, 19, 20).

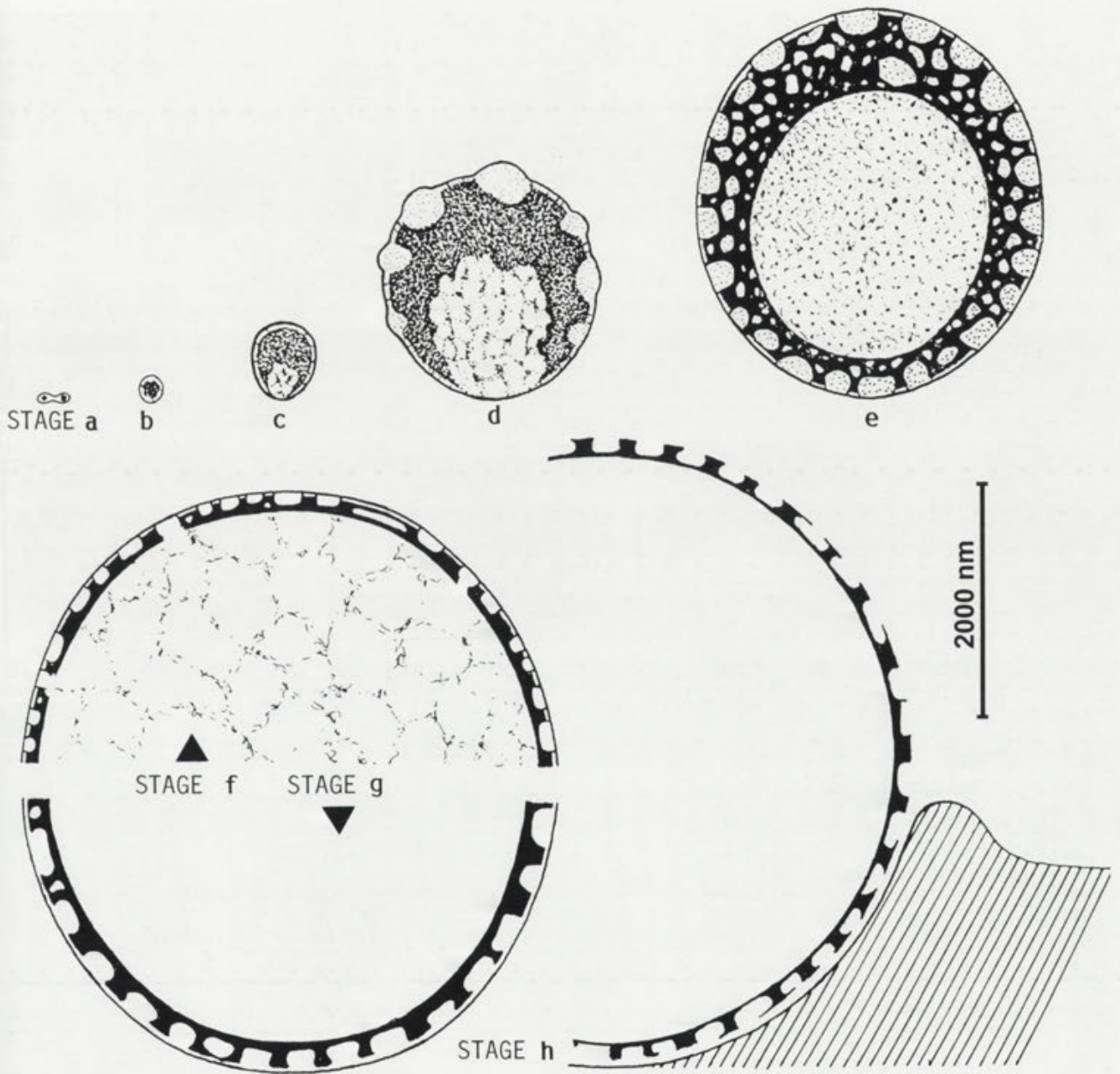
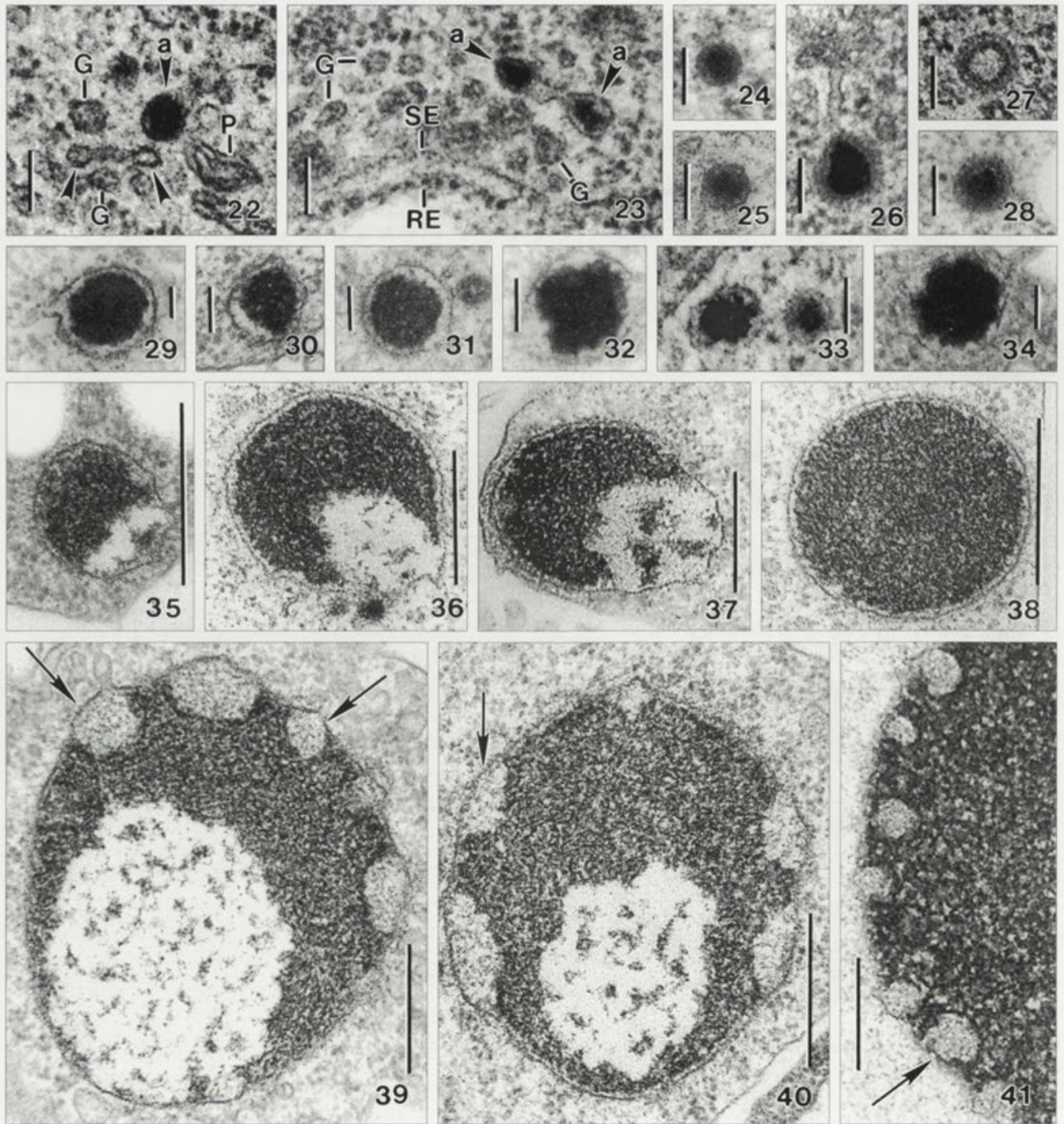


Fig. 21. *Meseres corlissi*, schematic figures drawn to scale of lepidosome genesis (a-g) and release (h). See text and Figures 22-58 for more detailed explanation.

resorbing type and have a conspicuous coat of extracellular organic scales, termed lepidosomes, embedded in a thick layer of mucus mainly composed of acid mucopolysaccharides. The lepidosomes, which likely consist of glycoproteins, are finely faceted, hollow spheres with a diameter of 2 - 14 μm (Fig. 3). The cyst wall is about 1.5 μm thick, smooth, and consists of five complex layers.

Genesis of the lepidosomes

Although lepidosome genesis is a continuous process, we have distinguished seven stages roughly correlating with the six encystment stages described above (Fig. 21). However, the sometimes high coefficients of variation indicate that several distinct stages have been



Figs 22-41. *Meseres corlissi*, transmission electron micrographs of stages (a-d) of lepidosome genesis. **22-25** - stage (a) shows that the lepidosomes are generated pairwise in dumbbell-shaped vesicles (arrowheads) of the medial Golgi cisternae. The vesicles, which have an average size of 85×78 nm, become filled with strongly osmiophilic material [arrowheads with (a)]. Figure 23 shows that the Golgi apparatus and vesicle production of *M. corlissi* correspond to textbook knowledge: transition vesicles arriving from the smooth side of the endoplasmic reticulum (SE) fuse with membranes of the cis-Golgi network, while lepidosome precursors bud off from the trans-Golgi network; **26-28** - coated transport vesicles; **29-34** - stage (b) precursors have a size of about 200 nm and show a cogged dense core when mature; **35-38** - stage (c) is very distinctive because a bright area develops at the margin of the vesicle. The bright area is not recognizable, if the section goes through the electron-dense portion, which is composed of finely reticular material; **39-41** - stage (d) is characterized by the occurrence of mesh precursors (arrows) in the periphery of the dense core. The lepidosome precursors have now light-microscopical dimension, i.e., a size of about $2 \mu\text{m}$. G - Golgi vesicles, P - cyst wall precursor, RE - rough endoplasmic reticulum, SE - smooth endoplasmic reticulum. Scale bars: 100 nm (22-34); 400 nm (35-41).

lumped or the process runs very fast (Table 2). The general fine structure of the cytoplasm of *M. corlissi* matches that of other ciliates and textbook knowledge, except of the endoplasmic reticulum and the Golgi apparatus which are comparatively distinct, likely because lepidosomes and cyst wall precursors are produced throughout the cell cycle (see above).

Stage (a): Lepidosome genesis commences with the appearance of dense core vesicles in the dilated rims of the medial and trans-Golgi cisternae. Thus, the lepidosomes originate in pairs, producing highly characteristic, dumbbell-shaped vesicles with an average size of 251×74 nm (Figs 21a, 23, Table 2). When the vesicles have pinched off, they become globular and have an average size of 85×78 nm (Figs 22, 24, 25, Table 2). Both the dense core and the surrounding membrane are more or less wrinkled. Usually, there is a minute space, often traversed by fibrogranular bridges, between membrane and core. The dense core is composed of strongly osmiophilic, very fine-grained material.

Two other vesicle types are also rather frequent and have the same size as the lepidosome precursors. They are coated by an about 30 nm thick, finely granular material, and one is filled with heavily osmiophilic material (Figs 26, 28), while the other appears bright (Fig. 27). Likely, these are transport vesicles.

Stage (b): The vesicles are globular to broadly ellipsoidal and doubled the average size to 206×182 nm (Table 2). Usually, the vesicle membrane and the dense core are less wrinkled than in stage 1, but the core surface often shows a cogged pattern (Figs 32-34). The dense core is very narrowly reticular and slightly smaller than the vesicle, leaving a narrow, bright space bridged by fine strands of fibrogranular material (Figs 21b, 29-31).

Stage (c): The lepidosome precursors are now broadly ellipsoidal and have a size of 615×525 nm on average (Table 2). Stage (c) is characterized by the appearance of a bright area at the margin of the dense core, which is connected to this area by many fine strands of fibrogranular material. The bright area, which has an average size of 465×312 nm, contains a loose reticulum of fibrogranular core material and, frequently, some patches of condensed core material (Figs 35, 37). Rarely, two or more bright areas occur, and sometimes the area distinctly projects from the vesicle proper, producing a rather irregular outline of the vesicle. The dense core has a finely spotted appearance, indicating a reticular arrangement of the material. Still, the core is separated

from the surrounding vesicle membrane by an about 15 nm wide space bridged by many fine strands of fibrogranular material (Figs 21c, 35-38, Table 2).

Stage (d): The next stage distinguishable has already light microscopical dimension, that is, has an average size of 2020×1827 nm (Table 2). Frequently, the precursors are broadly ovate with the bright portion being narrower and more or less protruding. The fine structure of the bright area and the dense core are as described in stage (c), but the plane of the former decreased from 45% to 26%. However, the main feature of this stage is the appearance of mesh precursors opposite to the bright area (Figs 21d, 39-41). The mesh precursors are pot-shaped blisters or concavities in the periphery of the dense core and contain fluffy, weakly stained material hardly distinguishable from the background; they are not bounded by a membrane, except distally, where the precursor membrane covers the blisters. The blisters have an average size of 228×174 nm and are comparatively rare, indicating that they will form the large meshes of the lepidosomes.

Stage (e): By further growth, the lepidosome precursors reached an average size of 3350×2962 nm, that is, are broadly ellipsoidal and have a tubercular outline due to the more or less distinctly protruding mesh blisters (Figs 42-44, Table 2). Morphologically, two main changes occur and can be followed *via* several transition stages (Figs 21e, 42-44). First, the dense core material, which has a finely granular structure (Fig. 46), becomes distinctly reticulate (Fig. 45), showing that it forms the lepidosome wall. Second, the bright area, which contains very fine-meshed, fibrogranular material, commences to move centripetally and grows distinctly, now occupying an average of 49% of the lepidosome plane (Figs 42-44). Obviously, the bright area forms the lepidosome cavity.

Stage (f): The lepidosome precursors have almost mature dimension, that is, show an average size of 4571×3831 nm (Table 2). Most precursors are globular or broadly ellipsoidal and very near to the ciliate's cortex (Figs 47, 49); rarely, they are impressed on one side and thus hemispherical or slightly wrinkled. Morphologically, the precursors are already highly similar to mature lepidosomes, that is, they consist of a thin, darkly stained wall and a large, bright cavity (Figs 21f, 47). However, details are still in work. The precursor wall material is still fibrogranular (Fig. 46), while the wall becomes distinctly reticular. However, the basal layer, which separates the wall from the central cavity, is still thin and partially lacking (Fig. 48); thus, cytoplasmic intrusions

Table 2. Morphometric data on lepidosome precursors. All measurements in nm and from transmission electron micrographs. CV - coefficient of variation in %, I - number of cysts investigated, M - median, Max - maximum, Min - minimum, n - number of precursors measured, SD - standard deviation, \bar{X} - arithmetic mean.

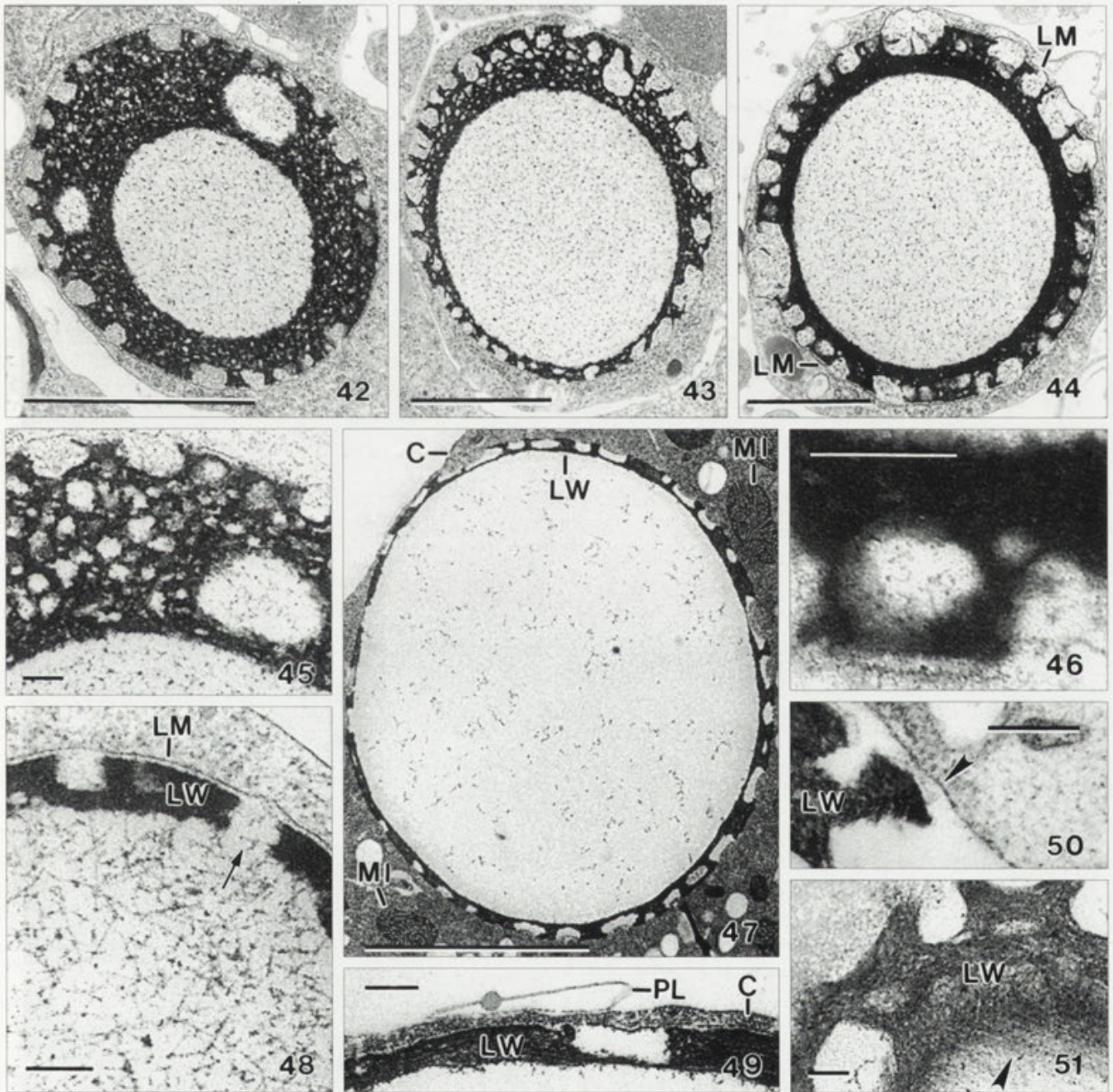
Characteristics ¹	\bar{X}	M	SD	CV	Min	Max	n	I
Stage (a), length ^a	251	225	72	28.8	183	413	11	2
width	74	75	16	22.2	47	100	11	2
Stage (a), length ^b	85	90	20	23.5	35	109	20	3
width	78	83	21	26.5	30	100	20	3
Stage (b), length	206	200	27	13.0	167	250	14	3
width	182	174	29	16.1	150	227	14	3
Stage (c), length	615	636	114	18.5	413	767	11	4
width	525	527	108	20.6	387	767	11	4
bright area, length	465	400	163	35.0	300	767	9	2
width	312	283	132	42.4	120	600	9	2
Stage (d), length	2020	1875	90	44.4	884	3947	26	6
width	1827	1675	84	46.2	714	3684	26	6
bright area, length	1081	1050	327	30.3	507	1682	13	5
width	894	975	262	29.3	453	1318	13	5
mesh precursors, length	228	250	69	30.4	120	320	13	5
width	174	150	68	39.3	107	319	13	5
Stage (e), length	3350	3107	1536	45.9	1679	6250	11	5
width	2962	2643	1356	45.8	1607	5833	11	5
bright area, length	2368	1884	1228	51.8	950	4750	10	5
width	2043	1590	1081	52.9	825	4250	10	5
Stage (f), length	4571	3737	2336	51.1	2250	9300	14	7
width	3831	3079	1911	49.9	1875	7895	14	7
wall, thickness	169	158	70	39.2	90	281	13	7
Stage (g), length	5842	5600	2227	38.1	3500	9700	12	7
width	4904	4500	2289	46.7	2500	9300	12	7
wall, thickness	250	211	103	41.1	158	500	10	7
Stage (h), length	5578	4500	2959	53.0	2400	10300	13	2
width	4754	4000	2622	55.2	1800	9000	13	2
wall, thickness	155	135	62	40.0	68	267	18	2
Just extruded lepidosomes, length	4490	4600	1625	36.2	2300	7600	12	2
width	3952	4035	1389	35.1	1895	6667	12	2

^adumbbell-shaped vesicles, ^bsingle vesicles.

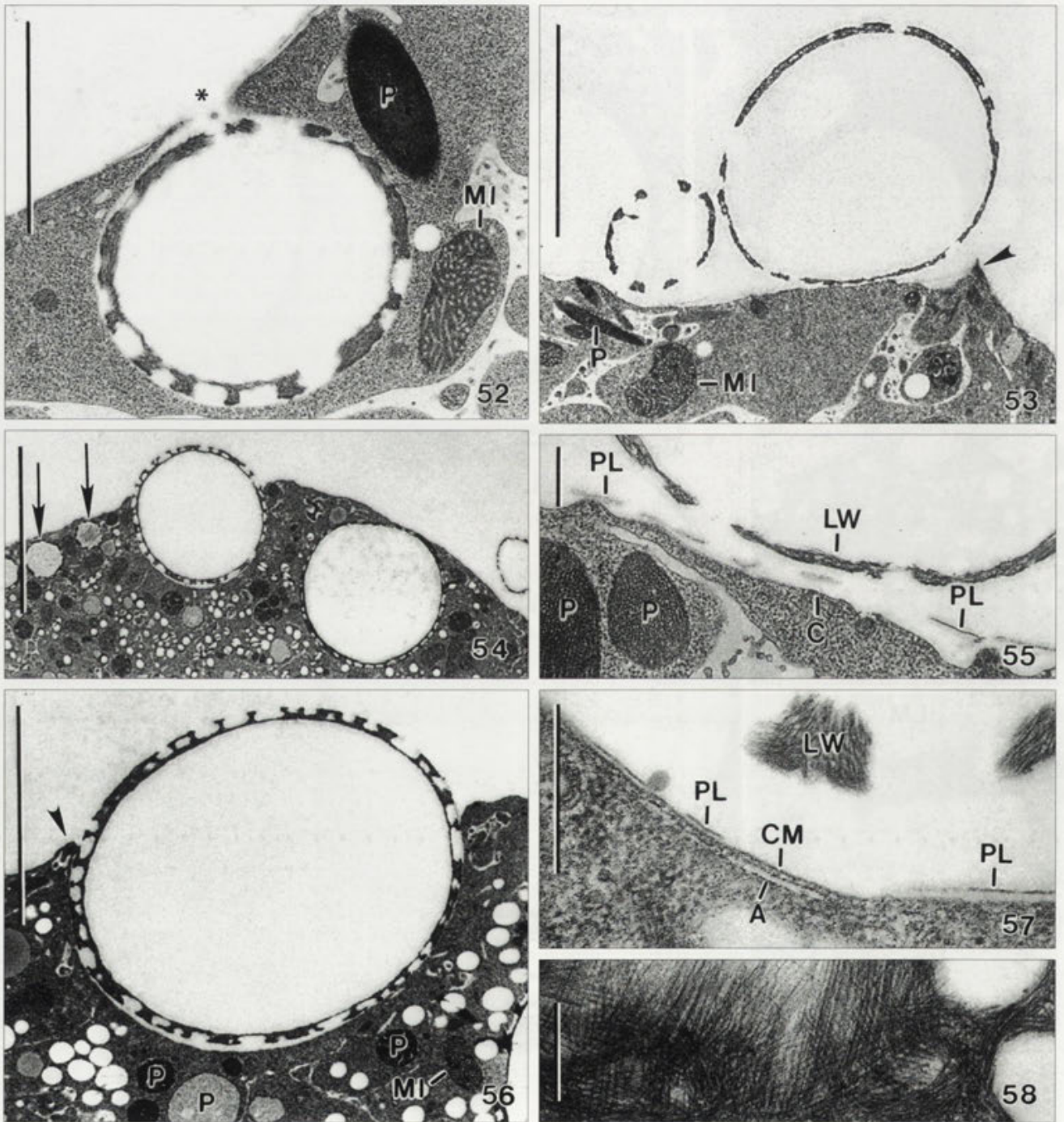
are sometimes found. The large, bright central cavity of the precursor contains a loose, sometimes very distinct (Fig. 48) fibrogranular reticulum (Fig. 47), which completes the precursor wall in the next stage.

Stage (g): By further growth, the precursors reached their mature size, that is, 5842 × 4904 nm on average (Table 2). Most-precursors are globular or slightly ellip-

soidal and very near to the cortex of the cell; rarely, they are impressed on one side and thus hemispherical or are near to the cell centre. Morphologically, two features change: (i) the wall material organizes to sheets, possibly via a microfibrillar transition stage, which are still finer and less distinct (Figs 50, 51) than in extruded lepidosomes (Fig. 58), and (ii) the central cavity becomes clear, likely



Figs 42-51. *Meseres corlissi*, transmission electron micrographs of stages (e-g) of lepidosome genesis. **42-46** - stage (e) precursors have a size of about 3 μm and show the rising lepidosome structure, viz., a thick, strongly osmiophilic wall surrounding a large, bright centre with fibrogranular contents (Figs 42-44). The wall, which evolved from the dense core described in the previous stages, still consists of finely granular material (Figs 45, 46) which, however, now forms a coarse reticulum with meshes increasing in size from proximal to distal (Figs 42-44); **47-49** - stage (f) precursors, which have a diameter of about 4 μm and are thus much larger than the mitochondria (Fig. 47), already resemble mature lepidosomes because the wall is much thinner than the central cavity (Fig. 47). Figure 49 is a few sections away from that shown in Figure 47 and demonstrates that the lepidosome is near to the ciliate's cortex and the wall is getting a microfibrillar structure. The central cavity is filled with fibrogranular material (Fig. 47), which is sometimes very distinct (Fig. 48). The lepidosome wall is still in work, often partially lacking the basal layer (Fig. 48, arrow); **50, 51** - stage (g) precursors are very similar to stage (f) precursors, but the microfibrillar structure of the wall changes to more distinct, sheet-like structures (Fig. 51, arrowhead), as typical for the mature lepidosome (Fig. 58). The arrowhead in Figure 50 marks the membrane surrounding the developing lepidosome. The lepidosome cavity becomes clear because the fibrogranular material (Figs 47, 48) attaches to the wall which thus becomes thicker (Table 2). C - ciliate cortex, LM - lepidosome membrane, LW - lepidosome wall, MI - mitochondria, PL - ciliate perilemma. Scale bars: 4000 nm (47); 2000 nm (42-44); 200 nm (45, 46, 48-51).



Figs 52-58. *Meseres corlissi*, transmission electron micrographs of lepidosome release. **52** - the cortex opens (asterisk) to release a lepidosome; **53** - (for an overview, see Figure 19) - two lepidosomes which just left the cell, as recognizable by the collar (arrowhead) surrounding leaving lepidosomes (cp. Fig. 56); **54, 56** - two sections of a lepidosome leaving the cell. Likely, the cell's turgor transports the lepidosome out of the cell. The lepidosome membrane closes the opening caused by the lepidosome and transforms into a new cell membrane (see also Figures 55, 57). The arrowhead marks the minute collar forming around the leaving lepidosome. The arrows denote some cyst wall precursors; **55, 57** - some fortunate sections show that the lepidosome membrane becomes part of the new ciliate cortex closing the lepidosome opening (see also Fig. 56). This process runs very fast, i.e., the new cortex becomes visible immediately after the lepidosome has left the cell. The cortex consists of a perilemma membrane (PL), the cell membrane (CM), and the membrane-bounded alveoli (A); **58** - the wall of the mature lepidosome consists of interwoven, very thin sheets, which form from the fibrogranular material composing the wall of the developing lepidosome (Figs 46, 49-51). A - cortical alveolus, C - cortex, CM - cell membrane, LW - lepidosome wall, MI - mitochondria, P - cyst wall precursors, PL - perilemma. Scale bars: 2 μ m (52); 4 μ m (53, 56); 10 μ m (54); 400 nm (55, 57, 58).

Table 3. Resting cyst volume as percentage of the vegetative cell volume. All calculations were done or redone by us, using simple geometric figures (cone, sphere etc.) and average size values as given by the authors cited. Pericyst excluded!

Species	Cyst volume %	Literature
Oligotrichs		
<i>Meseres corlissi</i>	28	This paper; see Table 1
<i>Halteria grandinella</i>	38	Foissner (unpubl.)
<i>Pelagostrombidium</i> spp.	58	Müller <i>et al.</i> (2002)
<i>Strombidium oculatum</i>	161	Jonsson (1994)
Stichotrichs		
<i>Oxytricha bifaria</i>	20	Ricci <i>et al.</i> (1985)
<i>Kahliella simplex</i>	20	Foissner and Foissner (1987)
<i>Engelmanniella mobilis</i>	33	Wirnsberger-Aeschl <i>et al.</i> (1990)
<i>Parakahliella halophila</i>	26	Foissner <i>et al.</i> (2002)
Heterotrichs		
<i>Condylostomides etoschensis</i>	3	Foissner <i>et al.</i> (2002)
<i>Blepharisma japonicum</i>	~100	Giese (1973)
<i>Blepharisma americanum</i>	92	Foissner (unpubl.)
Peritrichs		
<i>Vorticella echini</i>	51	Foissner <i>et al.</i> (2002)
<i>Opisthonecta henneguyi</i>	24	Rosenberg (1938)
<i>Opisthonecta henneguyi</i>	5	Walker <i>et al.</i> (1989)
Colpodids		
<i>Colpoda cucullus</i>	69	Foissner (1993)
<i>Maryna umbrellata</i>	52	Foissner <i>et al.</i> (2002)
<i>Kuehneliella namibiensis</i>	84	Foissner <i>et al.</i> (2002)
<i>Platyophrya spumacola</i>	71	Foissner (1993)
Haptorids		
<i>Enchelydium blattereri</i>	66	Foissner <i>et al.</i> (2002)
<i>Spathidium turgitorum</i>	~100	Foissner <i>et al.</i> (2002)
<i>Arcuospithidium cultriforme</i>	97	Xu and Foissner (2005)

due to the accumulation of the fibrogranular reticulum to the precursor's wall, whose thickness increases from 169 nm in stage (f) to 250 nm in the (g) stage (Figs 21g, 52, Table 2).

Stage (h): The precursor size is similar to that in the previous stage (Table 2), while the thickness of the precursor wall decreases from 250 nm in stage (g) to 155 nm in stage (h) and the wall sheets become distinct and thicker (Fig. 58), as typical for the mature state (Foissner 2005 and discussion below). The membrane surrounding the precursor is very near to the lepidosome wall (Figs 21g, 48, 50). The central cavity is clear and structureless (Figs 52, 56).

Release of the lepidosomes

When the mature lepidosome leaves the encysting cell, usually after the head stage (Fig. 1d), the cortex opens forming a low wall around the port (Figs 21h, 54, 56). Concomitantly, the precursor membrane is incorporated into the newly forming cortex consisting of perilemma, cell membrane and alveoli (Figs 21h, 53, 55,

57). Thus, the cytoplasm is membrane-covered during the whole extrusion process. We studied the release in nine lepidosomes and are thus sure that the lepidosome membrane is incorporated into the newly forming cortex.

DISCUSSION

Encystment

Encystment of *M. corlissi* shows two peculiarities, viz., body shape changes early and distinctly (Figs 4-7) and two phases of intense rotation occur (Figs 8, 11). The mature cyst has also two extraordinary features, viz., a coat of lepidosomes (Figs 3, 15) and a chitinous layer in the cyst wall (Foissner 2005, Foissner *et al.* 2005).

Distinct body changes during encystment occur in a variety of ciliates, for instance, in *Bursaria truncatella*, a colpodid ciliate (Foissner 1993). However, usually the shape becomes simpler, while the encysting *Meseres*

looks like another species (Figs 6, 7). Preliminary observations on *Halteria grandinella*, a close relative of *Meseres corlissi* (Katz *et al.* 2005), showed the same, that is, the globular vegetative cell becomes cylindroidal, and this stage has been described, indeed, as a distinct species (Foissner, unpubl.). *Strombidium oculatum*, the sole other oligotrich where detailed data are available on encystment, simply rounds up, as do many other ciliates (Montagnes *et al.* 2002).

The two rotation phases of the encysting *Meseres* are another extraordinary feature. In the literature, we found only one other ciliate doing the same, viz., *Strombidium oculatum*, suggesting that this phenomenon is characteristic for oligotrichs. Montagnes *et al.* (2002) described it as follows: "Cysts form in minutes on the bottom of tissue plates. A ciliate will swim to a surface, repeatedly bump into the surface, and begin to rotate around its long axis. The ciliate then presses against the surface and splays its adoral membranelles. After ~30 s, the ciliate begins to rotate, forms a ball, and within ~1 min it is covered by a cyst wall". Possible functions of these rotations will be discussed below. The peculiarities discussed above, motivated us to compare the cyst volume of *M. corlissi* with that of other ciliates (Table 3). However, *M. corlissi* is not special in this respect, while the cyst volume of *Strombidium oculatum* is considerably larger than that of the vegetative cell, an extraordinary feature not found in other ciliates. The cyst volume of colpodids and haptorids is between 50% and 100% and is thus usually larger than that of oligotrichs and stichotrichs (20%-60%). The wide volume ratios of the heterotrichs are also remarkable. Generally, the highly different ratios shown in Table 3 cry for more detailed investigations and a functional explanation. The data from *S. oculatum* suggest that the ratios could be related to the organism's ecology/biology (Jonsson 1994, Montagnes *et al.* 2002).

Lepidosome genesis

Many organelles of protists are produced in cisterns of the endoplasmic reticulum or in vesicles of the Golgi apparatus, for instance, trichocysts (Hausmann 1978, Peck *et al.* 1993) and the organic scales of various amoebae, flagellates and algae (Hibberd 1980, Romanovicz 1981, Pienaar 1994). In ciliates, the genesis of the cyst wall precursors is insufficiently known. Calvo *et al.* (1986) proposed that the wall precursors of a stichotrich ciliate, *Histiculus similis*, arise from the endoplasmic reticulum and the Golgi apparatus. This has been confirmed by Walker *et al.* (1989), who docu-

mented that the cyst wall precursor of a peritrich ciliate, *Tetotrochidium henneguyi*, develops pairwise in dilated Golgi cisterns, very similar to what we found in *M. corlissi* (Figs 21a, 23).

As yet, lepidosome genesis and development has been investigated only in *Colpoda cucullus*. Kawakami and Yagi (1963 a, b) showed that they develop from minute, dense vesicles which grow, *via* a granular stage, to about 1 μm -sized "network structures" composed of honey-combed units. The extrusion of these structures has been not documented, but the micrographs show that the extruded networks are globular and lack a surrounding membrane (see also Chessa *et al.* 2002), just as do the lepidosomes of *Meseres*. Obviously, lepidosome genesis is simpler in *Colpoda* than in *Meseres*. Seen from a more general aspect, the processes of pinching off vesicles from the smooth side of the endoplasmic reticulum and incorporating them into the dictyosome are as described in textbooks (Figs 21a, 23).

A few peculiarities in the genesis of the lepidosomes of *M. corlissi* should be mentioned, although we do not understand them. Why develops the central cavity asymmetrically? Why do the large meshes of the lepidosome wall develop earlier than the small ones? How do the lepidosomes grow? We never saw vesicles entering developing lepidosomes, although we studied hundreds of them. Thus, one may speculate that growth is carrier-mediated (Alberts *et al.* 1994). Accordingly, growth of the lepidosomes is different from that of trichocysts which grow by vesicle fusion (Peck *et al.* 1993).

Figure 21 shows a semi-schematic summary of lepidosome genesis and release in *M. corlissi*.

Lepidosome release

The lepidosomes are released rather early, viz., when the ciliary structures are still functioning (Figs 1d, 9, 10, 19). The release of the lepidosomes is a spectacular event because they are numerous and have an average size of 6 μm . Functionally, it is an exocytotic process par excellence, i.e., as described in textbooks (Alberts *et al.* 1994, Plattner and Hentschel 2002): the membrane surrounding the lepidosome fuses with the cortex membranes and becomes a new cell membrane; concomitantly, a new perilemma and cortical alveoli develop (Figs 52-57). This is different from trichocyst release, where the surrounding membrane remains in the cytoplasm and is recycled (Hausmann 1978). Likely, the huge number and the large size of the lepidosomes require that the lepidosomal membrane replaces the cortical membranes. Otherwise, the plasm would be

exposed to the environment because closing of an opening of up to 15 μm needs some time. Further, the about 200 lepidosomes are released almost concomitantly. It is difficult to imagine that the cell would not burst if the new cell membrane had to be generated *de novo*. Certainly, details of the process need to be studied with refined methods, e.g., marking the old cell membrane with ruthenium red.

The extrusion of the lepidosomes occurs within about 20 s and is followed by the release of four types of cyst wall precursors (Foissner and Pichler, submitted). Considering that there are about 200 lepidosomes with an average size of 6 μm , it can be calculated that two thirds of the cortex must be restored; and if the many wall precursors are added, this percentage increases to near 100%. Thus, production and release of the lepidosomes are extremely energy-demanding, suggesting that they have an important function which, however, is not known (Foissner *et al.* 2005). This situation resembles *Paramecium* which invests 40% of its total protein contents in the trichocysts, now known to have a protective function (Plattner 2002).

We did not find any structures, for instance, microtubules transporting the newly formed lepidosomes and cyst wall precursors to the cell periphery, while Walker *et al.* (1980) observed microtubules associated with the cyst wall precursors of *Gastrostyla steinii*, a stichotrich ciliate. Thus, we hypothesize that the intense first rotation phase, which occurs just before lepidosome release, slings the lepidosomes and wall precursors to the cell's periphery. The curious, breath-like inflation of the cell associated with the lepidosome release is possibly caused by a sudden influx of water ejecting the lepidosomes. The second, slower rotation phase might distribute the precursor material. At first glance, these hypotheses appear reasonable. However, many other ciliates produce the resting cyst without specific rotation phases. Thus, our speculations must be rigorously tested whether they are applicable at the low Reynold's numbers operating in the microscopic world.

Lepidosomes: composed of fibres or of thin sheets?

Foissner (2005) described the lepidosomes to be composed of "about 20 nm thick fibres likely longer than 1 μm ". However, when looking at the micrographs, it becomes obvious that the "fibres" must be very thin sheets because roundish or ring-like transverse sections, as typical for fibres and tubules, are not recognizable. This was confirmed by a reinvestigation of Foissner's unpublished materials and the present study. Both show

that the lepidosomes consist of very irregularly arranged, thin sheets (Fig. 58) which originate from a fribrogranular mass (Fig. 46). We could not determine the size of the sheets, but likely they are narrow (~20 nm ?), long bands or broad sheets folded like the bellows of a camera.

Acknowledgements. Financial support was provided by the Austrian Science Foundation (FWF project P 16796-B06) and the King Saud University, Riyadh, Saudi Arabia (contract LGP-7-9). The technical assistance of Andreas Zankl and Mag. Birgit Peukert is greatly acknowledged.

REFERENCES

- Alberts B., Bray D., Lewis J., Raff M., Roberts K., Watson J. D. (1994) *Molecular Biology of the Cell*, 3rd ed. Garland Publ. Inc., New York, London
- Calvo P., Torres A., Perez-Silva J. (1986) Ultrastructural and cytochemical study of the encystment in the hypotrichous ciliate *Histiculus similis*. *Arch. Protistenk.* **132**: 201-211
- Chessa M. G., Largana I., Trielli F., Rosati G., Politi H., Angelini C., Delmonte Corrado M. U. (2002) Changes in the ultrastructure and glycoproteins of the cyst wall of *Colpoda cucullus* during resting encystment. *Europ. J. Protistol.* **38**: 373-381
- Corliss J. O. (1979) *The Ciliated Protozoa. Characterization, Classification and Guide to the Literature*. 2nd ed. Pergamon Press, Oxford, New York, Toronto, Sydney, Paris, Frankfurt
- Foissner W. (1993) *Colpodea (Ciliophora)*. Fischer, Stuttgart, Protozoenfauna **4**: I-X + 1-793
- Foissner W. (2005) The unusual, lepidosome-coated resting cyst of *Meseres corlissi* (Ciliophora: Oligotrichea): transmission electron microscopy and phylogeny. *Acta Protozool.* **44**: 217-230
- Foissner I., Foissner W. (1987) The fine structure of the resting cysts of *Kahliella simplex* (Ciliata, Hypotrichida). *Zool. Anz.* **218**: 65-74
- Foissner W., Pichler M. (2006) The unusual, lepidosome-coated resting cyst of *Meseres corlissi* (Ciliophora: Oligotrichea): genesis of four complex types of wall precursors and assemblage of the cyst wall. *Acta Protozool.* **45**: 339-366
- Foissner W., Agatha S., Berger H. (2002) Soil ciliates (Protozoa, Ciliophora) from Namibia (Southwest Africa), with emphasis on two contrasting environments, the Etosha Region and the Namib Desert. *Denisia* **5**: 1-1459
- Foissner W., Müller H., Weisse T. (2005) The unusual, lepidosome-coated resting cyst of *Meseres corlissi* (Ciliophora: Oligotrichea): light and scanning electron microscopy, cytochemistry. *Acta Protozool.* **44**: 201-215
- Giese A. C. (1973) *Blepharisma*. The Biology of a Light-Sensitive Protozoan. Stanford Univ. Press, Stanford, California
- Gutiérrez J. C., Diaz S., Ortega R., Martín-González A. (2003) Ciliate resting cyst walls: a comparative review. *Recent Res. Devel. Microbiol.* **7**: 361-379
- Hausmann K. (1978) Extrusive organelles in protists. *Int. Rev. Cyt.* **52**: 197-276
- Hibberd D. J. (1980) Prymnesiophytes (= Haptophytes). In: *Phytoflagellates* (Ed. E. R. Cox). Elsevier, North Holland, New York, 273-318
- Jonsson P. R. (1994) Tidal rhythm of cyst formation in the rock pool ciliate *Strombidium oculatum* Gruber (Ciliophora, Oligotrichida): a description of the functional biology and an analysis of the tidal synchronization of encystment. *J. Exp. Biol. Ecol.* **175**: 77-103
- Katz L. A., McManus G. B., Snoeyenbos-West O. L. O., Griffin A., Pirog K., Costas B., Foissner W. (2005) Reframing the „Everything is everywhere” debate: evidence for high gene flow and diversity in ciliate morphospecies. *Aquat. Microb. Ecol.* **41**: 55-65

- Kawakami H., Yagiu R. (1963a) An electron microscopical study of the change of fine structures in the ciliate, *Colpoda cucullus*, during its life cycle. II. From the precyst stage to the early stage of the formation of the first layer of resting cyst membrane. *Zool. Mag.* **72**: 146-151
- Kawakami H., Yagiu R. (1963b) The electron microscopical study of the change of fine structure in the ciliate, *Colpoda cucullus*, during its life cycle. III. From the stage of completion of the first layer of resting cyst membrane to the completion of the resting cyst. *Zool. Mag.* **72**: 224-229
- Montagnes D. J. S., Lowe C. D., Poulton A., Jonsson P. R. (2002) Redescription of *Strombidium oculatum* Gruber 1884 (Ciliophora, Oligotrichia). *J. Eukaryot. Microbiol.* **49**: 329-337
- Müller H., Stadler P., Weisse T. (2002) Seasonal dynamics of cyst formation of strombidiid ciliates in alpine Lake Mondsee, Austria. *Aquat. Microb. Ecol.* **29**: 181-188
- Peck R. K., Swiderski B., Tourmel A.-M. (1993) Involvement of the trans-golgi network, coated vesicles, vesicle fusion, and secretory product condensation in the biogenesis of *Pseudomicrothorax* trichocysts. *Adv. Cell Molec. Biol. Memb.* **2**: 1-25
- Petz W., Foissner W. (1992) Morphology and morphogenesis of *Strobilidium caudatum* (Fromentel), *Meseres corlissi* n. sp., *Halteria grandinella* (Müller), and *Strombidium rehwaldi* n. sp., and a proposed phylogenetic system for oligotrich ciliates (Protozoa, Ciliophora). *J. Protozool.* **39**: 159-176
- Pienaar R. N. (1994) Ultrastructure and calcification of coccolithophores. In: Coccolithophores (Eds. A. Winter, W. G. Siesser). Cambridge Univ. Press, Cambridge, 13-37
- Plattner H. (2002) My favorite cell - *Paramecium*. *BioEssays* **24**: 649-658
- Plattner H., Hentschel J. (2002) Zellbiologie, 2nd ed. Thieme, Stuttgart, New York
- Ricci N., Verni F., Rosati G. (1985) The cyst of *Oxytricha bifaria* (Ciliata: Hypotrichida). I. Morphology and significance. *Trans. Am. microsc. Soc.* **104**: 70-78
- Romanovicz D. K. (1981) Scale formation in flagellates. *Cell Biol. Monogr.* **8**: 27-62
- Rosenberg L. E. (1938) Cyst stages of *Opisthonecta henneguyi*. *Trans. Am. microsc. Soc.* **57**: 147-152
- Sachs L. (1984) Angewandte Statistik. Springer, Berlin, Heidelberg, New York
- Walker G. K., Mangel T. K., Goode D. (1980) Encystment and excystment in hypotrich ciliates I. *Gastrostyla steinii*. *Protistologica* **16**: 511-524
- Walker G. K., Edwards C. A., Suchard S. J. (1989) Encystment in the peritrich ciliate *Telotrochidium henneguyi*. *Cytobios* **59**: 7-18
- Wirnsberger-Aeschl E., Foissner W., Foissner I. (1990) Natural and cultured variability of *Engelmanniella mobilis* (Ciliophora, Hypotrichida); with notes on the ultrastructure of its resting cyst. *Arch. Protistenk.* **138**: 29-49
- Xu K., Foissner W. (2005) Morphology, ontogenesis and encystment of a soil ciliate (Ciliophora, Haptorida), *Arcuospathidium cultriforme* (Penard, 1922), with models for the formation of the oral bulge, the ciliary patterns, and the evolution of the spathidiids. *Protistology* **4**: 5-55

Received on 12th April, 2006; revised version on 29th June, 2006; accepted on 23rd August, 2006

The Unusual, Lepidosome-coated Resting Cyst of *Meseres corlissi* (Ciliophora: Oligotrichea): Genesis of Four Complex Types of Wall Precursors and Assemblage of the Cyst Wall

Wilhelm FOISSNER and Maria PICHLER

Universität Salzburg, FB Organismische Biologie, Salzburg, Austria

Summary. We studied the genesis of the cyst wall precursors and the assemblage of the cyst wall in *Meseres corlissi* Petz and Foissner (1992), an oligotrichous ciliate closely related to the common *Halteria grandinella*, using transmission electron microscopy. *Meseres corlissi* has five types of cyst wall precursors, of which type (A), the lepidosomes of the pericyst, has been described by Foissner *et al.* (2006). Each precursor type has a complex genesis showing six to nine distinct stages described in detail. Types (A) and (C) develop from Golgi vesicles, while the origin of types (B), (D) and (E) remains obscure. None of the precursors is similar to those reported from other ciliates, suggesting the oligotrichs as a very distinct group of ciliates. Except of precursor (E), they develop and release their contents almost concomitantly by exocytosis, whereby the precursor membrane closes the exocytotic openings and the contents lose the property to be stained with the usual dyes. Thus, the assemblage of the cyst wall, which suddenly "condenses" out of the mass formed by the extruded contents of the wall precursors, could be followed only during the last stages when the precursor materials became stainable again. There is cortex reorganization and intense perilemma endocytosis before the cyst wall assembles, events not described in any other study. Thus, the perilemma is a real structure whose function, however, remains obscure. Based on the present and literature data, a high morphological diversity of cyst wall precursors and wall assemblage emerges. If this variety is added to that of overall cyst morphology (e.g., wall ornamentation), cyst wall composition (e.g., with or without chitin) and cell restructuring (e.g., the infraciliature may be maintained or resorbed), an overwhelming diversity emerges which should contain considerable phylogenetic and ecological information; unfortunately, the message is only partially understood, likely because detailed data are available from less than 40 species.

Key words: cortex reorganization, diversity, exocytosis, oligotrichine ciliates, perilemma endocytosis, phylogeny, review.

INTRODUCTION

Resting cysts are a special mode of protists to overcome detrimental periods of life. Thus, their morphology, physiology, and ecology are of wide interest and have been reviewed under several aspects (Corliss

and Esser 1974, Foissner 1993, Chessa *et al.* 1994, Gutiérrez and Martín-González 2002, Gutiérrez *et al.* 2003).

Attempts to use the morphological diversity of resting cysts for classifying higher systematic categories of ciliates are still at variance (Foissner 2005), while their value in distinguishing morphologically very similar species is increasingly acknowledged (Foissner 1993, Foissner *et al.* 2002, Xu and Foissner 2005). Our unpublished data even suggest that applying this feature more commonly will double the number of free-living ciliate species! For

Address for correspondence: Wilhelm Foissner, Universität Salzburg, FB Organismische Biologie, Hellbrunnerstrasse 34, A-5020 Salzburg, Austria; E-mail: Wilhelm.Foissner@sbg.ac.at

instance, four very similar populations of *Epispathidium amphoriforme*, a common moss and soil ciliate, have different resting cysts, suggesting classification as different species.

The morphological literature on resting cysts is comparatively rich for colpodid and stichotrichine ciliates (for reviews, see Foissner 1993, Berger 1999, Gutiérrez *et al.* 2003), while scant for oligotrichs, such as *Tintinnidium*, *Halteria* and *Meseres*. None the less, the few data available indicate a great diversity: the cysts may be globular (Foissner *et al.* 2005) or flask-shaped (Reid and John 1978, 1983; Jonsson 1994; Kim and Taniguchi 1995; Müller 1996, 2002); the cysts may have (Fauré-Fremiet 1948; Reid and John 1978, 1983; Kim and Taniguchi 1995; Müller 1996, 2002; Montagnes *et al.* 2002) or lack (Foissner *et al.* 2005) an escape opening; the cysts may have (Foissner *et al.* 2005) or lack (Fauré-Fremiet 1948, Reid and John 1978, Jonsson 1994) lepidosomes, that is, the cyst wall is smooth or covered with globular or spiny scales; the cyst wall may have (Reid 1987) or lack (Foissner 2005) a crystalline, calcium-rich layer; the cyst wall may have (Foissner *et al.* 2005) or lack (Foissner, unpubl. data on *Halteria*) a chitinous layer; and the endocyst may strongly swell (Foissner *et al.* 2005) or not swell (Fauré-Fremiet 1948, Jonsson 1994) during encystment.

We used *Meseres corlissi*, a close relative of the common *Halteria grandinella* (Katz *et al.* 2005), as a model to investigate encystment and cysts of oligotrich ciliates (Foissner 2005; Foissner *et al.* 2005, 2006; Müller *et al.* 2006). These investigations showed that the resting cyst of *M. corlissi* is unusual in having a chitinous layer in the wall and a pericyst with conspicuous, up to 15 µm large scales, now called lepidosomes (Foissner 2005, Foissner *et al.* 2005). The lepidosomes have a complex genesis in Golgi vesicles and are released by exocytosis (Foissner *et al.* 2006). The present study shows two further peculiarities: there are five types of complex cyst wall precursors, while other ciliates have four or less types with comparatively simple morphology and genesis; and there is cortex reorganization and intense perilemma endocytosis before the cyst wall condenses, events not described in any other study.

All these investigations were extraordinarily difficult and time-consuming because oligotrichs are notoriously difficult to prepare for transmission electron microscopy and five types of cyst wall precursors, each with six to nine distinct developmental stages in at least two orientations (longitudinal and transverse), had to be sorted.

This required investigating 25 different fixatives; sectioning of nearly 100 vegetative, precystic and cystic specimens; and analyzing more than 3000 micrographs.

MATERIALS, METHODS AND TERMINOLOGY

Material and cultivation. The population studied was isolated from meadow soil of Upper Austria, i.e., from the surroundings of the town of Kefermarkt, using the non-flooded Petri dish method (Foissner *et al.* 2002).

A culture of *M. corlissi* was established with about 20 cells on Eau de Volvic (French table water) enriched with some squashed wheat grains and *Cryptomonas lucens* (UK Culture Collection of Algae and Protozoa, CCAP, Windermere) as food sources. Cultivation occurred at room temperature and day light. The first, a clonal culture was used for all investigations because preservation of the fine structure distinctly decreases after even short periods of cultivation.

Induction of encystment. The various encystment stages were obtained by transferring about 2000 specimens from the exponentially growing culture with about 10% dividers into a Petri dish 5 cm across, together with 7 ml culture medium and the food contained therein. This isolated part of the culture was then controlled hourly with a dissecting microscope. Encysted specimens were recognized already after 5 hours, but epidemic encystment occurred after 20 hours when food was visibly reduced.

Morphological and cytological methods. For electron microscopy, the encysting culture mentioned above was fixed and embedded in toto as described in Foissner (2005). Briefly, cells were fixed in a mixture of 10 ml glutaraldehyde (25 %) + 6 ml aqueous osmium tetroxide (2 %) + 10 ml saturated aqueous mercuric chloride for 1 h and embedded in Epon 812 via a graded ethanol series and propylene oxide.

Six distinct stages can be distinguished during encystment (Foissner *et al.* 2006). Unfortunately, trials to trigger and synchronize the process failed. Thus, the appropriate stages were selected from the encysting, fixed and embedded culture described above, using a bright field microscope and a magnification of up to 250×.

Morphometry. As in our previous studies (Foissner 2005, Foissner *et al.* 2006), we provide basic morphometrics and statistics for the structures described. This is uncommon in cyst research and was criticized by some reviewers. However, we defend such data because they are much better, in spite of all the shortcomings they have, than the vague "about" so frequently seen in cyst literature. Furthermore, in the present study such data were indispensable for distinguishing the many developmental stages of the five cyst wall precursor types. For a more detailed discussion, see Foissner *et al.* (2006).

Terminology. General ciliate terminology follows Corliss (1979); cytological terminology is according to Plattner and Hentschel (2002) and Becker *et al.* (2006); and cyst terminology follows Gutiérrez *et al.* (2003), Foissner (2005), and Foissner *et al.* (2005). The various cyst wall precursors are termed « A, B, C, D, E » because we could not assign them to certain cyst layers, except of the (A) precursor which is the lepidosome and whose genesis has been described by Foissner *et al.* (2006).

RESULTS

Organization of description and morphometry (Fig. 1)

The vegetative species and its mature resting cyst have been described by Petz and Foissner (1992), Foissner (2005), and Foissner *et al.* (2005). The genesis and release of cyst wall precursor (A), that is, the lepidosomes, has been studied by Foissner *et al.* (2006).

Although precursor genesis is a continuous process, we distinguished several stages within each precursor type to emphasize the changes occurring and to make the description more clear. Further, the stages roughly correlate with the six encystment stages (Fig. 1) and may help to define the processes properly in more detailed research. Classifying a continuous process into

several stages is not uncommon. For instance, larval development is classified in over 40 stages in tadpoles.

The variability coefficients of mature structures of ciliates, for instance, body size and the number of ciliary rows, are usually between 5-15 % (Foissner 1984, 1993). In the present study, many variability coefficients are between 15 % and 30 %. Likely, this has several reasons: (i) the "stages" measured belong to a continuous process; (ii) some distinct stages may have been lumped; (iii) the maximum dimension of the structures may have been missed, though we measured only such precursors where crisp membrane profiles were recognizable, indicating that we were in or near to the centre.

The data compiled in Tables 1 and 2 and in Foissner *et al.* (2006) show that the five precursor types can be distinguished by their size, except of types (B) and (D): (A) 5842×4904 nm, (B) 1881×1363 nm, (C) $1734 \times$

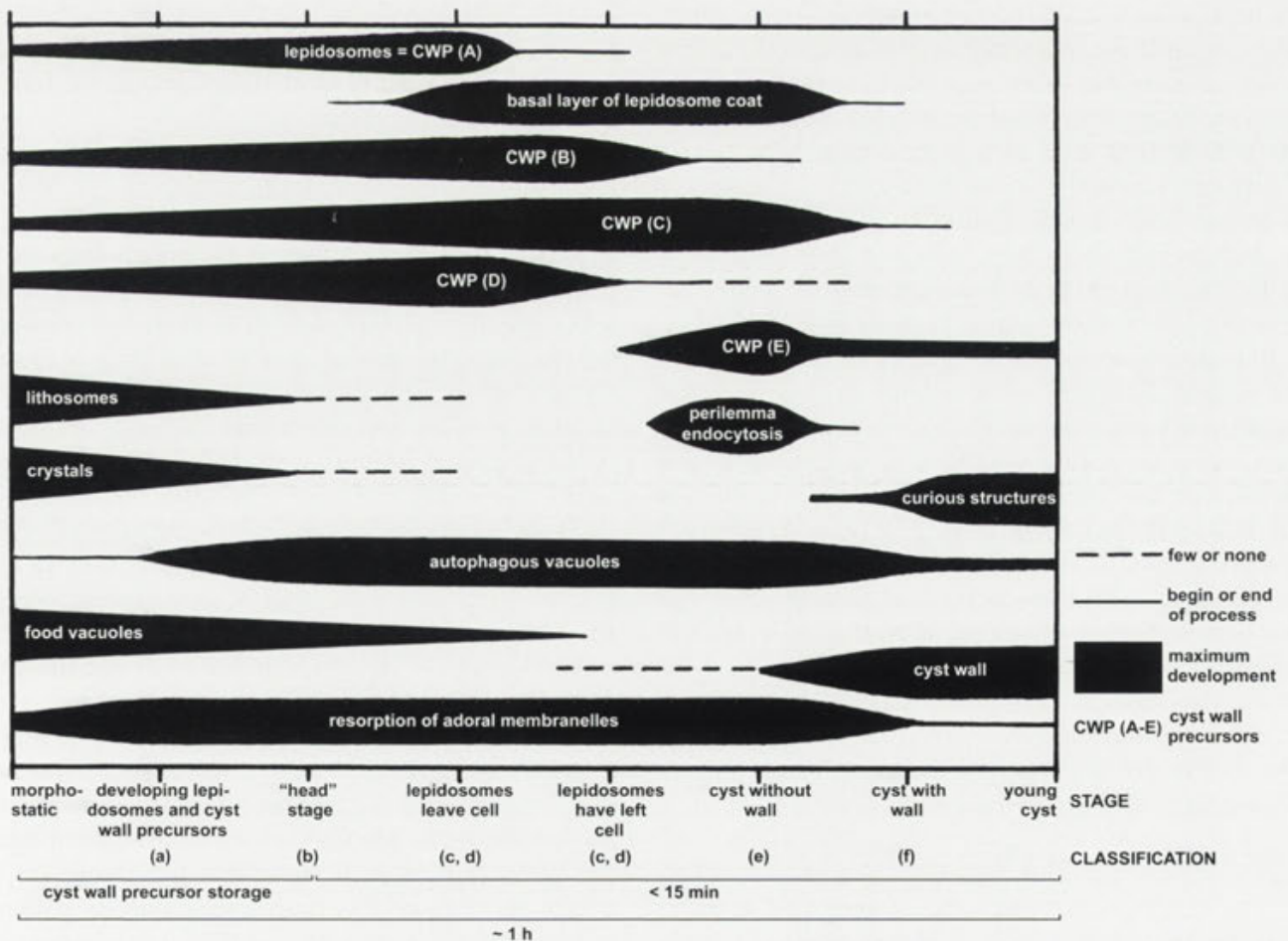


Fig. 1. *Meseres corlissi*, semiquantitative view of changes occurring during encystment. Note that the genesis of the lepidosomes has been described by Foissner *et al.* (2006); other structures not contained in the present study will be described in a forthcoming paper. Classification of encystment stages (a-f) is according to Foissner *et al.* (2006). See text for details.

257 nm, (D) 1855 × 1571 nm, (E) 443 × 293 nm. These data match those obtained from protargol-impregnated specimens, where all precursors can be seen (Figs 2, 3), except of precursor (E).

When encystment commences and the cyst wall precursors develop, the distinctness of the endoplasmic reticulum and the Golgi stacks strongly increases, as compared to morphostatic cells (Figs 32-34, 36, 39). The ordinary appearance is regained after the "head stage" (Foissner *et al.* 2006), that is, just before the lepidosomes are released.

Time course and relationship of processes (Fig. 1)

Encystment causes a complete transformation of the vegetative cell. Based on our previous investigations (Foissner 2005; Foissner *et al.* 2005, 2006), the present results, and some data from a forthcoming paper (Foissner and Pichler, in preparation), we are able to provide a scheme on the sequence and relationship of various main events occurring during encystment (Fig. 1). The time scale refers to the shortest period the processes can run. This was observed in specimens from the Dominican Republic, which were cultivated at 20-25°C (Weisse 2004). When transferred to 5°C, most specimens formed a mature resting cyst within 1 h (Foissner *et al.* 2005), while the cysts used for the present investigations were obtained after about 20 h from specimens kept at room temperature under decreasing food concentration (Foissner *et al.* 2006).

Protargol preparations show that cyst wall precursors are generated throughout the cell, but are most abundant in the broad anterior third (Figs 2, 3). As concerns the cyst wall precursors, types (A) to (D) are produced and released almost concomitantly, while precursor (E) is produced and released distinctly later (Fig. 1). Timing of precursors (A) to (D) is hampered not only by their almost concomitant production but also by cyst wall precursor storage, a remarkable phenomenon which will be described in a separate paper. Briefly, about one third of the specimens from exponentially growing cultures contain various developmental stages of precursor types (A) to (D); 10 % even contain few to many fully or almost fully differentiated precursors (Figs 2, 3).

Cyst wall precursor (B)

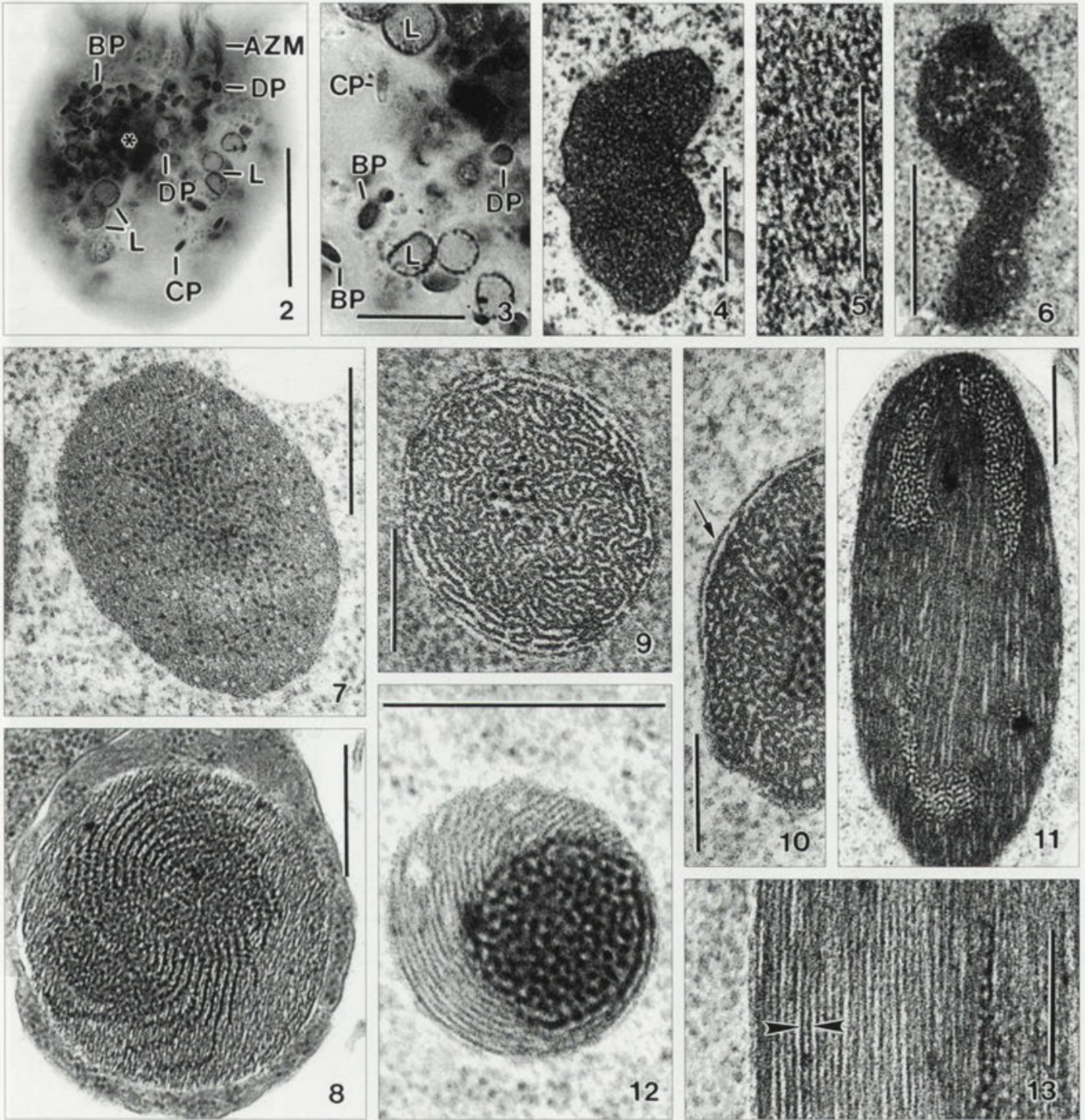
The cyst wall precursor (B) is generated together with precursors (A), (C) and (D), and released slightly later or almost concomitantly with precursor (A), that is, the lepidosomes. Precursor (B) is the largest precursor type, except of the lepidosomes, and is well recognizable

with the light microscope in protargol-impregnated specimens (Figs 2, 3). Beginning with stage (3), cyst wall precursor (B) is composed of a membranous matrix and fibrogranular material forming various patterns during the precursor's development. The about 12 nm thick sheets of the matrix are three-layered, that is, are composed of two osmiophilic outer layers and a bright inner layer each about 4 nm thick (Fig. 13). This composition is likely because three-layered sheets are distinct also in stage 8 (Figs 30, 31) and in some stages of the (C) precursor (Figs 35, 38, 40-42, 54).

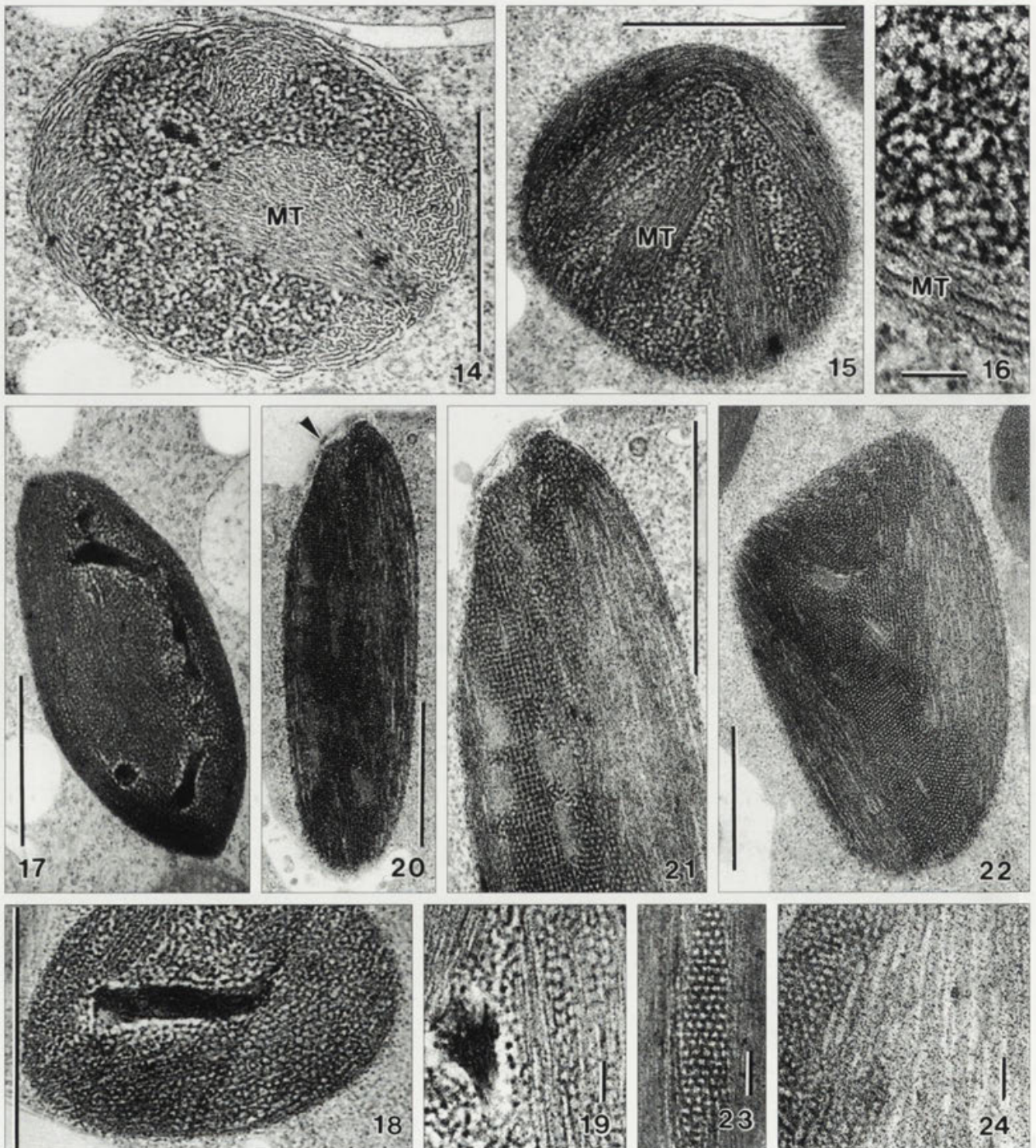
Stage (1): the earliest stages identified are roughly reniform, membrane-bound, dark vesicles with a rather irregular outline and an average size of 902 × 343 nm (Figs 4-6; Table 1). The vesicles are filled with amorphous or finely granular material; however, the best preparations reveal very narrowly meshed fibrous structures with a diameter of ≤ 2 nm (Figs 4, 5). In the central thirds of the vesicles are minute (~ 20 nm), bright areas in 60 out of 90 precursors investigated (Fig. 6). Possibly, these areas, which have a diffuse margin and provide the precursor with a white-spotted appearance, are formed by loosening of the matrix.

Stage (2): the precursors become broadly ellipsoidal because the width increases to an average of 669 nm (Table 1). The matrix is as in stage (1), that is, white-spotted, but now contains arrays of dark granules with a diameter of about 13 nm (Figs 7, 8). The granules, which are usually more densely spaced in the central portion of the precursor, frequently form lamellar patterns; rarely do they appear randomly distributed. It seems possible that the granular arrays are part of long, irregularly coiled sheets or strands with granules arranged like pearls on a string.

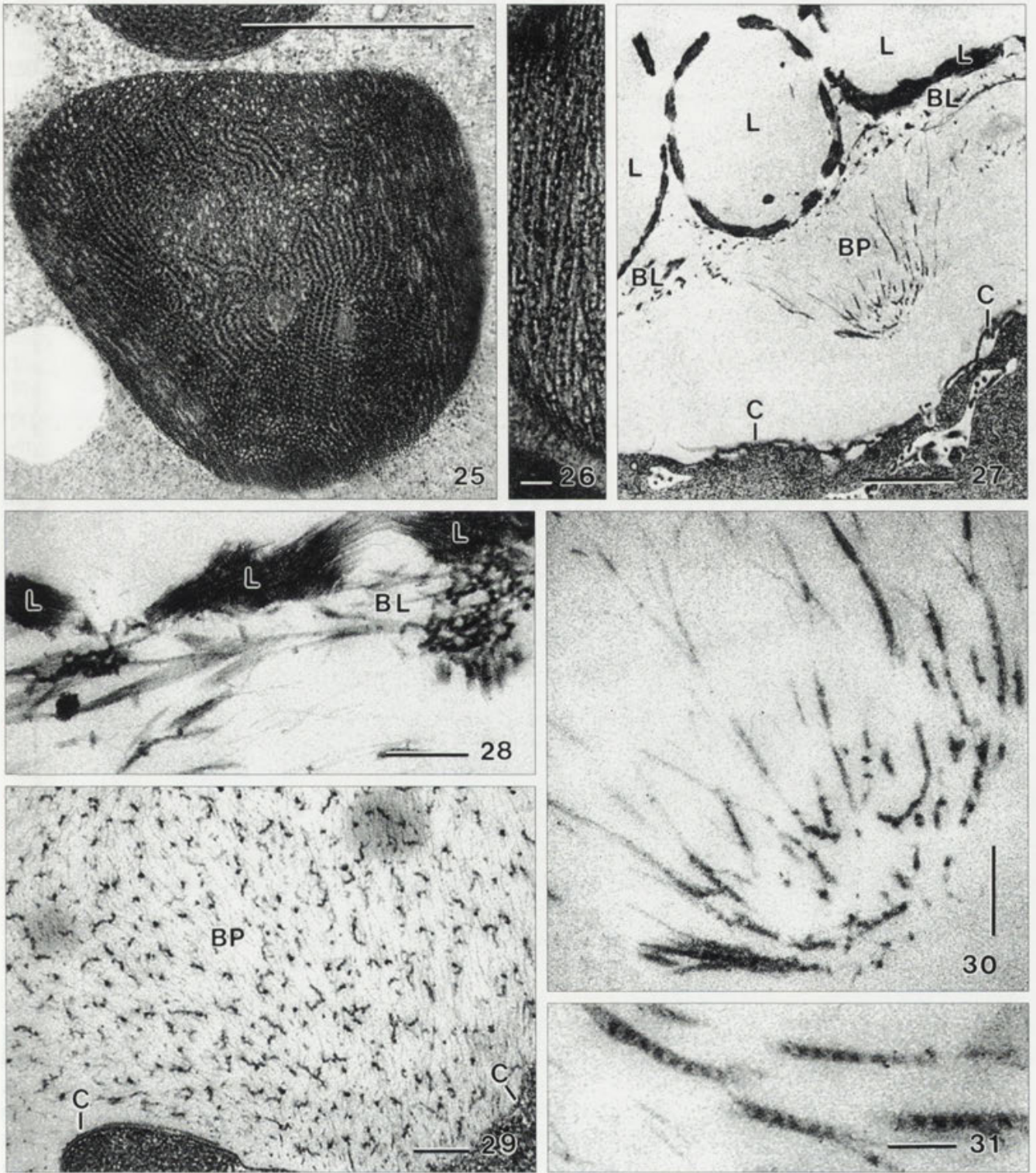
Stage (3): the precursors are now conspicuous, ellipsoidal to elongate ellipsoidal (2:1 - 6:1) structures of light microscopical dimension, that is, they have an average size of 2656 × 735 nm and rounded or bluntly pointed ends (Figs 9-12). Many transitions show that the great width variability (CV 45 %, Table 1) is natural, that is, not caused by lumping of two or more developmental stages. Longitudinal sections of well-preserved precursors now reveal the matrix as an array of bilamellate, membrane-like structures, as described above and shown in figure 13. Transverse sections show that the sheets are arranged in more or less pronounced sinuous patterns, making stage (3) highly distinct (Figs 9, 10); rarely, and mainly near to the ends of the precursor, the lamellae are helicoidally arranged (Fig. 12). The granular arrays described in stage (2) developed to a lobate, fibrogranular



Figs 2-13. *Meseres corlissi*, cyst wall precursors of morphostatic specimens in the light microscope (2, 3) and transmission electron micrographs of stages (1-3) of the genesis of cyst wall precursor (B) in encysting cells (4-13). **2, 3** - about 10 % of specimens from exponentially growing cultures contain developing lepidosomes (L) and cyst wall precursors (BP, CP, DP), which impregnate with protargol. The asterisk marks an accumulation of these structures; **4-6** - stage (1) cyst wall precursors (B) are reniform and have an average size of 902×343 nm. The osmiophilic, fibrogranular (4, 5) matrix often contains minute bright areas providing the precursor with a spotted appearance (6); **7, 8** - stage (2) precursors are broadly ellipsoidal and have an average size of 900×669 nm. Conspicuous granular arrays develop in the white-spotted matrix; **9-13** - stage (3) precursors are oblong (11) and have an average size of 2656×735 nm. The matrix now appears as an array of bilamellate, membrane-like structures (13, arrowheads) containing darkly stained, lobate areas of reticular, fibrogranular material (Figs 10-12). Transverse sections show that the lamellae form a sinuous or helical pattern (9, 10, 12). The arrow in figure 10 marks the membrane surrounding the precursor. AZM - adoral zone of membranelles, BP, CP, DP - cyst wall precursors, L - lepidosomes. Scale bars: 10 μ m (3); 30 μ m (2); 200 nm (5, 9, 10, 13); 400 nm (4, 6, 7, 8, 11, 12).



Figs 14-24. *Meseres corlissi*, transmission electron micrographs of stages (4-6) of the genesis of cyst wall precursor (B). **14-16** - stage (4) precursors are ellipsoidal and have an average size of 2450×1239 nm. In this stage, the lamellar matrix (MT) and the fibrogranular reticulum become strongly intertwined. Figure 14 shows a transition to stage (3), that is, the sinuous pattern of the matrix lamellae is still recognizable; **17-19** - stage (5) precursors are broadly ellipsoidal with an average size of 2343×1399 nm. Globular to oblong, compact inclusions appear in the fibrogranular reticulum and a honeycombed structure develops in the lamellar matrix; **20-24** - stage (6) precursors are ellipsoidal and have an average size of 2753×1080 nm. They are almost mature and thus typically found near or attached to the ciliate's cortex (20, arrowhead). Both, the fibrogranular reticulum and the compact inclusions recognizable in the previous stages have disappeared, while a highly characteristic, honeycombed structure developed throughout the precursor. MT - lamellar matrix. Scale bars: 1000 nm (14, 15, 17, 18, 20-22); 100 nm (16, 19, 23, 24).



Figs 25-31. *Meseres corlissi*, transmission electron micrographs of stages (7) and (8) of the genesis of cyst wall precursor (B). **25, 26** - mature (B) precursors have an average size of 1881×1363 nm, that is, are ellipsoidal to irregularly globular and composed of conspicuous granule strings sandwiched in two membranous sheets (Figs 26, 31); **27-31** - stage (8) comprises leaving and released precursors. As soon as the precursor is outside of the cell, it swells to a loose mass composed of countless fibres and wrinkled pieces (29) of the granule strings (30, 31). Likely, they form, after some transformation, the basal layer of the lepidosome coat (28). BL - basal layer, BP - cyst wall precursor (B), C - ciliate cortex, L - lepidosome and lepidosome wall. Scale bars: 100 nm (26, 30); 200 nm (28, 29, 31); 1000 nm (25, 27).

Table 1. Morphometric data on cyst wall precursors (B) and (C). Measurements in nm. CV - coefficient of variation in %, I - number of cysts investigated, M - median, Max - maximum, Min - minimum, n - number of precursors measured, SD- standard deviation, \bar{X} - arithmetic mean.

Characteristics	\bar{X}	M	SD	CV	Min	Max	n	I	
Precursor(B)									
Stage 1	length	902	900	173	19.2	600	1250	28	6
	width	343	300	96	28.0	250	600	28	6
Stage 2	length	900	850	183	20.3	700	1300	16	6
	width	669	600	178	26.6	400	1000	16	6
Stage 3	length	2656	2500	515	19.4	1800	3500	9	7
	width	735	600	332	45.1	300	1400	17	9
Stage 4	length	2450	2500	391	15.9	1800	3000	7	3
	width	1239	1200	184	14.9	950	1600	13	5
Stage 5	length	2343	2500	310	13.2	1700	2600	7	4
	width	1399	1300	306	21.9	1000	2100	14	8
Stage 6	length	2753	2900	650	23.6	1500	3800	15	3
	width	1080	1000	350	32.5	600	1750	15	3
Stage 7	length	1881	1787	531	28.2	1107	3000	10	4
	width	1363	1314	480	35.2	786	2000	10	4
Precursor(C)									
Stage 1	length	164	150	45	27.6	89	25	21	3
	width	85	75	27	32.0	49	147	21	3
Stage 2	length	399	384	104	26.2	267	600	10	2
	width	60	60	13	21.1	40	83	10	2
Stage 3	length	236	236	56	23.7	175	325	8	4
	width	177	170	37	20.9	133	232	8	4
Stage 4	length	274	282	50	18.3	211	320	4	2
	width	251	253	48	19.3	189	307	4	2
Stage 5	length	744	737	144	19.4	445	1000	18	4
	width	655	657	129	19.7	400	911	18	4
	length of dense strand	404	280	368	91.2	53	1429	28	4
	width of dense strand	149	138	58	38.9	55	267	26	4
	width of bright area	66	67	27	40.4	9	150	26	4
Stage 6	length	1576	1575	439	27.8	1000	2222	8	4
	width	404	415	112	27.8	240	573	8	4
Stage 7	length	1734	1689	202	11.7	1556	2000	4	3
	width	257	259	65	25.4	171	400	16	3
	length of dense plug	185	198	85	45.7	83	314	8	3
	width of dense plug	87	77	28	31.5	67	143	8	3
Stage 8	length	2338	2321	522	22.3	1450	3684	19	3
	width	275	267	61	22.1	200	421	19	3

reticulum extending in the anterior and posterior third of the precursor; rarely, the mass forms a rod-shaped array extending whole precursor length (Figs 10-12).

Stage (4): the precursors are now thicker than in stage (3) and have an average size of 2450×1239 nm (Table 1); likely, some are slightly flattened. In this stage, the lamellar matrix and the fibrogranular reticulum become intertwined, producing highly characteristic, irregular patterns; however, the lamellae still show a tendency to arrange longitudinally and peripherally (Figs 14, 15). Figure 14 shows a transition between stages (3) and (4), that is, the matrix lamellae are still sinuously arranged while the fibrogranular reticulum

forms a polygonal network with lobes distributed throughout the precursor (Figs 14-16).

Stage (5): the precursors are now broadly ellipsoidal and have a similar size as in stages (3) and (4), viz., 2343×1399 nm on average (Table 1). The overall fine structure is also as in stage (4), that is, the lamellar matrix and the fibrogranular reticulum are strongly intertwined, forming manifold patterns (Figs 17-19); the fibrogranular reticulum appears even more lobate than in stage (4), now extending between the individual lamellae of the matrix (Fig. 19). Stage (5) is characterized by the appearance of 1-7 (\bar{x} 2.8, $n = 27$) scattered, globular to oblong, dark inclusion in the fibrogranular reticulum

(Figs 17-19). These inclusions, which sometimes form long, lobate structures (Fig. 17), have an average size of 250×160 nm (n27) and possibly develop by uptake of electron-dense material in the meshes of the fibrogranular reticulum (Figs 17-19).

Stage (6): this stage appears when the lepidosomes are released or just left the ciliate (Foissner *et al.* 2006). The precursors now have an average size of 2753×1080 nm, and more than 90 % of them are near to or attached to the ciliate's cortex (Fig. 20, Table 1). The shape is highly variable: simple, short rods (Fig. 20) are side by side with oblong, polygonal precursors likely ready to be released (Fig. 22). The fine structure changed dramatically, that is, the fibrogranular reticulum (Figs 14-16) and the compact inclusions (Figs 17-19) recognizable in the previous stages have disappeared, while a highly characteristic, honeycombed structure with a mesh size of about 25 nm developed throughout the precursor and probably within the lamellar matrix (Figs 20-24). The (B)precursor now highly resembles "paracrystalline" ciliate mucocysts (Hausmann 1978).

Stage (7): usually, stage (7) is found in cells just having released the lepidosomes (Fig. 1). When the (B) precursor leaves the cell, it becomes globular to polygonal obtaining an average size of 1881×1363 nm (Table 1). Thus, the precursor is now shorter but thicker than in stages (5) and (6). The fine structure also changes considerably (Figs 25, 26). The honeycombed pattern arranges to highly characteristic strings composed of equidistantly spaced, about 12 nm-sized granules sandwiched between two membranous sheets each about 3 nm thick (Figs 25, 26); likely, the sheets represent the osmiophilic part of the matrix lamellae described in stage (3). This arrangement is well recognizable also in dissolving precursors (Fig. 30). The granule strings are embedded in fibrogranular, white-spotted material highly similar to that found in stage (2).

Stage (8): this stage comprises leaving and released precursors, which were found in four specimens having released the lepidosomes, suggesting that the (B) precursors are released slightly later than the (A) precursors (=lepidosomes). When leaving the cell, the vesicle's contents become loose and hyaline. As soon as it is outside, it swells to a globular mass up to 5 μ m across (Figs 27, 29). This mass, which accumulates at the proximal portion of the lepidosome coat, is composed of countless filaments and wrinkled pieces of the granule strings described in stage (7). Likely, the filaments are parts of the membranous sheets sandwiching the granule strings (Figs 30, 31). Soon, the filamentous

reticulum and the granule strings lose their staining property. Thus, their fate could not be followed, but likely they form the basal layer of the lepidosome coat (Figs 27, 28). The membrane surrounding the precursor vesicle becomes part of the ciliate cortex, as does that of the other precursors (Figs 59, 78; Foissner *et al.* 2006).

Cyst wall precursor (C)

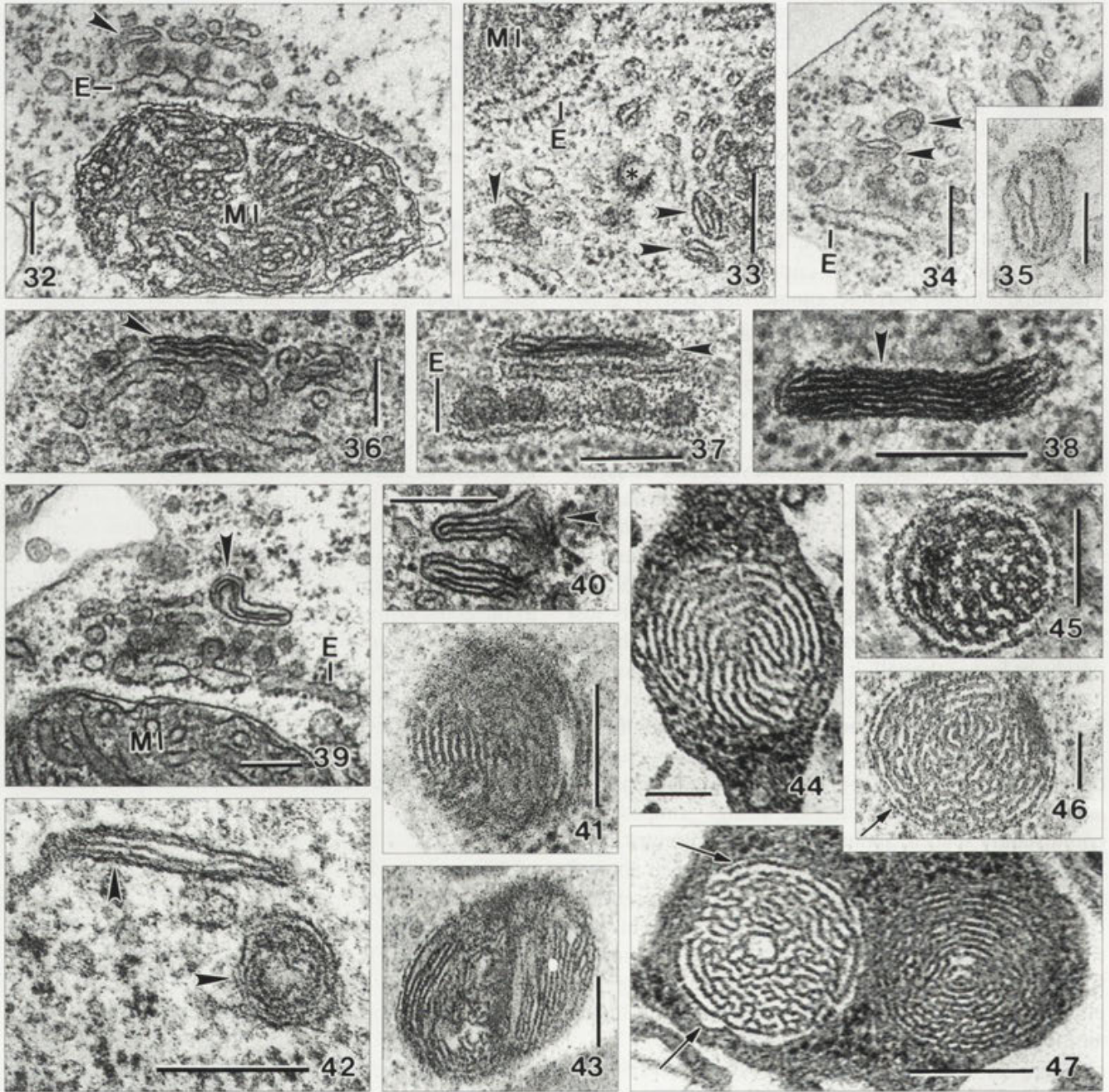
Cyst wall precursor (C) originates in vesicles of the Golgi apparatus, as does precursor (A). Its genesis is more complex and distinctive than that of the other precursors. Thus, the entire development process could be followed. In contrast, the structure is rather simple, i.e., the mature (C) precursor consists only of membranous sheets. Cyst wall precursor (C) is released slightly later than precursors (A), (B) and (D).

Stage (1): the first stage identifiable as developing (C) precursor is a broadly ellipsoidal vesicle at the distal side of the dictyosome (Fig. 32). These vesicles, which have an average size of 164×85 nm (Table 1), are made of a concentric array of two to three membranous lamellae, each about 6 nm thick and composed of two electron-dense sheets bordering an electron-lucent middle layer (Figs 32-35). Obviously, these vesicles were just produced by the dictyosome and migrated to the trans-Golgi network. No specific contents are recognizable between the lamellae (Fig. 35).

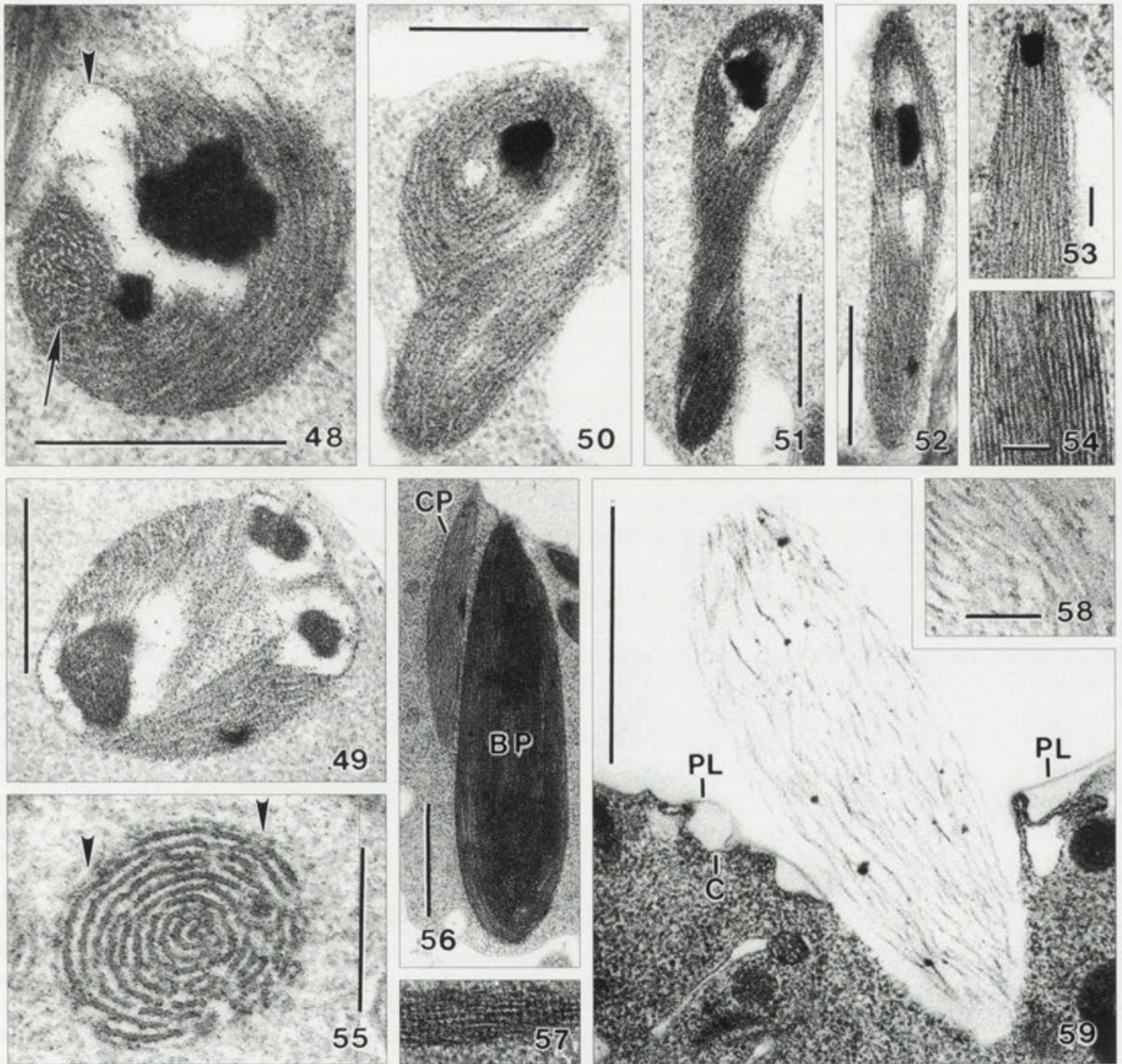
Stage (2): in stage (2), the globular vesicles of stage (1) grow to rod-shaped precursors with an average size of 399×60 nm (Figs 36-38, 42; Table 1). Like the stage (1) vesicles, they are at the distal side of the dictyosome and are composed of two to three concentric membranous lamellae. The space between the lamellae is clear.

Stage (3): the rod-shaped precursors of stage (2) roll up to broadly ellipsoidal, lamellar vesicles with an average size of 236×177 nm (Figs 39-43, Table 1). Likely, the involution occurs helically, as suggested by Fig. 43 and stage (6), where the vesicles unroll (Figs 48, 50). When reaching stage (4), the number of lamellae doubles and triples (Figs 41, 43).

Stage (4): the cyst wall precursors have grown to a size of 274×251 nm on average and became globular (Table 1). The membranous lamellae increased in number and form a conspicuous, sinuous pattern (Figs 44-47), highly similar to that found in stage (3) of the (B) precursor (Fig. 9). However, the stage (3) vesicles of the (B) precursor are much larger (2656×735 nm, Table 1) and usually contain a fibrogranular reticulum in the centre (Figs 9, 10, 12); further, we observed transi-



Figs 32-47. *Meseres corlissi*, transmission electron micrographs of stages (1-4) of the genesis of cyst wall precursor (C). **32-35** - the (C) precursor originates from vesicles of the trans-Golgi network on the distal side of the dictyosome (arrowheads). These vesicles have an average size of 164×85 nm and are composed of a concentric array of two to three membranous lamellae (Fig. 35). The active Golgi apparatus of *Meseres* is comparatively distinct and shows the classical structure, i.e., transition vesicles from the smooth surface of the endoplasmic reticulum form a Golgi stack composed of one to three cisterns. Note a coated transport vesicle (Fig. 33, asterisk); **36-38** - in stage (2), the ellipsoidal vesicles of stage (1) grow to rod-shaped precursors with an average size of 399×60 nm (arrowheads); **39-43** - during stage (3), the rod-shaped precursors of stage (2) roll up to broadly ellipsoidal, lamellar vesicles with an average size of 236×177 nm (Figs 39, 40, 42, arrowheads). Likely, the involution occurs helically (Fig. 43). Figure 42 shows a rod-shaped stage (2) precursor and a globular stage (3) precursor side by side (arrowheads). When reaching stage (4), the membranous lamellae double and treble (Figs 41, 43); **44-47** - stage (4) precursors have grown to an average size of 274×251 nm, that is, are globular. The membranous lamellae increased in number and form a sinuous pattern; note that the right precursor shown in figure (47) belongs to stage (8). Arrows mark the membrane surrounding the precursor. E - endoplasmic reticulum, MI - mitochondria. Scale bars: 100 nm (35); 200 nm (32-34, 36-46).



Figs 48-59. *Meseres corlissi*, transmission electron micrographs of stages (5-9) of the genesis and release of cyst wall precursor (C). **48, 49** - stage (5) cyst wall precursors (C) are globular and have an average size of 744×655 nm. The sinuous stage (4) matrix lamellae, remnants of which are recognizable in figure 48 (arrow), become helical and an electron-dense strand develops and appears in one to four pieces. Serial sections reveal the pieces as part of a peripheral helix performing one to two turns. Explanation of arrowhead in (48), see next figure; **50, 51** - stage (6) is characterized by the unfolding of the precursor. Unfolding commences with a blister (Fig. 48, arrowhead) and proceeds, via a retort-shaped transition stage (Fig. 50), to a rod-shaped vesicle with an average size of 1576×404 nm (Figs 51, 52, 56). The dense, peripheral helix present in stage (5) shortened to a small plug in the inflated anterior third of the precursor; **52, 53** - when approaching stage (7), the precursor has an average size of 1734×257 nm and is composed of a dense apical to subapical plug and 15-20 concentric, slightly helical lamellae; **54-56** - stage (8) precursors are mature and fusiform. They have an average size of 2338×275 nm and are thus three times thinner than the (B) precursors (Fig. 56). As concerns the fine structure, the fully developed (C) precursor is entirely composed of well preserved, concentric membranous sheets (lamellae) forming conspicuous arrays in transverse section (Figs 47, right specimen; 55, arrowheads mark the membrane surrounding the precursor); **57** - decomposing kinetodesmal fibres can be mixed up with late (C) precursors because they have a similar size and shape; **58, 59** (for an overview, see Fig. 107) - when released, the membranous sheets composing the (C) precursor lose their contour and dissolve. Unfortunately, the dissolved material does not stain, and thus we could not localize the cyst wall layer produced by the (C) precursor. BP - (B) cyst wall precursor, C - ciliate cortex, CP - (C) cyst wall precursor, PL - perilemma of the ciliate cortex. Scale bars: 100 nm (53, 54, 58); 200 nm (55); 500 nm (48-52); 1000 nm (56, 59).

tions between stages (4) and (5), excluding the possibility that the stage (4) precursors are misidentified (B) precursors (Fig. 48).

Stage (5): the (C) cyst wall precursor now reaches light microscopical dimension, that is, has an average size of 744×655 nm (Table 1); likely, most are globular. The fine structure changes markedly, that is, the sinuous matrix lamellae become helical and an electron-dense strand develops (Figs 48, 49). Usually, the matrix lamellae are poorly preserved, as compared to former and later stages, indicating that the transition from the sinuous to the helical state is still in progress. The dense strand appears in form of one to four scattered pieces or as a conspicuous semicircle (Figs 48, 49). Serial sections reveal the pieces as part of a peripheral helix performing one to two turns. The strand, which consists of a very fine-grained, heavily osmiophilic substance, has an irregular outline and an average width of 150 nm. It is surrounded by an about 66 nm wide bright zone traversed by many fibrogranular filaments connecting strand and matrix (Figs 48, 49; Table 1). When the precursor commences unfolding (see next stage), an electron-lucent blister becomes recognizable (Fig. 48, arrowhead).

Stage (6): now a remarkable process commences, viz., the globular vesicle unfolds, showing the helical arrangement of the matrix lamellae proposed in stage (3). Unfolding commences with an electron-lucent blister (Fig. 48, arrowhead) and proceeds via a retort-shaped transition stage (Fig. 50) to a clavate vesicle with an average size of 1576×404 nm (Fig. 51, Table 1). The clavate precursor is helically wound about the main axis and has a dense, globular plug embedded in the inflated anterior portion. Usually, the matrix lamellae are poorly preserved, suggesting that their reconstruction is still in progress. Further, the lamellae are usually absent from the centre and from small, scattered areas throughout the precursor, likely representing the sites of the dense peripheral helix (see previous stage), which shortened to the plug described above.

Stage (7): the (C) precursor is almost mature and has a size of 1734×257 nm on average, that is, it is rod-shaped and frequently attached to the cortex of the ciliate at angles ranging from perpendicular to almost parallel to the cell's surface. The precursor is now composed of a dense apical to subapical plug with an average size of 185×87 nm (Table 1) and 15-20 concentric, slightly helically arranged matrix lamellae (Figs 52, 53).

Stage (8): the mature stage (8) precursors are fusiform and can be recognized in the light microscope because they have an average size of 2338×275 nm (Figs 2, 3). As compared to the (B) precursors, the (C) precursors have a similar length but are three times thinner (Fig. 56, Table 1). The dense plug and the surrounding bright area disappear (Fig. 56), the membranous lamellae arrange longitudinally (Figs 54, 56), and the interlamellar space becomes clear (Figs 54, 56), showing that the reconstruction of the lamellae has finished. Thus, the fully differentiated (C) precursor is entirely composed of well preserved, about 6 nm thick, concentric membranous sheets (lamellae) forming conspicuous arrays in transverse section (Figs 47, right specimen; 55). They are easily mixed up with decaying kinetodesmal fibres which, however, usually have a distinct transverse striation (Fig. 57).

Stage (9): the (C) precursor is released slightly later than the lepidosomes, leaving its contents in a 1-3 μ m thick zone between the globular, encysting cell and the lepidosome coat. The membrane sac surrounding the precursor becomes part of the cortex, while the contents swell to an oblong mass with a size of about 2300×800 nm, that is, the length remains similar to that of the attached state, while width doubles; attachment and release of the precursor occur in a wide variety of angles, as described in stage (7). The emerging contents soon become a spongy mass with fading contours (Figs 58, 59). When the mass touches the lepidosome coat, it dissolves and seemingly disappears, that is, loses the property to be stained with uranyl acetate, lead citrate, and bismuth, quite similar to the other precursors (Fig. 27). When precursor release is disturbed by the fixation shock, the emerging contents often become enclosed in a sheet of cortical perilemma; rarely, the precursor explodes within the cell, showing that the membranous lamellae become "unsharp", that is, lose their integrity because they commence to dissolve.

Cyst wall precursor (D)

The very early and early developmental stages of the (D) precursor were difficult to identify. Thus, we performed a retrospective analysis using stage (4) as a template. This and the specific vesicle membrane [see stage (1)] clarified the early stages, while the very early stages remained obscure.

Stage (6) of the (D) precursor is similar to stages (e) and (f) of the (A) precursor (=lepidosomes; Foissner *et al.* 2006): both have a thick, deeply stained peripheral

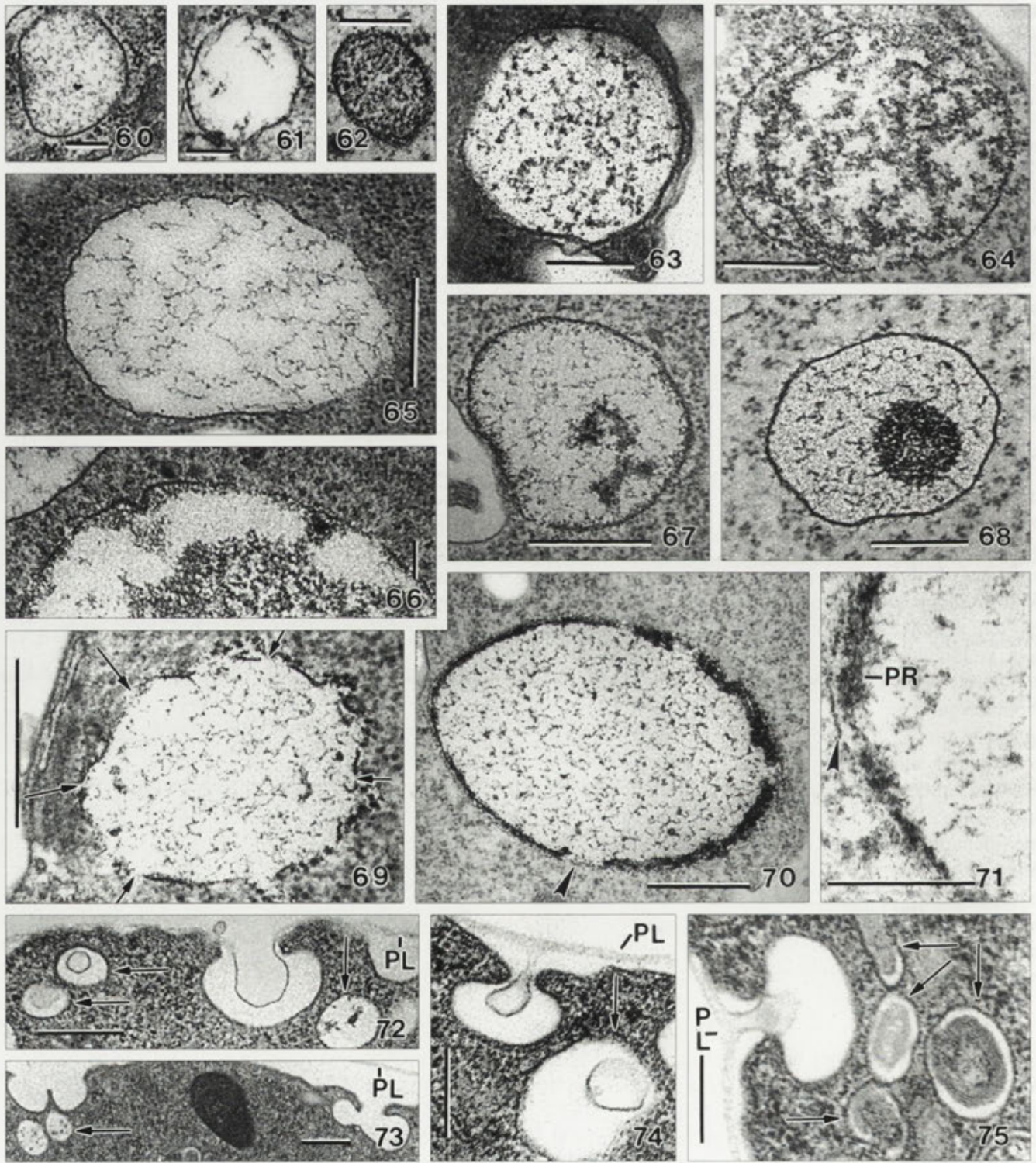
Table 2. Morphometric data on cyst wall precursors (D) and (E) of *Meseres corlissi*. Measurements in nm. CV - coefficient of variation in %, I - number of cysts investigated, M - median, Max - maximum, Min - minimum, n - number of precursors measured, SD- standard deviation, \bar{x} - arithmetic mean.

Characteristics	\bar{x}	M	SD	CV	Min	Max	n	I	
Precursor (D)									
Stage 1	length	323	296	153	47.3	147	524	8	6
	width	287	238	128	44.7	147	455	8	6
Stage 2	length	616	625	109	17.7	383	825	25	8
	width	505	548	113	22.4	308	700	25	8
Stage 3	length	1230	1161	389	31.7	683	2105	20	9
	width	960	889	306	31.9	483	1579	20	9
Stage 1-3	vesicle membrane, thickness	8	7	2	31.4	4	15	59	14
Stage 4	length	1022	1089	254	24.9	600	1325	15	5
	width	757	778	177	23.4	500	1000	15	5
Stage 6	length	1647	1705	266	16.2	1107	2036	20	5
	width	1426	1409	204	14.3	1107	1786	20	5
Stage 7	length	1503	1429	331	22.0	933	2321	21	5
	width	1299	1250	296	22.8	750	2000	21	5
Stage 8	length	1855	1875	224	12.1	1367	2286	23	7
	width	1571	1556	278	17.7	867	2071	23	7
	small net, length	125	120	45	36.0	75	275	16	6
	small net, width	85	85	16	19.0	50	111	16	6
	granules in net, ϕ	13	13	2	15.4	8	18	16	6
Stage 9	length within cell	1248	1179	203	16.2	1100	1533	4	2
	width within cell	813	748	196	24.1	667	1089	4	2
Stage 9	length outside cell	1989	1737	521	26.2	1400	2750	9	1
	width outside cell	1552	1458	381	24.6	1105	2105	9	1
Precursor (E)									
Stage 1	length	261	267	75	28.6	160	464	14	3
	width	202	200	61	30.1	133	357	14	3
Stage 2	length	585	598	89	15.2	420	700	8	2
	width	382	409	61	15.9	293	444	8	2
Stage 3	length	533	500	116	21.7	417	778	12	4
	width	210	223	41	19.4	133	275	12	4
Stage 4	total length	532	536	94	17.5	314	679	22	2
	total width	351	356	70	20.1	143	464	22	2
	core length	269	267	71	26.4	114	428	22	2
	core width	238	247	51	21.4	100	321	22	2
Stage 5	total length	443	440	63	14.1	371	556	9	4
	total width	293	283	60	20.4	200	400	9	4
	core length	337	333	85	25.2	229	467	9	4
	core width	190	171	49	26.1	133	286	9	4

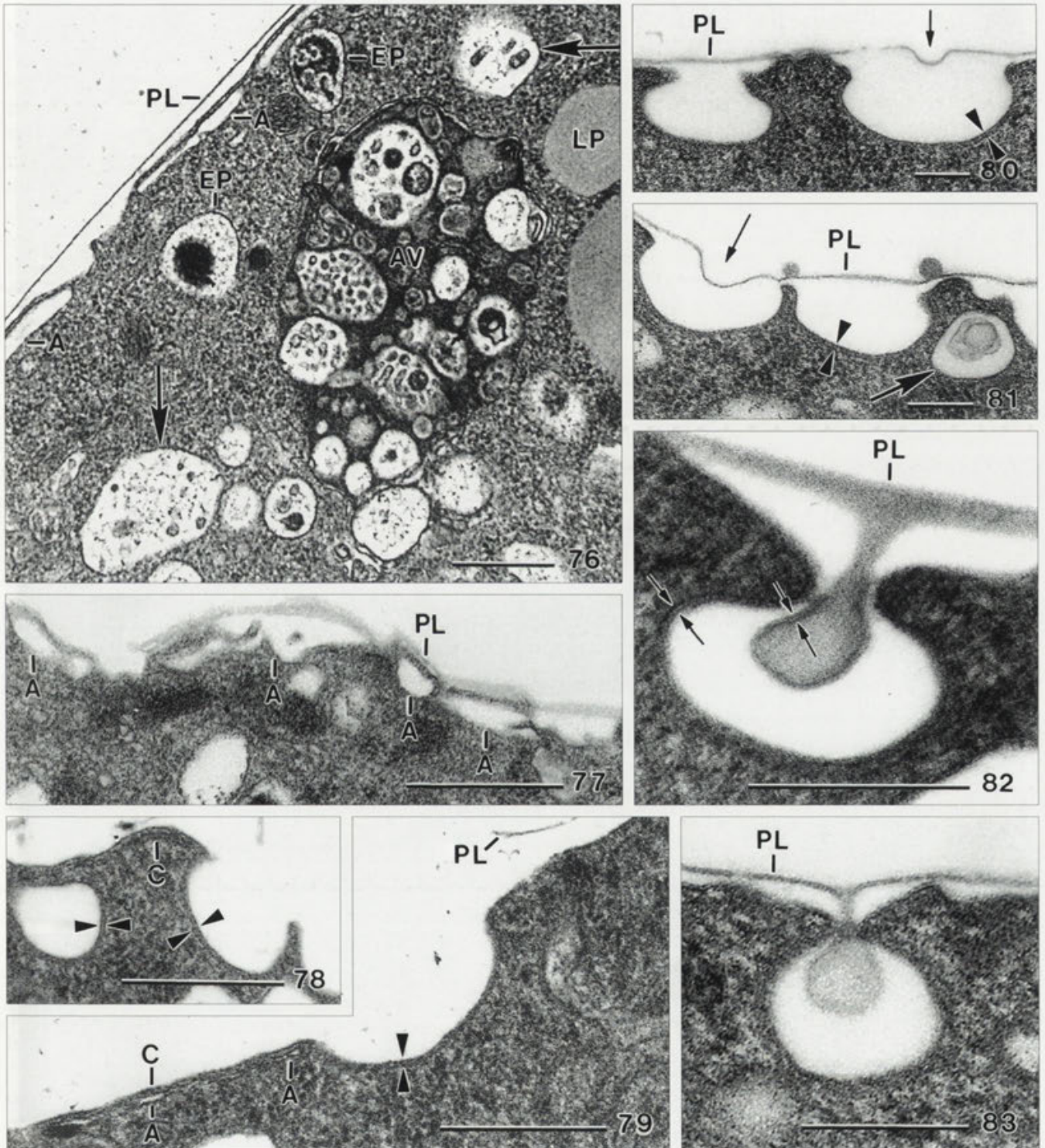
reticulum. However, they can be distinguished by three features. First, the lepidosomes have a thin, continuous base separating the wall meshes from the vesicle's contents. The (D) precursor lacks this base and thus the vesicle's contents are separated from the cytoplasm only by the membrane surrounding the vesicle (Figs 84, 85). Second, the peripheral reticulum of the (D) precursor develops on its surface (Figs 69-71, 84), while the reticulum of the lepidosome develops from the contents of the vesicle, that is, grows from the vesicle's centre to the periphery. Third, the fine structure of the peripheral

reticulum is different: very finely granular or filamentous in stage (e) and (f) lepidosomes, while distinctly reticular in the (D) precursor (Figs 84-86).

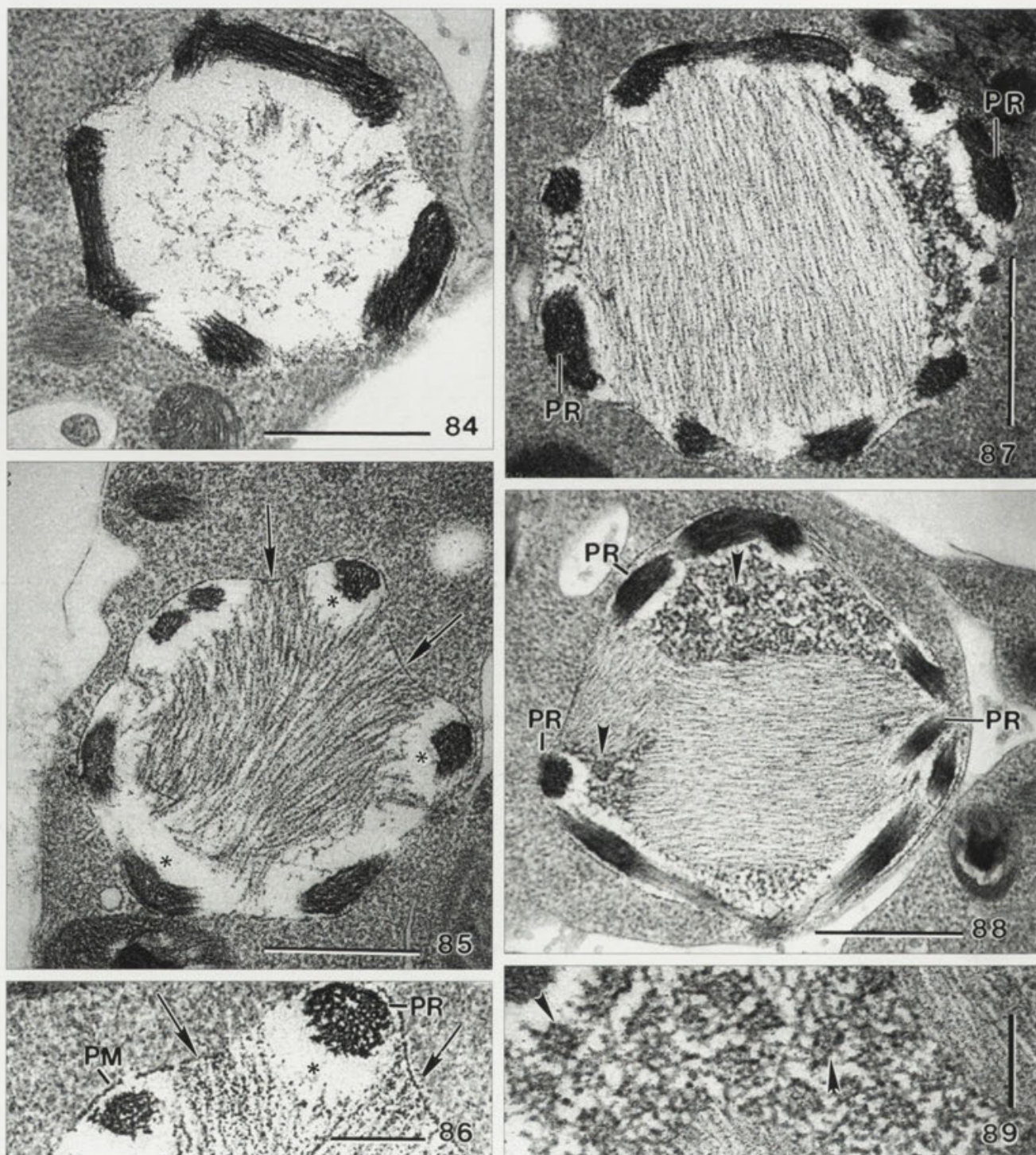
Stage (1): the earliest stage classified as developing (D) precursor are membrane-bound, slightly wrinkled vesicles with an average size of 323×287 nm (Table 2). The identification of the early development stages (1) to (3) is based not only on the retrospective analysis of stage (4), but mainly on the vesicle membrane which is more distinct (thicker) than in the corresponding stages of the other cyst wall precursors (Figs 60-68). Obviously,



Figs 60-75. *Meseres corlissi*, transmission electron micrographs of stages (1-5) of the genesis of the (D) cyst wall precursor (60-71) and of perilemma endocytosis (72-75). **60-68** - stage (1) to (3) vesicles differ mainly in size and have fibrogranular or alveolar contents. Note the characteristic, about 10 nm thick vesicle membrane; **69** - stage (4) precursors are unique in having bright areas in the vesicle membrane (arrows); **70, 71** - stage (5) shows that the osmiophilic membrane pieces recognizable in stage (4) become thicker, later forming the peripheral reticulum. Arrowheads mark the membrane surrounding the precursor. **72-75** - perilemma endocytosis during encystment stage (e; Fig. 1). Arrows mark internalized vesicles with decomposing perilemma. PL - perilemma, PR - growing peripheral reticulum. Scale bars: 200 nm (60-63, 66, 71, 74, 75); 400 nm (64, 65, 67-70, 72, 73).



Figs 76-83. *Meseres corlissi*, transmission electron micrographs of cortex reorganization (76, 77) and perilemma endocytosis (78-83). Opposed arrowheads mark the 12-22 nm thick coated membrane of endocytotic vesicles. Opposed arrows mark unit membranes of ordinary thickness (~ 6 nm). **76** - when cortical reorganization commences, the alveoli (A) become very distinct. Arrows mark large vesicles with decomposing perilemma. Note the large autophagous vacuole (AV); **77** - during reorganization, the cortex becomes heavily wrinkled and the alveoli increase in size; **78, 79** - forming endocytotic vesicles with coated wall (opposed arrowheads). The reorganized cortex has very small alveoli; **80-83** - perilemma endocytosis commences with a minute concavity (thin arrows) over the centre of the endocytotic vesicle (see also Figs 72-75). The thick arrow in (81) marks an internalized vesicle with perilemma. A - cortical alveoli, AV - autophagous vacuole, C - cortex, EP - (E) cyst wall precursor, LP - lipid droplet, PL - perilemma. Scale bars: 500 nm (76-79); 200 nm (80-83).



Figs 84-89. *Meseres corlissi*, transmission electron micrographs of stages (6) to (8) of the genesis of cyst wall precursor (D). **84** - stage (6) precursor vesicles have an average size of 1647×1426 nm and are thus recognizable in the light microscope (Figs 2, 3). The precursor now has a thick, dense peripheral reticulum encasing a loose, fibrogranular reticulum; **85, 86** - stage (7) is characterized by interwoven fibre bundles in the central two thirds of the precursor. The bundles are attached to the vesicle's membrane (arrows). The peripheral third of the precursor contains the loose, fibrogranular reticulum of stage (6), leaving an about 100 nm wide area (asterisks) around the branches of the dense peripheral reticulum (PR); **87-89** - stage (8) precursor vesicles have an average size of 1855×1571 nm. The central fibre bundles are straight and a fibrous network develops between the central bundles and the dense peripheral reticulum (Fig. 87). When fully developed, the network consists of roundish, narrowly meshed areas (arrowheads) within a more widely meshed basal network (Figs 88, 89). PM - precursor membrane, PR - dense peripheral reticulum. Scale bars: 200 nm (86, 89); 600 nm (84, 85, 87, 88).

some strongly osmiophilic material attaches to, or is contained in, the vesicle membrane which, indeed, is about 8 nm thick (Table 2), while ordinary organelle membranes are 6 nm thick (Sitte *et al.* 1991). These specialization is very likely related to the specific function the membrane has in the (D) precursor: it becomes the thick, strongly osmiophilic peripheral reticulum (see stages [4] and [5]). The vesicle's contents may be electron-lucent or fibrogranular forming an alveolar or smooth pattern (Figs 60-62). We found such vesicles in five specimens and with two fixation methods, suggesting that the varying aspect of the contents is not an artifact. However, the rather irregular outline of the vesicles may be caused by the coagulation of the cytoplasm.

Stage (2): this stage is very similar to stage 1, but the vesicles measure 616×505 nm on average, that is, doubled their size (Fig. 63, Table 2). When analyzed separately, the alveolar and finely granular vesicles have a very similar average size, suggesting that they represent a single vesicle type.

Stage (3): again, the size of the vesicles doubled, reaching light microscopical dimension, viz., 1230×959 nm on average (Table 2). Still, the vesicle's outline is rather irregular, while the contents are widely alveolar often showing denser, coarsely granular regions, sometimes even a dense globule (Figs 64-68).

Stage (4): the vesicles have similar size, shape, and contents as those of stage (3), but bright regions develop in the membrane (Fig. 69, Table 2). We could not clarify whether both, the membrane and the osmiophilic substance or only the latter disappear in these regions. Later stages show the bright areas as part of a coarse, peripheral reticulum (Figs 84, 85, 87, 88). This developmental stage is unique for the (D) precursor.

Stage (5): few stage (5) precursors were found, indicating rapid development between stages (3) to (6). The vesicles are similar to those of stage (4), but the wall is distinctly thicker (Figs 70, 71).

Stage (6): the (D) precursor has now an average size of 1647×1426 nm, that is, it is almost globular and recognizable in the light microscope (Figs 2, 3; Table 2). Morphologically, stage (6) is characterized by the thick, darkly stained peripheral reticulum, which is now fully developed (Fig. 84). The wall has an average thickness of 125 nm (SD 16.2, CV 13.0, Min 100, Max 150, $n = 15$) and is composed of fine fibres or sheets forming a reticular pattern in transverse section (Figs 84, 86). The vesicle's contents are lightly stained and show a loose,

fibrogranular reticulum, with a tendency to form more narrowly meshed, scattered accumulations.

Stage (7): there is further, slight growth of the precursor (Table 2). Stage (7) is characterized by the appearance of distinct fibre bundles mainly in the centre of the vesicle; many transitions occur between stages (6) and (7), suggesting comparatively slow development of the fibre bundles. When fully developed, the bundles are distinctly stained, more or less curved, and attached to the vesicle's membrane (Figs 85, 86). The fibres, which have a diameter of about 8 nm leave blank most of the peripheral third of the precursor, where the fibrogranular reticulum extends described in stage (6). This reticulum leaves blank an about 109 nm ($n = 16$) wide area around the peripheral reticulum, similar to the blank zone around the dense plug of the (C) precursor. However, both nets are connected by many fibrogranular strands (Figs 85, 86).

Stage (8): the (D) precursor is now fully developed and has an average size of 1855×1571 nm. Likely, most are globular because 40 % of the vesicles have a circular or nearly circular outline. Stage (8) is highly conspicuous and characterized by two features (Figs 87-89, Table 2): (i) the fibre bundles, which are now attached to both the vesicle's membrane and the peripheral reticulum, become straight and very dense, and (ii) the fibrogranular material between the fibre core and the vesicle's membrane becomes very distinct, forming a wide-meshed basal net containing many narrow-meshed areals with an average size of 125×85 nm. Many deeply stained granules with an average diameter of 13 nm are scattered in the net fibres. The peripheral reticulum is as described in stage (6).

Stage (9): the (D) precursors are released together with and slightly later than the lepidosomes. Just before extrusion, a series of changes occurs (Figs 90-92): the peripheral reticulum disappears without leaving any recognizable material; the fibres composing the central area reduce the diameter from about 8 nm in stage (8) to 4 nm in stage (9) and become reticular; the net around the central fibre core disappears, except of the narrowly meshed areas, which form highly characteristic curls, each composed of a wrinkled fibre and scattered, deeply stained granules; and the precursor decreases from an average size of 1855×1571 nm in stage (8) to 1247×813 nm in stage (9), likely due to the cell turgor which compresses the vesicle after the dissolution of the peripheral reticulum (Figs 90-92, Table 2). All these processes occur during a minute or so, that is, when the

lepidosomes are released, and they can be considerably altered by the fixation shock (see below).

As soon as the cortex opens, the cell turgor presses the contents of the precursor into the space between cortex and lepidosome coat, while the precursor membrane becomes part of the cortex. The perilemma opens like the other cortex membranes (Figs 90, 91); no specific structures are recognizable around the port. The further events could not be followed because the precursor's contents soon become stainless.

As mentioned above, the fixation shock can alter the processes considerably. Almost half of the 15 precursor extrusions seen still have the peripheral reticulum, both inside and outside the cell, where it disappears rapidly. That such stages are artifacts is indicated by the perilemma, which sometimes engages the extruded material.

Cyst wall precursor (E)

The (E) precursor appears late and is short-lived, that is, it becomes recognizable when the lepidosomes and the other cyst wall precursors have been released and disappears when the cyst wall develops, though late developmental stages are still recognizable in some young cysts (Fig. 1). They are numerous, i.e., there are about 80.000 (E) precursors in a cell, as calculated from their average size (~500 nm), the thickness of the sections (~80 nm), and the number of cuttings (~200) found in a transverse section through the middle third of a specimen. Further, (E) precursors are the simplest and smallest out of the five precursor types found. Thus, they reach the final size (~500 nm) already in developmental stage (2). During genesis of the (E) cyst wall precursor, cortex reorganization and perilemma endocytosis occur, as described below.

Stage (1): the first stage recognizable is a small, membrane-bound, rather distinctly wrinkled, bright vesicle with an average size of 261×202 nm (Figs 93, 94; Table 2). The origin of these vesicles could not be clarified. The fibrogranular contents form a wide-meshed pattern. Near the vesicle's margin, the contents show one or two minute, dark (electron-dense) accumulations, which distinguish this vesicle type from other ones.

Stage (2): the vesicles have grown to 585×382 nm on average, which is already the mature size (Table 2). They have a slightly wrinkled membrane and are pyriform (Figs 95, 96), a unique shape not found in any other precursor type of *Meseres*. As in stage (1), the fibrogranular contents form comparatively large alveoli

which, however, become filled with strongly osmiophilic material in the broader half of the precursor. Thus, this stage is conspicuously spotted (Figs 95, 96).

Stage (3): next, the precursor becomes ellipsoidal to oblong, i.e., gets an average size of 533×210 nm and a length:width ratio ranging from about 1.5:1-3.5:1 (Table 2). The vesicles have a rather wrinkled membrane and a bright, fibrogranular fringe. The central half is filled with darkly stained, narrowly meshed material, emphasizing the rod-like appearance of the precursor (Fig. 97).

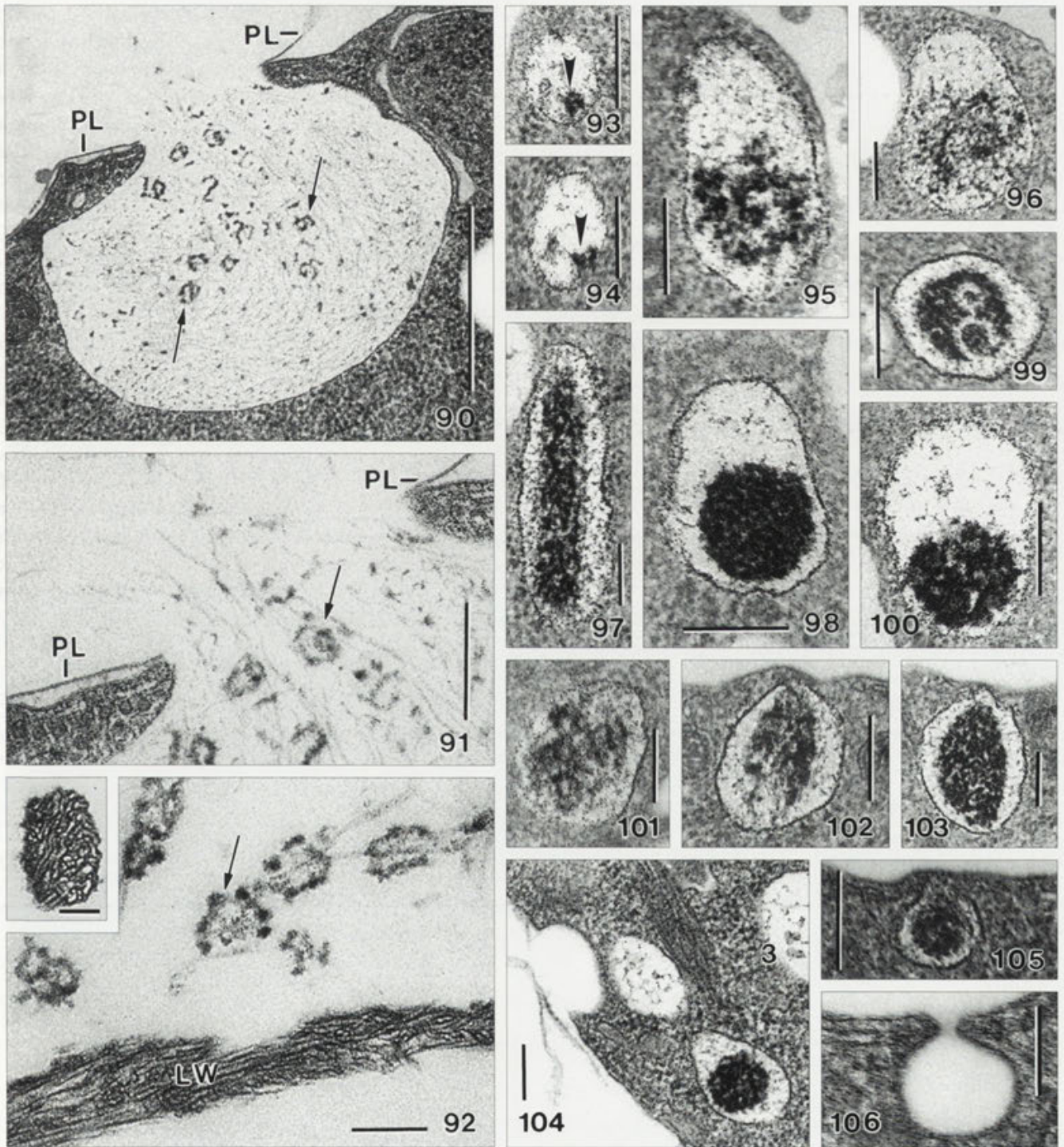
Stage (4): the precursor becomes pyriform again and has an average size of 532×351 nm; the surrounding membrane is more or less wrinkled (Figs 98-100, Table 2). The darkly stained central material described in the previous stages condensed to a narrowly meshed, conspicuous globule with an average size of 269×238 nm. This globule may occupy either the broader or narrower half of the precursor. The rest of the vesicle is filled with wide-meshed fibrogranular material very similar to that found in the previous stages (Figs 98-100).

Stage (5): when the precursor has attached to the cortex of the ciliate, it becomes broadly ellipsoidal showing an average size of 443×293 nm (Figs 101-103, Table 2). As compared to stage (4), the total size slightly decreased from 532×350 nm to 443×293 nm, while the size of the dense core increased from 269×238 to 337×190 nm. This matches the morphological changes, that is, the core loosened and is thus larger and less deeply stained (Figs 101-103).

Stage (6): although being numerous (see above), few extruding (E) precursors were found, indicating that most are released during a very short period. Further, the contents become stainless as soon as the vesicle opens. Thus, we could not follow the further way of the (E) precursor.

Cortex reorganization and perilemma endocytosis

The following data are based on four stage (e) cysts: two of them have a strongly alveolate, wrinkled cortex and few endocytotic vesicles, while the two others have a thin, reduced cortex with many endocytotic vesicles. All cells have small areas where either the original cortex is still present or has been fully reorganized (Fig. 76). Morphometric data of the process and structures described below are shown in Table 3. Briefly, the measurements show that all membranes have a usual thickness (6-7 nm) and four size-classes of vesicles can be distinguished.



Figs 90-106. *Meseres corlissi*, transmission electron micrographs of the extrusion of the (D) precursor (90-92), and the genesis (94-103) and extrusion (104-106) of the (E) precursor. **90-92** - emerging (D) precursor, showing the characteristic curls (arrows) produced by the narrowly meshed areas of the basal net (Fig. 89, arrowheads). The inset shows a transverse section of a branch of the peripheral reticulum, whose fine structure highly resembles that of the lepidosome wall; **93, 94** - stage (1) vesicles of the (E) precursor have a size of 261×202 nm and a unique accumulation of strongly osmiophilic material attached to the membrane (arrowheads); **95, 96** - stage (2) vesicles have a size of 585×382 nm and are pyriform. The wider part is filled with fibrogranular material; **97** - in stage (3), the precursor reaches a size of 533×210 nm. The central portion is filled with strongly osmiophilic material; **98-100** - when approaching stage (4), the precursor becomes pyriform again and has a size of 532×351 nm. The osmiophilic material condensed to a conspicuous globule; **101-103** - in stage (5), the precursor attaches to the cortex and has an average size of 443×293 nm. The core material loosens and thus appears less deeply stained than in stage (4); **104-106** - when extruded, the contents of the (E) precursor become stainless. LW - lepidosome wall, PL - perilemma. Scale bars: 100 nm (92, 106); 200 nm (91, 93-105); 600 nm (90).

During encystment stage (e), that is, when the cell significantly reduces its volume (Foissner *et al.* 2006 and Fig.1) and produces the (E) cyst wall precursor (Figs 93-103), the cortical alveoli double and treble their size and the cortex becomes heavily wrinkled; rarely occur endocytotic vesicles, as described below (Fig. 77). The cortical microtubule sheet has been decomposed earlier, that is, when the cell rounded up. These processes leave back a distinctly altered cortex with a cell membrane and few, very small alveoli (Figs 78, 79, 83). Then, an extraordinary process commences, viz., the formation of innumerable cortical vesicles which endocytose the surplus perilemma produced by the diminution of the cell and the reduction of the ciliary organelles. In the two appropriate cells studied, there were about 100-200 endocytotic events each in a single section through the mid of the cell, plus about 200 just internalized vesicles with decomposing perilemma.

Endocytotic vesicle formation commences with a flat concavity which soon grows and deepens to a bowl-shaped structure with a median size of 228×200 nm (Figs 72, 78-81; Table 3). Frequently, the vesicles are close together, forming breast-like figures (Figs 73, 81). The perilemma does not deepen during vesicle formation and thus covers the vesicle like the lid the pot (Figs 80, 81). Most of the vesicles have the cytoplasmic surface covered by a more or less distinct, electron-dense coat

with an average thickness of 10 nm (Figs 74, 78-81; Table 3). When the vesicles are fully developed, the internalization of the perilemma commences with a minute concavity over the centre of the vesicle (Fig. 80). This concavity grows (Fig. 81), eventually becoming a drop-shaped structure extending into the centre of the vesicle which commences to close by inclining the anterior margin (Figs 72, 74, 75, 82). Concomitantly, the surface coat disappears and then the vesicle pinches off, remaining underneath the cell surface and slightly increasing in size to an average of 352×269 nm (Fig. 72, 74, 81-83; Table 3).

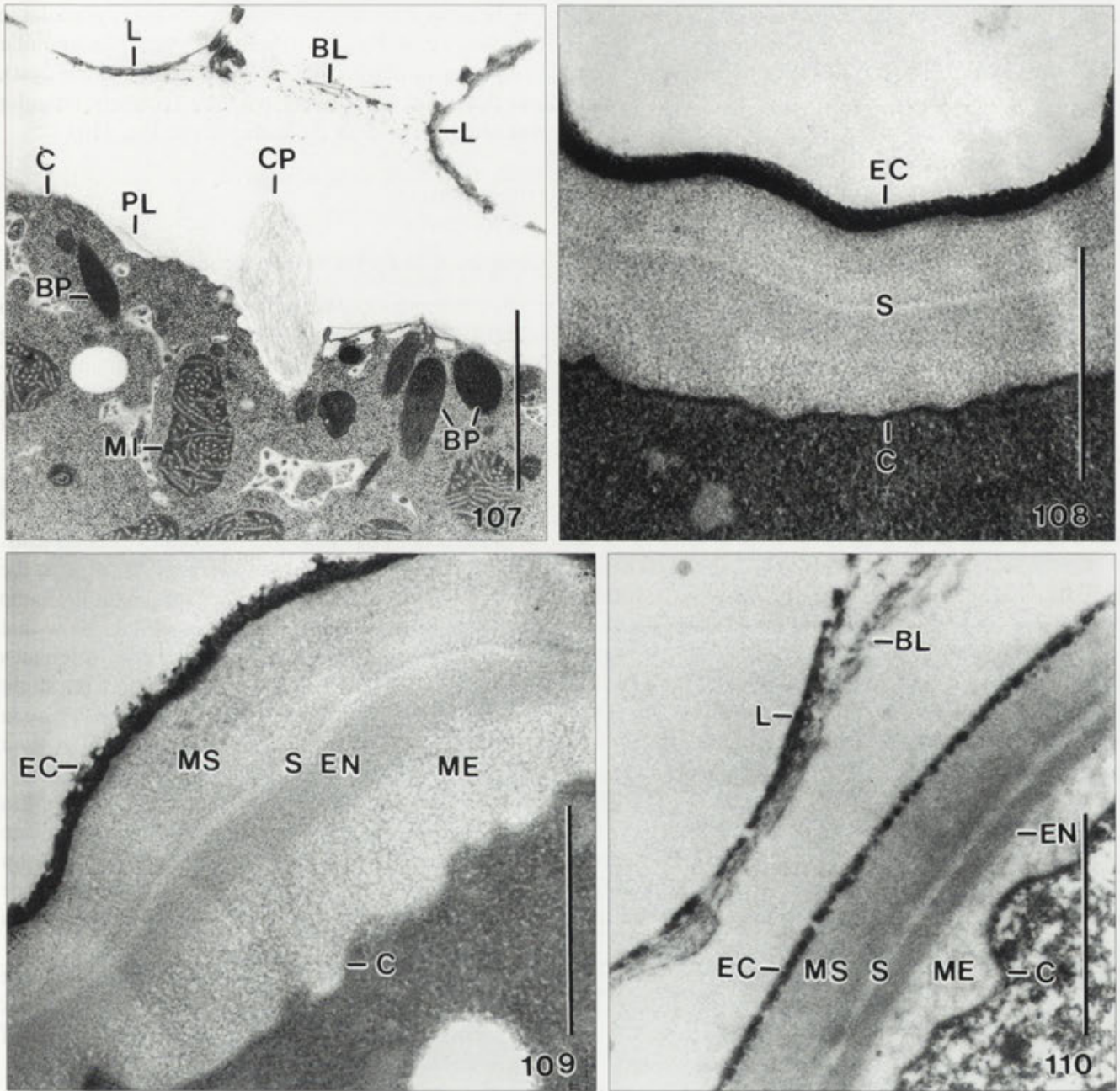
The following stages of perilemma decomposition were reconstructed from hundreds of micrographs. The analysis suggests that the vesicles and their contents become compacted to an average size of 218×157 nm. Thus, they appear dark, often showing myelin figures (Fig. 75). Still the vesicles are in the peripheral $1 \mu\text{m}$ of the cell, where they commence to fuse with each other and to move centripetally, forming bright vacuoles with membrane remnants and an average size of 612×439 nm (Fig. 76, Table 3). These vacuoles then fuse with autophagous vacuoles (Fig. 76).

Formation of basal layer and cyst wall

When the lepidosomes have been released, the encysting cell begins to rotate slowly for some minutes. During this period, an up to $10 \mu\text{m}$ wide, clear, structure-

Table 3. *Meseres corlissi*, morphometric data on reorganization of cortex and perilemma endocytosis. Arabic and Roman numerals ahead of the characteristics correspond to those shown in figure 112. Measurements in nm and from two cysts in encystment stage (e). CV - coefficient of variation in %, M - median, Max - maximum, Min - minimum, n - number of specimens measured, SD- standard deviation, \bar{x} - arithmetic mean.

Characteristics	\bar{x}	M	SD	CV	Min	Max	n
Membrane thickness							
I Cortex	32.1	33.0	4.6	14.3	24	40	11
2 Perilemma	6.2	7.0	1.0	15.8	5	7	11
3 Forming endocytotic vesicles (without coat)	6.4	6.0	0.9	14.4	5	8	11
4 Membrane plus coat of forming endocytotic vesicles	16.4	16.5	3.5	21.4	12	22	12
5 Internalized vesicles close to cell surface	6.6	6.5	1.3	19.9	5	9	16
6 Perilemma within internalized vesicles	6.8	7.0	1.2	18.2	5	8	13
Size of endocytotic vesicles							
I Fully developed vesicles, length	309.8	288	112	36.2	150	622	30
Fully developed vesicles, depth	209.4	200	80	38.0	100	400	30
II Internalized vesicles close to cortex, length	352.2	333	82	23.3	200	542	30
Internalized vesicles close to cortex, width	269.4	253	73	27.1	156	500	30
III Dark endocytotic vesicles, length	217.7	206	66	30.1	100	356	30
Dark endocytotic vesicles, width	155.6	148	49	31.2	58	250	30
IV Internalized vesicles in cytoplasm, length	612.2	573	162	26.4	367	1083	30
Internalized vesicles in cytoplasm, width	438.5	433	141	32.2	222	900	30



Figs 107-110. *Meseres corlissi*, formation of cyst wall. **107** - extrusion of a (C) precursor (CP; for higher magnifications, see figures 58, 59) in a specimen which has released the lepidosomes (L) and many (B), (C), and (D) precursors. All these materials, except of the lepidosomes and the basal layer, are in the space between basal layer (BL) and ciliate cortex (C), but cannot be seen because they do not stain with the methods used. Thus, the early stages of cyst wall formation could be not followed; **108** - middle stage of cyst wall formation, showing the deeply stained, structureless ectocyst and a thick, fibrogranular layer divided by a narrow, electron-lucent zone (S). The cytoplasm is very dense and poorly preserved in this stage; **109, 110** - a young (109) and a mature (110) cyst wall. They differ mainly by the ectocyst, which is structureless in the former and coarsely granular in the latter. BL - basal layer of pericyst, BP - cyst wall precursor (B), C - cortex of the ciliate, CP - cyst wall precursor (C), EC - ectocyst, EN - endocyst, L - lepidosomes, ME - metacyst, MI - mitochondrium, MS - mesocyst, PL - perilemma of the ciliate cortex, S - space. Scale bars: 600 nm (108, 109); 2000 nm (107, 110).

less zone, recognizable mainly due to adhering bacteria, develops around the globular cell (Foissner *et al.* 2006). This zone is formed by the materials released from cyst wall precursors (B-E).

Although we sectioned five appropriate specimens, we could not observe the formation of the cyst wall in the electron microscope, partially because the materials released by the wall precursors became stainless, as reported above. The wall either had not yet assembled or assemblage was almost finished, that is, we did not find transitions between the stages shown in Figures 107 and 108. Thus, cyst wall formation must be a fast "condensation" process, including a far-reaching restructuring of the materials so that they become visible again in the electron microscope. In this process, the slow rotation of the cell possibly mixes and transports the materials to the specific positions (Fig. 1, Foissner *et al.* 2006). What we could observe, is described in the following paragraphs.

The basal layer, upon which the lepidosomes lie or are partially embedded, is the proximal, denser portion of the slimy coat surrounding the cyst of *M. corlissi* (Foissner 2005; Foissner *et al.* 2005, 2006; Figs 27, 28, 107, 110). The developing lepidosomes are enclosed by a membrane which is very near to the lepidosome wall; thus, no space remains for slime (Foissner *et al.* 2006). Likewise, the lepidosome cavity does not contain slime because it does not stain with alcian blue (Foissner *et al.* 2005). Thus, the mucous coat of the *Meseres* cyst must be produced by one or several cyst wall precursors. Figures 27-31 and 90-92 indicate that the basal layer, and thus likely the entire slime coat, is formed by the (B) and (D) precursors because remnants (membranous sheets, curls) of them are recognizable in that layer. However, we cannot exclude that parts of the (B) and (D) precursors contribute to other layers of the cyst wall, too.

The just assembled (young) cyst wall is considerably thinner (\bar{x} 737 nm, Min 617 nm, Max 790 nm, n 5) than the mature wall (\bar{x} 1241 nm, Foissner 2005), but already shows the bright zone between mesocyst and endocyst (Figs 108, 110). Basically, two layers are recognizable in this stage (Fig. 108): the deeply stained, thin, structureless ectocyst (coarsely granular in the mature cyst; Fig. 110 and Foissner 2005) and a lightly stained, thick, fibrogranular layer divided by a narrow, electron-lucent zone present also in the mature wall (Fig. 110). In a later stage (Fig. 109), which is already very similar to the mature wall (Fig. 110), all cyst layers are recognizable,

but the ectocyst is still structureless (coarsely granular in the mature cyst; Fig. 110); the mesocyst is fibrogranular (usually with herring-bone pattern in the mature cyst); and the metacyst is finely reticular (coarsely reticular and often granular in the mature cyst; Fig. 110).

DISCUSSION

Genesis of the cyst wall precursors (Fig. 111)

According to Gutiérrez *et al.* (2003), "There is no reliable information on the origin of resting cyst wall precursors in the ciliate cytoplasm, although cytochemical evidence supports the notion that the origin of the cyst wall precursors is from ER and/or Golgi complex (Calvo *et al.* 1986)". However, Walker *et al.* (1989) provided convincing electron micrographs that the cyst wall precursor of a peritrich ciliate, *Telotrochidium henneguyi*, develops pairwise in dilated Golgi cisterns. This has been confirmed in *M. corlissi*, where the (A) wall precursor (= lepidosomes) originates the same way (Foissner *et al.* 2006). The present data show that cyst wall precursor (C) of *M. corlissi* also originates in Golgi vesicles (Figs 32-36). However, there is a slight difference: cyst wall precursor (A) originates pairwise in the dilated ends of Golgi cisterns, while cyst wall precursor (C) forms by growth of individual Golgi vesicles. Unfortunately, we could not find out the origin of cyst wall precursors (B), (D) and (E). Likely, they are also produced from saccules and vesicles of the Golgi complex, just like scales and various other surface structures of protists (Bovee 1991, Vickermann *et al.* 1991).

We could not clarify precursor growth; it is not vesicular endocytosis, suggesting material uptake across the precursor membrane *via* an active, carrier-mediated process.

Number and morphology of cyst wall precursors in ciliates (Fig. 111)

Literature data have been reviewed by Gutiérrez and Martín-González (2002) and Gutiérrez *et al.* (2003). Briefly, the cyst wall of ciliates consists of 2-4 layers (3-5 if the pericyst is recognized as a distinct layer; Foissner 2005), depending on the group of ciliates; rarely, there are differences between the species of a genus or the genera of a family. These layers are the pericyst, ectocyst, mesocyst, endocyst and metacyst. Usually,

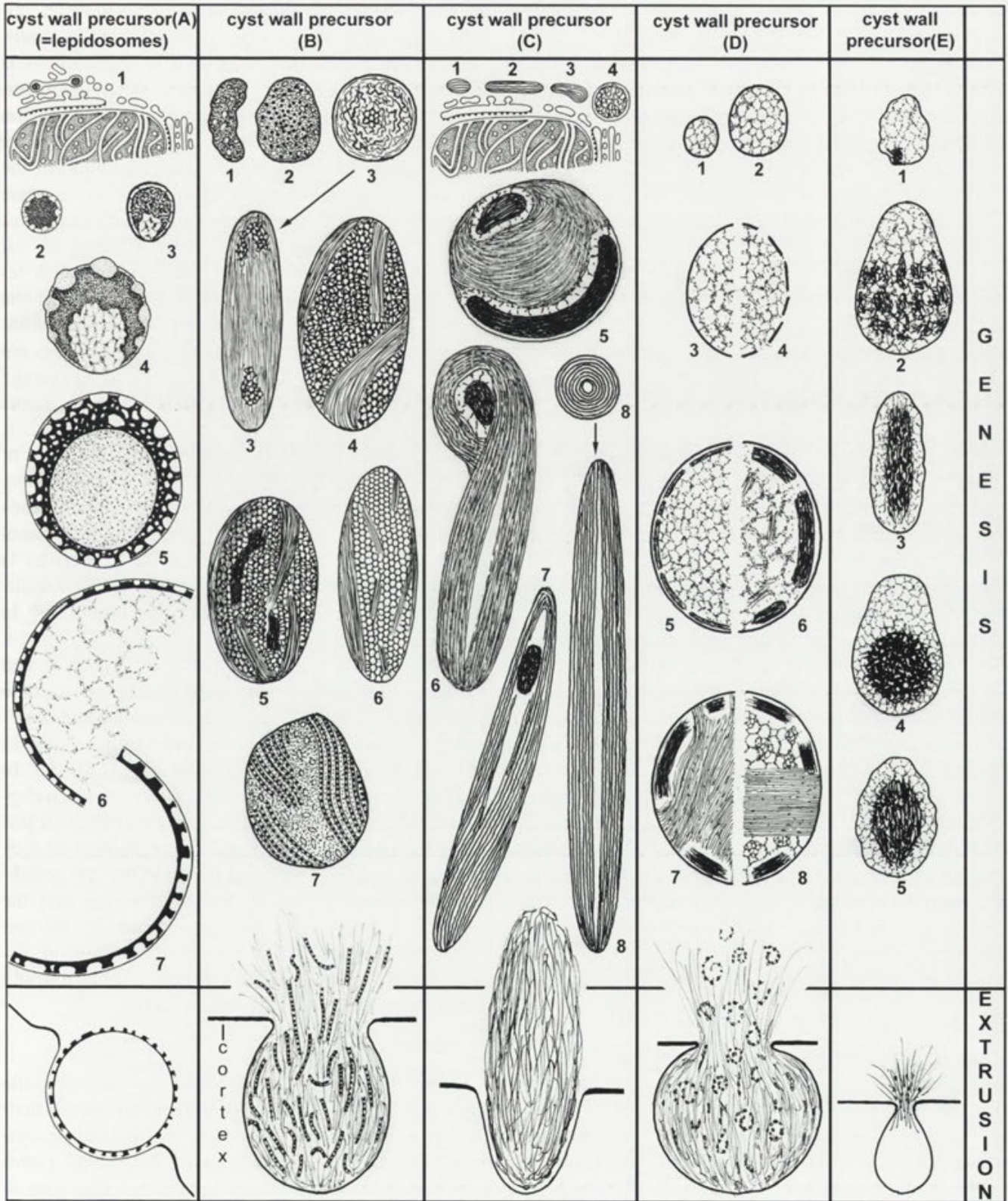


Fig. 111. *Meseres corlissi*, scheme of genesis and extrusion of cyst wall precursors (A-E). Genesis of precursor (A) is described in Foissner *et al.* (2006). Figures roughly drawn to scale within individual files. Numerals denote developmental stages as described in the text.

each layer originates from a distinct precursor whose development, unfortunately, rarely has been documented in detail.

With few exceptions, the cyst wall precursors are either mucocysts, for instance, in *Tetrahymena rostrata* (McArdle *et al.* 1980) and *Colpoda magna* (Frenkel 1994), or small ($\leq 1\mu\text{m}$) vesicles with fibrogranular or amorphous contents, for instance, in *Gonostomum* (Walker and Hoffman 1985) and *Telotrochidium henneguyi* (Walker *et al.* 1989). Well known exceptions are the plate-like ectocyst precursors of several stichotrichine spirotrichs (e.g. *Oxytricha*, *Coniculostomum*) and the hairpin-shaped clathrocysts which produce the mesocyst of *Didinium nasutum* (Holt and Chapman 1971). These precursors are some μm in size and show distinct developmental stages, just as those of *Meseres*.

Meseres corlissi highly resembles stichotrichine spirotrichs in the number of cyst wall precursors and wall layers. In contrast, the morphology of the wall precursors is entirely different from those described as yet, both in the developing and mature state (Fig. 111). There are some superficial similarities, for instance, the membranous structure of the (C) precursor resembles the ectocyst precursor of the stichotrichs. However, their genesis is different and when extruded the (C) precursor of *Meseres* dissolves and becomes stainless, while the plates of the stichotrichine ectocyst precursor remain structurally intact and form the lamellar ectocyst (Gutiérrez *et al.* 1983, 2003). The (E) precursor resembles the cyst wall precursor vesicles of several ciliates, for instance, *Gonostomum* (Walker and Hoffman 1985) and *Colpoda magna* (Frenkel 1994), but the details of genesis and fine structure are different. Accordingly, we conclude that the oligotrichine spirotrichs are a very distinct group of ciliates differing from other ones not only by their general morphology, but also in the genesis and mature structure of the cyst wall precursors.

Release of cyst wall precursors (Fig. 111)

Detailed data on the release of the cyst wall precursors are lacking in ciliates, except for *M. corlissi*, where Foissner *et al.* (2006) showed that cyst wall precursor (A), i.e., the lepidosomes are released by classical exocytosis (Plattner and Hentschel 2002, Becker *et al.* 2006), that is, the surrounding membrane fuses with the cortex membranes and is integrated into the newly forming cortex. Here, we show the same for the (B) precursor (Figs 27, 29), the (C) precursor (Fig. 59) and the (D) precursor (Fig. 90), while data for the (E)

precursor are insufficient due to problems in differentiating the release stages from perilemma endocytosis. Accordingly, exocytosis of the cyst wall precursors is different from extrusome exocytosis, where the enveloping membrane is recycled in the cytoplasm (Hausmann 1978, Vickerman *et al.* 1991, Peck *et al.* 1993, Plattner and Kissmehl 2003). In *Meseres*, augmentation of the surface area by the precursor membranes makes sense because about 1000 cyst wall precursors with a diameter of up to 15 μm (lepidosomes) are released almost concomitantly. The exocytotic openings produced occupy an average of about 87 % of the surface of the forming cyst (calculated surface area of *Meseres* without peristomial bottom where few or no precursors are released: ~ 8000 μm^2 ; 200 lepidosomes with an average diameter of 6 μm : ~ 5700 μm^2 ; 800 (B, C, D) precursors with an average diameter of 1 μm : ~ 1260 μm^2). Thus, resealing of the exocytotic openings requires a lot of membrane obviously provided by the vesicles containing the cyst wall precursors. Certainly, further investigations have to clear the details of the process, but our basal observation that the membrane of the precursors is integrated into the newly forming cortex is well documented (Figs 27, 29, 59, 90, 111 and Figs 52-57 in Foissner *et al.* 2006).

We could not clarify the precursor transport and release *s. str.* The cyst wall precursors of the stichotrichine ciliate *Gastrostyla steinii* and the scales of chrysophytes are guided to the cortex by microtubules (Walker *et al.* 1980, Vickerman *et al.* 1991). In *M. corlissi*, microtubules or other fibres are not recognizable. However, there is fast rotation of the cell just before the precursors are released, suggesting that they are transported by centrifugal forces to the cell periphery. The release *s. str.* of the lepidosomes and the contents of the vesicles may be achieved by the cell turgor, which probably increases before extrusion, because the cell becomes slightly inflated, just like it would take a deep breath (Foissner *et al.* 2006).

Formation of cyst wall

One of the firm findings in ciliate cyst research is the sequential formation of the cyst wall precursors and their successive secretion to generate the individual cyst layers (Grimes 1973; Gutiérrez *et al.* 1983, 2003; Calvo *et al.* 1986). *Meseres corlissi* breaks this rule: four of the five wall precursors are generated and released almost concomitantly, and the cyst wall suddenly “condenses” out of the stainless mass formed by the extruded contents of the wall precursors.

Unfortunately, authors often do not comment on cyst wall assemblage *s. str.* However, those studies which do show that the secreted precursors basically maintain their structure and visibility, that is, stain with the ordinary methods. Good examples are *Didinium nasutum* (Holt and Chapman 1971), *Colpoda magna* (Frenkel 1994), *Oxytricha fallax* (Grimes 1973), *Laurentiella acuminata* (Gutiérrez *et al.* 1983), and *Conciculostomum monilata* (Kamra and Sapra 1993). This contrasts *M. corlissi*, where the released precursors change their structure so distinctly that they become invisible (Figs 27, 59, 90, 105, 107), except of precursor(A) which, however, is assembled within the cell (Foissner *et al.* 2006).

We could not observe which precursors form the individual cyst layers of *M. corlissi* because the materials become stainless when released. Possibly, this is unique to *Meseres* or the oligotrichs. However, it might occur also in some other ciliates, for instance, in *Oxytricha bifaria*, where the seemingly empty pericellular space could contain stainless mesocyst material because all other cyst layers have already formed (Verni *et al.* 1984; Figs 5, 6, 9).

Three further general aspects on cyst wall precursors and wall assemblage can be extracted from our investigations and the literature. First, the cyst wall can be formed (i) from precursors generated *de novo*, for instance, in *Meseres* and many other ciliates (Gutiérrez *et al.* 2003); (ii) mainly by organelles present in the morphostatic cell, for instance, the mucocysts in *Tetrahymena rostrata* (McArdle *et al.* 1980); (iii) by a combination of precursors and organelles present in the morphostatic cell, for instance, in *Colpoda magna* (Frenkel 1994) and *Engelmanniella mobilis* (Wirnsberger-Aeschl *et al.* 1990); and (iv) without recognizable, membrane-bound precursors, for instance, in the parasitic ciliate *Hyalophysa chattoni* (Landers 1991). Second, the cyst wall is assembled either outside the cell's cortex (usual way, Gutiérrez *et al.* 2003) or part of the wall is assembled within the cell, for instance, the lepidosomes of *Meseres* (Foissner *et al.* 2006) and *Halteria* (Foissner, unpubl.). Third, the cyst wall forms outside the cell (usual way, as in *Meseres*) or subcortically (known only from *Colpoda steinii*, Ruthmann and Kuck 1985). There are some reports that the cyst wall forms between the cell membrane and the perilemma in stichotrichine spirotrichs (Grimes 1973, Matsusaka 1976, Walker *et al.* 1980, Calvo *et al.* 1986). However, convincing micrographs are lacking (Foissner *et al.* 2006 and next chapter).

Cortex reorganization and perilemma endocytosis (Fig. 112)

To our best knowledge, cortex reorganization and/or perilemma endocytosis have not been reported in encysting ciliates. This is surprising, considering that body volume (size) and body surface are usually considerably reduced. For instance, the cyst volume of *M. corlissi* is only 28% of that of the vegetative cell and only 5% in *Opisthonecta*, a peritrich ciliate (Foissner *et al.* 2006). Even more surprising is the absence of reports on perilemma endocytosis in several well investigated stichotrichs, for instance, *Oxytricha* (Grimes 1973), *Laurentiella* (Gutiérrez *et al.* 1983) and *Conciculostomum* (Kamra and Sapra 1993). This indicates that perilemma endocytosis is a specific trait of oligotrichs. However, endocytosis occurs only during a short period of the encystment process (Fig. 1). Thus, it cannot be excluded that previous studies missed it by bad luck.

Preservation of the fine structure is difficult in resting cysts, even if the protecting wall has not yet formed, because encystment involves a complete restructuring of the cell which thus becomes fragile and difficult to fix. None the less, we are sure that our micrographs (Figs 76-79) show cortex reorganization because the wrinkled cortex and the large alveoli appear just when the cell significantly reduces its size and thus much surplus cortex has to be removed. The reorganization occurs without special Anlagen and is thus unspectacular and rather difficult to recognize, possibly explaining the lack of previous reports.

The perilemma is a unit membrane-like structure covering body and cilia of oligotrichine and stichotrichine spirotrichs, except of the curious lack in *Halteria*, the closest relative of *Meseres* (Fauré-Fremiet and Ganier 1970, Grain 1972, Laval-Peuto 1975, Bardele 1981, Wirnsberger-Aeschl *et al.* 1989, Katz *et al.* 2005). In *M. corlissi*, up to five perilemma membranes occur in the vegetative specimens and two in cystic cells (Foissner 2005). Our investigations show that only part of the perilemma is removed by endocytosis, likely mainly the surplus portion originating from body size and cilia reduction.

In conventional electron micrographs, there is no absolute marker for distinguishing endocytosis and exocytosis. However, often this is possible when other aspects are taken into account. In *Meseres*, we interpret the cortical vesicles as an endocytotic process for the following reasons: (i) Cortex reorganization and perilemma

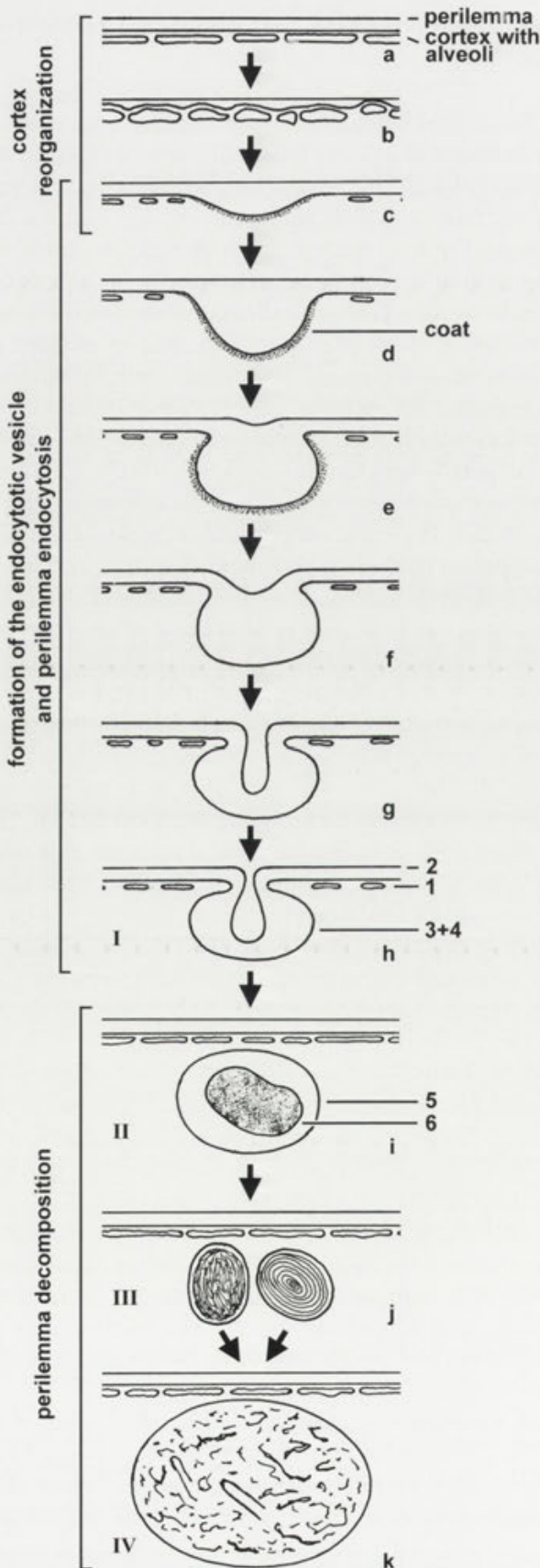


Fig. 112. *Meseres corlissi*, scheme of reorganization of cortex (a-c), formation of the endocytotic vesicle and perilemma endocytosis (c-h), and perilemma decomposition (i-k). Drawn to scale, according to data compiled in Table 3. Unit membranes shown as simple lines. Arabic (1-6) and Roman (I-IV) numerals correspond to structures measured in Table 3. See text and discussion for more detailed explanations.

endocytosis take place during encystment stage (e), that is, when the cell significantly reduces its size (Foissner *et al.* 2006), decomposes the ciliary organelles, and the number of autophagous vacuoles reaches a maximum (Fig. 1); (ii) The vesicles are coated only during formation and only on the cytoplasmic surface (Figs 74, 78, 79); (iii) The vesicles are most numerous in the oral area, where plenty of ciliary perilemma must be removed; (iv) The vesicles contain membrane pieces. To our best knowledge, it never has been described that membrane pieces are produced deep in the cytoplasm, transported to the cell's surface, and then integrated into an existing membrane; (v) The vesicles develop to vacuoles with myelin figures, which are typical for decomposing membranes; (vi) Last but not least, the micrographs (Figs 72-83) strongly suggest endocytosis, that is, progress of the processes as shown in the scheme (Fig. 112). This applies especially for the stages shown in figures 80 and 81, which can occur only during an endocytotic process.

No data are available on the composition and function of the perilemma as well as how it is derived and replenished. Lynn and Corliss (1991) speculate that it may be a special kind of fixation artifact of the glycocalyx, while Bardele (1981) proposes: "I believe that the perilemma is a temporary structure which is renewed quite often, for numerous layers of the perilemma are usually seen in the buccal cavity. It is not known whether the perilemma is involved in food gathering under certain physiological conditions, for example, starvation, or is a prerequisite to encystation, where it certainly forms the outer layer during early stages of cyst formation (Grimes 1973)". As concerns participation in cyst wall formation, the evidences are weak, that is, convincing electron micrographs are lacking that the ectocyst precursor is entrapped between the perilemma and the cell membrane. And it contradicts the observations on *Meseres*, where the perilemma disappears at the sites where the wall precursors leave the cell (Figs 59, 90, 91, 107 and Foissner *et al.* 2006). Our investigations also rule out that the perilemma is a temporary structure or a fixation artifact because it is present throughout the life cycle and becomes reduced by endocytosis with defined decomposition stages in the internalized vesicles (Fig. 75).

Some function in food gathering cannot be excluded, but is unlikely considering that it covers the whole body. Thus, nothing remains except of the morphological facts. Our investigations suggest that structure and composition of the perilemma are considerably different from those of ordinary cortex membranes; otherwise, it would not need so prominent endocytosis to be removed.

Phylogenetic implications

The compilation above shows a considerable diversity of the processes associated with cyst wall formation in ciliated protozoa. Likely, many more possibilities remain to be discovered. If this diversity is added to that of overall cyst morphology (e.g., wall ornamentation), cyst wall composition (e.g., with or without chitin) and cell restructuring (e.g., the infraciliature may be maintained or partially or completely resorbed), an overwhelming diversity emerges which should contain considerable ecological and phylogenetic information; unfortunately, the message is only partially understood, likely because detailed data on resting cyst formation and structure are available from less than 40 species (Gutiérrez *et al.* 2003). For instance, when one compares the very different modes of cyst wall formation in *Colpoda steinii* (Ruthmann and Kuck 1985) and *C. magna* (Frenkel 1994), then it seems likely that both belong to different genera or even families, although taxonomists consider them as congeneric (Foissner 1993).

When discussing the classification of the halteriine spirotrichs, to which *Meseres* belongs (Katz *et al.* 2005), Foissner *et al.* (2004) reached the conclusion that further data are necessary to decide whether they are oligotrichine or stichotrichine spirotrichs, as suggested by the ontogenetic, respectively, molecular investigations. The present study supports the classical view that the halteriids belong to the oligotrichs because the cyst wall precursors are quite different from those of the stichotrichs. Specifically, *Meseres* lacks the highly characteristic stacks of membrane-like ectocyst precursors of the stichotrichine spirotrichs, and thus has a different mature ectocyst (Foissner 2005). Likewise, there are no similarities to the urostylid ectocyst (Rios *et al.* 1985), while the kahliellid ectocyst is as thin as that of *Meseres* and thus looks rather similar (Foissner and Foissner 1987). However, it is composed of a membranous sheet in *Kahliella*, while coarsely granular in *Meseres* (Foissner 2005).

Acknowledgements. Financial support was provided by the Austrian Science Foundation, FWF project P 16796-B06. The technical

assistance of Andreas Zankl and Mag. Birgit Peukert is greatly acknowledged.

REFERENCES

- Bardele C. F. (1981) Functional and phylogenetic aspects of the ciliary membrane: a comparative freeze-fracture study. *BioSystems* **14**: 403-421
- Becker, W. M., Kleinsmith L. J., Hardin J. (2006) *The World of the Cell*, 6th ed. Pearson, San Francisco and Toronto
- Berger H. (1999) Monograph of the Oxytrichidae (Ciliophora, Hypotrichia). Kluwer, Dordrecht, Boston, London
- Bovee E. C. (1991) Sarcodina. *Microsc. Anat. Invert.* **1**: 161-259
- Calvo P., Torres A., Perez-Silva J. (1986) Ultrastructural and cytochemical study of the encystment in the hypotrichous ciliate *Histiculus similis*. *Arch. Protistenk.* **132**: 201-211
- Chessa M. G., Delmonte Corrado M. U., Carcupino M., Pelli P. (1994) Ultrastructural cortical aspects of cell differentiation during long-term resting encystment in *Colpoda inflata*. In: *Contribution to Animal Biology* (Eds. R. Argano, C. Cirotto, E. Grassi Milano, L. Masfrolia). Halocynthia Association, Palermo, 169-172
- Corliss J. O. (1979) *The Ciliated Protozoa. Characterization, Classification and Guide to the Literature*. 2 ed. Pergamon Press, Oxford, New York, Toronto, Sydney, Paris, Frankfurt
- Corliss J. O., Esser S. C. (1974) Comments on the role of the cyst in the life cycle and survival of free-living protozoa. *Trans. Am. microsc. Soc.* **93**: 578-593
- Fauré-Fremiet E. (1948) Le rythme de marée du *Strombidium oculatum* Gruber. *Bull. biol. France Belg.* **82**: 3-23
- Fauré-Fremiet E., Ganier M.-C. (1970) Structure fine du *Strombidium sulcatum* Cl. et L. (Ciliata Oligotrichida). *Protistologica* **6**: 207-223
- Foissner W. (1984) Infraciliatur, Silberliniensystem und Biometrie einiger neuer und wenig bekannter terrestrischer, limnischer und mariner Ciliaten (Protozoa: Ciliophora) aus den Klassen Kinetofragminophora, Colpodea und Polyhymenophora. *Stapfia*, Linz **12**: 1-165
- Foissner W. (1993) Colpodea (Ciliophora). *Protozoenfauna* **4**: I-X + 798 p
- Foissner W. (2005) The unusual, lepidosome-coated resting cyst of *Meseres corlissi* (Ciliophora: Oligotricha): transmission electron microscopy and phylogeny. *Acta Protozool.* **44**: 217-230
- Foissner I., Foissner W. (1987) The fine structure of the resting cysts of *Kahliella simplex* (Ciliata, Hypotrichida). *Zool. Anz.* **218**: 65-74
- Foissner W., Agatha S., Berger H. (2002) Soil ciliates (Protozoa, Ciliophora) from Namibia (Southwest Africa), with emphasis on two contrasting environments, the Etosha Region and the Namib Desert. *Denisia* **5**: 1-1459
- Foissner W., Moon-van der Staay S.Y., van der Staay G. W. M., Hackstein J. H. P., Krautgartner W.-D., Berger H. (2004) Reconciling classical and molecular phylogenies in the stichotrichines (Ciliophora, Spirotrichea), including new sequences from some rare species. *Europ. J. Protistol.* **40**: 265-281
- Foissner W., Müller H., Weisse T. (2005) The unusual, lepidosome-coated resting cyst of *Meseres corlissi* (Ciliophora: Oligotricha): light and scanning electron microscopy, cytochemistry. *Acta Protozool.* **44**: 201-215
- Foissner W., Pichler M., Al-Rasheid K., Weisse T. (2006) The unusual, lepidosome-coated resting cyst of *Meseres corlissi* (Ciliophora: Oligotricha): encystment and genesis and release of the lepidosomes. *Acta Protozool.* **45**: 323-338
- Frenkel M. A. (1994) The cyst wall formation in *Tillina magna* (Ciliophora, Colpodidae). *Arch. Protistenk.* **144**: 17-29
- Grain J. (1972) Etude ultrastructurale d'*Halteria grandinella* O.F.M., (Cilié Oligotriche) et considérations phylogénétiques. *Protistologica* **8**: 179-197
- Grimes G. W. (1973) Differentiation during encystment and excystment in *Oxytricha fallax*. *J. Protozool.* **20**: 92-104

- Gutiérrez J. C., Martín-González A. (2002) Ciliate encystment-excystment cycle: a response to environmental stress. In: Microbial Development Under Environmental Stress (Ed. J. C. Gutiérrez). Research Signpost 37/661(2), Trivandrum - 695 023, Kerala, India, 29-49
- Gutiérrez J. C., Torres A., Perez-Silva J. (1983) Structure of cyst wall precursors and kinetics of their appearance during the encystment of *Laurentiella acuminata* (Hypotrichida, Oxytrichidae). *J. Protozool.* **30**: 226-233
- Gutiérrez J. C., Diaz S., Ortega R., Martín-González A. (2003) Ciliate resting cyst walls: a comparative review. *Recent Res. Devel. Microbiol.* **7**: 361-379
- Hausmann K. (1978) Extrusive organelles in protists. *Int. Rev. Cyt.* **52**: 197-276
- Holt P. A., Chapman G. B. (1971) The fine structure of the cyst wall of the ciliated protozoan *Didinium nasutum*. *J. Protozool.* **18**: 604-614
- Jonsson P. R. (1994) Tidal rhythm of cyst formation in the rock pool ciliate *Strombidium oculatum* Gruber (Ciliophora, Oligotrichida): a description of the functional biology and an analysis of the tidal synchronization of encystment. *J. Exp. Mar. Biol. Ecol.* **175**: 77-103
- Kamra K., Sapra G. R. (1993) Morphological and ultrastructural changes during encystment in *Coniculostomum monilata* (Ciliophora, Hypotrichida, Oxytrichidae). *Zoology* **3**: 273-302
- Katz L. A., McManus G. B., Snoeyenbos-West O. L. O., Griffin A., Pirog K., Costas B., Foissner W. (2005) Reframing the "Everything is everywhere" debate: evidence for high gene flow and diversity in ciliate morphospecies. *Aquat. Microb. Ecol.* **41**: 55-65
- Kim Y.-O., Taniguchi A. (1995) Excystment of the oligotrich ciliate *Strombidium conicum*. *Aquat. Microb. Ecol.* **9**: 149-156
- Landers S. C. (1991) The fine structure of secretion in *Hyalophysa chattoni*: formation of the attachment peduncle and the chitinous phoretic cyst wall. *J. Protozool.* **38**: 148-157
- Laval-Peuto M. (1975) Cortex, périmelle et réticulum vésiculeux de *Cyttarocylis brandti* (cilié tintinnide). Les ciliés à périmelle. *Protistologica* **11**: 83-98
- Lynn D. H., Corliss J. O. (1991) Ciliophora. *Microsc. Anat. Invert.* **1**: 333-467
- Matsusaka T. (1976) An ultrastructural study of encystment in the hypotrichous ciliate *Pleurotricha* sp. *Kumamoto J. Sci., Biol.* **13**: 13-26
- McArdle E. W., Bergquist B. L., Ehret C. F. (1980) Structural changes in *Tetrahymena rostratum* during induced encystment. *J. Protozool.* **27**: 388-397
- Montagnes D. J. S., Lowe C. D., Poulton A., Jonsson P. R. (2002) Redescription of *Strombidium oculatum* Gruber 1884 (Ciliophora, Oligotrichia). *J. Eukaryot. Microbiol.* **49**: 329-337
- Müller H. (1996) Encystment of the freshwater ciliate *Pelagostrombidium fallax* (Ciliophora, Oligotrichida) in laboratory culture. *Aquat. Microb. Ecol.* **11**: 289-295
- Müller H. (2002) Laboratory study of the life cycle of a freshwater strombidiid ciliate. *Aquat. Microb. Ecol.* **29**: 189-197
- Müller H., Foissner W., Weisse T. (2006) Role of soil in the life cycle of *Meseres corlissi* (Ciliophora: Oligotrichia): experiments with two clonal strains from the type locality, an astatic meadow pond. *Aquat. Microb. Ecol.* **42**: 199-208
- Peck R. K., Swiderski B., Tourmel A.-M. (1993) Involvement of the trans-Golgi network, coated vesicles, vesicle fusion, and secretory product condensation in the biogenesis of *Pseudomicrothorax* trichocysts. *Adv. Cell Molec. Biol. Memb.* **2**: 1-25
- Petz W., Foissner W. (1992) Morphology and morphogenesis of *Strombidium caudatum* (Fromentel), *Meseres corlissi* n. sp., *Halteria grandinella* (Müller), and *Strombidium rehwaldi* n. sp., and a proposed phylogenetic system for oligotrich ciliates (Protozoa, Ciliophora). *J. Protozool.* **39**: 159-176 ed. Thieme, Stuttgart, New York
- Plattner H., Kissmehl R. (2003) Molecular aspects of membrane trafficking in *Paramecium*. *Int. Rev. Cyt.* **232**: 185-216
- Reid P. C. (1987) Mass encystment of a planktonic oligotrich ciliate. *Mar. Biol.* **95**: 221-230
- Reid P. C., John A. W. G. (1978) Tintinnid cysts. *J. mar. biol. Ass. U.K.* **58**: 551-557
- Reid P. C., John A. W. G. (1983) Resting cysts in the ciliate class Polyhymenophorea: phylogenetic implications. *J. Protozool.* **30**: 710-713
- Rios R. M., Torres A., Calvo P., Fedriani C. (1985) The cyst of *Urostyla grandis* (Hypotrichida, Urostylidae): ultrastructure and evolutionary implications. *Protistologica* **21**: 481-485
- Ruthmann A., Kuck A. (1985) Formation of the cyst wall of the ciliate *Colpoda steinii*. *J. Protozool.* **32**: 677-682
- Sitte P., Ziegler H., Ehrendorfer F., Bresinsky A. (1991) Lehrbuch der Botanik. Fischer, Stuttgart
- Verni F., Rosati G., Ricci N. (1984) The cyst of *Oxytricha bifaria* (Ciliata Hypotrichida). II. The ultrastructure. *Protistologica* **20**: 87-95
- Vickerman K., Brugerolle G., Mignot J.-P. (1991) Mastigophora. *Microsc. Anat. Invert.* **1**: 13-159
- Walker G. K., Hoffman J. T. (1985) An ultrastructural examination of cyst structure in the hypotrich ciliate *Gonostomum* species. *Cytobios* **44**: 153-161
- Walker G. K., Mangel T. K., Goode D. (1980) Encystment and excystment in hypotrich ciliates I. *Gastrostyla steinii*. *Protistologica* **16**: 511-524
- Walker G. K., Edwards C. A., Suchard S. J. (1989) Encystment in the peritrich ciliate *Telotrochidium heneguyi*. *Cytobios* **59**: 7-18
- Weisse T. (2004) *Meseres corlissi*: a rare oligotrich ciliate adapted to warm water and temporary habitats. *Aquat. Microb. Ecol.* **37**: 75-83
- Wirnsberger-Aescht E., Foissner W., Foissner I. (1989) Morphogenesis and ultrastructure of the soil ciliate *Engelmanniella mobilis* (Ciliophora, Hypotrichida). *Europ. J. Protistol.* **24**: 354-368
- Wirnsberger-Aescht E., Foissner W., Foissner I. (1990) Natural and cultured variability of *Engelmanniella mobilis* (Ciliophora, Hypotrichida); with notes on the ultrastructure of its resting cyst. *Arch. Protistenk.* **138**: 29-49
- Xu K., Foissner W. (2005) Descriptions of *Protospathidium serpens* (Kahl, 1930) and *P. fraterculum* n. sp. (Ciliophora, Haptoria), two species based on different resting cyst morphology. *J. Eukaryot. Microbiol.* **52**: 298-309

Received on 11th July, 2006; revised version on 29th August, 2006; accepted on 6th October, 2006

Molecular Characterization of *Blastocrithidia culicis* L17 Ribosomal Protein

Lívia Regina MANZINE¹, Marco Túlio Alves DA SILVA¹, Otávio Henrique THIEMANN² and Regina Maria Barretto CICARELLI¹

¹UNESP - Universidade Estadual Paulista, Faculdade de Ciências Farmacêuticas, Departamento de Ciências Biológicas, Rodovia Araraquara-Jaú, Araraquara, São Paulo; ²Universidade de São Paulo, Instituto de Física de São Carlos, São Carlos, São Paulo, Brazil.

Summary. *Blastocrithidia culicis* is a protozoan of the family Trypanosomatidae. It is a parasite of insects, but the presence of bacterium-like endosymbionts in its cytoplasm led some investigators to study this protozoan. This trypanosomatid does not infect humans and although it is phylogenetically distant from *Trypanosoma cruzi*, it presents many morphological characteristics, which are similar. In previous studies our group showed the presence of a L27 ribosomal protein in *T. cruzi* (named TerL27) using a RT-PCR, which also resulted in the cloning, sequencing and expression of an unexpected ribosomal protein, L17, in *Blastocrithidia culicis* (BcL17). In this paper, Western blot analysis demonstrated that the anti-BcL17 antibody recognizes the presence of the same ribosomal protein either in *Blastocrithidia culicis* and *T. cruzi* nuclear extracts. Besides, two similar bands (40 and 47 kDa) appeared also in *T. cruzi* isolated ribosomal proteins and *B. culicis* nuclear extract corroborating with the findings showed in the phylogenetic reconstruction. With respect to their localization within the ribosome, both the L17 and L27 ribosomal proteins appear to belong to the peptidyl-transferase site, and are therefore part of the key step in protein synthesis. Both ribosomal proteins bind spiramycin derivatives, being therefore compounds of the macrolides connection sites in the ribosome. These findings would open a possibility to better evaluate this issue.

Key words: *Blastocrithidia culicis*, L17 ribosomal protein, recombinant ribosomal protein, trypanosomatids.

INTRODUCTION

Trypanosomatid ribosomal proteins, such as histones and heat shock proteins, have an elevated sequence identity and preserved cellular function on an evolution-

ary timescale (González *et al.* 2004). The order Kinetoplastida is divided into two sub-orders: Trypanosomatina and Bodonina; the sub-order Bodonina is divided in two families: Bodonidae and Cryptobiidae and the sub-order Trypanosomatina includes only one family: Trypanosomatidae. In this family the genera *Trypanosoma*, *Leishmania* and *Blastocrithidia* are included. These genera were defined as monophyletics (a group that involves an ancestral species and all its descendants) (Lukes *et al.* 1997, Wright *et al.* 1999, Stevens and Gibson 1999). However, recently Maslov *et*

Address for correspondence: Regina Maria Barretto Cicarelli, Departamento de Ciências Biológicas, Faculdade de Ciências Farmacêuticas, Universidade Estadual Paulista - UNESP, Rodovia Araraquara-Jaú, Km 01, 14801-902, CP 502, Araraquara, SP, Brazil; Fax: +55 16 3301 6940; E-mail: cicarell@cfar.unesp.br

al. (2001) defined the gender *Blastocrithidia* as polyphyletic (a group derived from two or more ancestral species) suggesting that the morphological classification of the Kinetoplastida order may not be general to the family Trypanosomatidae. The genus *Blastocrithidia* is classified as monogenetic while the *Trypanosoma* and *Leishmania* are digenetic (Neves *et al.* 2000). More than 30 species belonging to the genus *Blastocrithidia* have been described, which infect dipters (mosquitoes and flies) and hemipters. The epimastigote forms of *Blastocrithidia* sp can be cultivated *in vitro* and the cells measure between 10 and 50 μm in length, with flagella of about 5 to 12 μm . This trypanosomatid does not infect humans and although it is phylogenetically distant from *Trypanosoma cruzi*, presents many morphological, biochemical and immunological characteristics, which are similar; in *B. culicis* culture some trypomastigotes can occur ranging from 2-7 % (Souza 1994, d'Ávila-Levy *et al.* 2005). Due to these morphological similarities among trypanosomatids, the gender *Blastocrithidia* provides to be an excellent model system for the investigation of *Trypanosoma cruzi* and Chagas' disease.

In previous studies we showed the presence of a L27 ribosomal protein in *T. cruzi* (Perone *et al.* 2003) using RT-PCR; this strategy resulted in the cloning sequencing and expression of an unexpected protein, which codes for another ribosomal protein, L17, in *Blastocrithidia culicis* (BcL17). Both the L17 and L27 ribosomal proteins appear to belong to the peptidyl-transferase site within the ribosome, and are therefore part of the key step in protein synthesis (Monro *et al.* 1969). However, studies in *Escherichia coli* have shown that the location of the L17 protein in the ribosome is still controversial (Bischof *et al.* 1995). Both ribosomal proteins (L17 and L27) bind spiramycin derivatives (Bischof *et al.* 1995), being therefore, compounds of the macrolides connection sites in the ribosome (Vazquez 1979). Spiramycin macrolide derivatives act in the initial stages of peptide formation and compete with aminoacyl-tRNAs for the A site (Dinos *et al.* 1993). This effect is comparable with the typical inhibition of the peptidyl-transferase provoked by chloramfenicol (Vazquez 1979).

We report herein the cloning, sequencing, structural analysis and gene expression of the L17 ribosomal protein from *Blastocrithidia culicis* (BcL17). The results show details of the amino acid sequence of the protein, features of its physical chemistry and its similarity with homologues from other trypanosomatids. The

expressed recombinant protein was used to produce antibody that reacted with the native protein in parasite extracts.

MATERIALS AND METHODS

***Blastocrithidia culicis* parasites.** *Blastocrithidia* epimastigotes (ATCC14806) were cultured *in vitro* at 28°C in LIT medium (Fernandes and Castellani 1966) supplemented with 10% fetal bovine serum, until reaching a total cell count of approximately 10⁷ forms.

Genomic DNA, total RNA and nuclear extract preparation. The genomic DNA and total RNA were prepared using DNAzol® and Trizol® reagents (Invitrogen), respectively. 400 μl of nuclear extract were prepared using protease inhibitors (50 mM PMSF, leupeptin 2 $\mu\text{g}/\text{ml}$, 0.5M DTT) following the protocol described by Kovacs *et al.* (1993). The proteins were precipitated with 100 % cold acetone.

cDNA preparation, amplification and sequencing. RT-PCR was carried out using the 3'RACE kit (Life Technologies) for cDNA synthesis in the case of the trypanosomatid. The PCR reaction was performed using the oligonucleotide (5'-GCTGTACTATATTGTGGCTTC-3') designed from the nucleotide sequence of the 5'-UTR gene region that codes for the L27 ribosomal protein in *Trypanosoma cruzi*. The PCR product was sized on agarose electrophoresis and purified from the gel using the Qiaquick gel extraction kit (Qiagen). The PCR product was cloned using the TOPO TA Cloning for sequencing kit (pCR®4-TOPO® vector - Invitrogen), transformed in *E. coli* competent cells and sequenced on an ABI PRISM 377 DNA Sequencer (Perkin Elmer), using Big Dye Terminator (Applied Biosystem). Sequence-comparison analysis of the protein BcL17 was carried out using the program GENE RUNNER version 3.0 (Hastings Software, Inc.).

Sequence analysis. The BLASTn and BLASTp tools were used for the identification of sequences of interest (www.ncbi.nlm.nih.gov/blast). The BcL17 sequence was analyzed for functional motifs or domains using the PROSITE (http://myhits.isb-sib.ch/cgi-bin/motif_scan) and Conserved Domain (www.ncbi.nlm.nih.gov/Structure/) databases. Secondary structure prediction was accomplished using the PSIPRED Protein Structure Prediction Server (<http://bioinf.cs.ucl.ac.uk/psipred/>) and the isoelectric point predicted using GENE RUNNER version 3.0 (Hastings Software, Inc.). The BcL17 sequence was aligned with other sequences of ribosomal proteins obtained from the NCBI database (www.ncbi.nlm.nih.gov) using the BioEdit Sequence Alignment Editor (Hall 1999).

Phylogenetic analysis. For the phylogenetic studies, the BcL17 sequence was aligned with ribosomal proteins of the other organisms using BioEdit version 7.0.0 (Hall 1999) and the phylogenetic tree was built using MEGA (Molecular Evolutionary Genetics Analysis) version 2.1 (Kumar *et al.* 2001) with the distance methodology (distance-p) and neighbor-joining algorithm. Bootstrap values of 1,000 replications were used.

Southern blot analysis. Ten μg of *Blastocrithidia culicis* genomic DNA were fully digested with *Hind*III (0.6 U/ml - Amersham Biosciences) and *Pst*I (0.4 U/ml - Life Technologies), which does not

cut inside the ORF, electrophoresed on 0.8% agarose gel and transferred to a nylon membrane (Amersham Biosciences) using 10X SSC (0.3 M sodium citrate, pH 7.0 and 3 M sodium chloride). Labeling and hybridization were performed using the ECL Nucleic Acids Labelling and Detection System kit (Amersham Biosciences) following the manufacturer's instructions. The membrane was exposed to the film for 30 min at room temperature.

Expression of His-tagged 20 kDa protein and immunization of rabbits. To clone the 20 kDa cDNA into the pET28a vector (Novagen), *Nde*I and *Xho*I restriction sites were added via PCR amplification to the N and C termini, respectively, of the 20 kDa EST. The PCR fragment was cloned into the pET expression vector thus encoding the full-length 20 kDa protein fused to a N-terminal His tag. Correct orientation and the presence of an ORF were verified by DNA sequencing. The recombinant protein was expressed in *Escherichia coli* BL21 cells for 3 h at 37°C after induction with 1 mM IPTG (isopropyl- β -D-thiogalactopyranoside). The protein was found both on inclusion bodies (insoluble) and supernatant (soluble fraction); this latter was separated by preparative 15 % SDS-PAGE, and the interest band (approximately 17 kDa) was excised the gel, cut with sterile scissor, mixed with 1 ml of saline solution and stored -20°C. The concentration of the protein was estimated using the standard molecular weight according with the manufacturer (Bio-Rad). The excised band (approximately 200 μ g of recombinant protein) was homogenized in 1X PBS (Phosphate Buffer Saline) plus complete Freund adjuvant (GibcoBRL) and then inoculated in rabbits (70-75 μ g of protein/inoculation). Two boosters with incomplete Freund adjuvant were done after 15 days each one. Pre-immune serum (non-absorbed with *E. coli* total protein lysate) was collected before rabbit immunization. The immune serum was previously absorbed with *E. coli* total protein lysate and the polyclonal antibodies were tested by Western blot against the BcL17 recombinant protein to titration.

Trypanosoma cruzi nuclear extracts and ribosomal proteins. *T. cruzi* epimastigotes of two different strains (Bol and Y) were cultured *in vitro* at 28°C in LIT medium (Fernandes and Castellani 1966) supplemented with 10 % fetal bovine serum for 7-8 days and the parasites were used to prepare 400 μ l of nuclear extracts using protease inhibitors (50 mM PMSF, leupeptin 2 μ g/ml, 0.5 M DTT) following protocol described by Kovacs *et al.* (1993). The proteins were precipitated with 100 % cold acetone and resuspended in 40 μ l SDS-PAGE loading buffer (20 μ l of samples were loaded per slot). *T. cruzi* (Tulahuen strain) ribosomal fraction proteins were kindly provided by Dr. Mariano Levin lab (INGEBI-CONICET, Buenos Aires, Argentina).

Western blot analysis. Protein fractions (recombinant BcL17 and *T. cruzi* ribosomal proteins) and total and nuclear parasite extracts were separated on 15 % SDS-PAGE gel and transferred to nitrocellulose using Hoefer SemiPhor (Pharmacia) and transfer buffer (25 mM Tris, 192 mM glycine, 20 % methanol). The membrane was blocked using 3 % low fat milk (1h at room temperature), washed 3 times with PBS-Tween 20 and incubated with anti-BcL17-antibody diluted in 2 % low fat milk/PBS for 18 hours at 4°C under agitation. After washings (PBS-Tween 20), the blot was incubated 1 hour with protein-A-horseradish peroxidase (Sigma, 1:5,000 in 2 % low fat milk/PBS) at room temperature and revealed using DAB (0.6 g in 5 ml of 0.05 M Tris-HCl, pH 7.6, and 1 μ l/ml H₂O₂) for 10 min. Scanner captured the bands.

RESULTS

The cDNA insert of the BcL17 clone contains 534 nucleotides and includes a single open reading frame together with the 3' flanking region. The open reading frame of 420 nucleotides codes for a 139 amino acid protein, with an estimated molecular mass of 15,044 Da. The nucleotide sequence (GenBank accession number AAY78546) and the deduced amino acid sequence are shown in Fig. 1. The initiation codon is located at position one and the stop codon (TAA) at position 420. The BcL17 protein shows an excess of basic residues (9.22 % arginine and 9.22 % lysine) over acidic ones and a theoretical isoelectric point (pI) of 10.11. These residues confer a high level of positive charge to the protein, a common feature of ribosomal and histone proteins, which are involved in interactions with nucleic acids in eukaryotic organisms (Aslund *et al.* 1994).

BLAST analysis of the *Blastocrithidia culicis* L17 protein with other L17 sequences of different trypanosomatids demonstrated 96% identity with the homologue from *Leishmania infantum* and 82% with that from *Trypanosoma cruzi*. The identity detected with other L17 sequences belonging to different non-trypanosomatid organisms was lower than expected: 76 % with *Pan troglodytes* (XP_511444) and *Arabidopsis thaliana* (AAB70426), 70 % with *Homo sapiens* (AAH62716) and 67 % with *Drosophila melanogaster* (NP_523813).

The protein displays highly conserved regions with respect to other members of the protein family as well as zones with remarkable differences. The L17 signature sequence is located between amino acid positions 78 and 104, which is similar to that of trypanosomatids but differs from that shown by proteins from the other species considered. There are two myristoylation sites at position 18-GLPVGA and 123-GSTIAG and three protein kinase C (PKC) phosphorylation sites at positions 40, 63 and 86, respectively (Fig. 1).

The macrolide binding sequence (Bischof *et al.* 1995) is present between Cys¹¹ and Lys³⁷ and is highly conserved, displaying high levels of sequence identity (close to 90 %) not only with those from other Trypanosomatidae, but also with *Arabidopsis thaliana*, *Drosophila* and humans. In the case of the L17 ribosomal protein from *Blastocrithidia culicis*, the possible lysine for ligation to the macrolide seems to be present at position 35. Between positions 73 and 88 (KKVLANAVIIRQRKSWR) a nuclear location sequence

```

      10      20      30      40      50      60
...|...|...|...|...|...|...|...|...|...|...|...|
ATGGGTAAGGAACAGATCAACGTTAAGGGTTGCCGCTTCCGCGTGTCCGTCGGTCTCCCC
(M) G K E Q I N V K G C R F R V S V G L P

      70      80      90      100     110     120
...|...|...|...|...|...|...|...|...|...|...|...|
GTCGGCGCCGTCGTGAACTGCGCGGATAACACCGGTGCCAAGAACCTGTACGTGATTTC
V G A V V N C A D N T G A K N L Y V I (S)

      130     140     150     160     170     180
...|...|...|...|...|...|...|...|...|...|...|...|
GTC AAGGGTTACCACGGCCGCTGAACCGTCTGCCCTCTGCGGCCCTCGGCGATATGGT
(V K) G Y H G R L N R L P S A A L G D M V

      190     200     210     220     230     240
...|...|...|...|...|...|...|...|...|...|...|...|
ATGTGCTCCGTGAAGAAAGGCAAGCCGGA ACTCCGCAAGAAGGTGCTCAACGCTGTCATC
M C (S V K) K G K P E L R K K V L N A V I

      250     260     270     280     290     300
...|...|...|...|...|...|...|...|...|...|...|...|
ATCCGTCAGCGCAAGAGCTGGCGCCGCAAGGACGGCACCCTCATCTACTTTGAGGATAAC
I R Q R K (S W R R) K D G T V I Y F E D N

      310     320     330     340     350     360
...|...|...|...|...|...|...|...|...|...|...|...|
GCTGGCGTCATCGTTAACCCCAAGGGTGAGATGAAGGGCTCCACCATTGCCGGCCCCGTC
A G V I V N P K G E M K G S T I A G P V

      370     380     390     400     410     420
...|...|...|...|...|...|...|...|...|...|...|...|
GCGAAGGAATCTGCGGACCTCTGGCCCAAGATCTCCACCACGCCCTGCCATCGTCTAA
A K E S A D L W P K I S T H A P A I V *

```

Fig. 1. Nucleotide and amino acid sequences of *Blastocritidia culicis* L17 ribosomal protein (BcL17). The nucleotide sequence is given in the 5' to 3' direction. Grey circle - methionine (start codon); grey rectangle - L17 signature; circle - PKC sites; rectangle - N-myristoylation sites; * - stop codon.

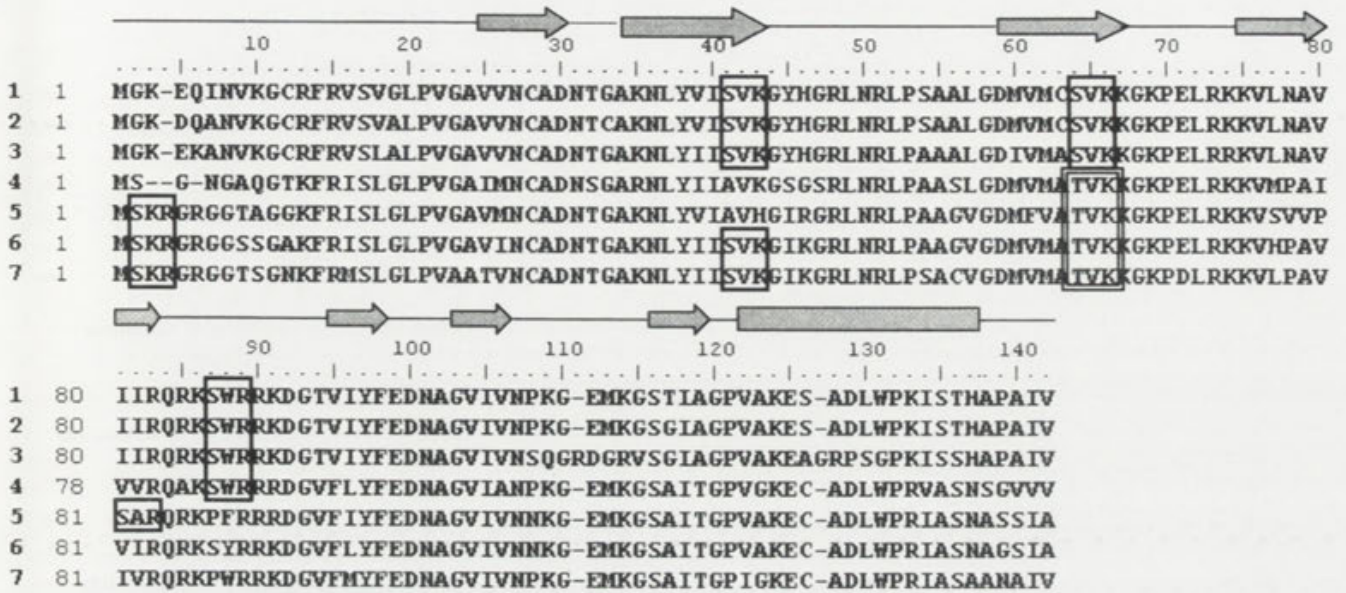


Fig. 2. Comparison of the amino acid sequences of L17 ribosomal proteins among eukaryotic species. 1 - *Blastocrithidia culicis* (AAY78546); 2 - *Leishmania infantum* (AF097022); 3 - *Trypanosoma cruzi* (gi 2500266); 4 - *Saccharomyces cerevisiae* (gi 13274); 5 - *Drosophila melanogaster* (gi 1350673); 6 - *Homo sapiens* (gi 266927); 7 - *Arabidopsis thaliana* (gi 2459420). Single line boxes, PKC phosphorylation sites associated with serine; double line boxes, threonine phosphorylation sites. Regions of secondary structure in *Blastocrithidia culicis* L17 are indicated above the alignment. The α -helices are displayed as open bars; β -strands as large arrows and coil as lines.

(NLS) was detected, which facilitates protein transport between nucleus and cytoplasm (Miyamoto *et al.* 1999).

Figure 2 shows the comparison between L17 from *Blastocrithidia culicis* and the corresponding L17 ribosomal proteins from different sources, representing both lower and higher eukaryotes. In the protozoan proteins there are three PKC phosphorylation sites, all of which are associated with serine. In all other species considered, threonine is present in the most highly conserved site, at position 63. Protozoan proteins do not possess the phosphorylation sites at position 2, whilst *Saccharomyces cerevisiae* and *Drosophila melanogaster*, lack the site at position 40. On the other hand, *D. melanogaster* presents an additional site at position 81. The secondary structure prediction of *Blastocrithidia culicis* L17 protein showed that there is a predominance of β -strand and coil, with the prediction of only one α -helix in the C-terminal region. The conservation of this region among the different organisms analyzed indicates that the helix is probably maintained in all such species.

The multiple sequence alignments that were used for the phylogenetic analyses revealed that the first ten amino acids are only conserved among the trypanosomatids (data not shown). The phylogenetic

reconstruction showed the presence of well-divided groups (Chordata, Nematoda, Arthropoda, Kinetoplastida, Coccidia, Fungi and Plantae). Among Trypanosomatidae, the L17 protein of *Blastocrithidia culicis* is closer to *Leishmania infantum* than *Trypanosoma cruzi*, as shown in Figure 3.

Southern blot analysis of *Blastocrithidia culicis* genomic DNA (Fig. 4) digested with two restriction enzymes, which did not cleave inside the ORF of the BcL17 probe, suggested that this parasite presents only a single copy of the gene.

Western blot results demonstrate that the anti-BcL17 antibody recognizes the presence of the same ribosomal protein (L17) either in *Blastocrithidia culicis* and *T. cruzi* strains nuclear extracts (Figs 5A and B: lane 4, Blas, Bol, Y), even slightly different patterns of molecular weight size as compared with the *T. cruzi* purified ribosomal proteins (Rib). An arrow indicates the 17 kDa recombinant protein (Figs 5A, lane 3 and B, L17). The reactivity bands that appeared in pre-immune serum are due to the lack of absorption with *E. coli* proteins, since there was not any reaction with trypanosomatid total and nuclear extracts (data not shown). As expected, no reaction occurred after second conjugate incubation

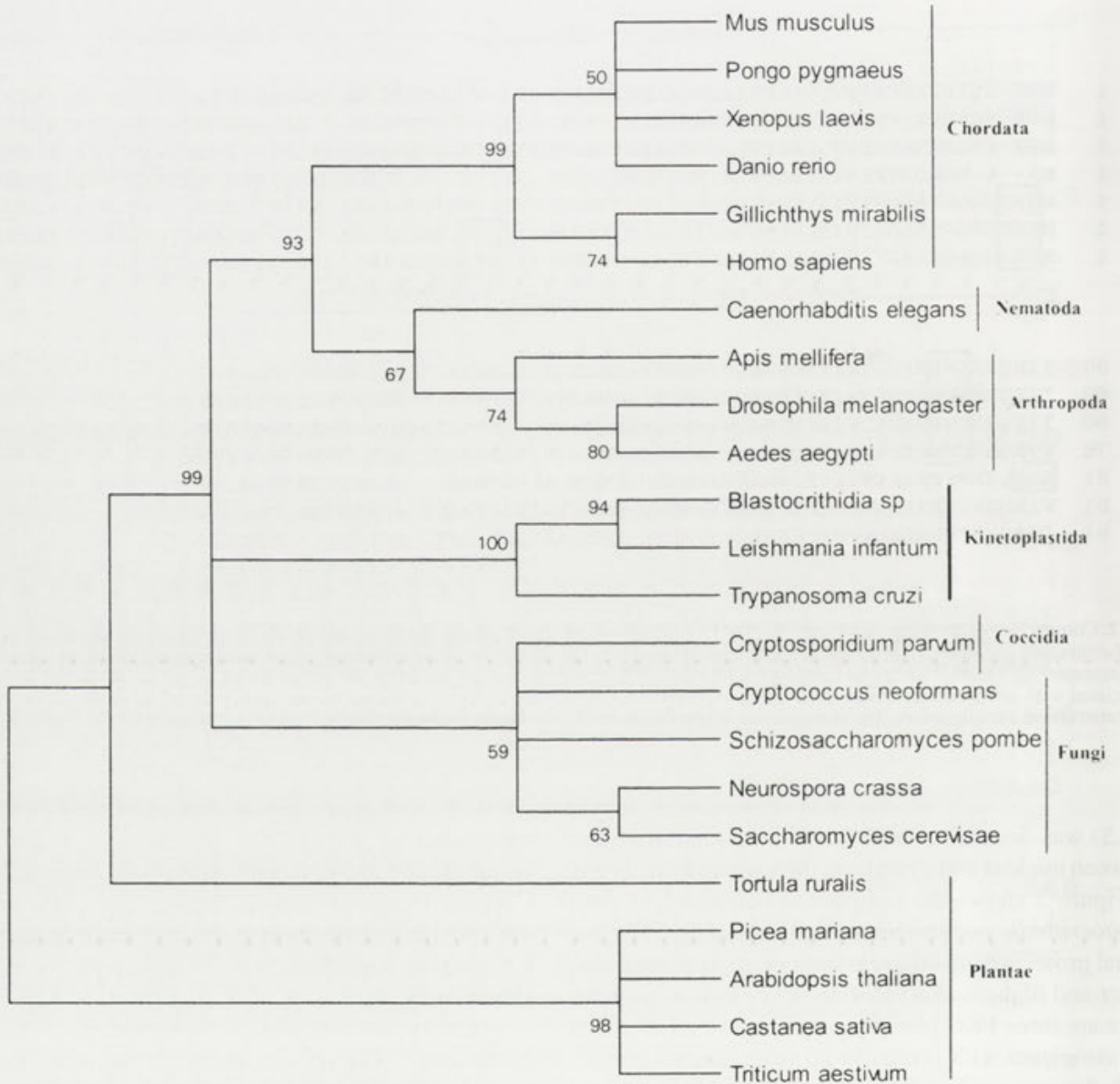


Fig. 3. Molecular phylogenetic tree based on comparison of amino acid sequences of *Blastocrithidia culicis* (AAY78546) L17 ribosomal protein with those of others species: *Leishmania infantum* (gi 3851618); *Trypanosoma cruzi* (gi 2500266); *Arabidopsis thaliana* (AA042332); *Caenorhabditis elegans* (AAK18857.1); *Castanea sativa* (AAK25758.1); *Apis mellifera* (XP_392812.1); *Triticum aestivum* (AAW50991.1); *Picea mariana* (AAC32130.1); *Danio rerio* (NP_957026.1); *Mus musculus* (NP_075029.1); *Gillichthys mirabilis* (AF266222); *Cryptococcus neoformans* (CNBK0380); *Homo sapiens* (AAH62716.1); *Pongo pygmaeus* (CAH89715.1); *Drosophila melanogaster* (NP_523813.1); *Tortula ruralis* (AAD23966.1); *Aedes aegypti* (AAL85622.1); *Schizosaccharomyces pombe* (CAA15912.1); *Cryptosporidium parvum* (EAK90115.1); *Neurospora crassa* (XP_330093.1), *Saccharomyces cerevisiae* (gi 132744); *Xenopus laevis* (AAH73541.1). Outgroup: *Triticum aestivum*.

(Fig. 5A, lane 5). Two ribosomal proteins (40 and 47 kDa, approximately, indicated by arrows in the Fig. 5B, Rib) appeared either in *T. cruzi* isolated ribosomal proteins and *B. culicis* total (Fig. 5A, lane 4) and

nuclear (Fig. 5B, Blast) extracts corroborating with the findings showed in the phylogenetic reconstruction (Fig. 3). The differences on the reactivity among the trypanosomatid strains are still unknown.

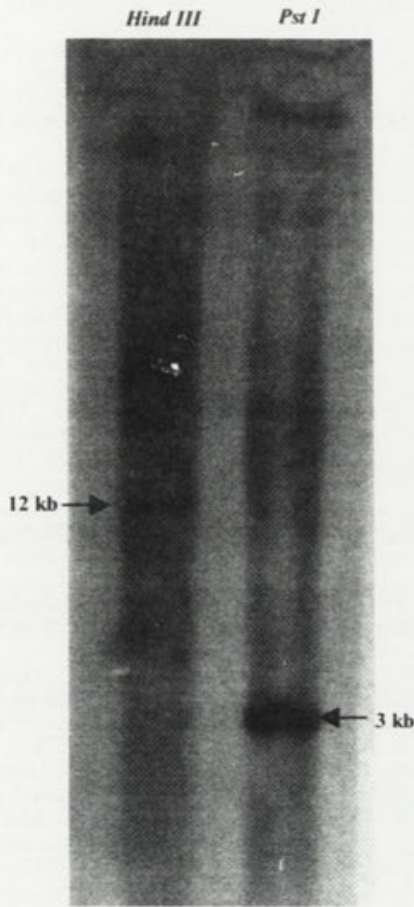


Fig. 4. Southern blot analysis of BcL17 encoding gene in *Blastocrithidia culicis* genomic DNA using *Hind*III and *Pst*I as restriction enzymes. The molecular weight (kb) of the bands is indicated.

DISCUSSION

This work presents results of the cloning and sequencing of the gene encoding the L17 ribosomal protein from the parasite *Blastocrithidia culicis*. The analysis of sequence alignments showed that the nucleotide sequence of the *Blastocrithidia culicis* L17 gene is very similar to those of the L17 ribosomal proteins from *Leishmania infantum* (96 %) and *Trypanosoma cruzi* (82 %) (gi: D87216 and gi: AF097022, respectively). The BcL17 amino acid sequence also showed high levels of identity with ribosomal proteins present in other higher eukaryotes, but presented structural differences when compared with homologous proteins from other organisms. These differences include the length of the amino acid sequence, 139 residues in the case of BcL17

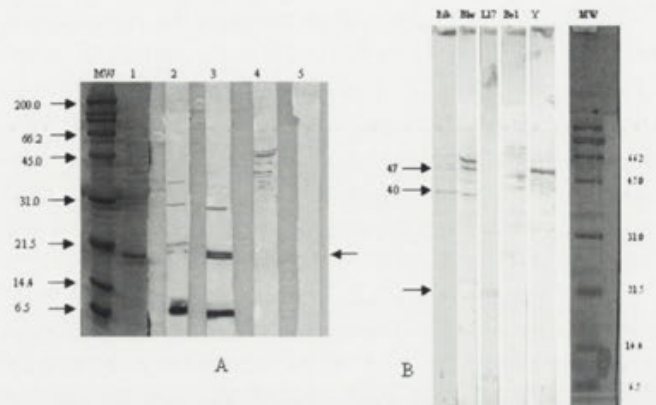


Fig. 5. Western blot analysis of BcL17-recombinant protein (A), *Blastocrithidia culicis* and *T. cruzi* native proteins (B) with anti-BcL17 antibody. **A:** 1 - SDS-PAGE (15%) of recombinant protein lysate (soluble fraction); 2, 3, 5 - semi-purified BcL17 (17 kDa) assayed, respectively, with pre-immune serum (1:400, non-*E. coli* adsorbed), anti-BcL17 antibody (1:50, *E. coli*-adsorbed) and protein A-peroxidase conjugate as a negative control; 4 - *B. culicis* total extract. **B:** *T. cruzi* (Tulahuen strain) purified ribosomal proteins (Rib), *T. cruzi* nuclear extracts (Bol and Y strains) and *Blastocrithidia culicis* nuclear extract (Blas) and BcL17-recombinant protein (L17). The arrows indicate the BcL17-recombinant protein and the putative native proteins present in the parasite extracts comparing with purified ribosomal proteins (40 and 47 kDa). MW - molecular weight standards in kDa.

protein, which is smaller than that found in *Sacharomyces cerevisiae*, *Drosophila* or humans (Mukhopadhyay *et al.* 1988, Suzuki and Wool 1991).

The positions of the PKC phosphorylation sites are identical among the trypanosomatids. Although these are also highly conserved in higher eukaryotes, even the most conserved site presents the substitution of a serine in Trypanosomatidae by a threonine in the other organisms analyzed. *N*-miristylation and a bipartite nuclear localization sequence (NLS) were also identified. These regions are also conserved in other ribosomal proteins, for example, L14 of *Leishmania brasiliensis* (González *et al.* 2004).

The phylogenetic proximity among the trypanosomatids was confirmed by analysis of the amino acid sequences, demonstrating that *Blastocrithidia culicis* is closest to *Leishmania infantum*. However, the Western blot results also suggest that the BcL17 ribosomal proteins share common epitopes with isolated *T. cruzi* ribosomal proteins, even in TriTryp genomes (*T. brucei*, *T. cruzi* and *Leishmania*), this protein has been described as a 50S putative ribosomal protein L17.

Southern blot analysis demonstrated the presence of only one copy of L17 in *Blastocrithidia culicis*. Similar experiments with *Leishmania infantum* also demonstrated the presence of only one copy in genomic DNA, despite the fact that Northern blot analysis suggested the existence of two non-identical copies. However, in this latter case allele polymorphism of the gene cannot be discharged (González-Aseguinolaza *et al.* 2000).

The affinity of the L17 ribosomal protein for spiramycin and derivatives, also observed in other organisms, may represent a useful means to investigate the structural components of the peptidyl-transferase center of the ribosome, because the proteins that interact strongly with the spiramycin molecule have been shown to be close to or part of this region (Walleczek *et al.* 1988, 1990). Analysis of a multiple alignment involving ribosomal proteins from different organisms which vary from lower eukaryotes to man demonstrated that a lysine residue is possibly involved in macrolide binding. This was predicted to be position Lys³⁵ in *Blastocrithidia culicis*, which is highly conserved. Among the 23 organisms used in these analyses, only a hypothetical protein from *Neurospora crassa* (XP_330093.1) and a ribosomal L23 (L17) of *Saccharomyces cerevisiae* (gi 132744) presented an arginine substituting the lysine residue at this position (data not shown).

The mode of action of the macrolides has been mainly attributed to the different sugars moieties, which are part of the lactone-ring (Vazquez 1979). The knowledge of the possible mechanism of action of this therapeutic class of compounds associated with the understanding of the structure and function of each structural component of the ribosome may represent an important tool for the discovery of new and more specific therapeutic agents. The findings about BcL17-common epitopes sharing with *T. cruzi* ribosomal protein would open a possibility to better evaluate this issue.

Acknowledgements. This research was partially supported by a grant from PADC-FCF-UNESP (2001/06-1). L.R.M. was the recipient of a fellowship from FAPESP (03/13830-0). *Blastocrithidia culicis* (ATCC14806) were a kind gift from Dr. Wanderley de Souza Lab (Instituto de Biofísica Carlos Chagas Filho - Universidade Federal do Rio de Janeiro - Brazil). We are indebted to Richard Garratt for aiding in the elaboration of the final text.

REFERENCES

- Aslund L., Carlsson L., Henriksson J., Rydaker M., Toro G. G., Galanti N., Pettersson U. (1994) A gene family encoding heterogeneous histone H1 proteins in *Trypanosoma cruzi*. *Mol. Biochem. Parasitol.* **65**: 317-330
- d'Ávila-Levy C. M., Araujo F. M., Vermelho A. B., Soares R. M. A., Santos A. L. S., Branquinha M. H. (2005) Proteolytic expression in *Blastocrithidia culicis*: influence of the endosymbiont and similarities with virulence factors of pathogenic trypanosomatids. *Parasitology* **130**: 413-420
- Bischof O., Urlaub H., Kruff V., Wittman-Liebold B. (1995) Peptide environment of the peptidyl transferase center from *Escherichia coli* 70S ribosomes as determined by thermoaffinity labeling with dihydrospiramycin. *J. Biochem.* **270**: 23060-23064
- Dinos G., Synetos D., Coutsogeorgopoulos C. (1993) Interaction between the antibiotic spiramycin and a ribosomal complex active in peptide bond formation. *Biochemistry* **32**: 10638-10647
- Fernandes J. F., Castellani O. (1966) Growth characteristics and chemical composition of *Trypanosoma cruzi*. *Exp. Parasitol.* **18**: 195-202
- González A. C., Thomas M. C., Martínez-Carretero E., Carmelo E., López M. C., Valladares B. (2004) Molecular and immunological characterization of L14 ribosomal protein from *Leishmania brasiliensis*. *Parasitology* **128**: 139-147
- González-Aseguinolaza G., Taladriz S., Marquet A., Larraga V. (2000) Differential protein kinase C phosphorylation sites in the L17 ribosomal protein from *Leishmania infantum*. *Parasitol. Res.* **86**: 36-40
- Hall T. A. (1999) BioEdit: a user-friendly biological sequence alignment editor and analysis program for Windows 95/98/NT. *Nucl. Acids. Symp. Ser.* **41**: 95-98
- Kovacs S., O'Neil J., Watcharapijarn J., Moe-Kivan C., Vijay S., Silva V. (1993) Eubacterial components similar to small nuclear ribonucleoproteins and capped RNAs in a cyanobacterium and gram-positive eubacterium. *J. Bacteriol.* **175**: 1871-1878
- Kumar S., Koichiro T., Ingrid B. J., Nei M. (2001) Molecular Program Evolutionary Genetics Analysis (MEGA - Version 2.1)
- Lukes J., Jirku M., Dolezel D., Kral'ová I., Hollar L., Maslov D. A. (1997) Analysis of ribosomal RNA genes suggests that *Trypanosoma* are monophyletic. *J. Mol. Evol.* **44**: 521-527
- Maslov D. A., Podlipaev S. A., Lukes J. (2001) Phylogeny of the kinetoplastida: Taxonomic problems and insights into evolution of parasitism. *Mem. Inst. Oswaldo Cruz* **96**: 397-402
- Miyamoto L. C., Azeredo V. M., Dietze R., Callahan H. L., Bernan J. D., Grogl M. N. (1999) Humoral immune response among mucosal and cutaneous leishmaniasis patients caused by *Leishmania*. *J. Parasitol.* **85**: 1076-1083
- Monro R. E., Staehelin H. F., Celma M. I., Vazquez D. (1969) The peptidyl-transferase activity of ribosomes. *Cold Spring Harbor Symp. Quant. Biol.* **34**: 357-368
- Mukhopadhyay N. K., Saha A. K., Lovelace J. K., Silva R. D., Sacks D. L., Glew R. H. (1988) Comparison of the protein kinase and acid phosphatase activities of five species of *Leishmania*. *J. Protozool.* **35**: 601-607
- Neves D. P., Melo A. L., Genaro O., Linardi P. M. (2000) Parasitologia Humana. (Ed. Atheneu). Sao Paulo, SP, 27-72
- Perone D., Santos M. A. M., Peixoto M. S., Cicarelli R. M. B. (2003) *Trypanosoma cruzi*: identification and characterization of a novel ribosomal protein L27 (TrL27) that cross-reacts with an affinity-purified anti-Sm antibody. *Parasitology* **126**: 577-583
- Stevens J. R., Gibson W. (1999) The molecular evolution of trypanosomes. *Parasitol. Today* **15**: 432-437
- Souza M. A. (1994) Trypomastigotes in cultures of *Blastocrithidia culicis* (Novy, MacNeal *et* Torrey, 1907) (Kinetoplastida: Trypanosomatidae). *Mem. Inst. Oswaldo Cruz* **89**: 111-112
- Suzuki K., Wool G. I. (1991) The primary structure of rat ribosomal protein L17. *Biochem. Biophys. Res. Commun.* **178**: 322-328
- Vazquez D. (1979) Inhibitors of protein synthesis. *Mol. Biol. Biochem. Biophys.* **30**: 120-126
- Walleczek J., Schüler D., Stöffler-Meilicke M., Brimacombe R., Stöffler G. (1988) A model for the spatial arrangement of the proteins in the large subunit of the *Escherichia coli* ribosome. *EMBO J.* **7**: 3571-3576

- Walleczek J., Albrecht-Ehrlich R., Stoffler G., Stoffler-Meilicke M. (1990) Three-dimensional localization of the NH₂- and carboxyl-terminal domain of ribosomal protein S1 on the surface of the 30S subunit from *Escherichia coli*. *J. Biol. Chem.* **265**: 11338-11344
- Wright A. D., Feng S. L. S., Martin D. S., Lynn D. H. (1999) Phylogenetic position of the kinetoplastids, *Cryptobia bullocki*, *Cryptobia catostomi* and *Cryptobia salmositica* and monophyly

of the genus *Trypanosoma* inferred from small subunit ribosomal RNA sequences. *Mol. Biochem. Parasitol.* **99**: 69-76

Received on 21st March, 2006; revised version on July 3rd, 2006; accepted on 13th September, 2006

Journal of Cellular Biochemistry
Volume 80, Number 1, 2000
© 2000 Wiley-Liss, Inc.

Journal of Cellular Biochemistry
Volume 80, Number 1, 2000
© 2000 Wiley-Liss, Inc.

Journal of Cellular Biochemistry
Volume 80, Number 1, 2000
© 2000 Wiley-Liss, Inc.

Journal of Cellular Biochemistry
Volume 80, Number 1, 2000
© 2000 Wiley-Liss, Inc.

Journal of Cellular Biochemistry
Volume 80, Number 1, 2000
© 2000 Wiley-Liss, Inc.

Journal of Cellular Biochemistry
Volume 80, Number 1, 2000
© 2000 Wiley-Liss, Inc.

Journal of Cellular Biochemistry
Volume 80, Number 1, 2000
© 2000 Wiley-Liss, Inc.

Journal of Cellular Biochemistry
Volume 80, Number 1, 2000
© 2000 Wiley-Liss, Inc.

Journal of Cellular Biochemistry
Volume 80, Number 1, 2000
© 2000 Wiley-Liss, Inc.

Intraspecific Genetic Divergence of *Paramecium bursaria* and Re-construction of the Paramecian Phylogenetic Tree

Ryo HOSHINA, Sayaka HAYASHI and Nobutaka IMAMURA

Department of Bioscience and Biotechnology, Faculty of Science and Engineering, Ritsumeikan University, Kusatsu, Shiga, Japan

Summary. *Paramecium bursaria*, a species belonging to the genus *Paramecium*, is quite unique in that the species intracellularly maintains several hundreds of symbiotic algae. This species has been regarded as firstly branched-off species within this genus, and reported its higher genetic variation. We determined rDNA 5' half regions of 13 strains of *P. bursaria*, and investigated their intraspecific genetic divergences with comparisons of 18S rDNA and internal transcribed spacer 2 (ITS2). The 18S rDNA divergence among the strains of *P. bursaria* reached 1.61% which definitely greater than that of *P. caudatum*, *P. multimicronucleatum* and *P. aurelia* complex, and also greater than some interspecific relations (e.g. between *P. jenningsi* and *P. schewiakoffi*). These results seemed to be caused by the strains used for the experiments; we used large number (14) of *P. bursaria* strains and small number of others (four *P. caudatum*, three *P. multimicronucleatum* and three *P. aurelia* complex strains). Comparison of the ITS2 region using 10 *P. bursaria*, 13 *P. caudatum*, 11 *P. multimicronucleatum* and 18 *P. aurelia* complex strains showed inverted results: *P. multimicronucleatum* and *P. aurelia* complex diverged greater than *P. bursaria* in the quantitative (number of nucleotide substitutions) as well as the qualitative sense (presence/absence of [hemi-] compensatory base change). Increasing the divergent sequence number occasionally changed the topology of the phylogenetic tree. We re-evaluated the phylogenetic relationships of *Paramecium* spp. as inferred from 18S rDNA with our 20 added paramecian sequences. The trees indicated that paramecia divided into four lineages: i) *P. bursaria*, ii) *P. duboscqui* and *P. putrinum*, iii) *P. calkinsi*, *P. jenningsi*, *P. nephridiatum*, *P. polycaryum*, *P. woodruffi*, and *P. aurelia* complex, and iv) *P. caudatum*, *P. multimicronucleatum* and *P. schewiakoffi*; in strict correspondence with the latest subgeneric concept of „*Chloroparamecium*“, „*Helianter*“, „*Cypriostomum*“ and „*Paramecium*“, respectively. „*Chloroparamecium*“ and „*Helianter*“ of which there are similar characteristics were claded, as were „*Cypriostomum*“ and „*Paramecium*“.

Key words: CBC, „*Chloroparamecium*“, „*Cypriostomum*“, „*Helianter*“, ITS2, „*Paramecium*“, 18S rDNA, phylogeny.

Abbreviations: CBC - compensatory base change, ITS - internal transcribed spacer, ML - maximum likelihood, MP - most parsimonious, NJ - neighbor joining, OTU - operational taxonomic unit.

INTRODUCTION

The common freshwater ciliate, *Paramecium* spp. has been well and widely studied for two hundred

years. Early microscopic technology caused insufficient descriptions, and undeveloped methods concerning species identification resulted in many dubious species (Wichterman 1953, 1986). With the development of modern techniques, e.g., electron microscopy and staining techniques (Fokin 1986, 1997; Shi *et al.* 1997; Fokin and Chivilev 1999; Fokin *et al.* 1999), the species concepts have been reorganized. Consequently, 17 paramecian species (as the *P. aurelia* complex con-

Address for correspondence: Nobutaka Imamura, Department of Bioscience and Biotechnology, Faculty of Science and Engineering, Ritsumeikan University, 1-1-1 Noji Higashi, Kusatsu, Shiga 525-8577, Japan; Fax: +81-77-561-2659; E-mail: imamura@se.ritsumei.ac.jp

verted into one species) are now recognized as valid (Fokin *et al.* 2004).

Among *Paramecium* spp., morphology and other characteristics are diverse, which have brought subgeneric concepts into this genus (Woodruff 1921; Jankowski 1969, 1972). The latest concept based upon morphometric, biological and molecular differences divides the above 17 species into four subgenera: „*Chloroparamecium*”, „*Helianter*”, „*Cypriostomum*” and „*Paramecium*” (Fokin *et al.* 2004). „*Chloroparamecium*” is composed of only one species *P. bursaria*, and prior studies (Strüder-Kypke *et al.* 2000a, b; Fokin *et al.* 2004) have suggested this species diverged first in the genus *Paramecium*.

If *P. bursaria* is regarded as an “old species”, the intraspecific genetic divergence is possibly larger. In fact, Stoeck *et al.* (1998) reported higher genetic diversities than in other paramecian species. The highest 18S rDNA pairwise distance seen in *P. bursaria* reached 1.57% (gaps were included, Hoshina *et al.* 2005); e.g. the recently described species *P. schewiakoffi* (Fokin *et al.* 2004; GenBank accession no., AJ548821) differed by 0.73% from *P. jenningsi* (AF100311) and by 1.11% from *P. tetraurelia* (X03772).

The sibling species concept seen in *Paramecium* spp. has been investigated with various methods e.g. with isozymes (Allen and Gibson 1971) and random amplified polymorphic DNA (RAPD, Stoeck *et al.* 1998, 2000; Stoeck and Schmidt 1998). However, it is problematic to consider their phylogeny or distance. Coleman (2000, 2005) proposed the utility of internal transcribed spacer 2 (ITS2) sequence comparison for such species or non-species affair. Although this region is a non gene-coding region, it might be limited to primary and secondary sequence variation in the potential gene exchange group. She also showed the applicability of this region for paramecian species, and indicated the linkage between sequence variation and gene exchange. Although the precise cause of above genetic distances in *P. bursaria* are as yet not well known, in this study we compared their ITS2 sequences as well as the 18S rDNA sequences.

We have collected *P. bursaria* strains from studies relating their symbionts (Hoshina *et al.* 2004, 2005) and the other comparative paramecian stocks, and have used 18S rDNA sequence comparison. As a result, we obtained 20 operational taxonomic units (OTUs) of 18S rDNA sequences from *Paramecium* spp. (Hoshina *et al.* 2005 and this study), which more than doubles the number of available sequences compared to other phy-

logenetic assessments based on this sequence (Fokin *et al.* 2004). It is well known that increases in the numbers of sequences frequently changes the phylogenetic tree topology (e.g. Graur and Li 2000, Nei and Kumar 2000). Consequently, we attempted to re-construct the paramecian phylogenetic tree.

MATERIALS AND METHODS

Paramecium bursaria, *P. caudatum*, *P. multimicronucleatum* and *P. tetraurelia* stocks (Table 1) were maintained in aka-endoumame medium (Tsukii *et al.* 1995) or in accordance with CCAP (Culture Collection of algae and Protozoa, UK) instructions, at 25°C with cool white light illumination (16 L: 8 D, 100 µmol photons m⁻² s⁻¹).

For DNA extraction, we used the modified CTAB method (outlined in Hoshina *et al.* 2004), or the DNeasy plant mini kit (Qiagen, GmbH, Düsseldorf, Germany) according to manufacturer's directions. A part of the total DNA used for the following analyses were those obtained by Hoshina *et al.* (2005).

DNA amplification and sequencing primers for ribosomal DNAs are described in Hoshina *et al.* (2005). For ITS amplification, we used the alternative primer sets of *Paramecium*500F (Hoshina *et al.* 2005)/ITS4 (White *et al.* 1990) or *Paramecium*730F (5'-GTGTTTCAGGCAGGTTTCG-3', forward direction)/ITS4. The PCR products were once sequenced directly. Low-quality electrophorograms were observed in the sequences of ITS regions of *P. bursaria* CCAP 1660/12 and 1660/13, which were cloned using the TArget Clone kit (Toyobo, Osaka, Japan) according to manufacturer's recommended protocols.

We compared all available (published by Strüder-Kypke *et al.* 2000a, b; Coleman 2005; Barth *et al.* 2006) and our (Table 1) sequences of *P. bursaria*, *P. caudatum*, *P. multimicronucleatum* and *P. aurelia* complex. 18S rDNA sequences (14 strains of *P. bursaria*, four *P. caudatum*, three *P. multimicronucleatum* and three *P. aurelia* complex) were manually aligned using Clustal X version 1.81 (Thompson *et al.* 1997). For ITS2 comparison, once we made secondary structural models for every sample, these were referred to that of *P. tetraurelia* (Coleman 2005; a brief diagram is shown in Fig. 1). Helix constructions were predicted by mfold version 3.2 (Zuker 2003) and ITS2 sequences (10 *P. bursaria*, 13 *P. caudatum*, 11 *P. multimicronucleatum* and 18 *P. aurelia* complex) were aligned by considering the above secondary structure. Unrooted distance trees based on each 18S rDNA and ITS2 were constructed (Fig. 2) by Neighbor Joining (uncorrected “p” distance) in PAUP version 4.0b10 (Swofford 2000).

For the re-constructing of the paramecian phylogenetic tree, we employed all available paramecian sequences (published by Strüder-Kypke *et al.* 2000a, b; Fokin *et al.* 2004) with 15 other ciliates (see Fig. 3). Once we aligned them using Clustal X, they were compared to available 18S rRNA structures (Comparative RNA Web Site, Cannone *et al.* 2002), manually adjusted, and ambiguous regions lying at hairpin loops, internal loops or bulges were removed. Phylogenetic trees based on this 18S rDNA dataset were constructed using PAUP. For maximum likelihood (ML) analyses, optimal likelihood settings for evolutionary models were determined by Modeltest version 3.6 (Posada and Crandall 1998), which resulted in a model and respective

parameters or proportions for each dataset. With those settings, a heuristic search was performed (nearest-neighbor interchange algorithm, starting tree obtained via neighbor joining). Maximum parsimony (MP) analysis was performed using a heuristic search with the bisection-reconnection option and random sequence addition with 10 replications; gaps were treated as a fifth base. Neighbor Joining (NJ) analysis of Saito and Nei was also performed. The bootstrap probabilities were calculated by all ML (100 replicates), MP (1000) and NJ (1000) analyses.

RESULTS

Sequences and genetic intraspecies diversity of *P. bursaria*

The variation seen in multiple copies of a single locus has been reported in a paramecium (Preer *et al.* 1999). However, most of our electrophorograms from direct sequencing showed definite single peaks. If different sequences were present, their copy number in the genome seems proportionately below our detection level. It probably needs tens or hundreds of subcloning procedure to detect such minor variation, and truthfully, the quest for all minor variation is never ending without

whole genome analysis. Indeed, recent intraspecific studies of paramecia using rDNA cistron also chose

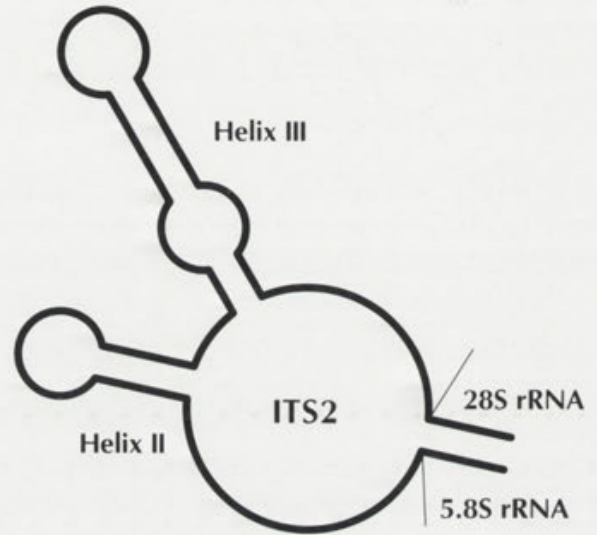


Fig. 1. Secondary structural diagram of paramecian ITS2 modified from Coleman, 2005. ITS2 usually forms a four-fingered hand structure in eukaryotic organisms (Coleman 2003); helices I and IV occasionally evolve rapidly, and in paramecia, these are absent (see Coleman 2005).

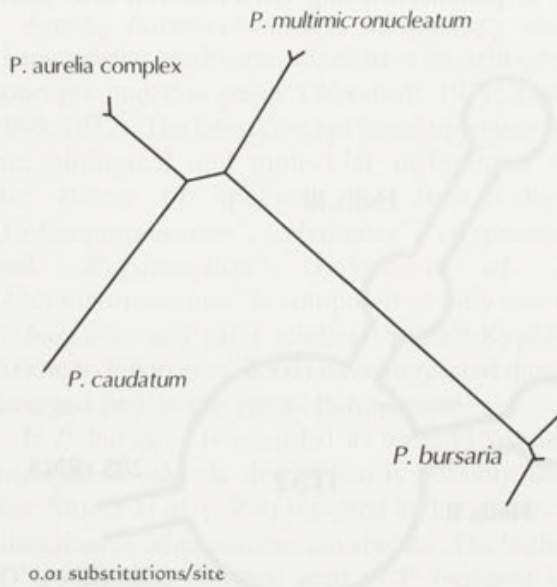
Table 1. Paramecian strains of which DNA sequence were obtained in this study.

Strains	syngen/mating	Collection site	Accession	
			18S rDNA	ITS
<i>P. bursaria</i> OK1	1/I	Aich, Japan	AB206537 ^a	AB252010
<i>P. bursaria</i> So13	1/I	Nagano, Japan	AB206538 ^a	AB252011
<i>P. bursaria</i> F36	1/II	^b	AB206539 ^a	AB252012
<i>P. bursaria</i> KM2	1/I	Shimane, Japan	AB206540 ^a	
<i>P. bursaria</i> Dd1	1/II	Ibaraki, Japan	AB206541 ^a	
<i>P. bursaria</i> Bnd1	1/III	Hiroshima, Japan	AB206542 ^a	
<i>P. bursaria</i> Cs2	1/II	Shanghai, China	AB206543 ^a	AB252013
<i>P. bursaria</i> MRBG1	?	Melbourne, Australia	AB219526 ^a	AB252014
<i>P. bursaria</i> PB-SW1	?	Schwarzwald, Germany	AB206544 ^a	AB252015
<i>P. bursaria</i> CCAP1660/10	2/IV	?	AB252000	AB252016
<i>P. bursaria</i> CCAP1660/11	2	Cambridge, UK	AB206545 ^a	AB252017
<i>P. bursaria</i> CCAP1660/12	?	Cambridge, UK	AB252001	AB252018-24
<i>P. bursaria</i> CCAP1660/13	?	Cambridge, UK	AB252002	AB252025-38
<i>P. caudatum</i> Isn4	12/XXIII	Iwate, Japan	AB252003	AB252039
<i>P. caudatum</i> KNZ2	3/VI	Kanazawa, Japan	AB252004	AB252040
<i>P. caudatum</i> Yhm	?	Yamaguchi, Japan	AB252005	AB252041
<i>P. multimicronucleatum</i> TH105	2/IV	?	AB252006	AB252042
<i>P. multimicronucleatum</i> YM25	cycler ^c	Ishinomaki, Japan	AB252007	AB252043
<i>P. tetraurelia</i> 51	4/VII	USA	AB252008	AB252044
<i>P. tetraurelia</i> hrd	4/VIII	?	AB252009	AB252045

^a Accessions obtained in Hoshina *et al.* (2005); ^b One of F1 crossbreed between T151 (1/IV, Ibaraki, Japan) and Mts4 (1/I, Nagano, Japan);

^c Janiform entity of 2/III and 2/IV, see Barnett (1966).

a. 18S rDNA tree



b. ITS2 tree

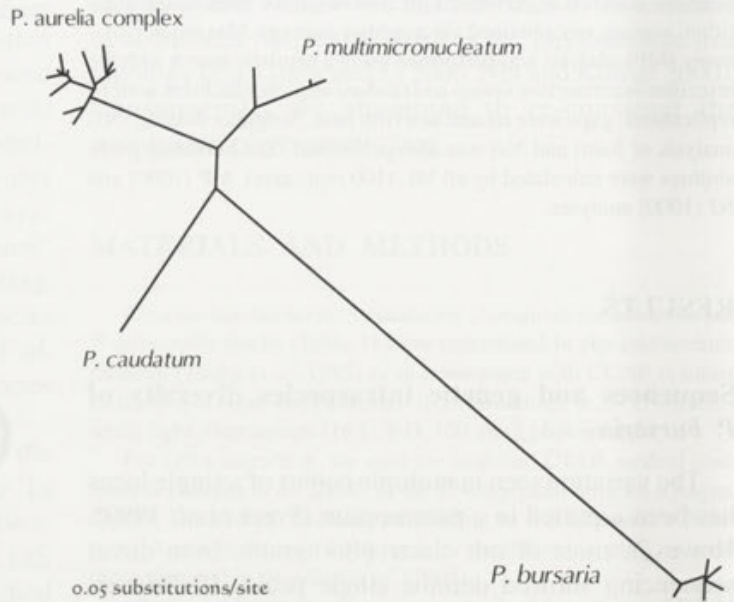


Fig. 2. Unrooted phylograms showing genetic divergences among *Paramecium bursaria*, *P. caudatum*, *P. multimicronucleatum* and *P. aurelia* complex: a, based on 18S rDNA; b, based on 163 aligned nucleotides (gaps included) of ITS2.

direct sequencing method (Coleman 2005, Barth *et al.* 2006). Thus, we quit subsequent clonings for the PCR products of which electrophorograms have undoubted peaks. The visible double peaks or dubious electrophorograms were seen only in spacer regions of two strains of *P. bursaria*, which were defined by a subcloning method. Seven clones detected a single nucleotide polymorphism (SNP, C/T mixtures) and 19 nucleotide insertion/deletions in ITS1 of CCAP 1660/12; and in 14 clones a C/T variation was detected in the 5.8S rDNA and two C/T and two A/G variations in the ITS2 region of CCAP 1660/13. The positions of SNPs corresponded to those of the double peaks seen when sequenced directly.

Four types of 18S rDNA sequences were found in *P. bursaria* (Fig. 4a): A) CCAP 1660/12 and 1660/13; B) 1660/10 and a Canadian strain (Strüder-Kypke *et al.* 2000a, AF100314); C) PB-SW1 and 1660/11; D) OK1, So13, F36, KM2, Dd1, Bnd1, Cs2, MRBG1. The intraspecific distance reached 23 substitutions + 4 insertion/deletions between genetic group of C and D. Oppositely, there were only two transitions between A and B. The unrooted 18S rDNA tree (Fig. 2a) revealed big intraspecific distances of *Paramecium bursaria* com-

pared to the other three species; five substitutions were seen in *P. multimicronucleatum* and in *P. aurelia* complex, and no divergence in *P. caudatum*.

Six different ITS2 sequences were recognized when 14 clones of CCAP 1660/13 were regarded as independent OTUs (Fig. 4b): i) CCAP 1660/10, 1660/11, 1660/12 and 1660/13 clones 01-03, 05-07 and 11-14; ii) PB-SW1 and CCAP 1660/13 clone 08; iii) CCAP 1660/13 clone 04; iv) CCAP 1660/13 clone 09; v) CCAP 1660/13 clone 10; vi) OK1, So13, F36, Cs2 and MRBG1. There were only one or two transitions among the genetic groups i through v, and the group vi differed two or more nucleotides + one insertion/deletions from the others. The ITS2 tree (Fig. 2b) showed the reverse result to that of the 18S rDNA. Up to 6 substitutions were seen both in *P. multimicronucleatum* and in *P. aurelia* complex, yet 3 substitutions + 1 insertion/deletion was found among *P. bursaria* strains as a maximum (group i vs. groups iii-vi). No divergence was seen in *P. caudatum*.

Depending on species (-complex), there were several varieties such as helix length and bulges, although the general structure of ITS2 was common to all four species. For intraspecific comparison, while most of the

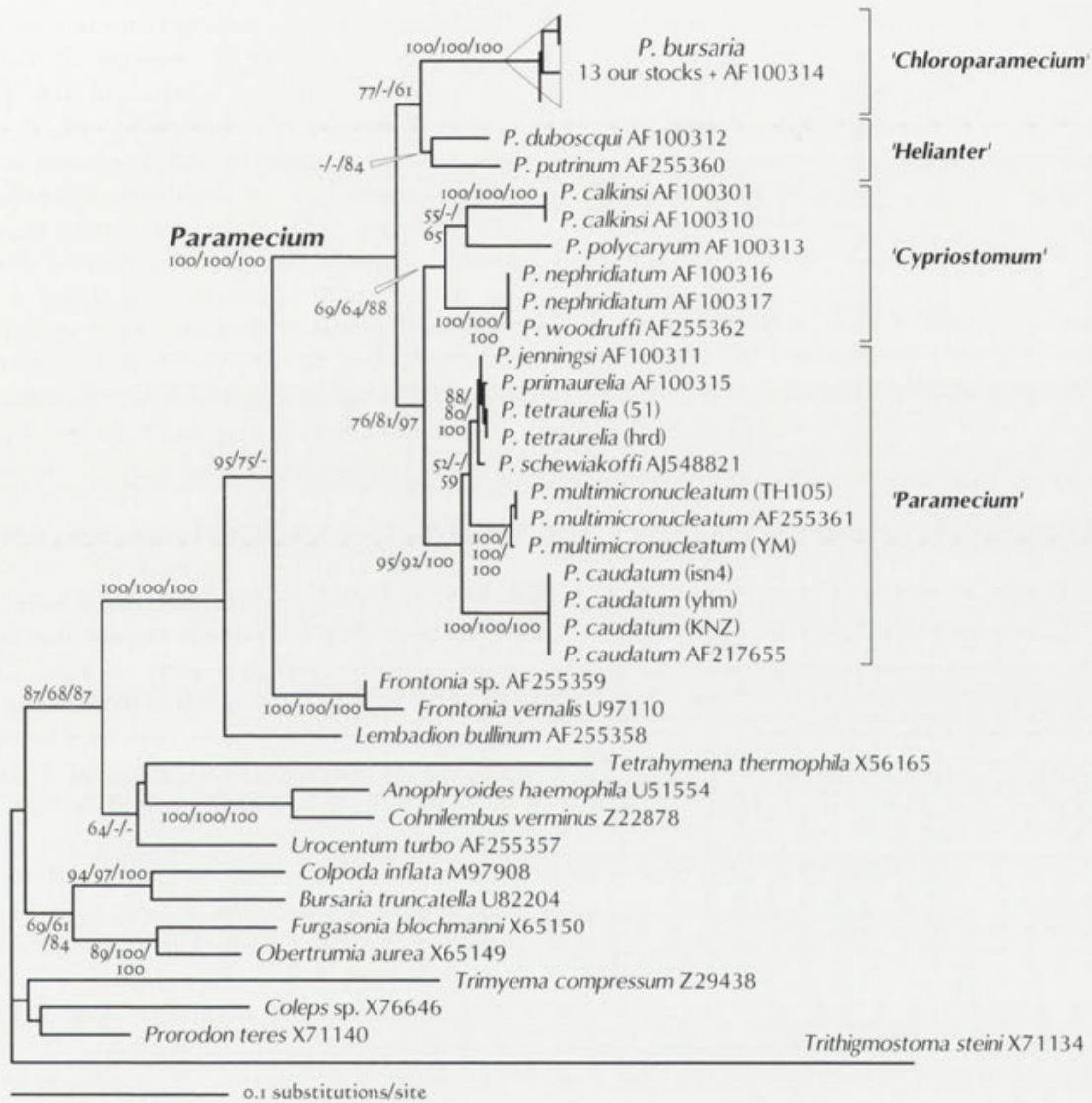


Fig. 3. Phylogenetic tree of paramecia constructed from an analysis of 18S rRNA gene sequences. Tree topology was obtained by ML analysis. Numerals at each nodes are bootstrap probabilities of ML (100 replicates) / MP (1000 replicates) / NJ (1000 replicates) analyses; only values above 50% support are shown.

nucleotide substitutions or insertion/deletions were seen at single loops (including bulges), two compensatory nucleotide substitutions without structural changes were also seen. One was hemi-CBC (compensatory change on only one side of a helix pairing: U-A/U-G) at helix III (Fig. 1) in *P. aurelia* complex, which was reported by Coleman (2005). The other was CBC (compensatory base change: U-A/C-G) found at the tip of helix II (Fig. 1) of *P. multimicronucleatum*. Neither CBC nor hemi-CBC was found in species of *P. bursaria*.

Paramecian phylogeny

Phylogenetic analyses of the 34 paramecian 18S rDNA sequences were performed with 15 other ciliates. Once we tried multiple alignment with the out group taxa as employed by Strüder-Kypke *et al.* (2000b). Although they instructed on gap-handlings for length polymorphic region Helix E10_1 among them, such length polymorphic regions were abundant when compared to the outermost spirotrich taxa. We therefore employed

evolutionary event, when a species diverges into two or more species, requires a long time for completion. Consequently, any species is just in the process of speciation. When we look at organisms around us, we can occasionally recognize plural different units within a species. In protists, it is well known that sexually isolated groups are present in a morphologically identical taxon (Finlay and Esteban 2001, Coleman 2002). In the case of *Paramecium* spp., such sexually isolated groups are called syngens. It is a fact that an entity of paramecia (hitherto *P. aurelia*) was re-described as 14 independent species with the findings of a separated character for each syngen (Sonneborn 1975). Later, *P. sonnebornii* was added to this group as 15th species (Aufderheide *et al.* 1983). As each of the other paramecia remains inclusive of several syngens within a species, the above separation has created active debate over its pros and cons, and is now evolving into "what is a species?" All of the species derived from hitherto *P. aurelia* are generally collectively called *P. aurelia* complex (Allen *et al.* 1983).

To fill a gap between morphological species and biological (producing fertile offspring) species, Coleman (2000) proposed the Z clade concept which indicates the zygote formation group, regardless of whether they produce fertile offspring or not. Furthermore, to assess delimits of Z clades, the utility of a region of ribosomal DNA cistron, the internal transcribed spacer 2 (ITS2), has been advocated (Fabry *et al.* 1999; Coleman 2000, 2005; Coleman and Vacquier 2002; Young and Coleman 2004). ITSs organize certain secondary structures, which helps splicing for 18S (SSU), 5.8S and LSU rRNA. Therefore, ITSs are not mere spacers but may be regarded as genes. Compensatory Base Change (CBC) is a phenomenon when one side base of a pair changes, the opposite side base also changes, compensating to conserve that base pair in a double strand helix. Only one side change also remaining a structure called hemi-CBC. Both are used to establish the confidential folding pattern for rRNAs (Gutell *et al.* 1994). Although the ITS2 sequence has nothing directly to do with whether two organisms can mate or not, when there is a CBC in ITS2 there is no sexual compatibility (Coleman 2000, Coleman and Vacquier 2002, Behnke *et al.* 2004). There was a hemi-CBC (indicating incompatibility next to CBC) in *P. aurelia* complex (Coleman 2005), and we here found a CBC intraspecies of *P. multimicronucleatum*. However, neither CBC nor hemi-CBC was found among our 10 strains of *P. bursaria*. It is a fact that intraspecific divergence of

P. bursaria looked higher than those of the other species by 18S rDNA comparison (Fig. 2a), but this is different with ITS2 (Fig. 2b). Definitely, ITS2 divergence of *P. bursaria* was lower in quality and quantity than that of *P. aurelia* complex and of *P. multimicronucleatum*. The principal factor of the above reversion might be the number of strains (see Materials and methods) and syngens; for instance, we could have used only two (or more) *P. bursaria* syngens, but compared them with 13 syngens of *P. aurelia* complex for ITS2 analysis (most of *P. multimicronucleatum* sequence were obtained in Barth *et al.* (2006), of which syngens have not been made public). Although CBC indicates different biological species, the converse is not always true (Coleman 2005). To assess the degree of *P. bursaria* speciation, all six syngens should be analyzed.

We detected five different sequence variants in CCAP 1660/13 ITS2 region. We handled them as independent OTUs for the comparisons, although it might be inappropriate procedure. As a matter of course, it is not certain the other strains have same sequence copies within the genome. The genetic groups of which based on 18S rDNA and ITS2 were not congruent (see Fig. 4). 18S rDNA group C can be taken as a simple example; PB-SW1 belongs to ITS2 group ii with one of 1660/13 (group A) cloning products, and 1660/11 belongs to group i with those 18S group A (1660/12 and 1660/13 clones) and B (1660/10). The other hand, the member of 18S group D congruently belonged to ITS2 group vi. The genetic group D = vi is also characterized by that they commonly possess "American" type symbionts (Hoshina *et al.* 2005). From the geographical viewpoint, although sampling is meager, group D distributes to Asia and Oceania whereas groups A, B and C distribute to Europe and Northern America (Table 1). We defined four genetic groups intraspecies of *P. bursaria* based on 18S rDNA, however, it might be regarded that the greater autonomy of group D.

Tree topologies can differ according to outgroup selections, multiple alignment, increasing OTUs and tree construction models (Graur and Li 2000, Nei and Kumar 2000). Although the number of paramecian species was not changed from the previous analysis (Fokin *et al.* 2004), we increased genetic diversity of paramecian materials. For example, although only one *P. bursaria* sequence has ever been published, we sprinkled several new sequences of *P. bursaria*, of which the diversity is equivalent to some interspecific diversities (mentioned above). After the first paramecian analysis (Strüder-Kypke *et al.* 2000a), the organisms

phylogenetically surrounding the peniculines were stable, offering a choice of the closer outermost group to construct a phylogenetic tree. Closer outgroups resulted in more accurate alignment. In addition, we relentlessly removed doubtful regions which corresponded to loops or bulges in SSU rRNA foldings.

The accumulation of such tiny differences generated the unique topology. The point with the greatest difference is the first division of *Paramecium* spp. The topologies conducted by Strüder-Kypke *et al.* 2000a, b; Fokin *et al.* 2004 commonly showed that *P. bursaria* diverged at first at the genus and the monophyly of the rest of the species were moderately to highly supported. In our analyses, however, the paramecia branched into two, the clade of *P. bursaria*, *P. duboscqui* and *P. putrinum* and the clade constructed of *P. calkinsi*, *P. polycaryum*, *P. nephridiatum*, *P. woodruffi*; *P. jenningsi*, *P. aurelia* complex, *P. schewiakoffi*, *P. multimicronucleatum* and *P. caudatum* (Fig. 3). Although Fokin *et al.* (2004) acknowledged that *P. duboscqui* and *P. putrinum* were secondary branching species, they pointed out the similarities to *P. bursaria*, for example by the multiple mating-type system and nuclear reorganization process. This monophyly was supported up to 77% obtained by ML analysis, and six MP and NJ trees also showed the same topology.

Although there are negative aspects to some lower bootstraps (except NJ analysis) or some shorter internodes, the members of the paramecia can be perceived as four phylogenetic groups, namely, *P. bursaria*; *P. duboscqui* and *P. putrinum*; *P. calkinsi*, *P. polycaryum*, *P. nephridiatum*, and *P. woodruffi*; *P. jenningsi*, *P. aurelia* complex, *P. schewiakoffi*, *P. multimicronucleatum* and *P. caudatum*. This separation is consistent with the subgeneric concept of Fokin *et al.* (2004) emphasizing morphometric analysis. Each corresponds to „*Chloroparamecium*”, „*Helianter*”, „*Cypriostomum*” and „*Paramecium*”, respectively (see Fig. 3). All topologies obtained from ML, MP and NJ analyses are congruent even at the most unreliable branch, indicating „*Helianter*” (*P. duboscqui* and *P. putrinum*) and NJ analysis gives strong bootstrap support. Therefore, we generally support the subgeneric classification of Fokin *et al.* (2004) from the phylogenetic view point.

The same as with published trees (Strüder-Kypke *et al.* 2000b, Fokin *et al.* 2004), *Paramecium* spp.

constructed a robust clade with *Frontonia* and *Lembadion* spp. (Subclass Peniculia, see Strüder-Kypke *et al.* 2000b) which share the short helix E10_1 in the 18S rDNA (Strüder-Kypke *et al.* 2000b) and the morphological characteristics of nematodesmata (Didier 1970). In this clade, *Paramecium* spp. were derivatively divided in ML and MP analyses; incongruently, *Frontonia* and *Lembadion* were claded as a sister to *Paramecium* in NJ analysis. Referring to their cell shape, the alternative foot shape or cigar shape which was the first dividing concept for paramecia (Woodruff 1921) resulted in cigar shaped species aggregated to a clade of the subgenus „*Paramecium*” (Fig. 3). The other three subgenera have a foot shaped body in common. *Frontonia* and *Lembadion* also appear to be foot shaped. Consequently, it can be said that the foot shape is the plesiomorphic character for the genus *Paramecium* and the cigar shape is the synapomorphic one for the subgenus „*Paramecium*”. Can we say that „*Chloroparamecium*” is the lineage acquiring algal-holding ability? When we glance around the Peniculia, there is another green ciliate, *Frontonia vernalis* Ehrenberg, which is a typical algae-hold host (Berninger *et al.* 1986). If the algal-holding ability was obtained at the lineage to „*Chloroparamecium*”, the same ability must have been independently gained at the lineage to *Frontonia vernalis*. It is also possible that the ancestor of Peniculia (because the relationship between *Frontonia* and *Lembadion* was unresolved, as mentioned above) had already gained this ability. This needs at least five evolutionary instances of one gain and four independent losses: the lineages to (i) *Lembadion*, (ii) heterotrophic *Frontonia*, (iii) „*Helianter*”, (iv) the ancestor of „*Cypriostomum*” and „*Paramecium*”. Derived characters are usually equally weighted in cladistics, but it is an accepted norm in evolution that the loss of a character is easier than the gain of a character. With the example of eyes in arthropods, it is occasionally taken as a central role of evolution that eyes are lost over 30 times as often as they are gained (Oakley and Cunningham 2002). Another example is the trophically diverse group, the dinoflagellates, although it is not clear when they got plastid-control ability. At least eight independent instances of plastid loss (with three of replacement) have been shown (Saldarriaga *et al.* 2001). The evolutionary facts will be settled once the gene permitting algal control has been elucidated.

Acknowledgements. The colorless paramecia sequenced were kindly obtained from Prof. Isoji Miwa, Ibaraki Univ.

REFERENCES

- Aufderheide K. J., Daggett P.-M., Nerad, T. A. (1983) *Paramecium sonneborni* n. sp., a new member of the *Paramecium aurelia* species-complex. *J. Protozool.* **30**: 128-131
- Allen S. L., Gibson I. (1971) Interspecific variations in the esterases of axenic stocks of *Paramecium aurelia*. *Biochem. Genet.* **5**: 161-181
- Allen S. L., Adams J., Rushford C. L. (1983) Interspecific relationships in the *Paramecium aurelia* complex: acid phosphatase variation. *J. Protozool.* **30**: 143-147
- Barnett A. (1966) A circadian rhythm of mating type reversals in *Paramecium multimicronucleatum*, syngen 2, and its genetic control. *J. Cell. Physiol.* **67**: 239-270
- Barth D., Krenek S., Fokin S. I., Berevdonk T. U. (2006) Intraspecific genetic variation in *Paramecium* revealed by mitochondrial cytochrome *c* oxidase I sequences. *J. Eukaryot. Microbiol.* **53**: 20-25
- Behne A., Friedl T., Chepurnov V. A., Mann D. G. (2004) Reproductive compatibility and rDNA sequences analyses in the *Sellaphora pupula* species complex (Bacillariophyta). *J. Phycol.* **40**: 193-208
- Berninger U.-G., Finlay B. J., Canter H. M. (1986) The spatial distribution and ecology of zoochlorellae-bearing ciliates in a productive pond. *J. Protozool.* **33**: 557-563
- Cannone J. J., Subramanian S., Schnare M. N., Collett J. R., D'Souza L. M., Du Y., Feng B., Lin N., Madabusi L. V., Müller K. M., Pande N., Shang Z., Yu N., Gutell R. R. (2002) The comparative RNA web (CRW) site: an online database of comparative sequence and structure information for ribosomal, intron, and other RNAs. *BMC Bioinformatics* **3**: 15
- Coleman A. W. (2000) The significance of a coincidence between evolutionary landmarks found in mating affinity and a DNA sequence. *Protist* **151**: 1-9
- Coleman A. W. (2002) Microbial eukaryote species. *Science* **297**: 337
- Coleman A. W. (2003) ITS2 is a double-edged tool for eukaryote evolutionary comparisons. *Trends Genet.* **19**: 370-375
- Coleman A. W. (2005) *Paramecium aurelia* revisited. *J. Eukaryot. Microbiol.* **52**: 68-77
- Coleman A. W., Vacquier V. D. (2002) Exploring the phylogenetic utility of ITS sequences for animals: A test case for abalone (*Halotis*). *J. Mol. Evol.* **54**: 246-257
- Fabry S., Köhler A., Coleman A. W. (1999) Intraspecific analysis: Comparison of ITS sequence data and gene intron sequence data with breeding data for a worldwide collection of *Gonium pectorale*. *J. Mol. Evol.* **48**: 94-101
- Finlay B. J., Esteban G. F. (2001) Exploring Leeuwenhoek's legacy: the abundance and diversity of protozoa. *Int. Microbiol.* **4**: 125-133
- Fokin S. I. (1986) Morphology of the contractive vacuoles in ciliated protozoa of the genus *Paramecium* (Hymenostomatida, Peniculina) as a species-specific character. *Zoologicheskii Zhurnal* **48**: 30-39 (in Russian with English summary)
- Fokin S. I. (1997) Morphological diversity of the micronuclei in *Paramecium*. *Archiv für Protistenk.* **148**: 375-387
- Fokin S. I., Chivilev S. M. (1999) Brackish water *Paramecium* species and *Paramecium polycaryum*. Morphometric analysis and some biological peculiarities. *Acta Protozool.* **38**: 105-117
- Fokin S. I., Stoeck T., Schmidt H. J. (1999) Rediscovery of *Paramecium nephridiatum* Gelei, 1925 and its characteristics. *J. Eukaryot. Microbiol.* **46**: 416-426
- Fokin S. I., Przybos E., Chivilev S. M., Beier C. L., Horn M., Skotarczak B., Wodecka B., Fujishima M. (2004) Morphological and molecular investigations of *Paramecium schewiakoffi* sp. nov. (Ciliophora, Oligohymenophorea) and current status of distribution and taxonomy of *Paramecium* spp. *Eur. J. Protistol.* **40**: 225-243
- Graur D., Li, W.-H., (2000) Fundamentals of molecular evolution second edition. Sinauer Associates, Sunderland, Massachusetts
- Gutell R. R., Larsen N., Woese C. R. (1994) Lessons from an evolving rRNA: 16S and 23S rRNA structures from a comparative perspective. *Microbiol. Rev.* **58**: 10-26
- Hoshina R., Kamako S.-i., Imamura N. (2004) Phylogenetic position of endosymbiotic green algae in *Paramecium bursaria* Ehrenberg from Japan. *Plant Biology* **6**: 447-53
- Hoshina R., Kato Y., Kamako S.-i., Imamura, N. (2005). Genetic evidence of "American" and "European" type symbiotic algae of *Paramecium bursaria* Ehrenberg. *Plant Biology* **7**: 526-32
- Jankowski A. W. (1969) A proposed taxonomy of the genus *Paramecium* Hill, 1752 (Ciliophora). *Zoologicheskii Zhurnal* **48**: 30-40 (in Russian with English summary)
- Jankowski A. W. (1972) Cytogenetics of *Paramecium putrinum* C. et L. (1858) *Acta Protozool.* **10**: 285-394
- Nei M., Kumar S. (2000) Molecular Evolution and Phylogenetics. Oxford University Press, Oxford, New York
- Oakley T. H., Cunningham C. W. (2002) Molecular phylogenetic evidence for the independent evolutionary origin of an arthropod compound eye. *P. Natl. Acad. Sci. USA* **99**: 1426-1430
- Posada D., Crandall K. A. (1998) MODELTEST: testing the model of DNA substitution. *Bioinformatics* **14**: 817-818
- Preer L. B., Rudman B., Pollack S., Preer J. R. Jr. (1999) Does ribosomal DNA get out of the micronuclear chromosome in *Paramecium tetraurelia* by means of a rolling circle? *Mol. Cell. Biol.* **19**: 7792-7800
- Saldarriaga J. F., Taylor F. J. R., Keeling P. J., Cavalier-Smith T. (2001) Dinoflagellate nuclear SSU rRNA phylogeny suggests multiple plastid losses and replacements. *J. Mol. Evol.* **53**: 204-213
- Shi X., Jin M., Liu G. (1997) Rediscovery of *Paramecium duboscqui* Chatton & Brachon, 1933 and a description of its characteristics. *J. Eukaryot. Microbiol.* **44**: 134-141
- Sonneborn T. M. (1975) The *Paramecium aurelia* complex of fourteen sibling species. *Trans. Am. Microsc. Soc.* **94**: 155-178
- Stoeck T., Schmidt H. J. (1998) Fast and accurate identification of European species of the *Paramecium aurelia* complex by RAPD-fingerprints. *Microbial Ecol.* **35**: 311-317
- Stoeck T., Przybos E., Schmidt H. J. (1998) A combination of genetics with inter- and intra-strain crosses and RAPD-fingerprints reveals different population structures within the *Paramecium aurelia* complex. *Eur. J. Protistol.* **34**: 410-420
- Stoeck T., Welter H., Seitz-Bender D., Kusch J., Schmidt H. J. (2000) ARDRA and RAPD-fingerprinting reject the sibling species concept for the ciliate *Paramecium caudatum* (Ciliophora, Protoctista). *Zool. Scr.* **29**: 75-82
- Strüder-Kypke M. C., Wright A. G., Fokin S. I., Lynn D. H. (2000a) Phylogenetic relationships of the genus *Paramecium* inferred from small subunit rRNA gene sequences. *Mol. Phylogen. Evol.* **14**: 122-130
- Strüder-Kypke M. C., Wright A. G., Fokin S. I., Lynn D. H. (2000b) Phylogenetic relationships of the Subclass Peniculia (Oligohymenophorea, Ciliophora) inferred from small subunit rRNA gene sequences. *J. Eukaryot. Microbiol.* **47**: 419-429
- Swofford D. L. (2000) PAUP* Phylogenetic analysis using parsimony (*and other methods), version 4. Sinauer Associates, Sunderland, Massachusetts
- Thompson J. D., Gibson T. J., Plewniak F., Jeanmougin F., Higgins D. G. (1997) The Clustal X Windows interface: flexible strategies for multiple sequence alignment aided by quality analysis tools. *Nucleic Acids Res.* **25**: 4876-4882
- Tsukii Y., Harumoto T., Yazaki K. (1995) Evidence for a vial macronuclear endosymbiont in *Paramecium caudatum*. *J. Eukaryot. Microbiol.* **42**: 109-15
- White T. J., Bruns T., Lee S., Taylor J. (1990) Amplification and direct sequencing of fungal ribosomal RNA genes for phylogenetics. In: PCR Protocols: a Guide to Methods and Applications. (Eds. M. Innis, D. Gelfand, J. Sninsky and T. White). Academic Press, San Diego, 315-322
- Wichterman R. (1953) The Biology of *Paramecium*. Blakiston, New York
- Wichterman R. (1986) The Biology of *Paramecium*. 2nd Edition. Plenum Press, New York

- Woodruff L. L. (1921) The structure, life history, and intrageneric relationships of *Paramecium calkinsi*, sp. nov. *Biol. Bull.* **41**: 171-180
- Young I., Coleman A. W. (2004) The advantages of the ITS2 region of the nuclear rDNA cistron for analysis of phylogenetic relationships of insects: a *Drosophila* example. *Mol. Phylogenet. Evol.* **30**: 236-242
- Zuker M. (2003) Mfold web server for nucleic acid folding and hybridization prediction. *Nucleic Acids Res.* **31**: 3406-3415

Received on 4th May, 2006; revised version on 23rd June, 2006; accepted on 16th July, 2006

Sibling Species within *Paramecium jenningsi* Revealed by PCR-RFLP

Agnieszka MACIEJEWSKA

Department of Genetics, University of Szczecin, Szczecin, Poland

Summary. *Paramecium jenningsi* Diller *et* Earl, 1958 is classified in the so-called "aurelia" subgroup. The original assumption of the monomorphic status of *P. jenningsi* (Sonneborn 1970) has been repeatedly challenged over the years with the application of increasingly sophisticated methods and knowledge of the geographic distribution of particular strains of this species. Investigations concerning genetic polymorphism suggested the existence of two sibling species in *P. jenningsi*, comprised of strains inhabiting India, Saudi Arabia, China and Japan. In order to confirm the existence of these sibling species, here we apply the PCR-RFLP method for analysis of a fragment of the *hsp70* gene coding for the Hsp70 cytosol heat shock protein. PCR-RFLP with enzymes *Alu*II and *Eco*RI did not reveal size polymorphism of restriction fragments. Band patterns obtained with enzyme *Tru*II showed variation corresponding to genetic polymorphism and were subject to comparative analysis using the BIOID program which applies Nei and Li's and Jaccard's similarity coefficients. The results of these analyses are homology trees showing the genetic similarity between West-Central Asian and Japanese groups, the intra-group similarity coefficients had a value of 1, i.e. the strains were 100% homologous. The similarity between both of these groups was calculated as 32% and 20% depending on which coefficient was used. West-Central Asian and Japanese groups detected in this study on the basis of PCR-RFLP result can be considered separate species after interpretation of inter-strain crosses, which have shown the existence of reproductive isolation barriers between West-Central Asian and Japanese strains on the basis of the percentage of surviving clones.

Key words: *Paramecium aurelia*, *P. jenningsi*, PCR-RFLP, sibling species.

INTRODUCTION

Protozoans are particularly valuable research subjects for many biological disciplines because their exceptional diversity (morphological as well as physiological) allows for wide-ranging analyses using contemporary methods (electron microscopy, *in vitro* cultures, biochemical and genetic methods) (Kazubski 1988). The genus *Paramecium* has been known for 250 years

and its representatives include some of the most commonly studied ciliates. They are model organisms for many investigations concerning questions in protozoology, cytology, genetics, ecology, general biology and many other fields in biology. The cosmopolitan distribution, straightforward culture and relatively large size (80-400 μ m) of paramecia have made them universal laboratory organisms (Fokin *et al.* 2001).

Paramecium jenningsi Diller *et* Earl, 1958 is classified in the so-called "aurelia" subgroup including *P. caudatum*, *P. multimicronucleatum*, *P. schewiakoffi* and species of the *P. aurelia* complex (Przyboś 1975, 1978; Fokin *et al.* 2001, 2004). Many studies using

Address for correspondence: Agnieszka Maciejewska, Department of Genetics, University of Szczecin, al. Piastów 40B, Blok 6, 71-065 Szczecin, Poland; Fax: 091 444 2780; E-mail: maciejew@univ.szczecin.pl

traditional and molecular methods of analysis have shown that *P. jenningsi* is closely related with species comprising the *P. aurelia* complex (Strüder-Kypke *et al.* 2000a, b; Fokin *et al.* 2001, 2004). It has even been suggested that *P. aurelia* and *P. jenningsi* are sibling species, and that the *P. aurelia* complex evolved from a *P. jenningsi* lineage (Yamauchi *et al.* 1995). Recent comparative analyses of SS rRNA sequences (Fokin *et al.* 2004) have also shown that *P. jenningsi* is the sister species to the newly described *P. schewiakoffi* from the monophyletic "aurelia" subgroup. The original assumption of the monomorphic status of *P. jenningsi* (Sonneborn 1970) has been repeatedly challenged over the years with the application of increasingly sophisticated methods and knowledge of the geographic distribution of particular strains of this species. At first, traditional cytogenetic and karyological studies (Przyboś 1975, 1978, 1980, 1986a, b; Jurand and Przyboś 1984) as well as biochemical analyses (Allen *et al.* 1983) supported the monomorphic status of *P. jenningsi*. Investigations concerning genetic polymorphism in *P. jenningsi* were commenced after the morphological and biochemical stability of paramecia was contrasted with the discovery of substantial variation at the molecular level (Strüder-Kypke *et al.* 2000a, b; Fokin *et al.* 2001). This suggested the existence of genetic polymorphism decoupled with detectable polymorphism at other organizational levels of the cell. Another important determinant of further studies on the genetic polymorphism of *P. jenningsi* was the discovery of new habitat of this species in Japan, China and Saudi Arabia (Przyboś *et al.* 2003b). The results of comparative genomic analyses using RAPD-PCR fingerprinting contested the assumed monomorphic nature of this species because they suggested the existence of two sibling species in *P. jenningsi*, comprised of strains inhabiting India, Saudi Arabia, China and Japan (Przyboś *et al.* 2003b; Skotarczak *et al.* 2004a, b).

In order to confirm the existence of these sibling species, here we apply the PCR-RFLP method, also known as CAPS (Cleaved Amplified Polymorphic Sequence), based on sequential amplification and restriction. This method can be used if the amplified products do not possess length variation and nucleotide variation at sites complementary to the applied primers. Restriction enzymes reveal nucleotide variation at enzyme-specific sites in the amplified fragments (Jerome and Lynn 1996, Buruoca *et al.* 1999). An alternative and more detailed method involves sequencing, however, it considerably increases costs.

MATERIALS AND METHODS

Genetic material isolated from 9 strains of *P. jenningsi* was used as listed in Table 1. Paramecia were raised in a lettuce culture inoculated with *Enterobacter aerogenes* at room temperature in daylight according to the method of Sonneborn (1970).

Paramecia DNA was isolated using the DNeasy™ Tissue Kit (Qiagen, Germany). For PCR-RFLP a fragment of the *hsp70* gene coding for the Hsp70 cytosol heat shock protein of 70 kDa (Budín and Philippe 1998) was used for digestion with restriction enzymes. The primer pair Afor (5'GAG GAG AAG ATT TCG ATA AC3') and Arev (5'GCT TCA TCT GGG TTG ATT GA3'), amplifying a 440 bp fragment of the aforementioned gene (Przyboś *et al.* 2003a), was used in PCR. The 50 µl PCR consisted of 5 µl DNA isolate; 2.5 U DNA recombinant *Taq* polymerase in buffer (20 mM Tris-HCl, 100 mM KCl, 1 mM DTT, 0.1 mM EDTA, 0.5% Nonidet P-40, 0.5% Tween 20, 50% glycerol; pH 8.0) (Qiagen, Germany); 1x PCR buffer (Tris-HCl, KCl, (NH₄)₂SO₄, 15 mM MgCl₂; pH 8.7) (Qiagen, Germany); 87.5 mM MgCl₂; 25 pM primer Afor and Arev (Biomers, Germany) in TE buffer (10 mM Tris-HCl, 1 mM EDTA; pH 8); 5 µM of each dNTP. Amplification of the *hsp70* gene in the 9 strains of *P. jenningsi* was performed in a Peltier Thermal Cycler PTC-200 MJ Research (USA) and a T-Gradient Biometra (Germany). The thermal-time PCR profile of Przyboś *et al.* (2003a) was used: initial denaturation at 94°C for 2 min, 30 cycles (denaturation at 94°C for 45 s, primer annealing at 50°C for 60 s, chain extension at 72°C for 60 s) and final extension at 72°C for 5 min. The reaction was performed in 18 samples, i.e. 2 samples per isolate from 9 cultured strains of *P. jenningsi*.

PCR products were purified and precipitated using a 96% and 70% ethanol/sodium acetate protocol. Purified PCR products were subsequently digested with three restriction enzymes: *AluI*, *EcoRI*, *TruII* (*MseI*) (Fermentas, Lithuania), using 3U in 20 µl reactions.

RESULTS

Amplification with primers Afor and Arev in 18 samples (2 samples per isolate from 9 cultured strains of *P. jenningsi*) gave a 440 bp product representing a fragment of the *hsp70* gene (Fig. 1).

No size polymorphism of restriction fragments was detected after restriction of the purified PCR products with *AluI* and *EcoRI*. For each sample the same number of products of identical size was obtained: 5 and 4 fragments for *AluI* and *EcoRI* restrictases, respectively (Figs 2, 3). The application of *TruII* revealed restriction site polymorphism in the sequence of the *hsp70* gene in *P. jenningsi*. The number of obtained restriction fragments was the same for all studied strains however, their lengths were different for West-Central Asian and Japanese strains. No intra-strain polymorphism was detected (Fig. 4). Approximate sizes of all fragments are compared in Table 2.

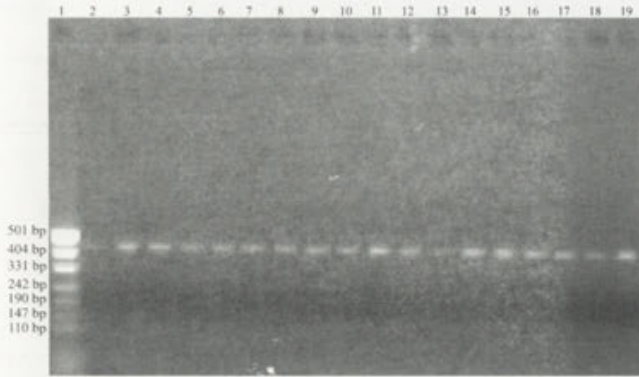


Fig. 1. Amplification products of *hsp70* from 9 strains of *P. jenningsi*. Lanes: 1 - molecular mass marker MW 501, 2 and 3 - *P. jenningsi* strain from India (Bangalore), 4 and 5 - strain from Saudi Arabia, 6 and 7 - strain from China (Shanghai), 8 and 9 - strain from Japan (Yamaguchi), 10 and 11 - strain from Japan (Hagi), 12 and 13 - strain from Japan (Ube), 14 and 15 - strain from Japan (Nagato), 16 and 17 - strain from Japan (Shinnamyou), 18 and 19 - strain from Japan (Okinawa, Hujigawa).

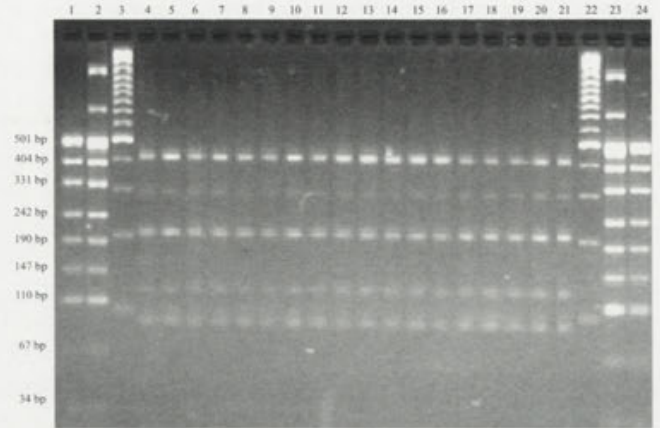


Fig. 2. Restriction products of the *hsp70* gene with enzyme *AluI* in 9 strains of *P. jenningsi*. Lanes: 1 and 24 - mass marker MW 501, 2 and 23 - mass marker MW 1444, 3 and 22 - mass marker GeneRuler, 4 and 5 - strain of *P. jenningsi* from India (Bangalore), 6 and 7 - strain from Saudi Arabia, 8 and 9 - strain from China (Shanghai), 10 and 11 - strain from Japan (Yamaguchi), 12 and 13 - strain from Japan (Hagi), 14 and 15 - strain from Japan (Ube), 16 and 17 - strain from Japan (Nagato), 18 and 19 - strain from Japan (Shinnamyou), 20 and 21 - strain from Japan (Okinawa, Hujigawa).

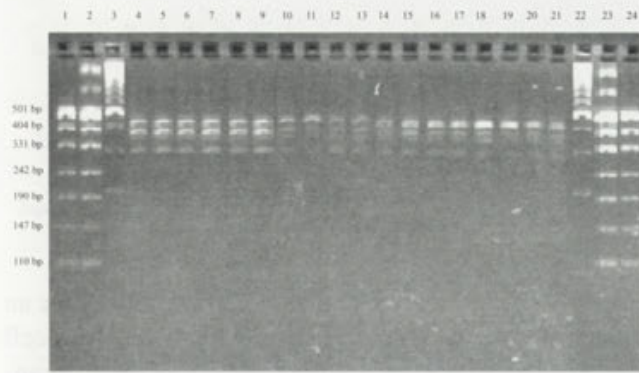


Fig. 3. Restriction products of the *hsp70* gene with enzyme *EcoRI* in 9 strains of *P. jenningsi*. Lanes as in Fig. 2.

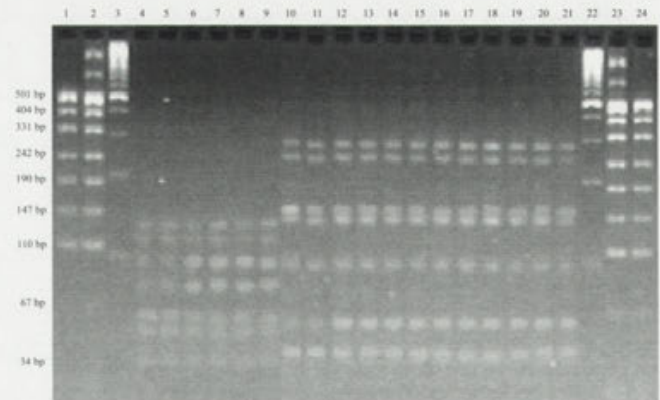


Fig. 4. Restriction products of the *hsp70* gene with enzyme *TruII* in 9 strains of *P. jenningsi*. Lanes as in Fig. 2.

PCR-RFLP with enzymes *AluI* and *EcoRI* did not reveal size polymorphism of restriction fragments, because all fragments were identical. As so, the patterns were not analyzed further. The results of comparative analysis of band patterns obtained by PCR-RFLP with enzyme *TruII* using the BIOID program which applies Nei and Li's and Jaccard's similarity coefficients are homology trees showing the genetic similarity in percent-

age values for each strain of *P. jenningsi* from different geographical localities (Figs 5, 6).

DISCUSSION

The taxonomic structure of ciliates is characteristically complicated. At present the systematics of this

Table 1. Strains of *Paramecium jenningsi* and their origin.

Strain Symbol	Collection site	Collection date of sample for first culture	Collector
B	India, Bangalore	1955	P. B. Padmavathi
SA	Saudi Arabia, vicinity of Riyadh	July 1999	K. A. S. AL Rasheid
C2	China, Shanghai	November 1999	M. Fujishima
JAP	Japan, Honshu Island, Yamaguchi	November 1999	S. Fokin
JYR	Japan, Honshu Island, Hagi	September 1997	S. Fokin
J1	Japan, Honshu Island, Ube	October 2000	M. Fujishima
J2	Japan, Honshu Island, Nagato	September 2000	M. Fujishima
J3	Japan, Honshu Island, Shinnamyou	October 2000	M. Fujishima
JOH	Japan, Okinawa Island, Hujigawa	2000	M. Fujishima

Table 2. Approximate lengths of restriction fragments after digestion of gene *hsp70* with enzymes *AluI*, *EcoRI* and *TruI*. Lengths in base pairs.

<i>AluI</i>	<i>EcoRI</i>	<i>TruI</i>	
All - <i>P. jenningsi</i> strains		West-Central Asian strains of <i>P. jenningsi</i>	Japanese strains of <i>P. jenningsi</i>
200	171	59	120
90	91	54	110
80	81	40	63
61	79	34	59
43		29	40
		24	25
		13	16

group is rapidly changing because of an immense increase of information, including the discovery of new, oftentimes substantial differences between groups of ciliates which leads to the description of new taxa (Kazubski 2000). Representatives of many genera, including *Paramecium*, show incredible species diversity. We now have described many more species of paramecia than had been estimated beforehand (Sonneborn 1957). In evolutionary studies, sibling species seem to be particularly important, such as those detected in *Paramecium*. Sibling species are considered to be real biological species in which reproductive isolation is fully developed, but are morphologically similar or even identical (Sonneborn 1975), due to recent common ancestry. In evolutionary terms, not much time has past since sibling species have diverged, thus these organisms are relatively young and useful for the study of evolutionary processes. The anatomy and functioning of *Paramecium* cells, and especially their life strategy guaranteeing

a fast rate of evolution (Fokin *et al.* 2001), allows for an in-depth look into these processes at many levels of cell organization, which particularly predestines these organisms to evolutionary and phylogenetic study.

PCR-RFLP allows for the detection of genetic polymorphism due to nucleotide variation at enzyme-specific sites in amplified DNA fragments. Various band patterns can be used as RFLP markers for identification purpose or for further phylogenetic analyses describing the evolutionary relationships between these organisms (Jerome and Lynn 1996, Burucoa *et al.* 1999). In this paper, we applied PCR-RFLP to a fragment of the *hsp70* gene coding for the Hsp70 cytosol heat shock protein. Recently, *hsp70* genes have been shown to be reliable as a phylogenetic marker in protozoa and to be suitable for separating sibling species among *Paramecium* genus (Hori *et al.* 2006). These genes has also been previously used in phylogenetic analyses of diverse organisms, including ciliates and other protozoans, by many indepen-

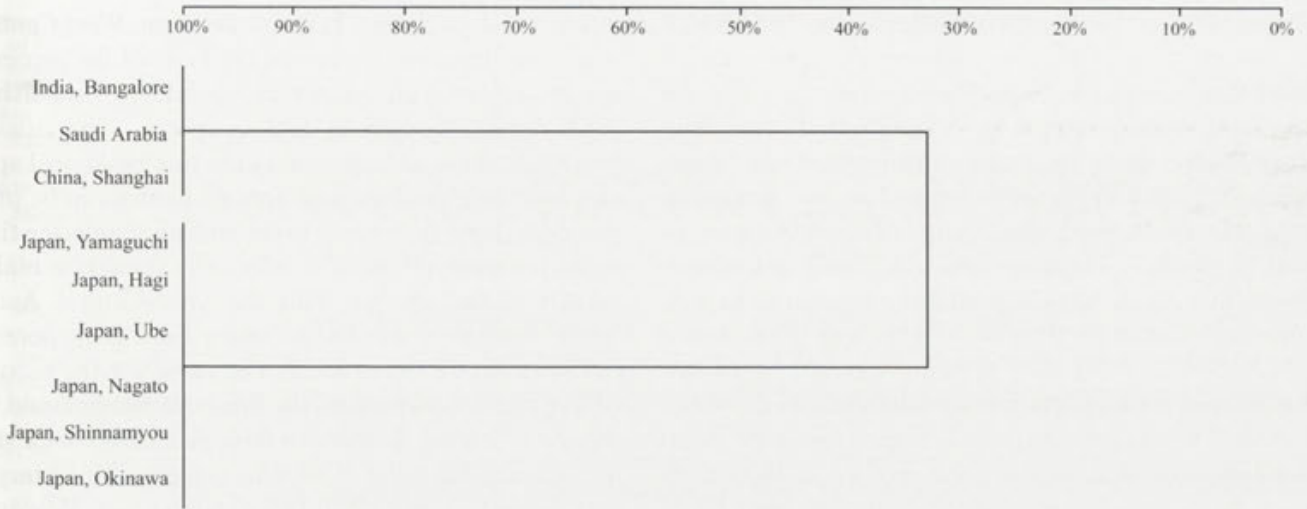


Fig. 5. Homology diagram calculated on the basis of Nei -Li coefficients for *P. jenningsi* strains through PCR-RFLP with *Tru*II on the basis of a fragment of the *hsp70* gene.



Fig. 6. Homology diagram calculated on the basis of Jackard's coefficients for *P. jenningsi* strains through PCR-RFLP with *Tru*II on the basis of a fragment of the *hsp70* gene.

dent research groups (Gupta and Golding 1993, Boorstein *et al.* 1994, Rensing and Maier 1994, Budin and Philippe 1998, Przyboś *et al.* 2003a).

Very recently one more molecular marker for testing genetic variation in ciliates, which has very good resolu-

tion, the mitochondrial cytochrome *c* oxidase I (Barth *et al.* 2006) was successfully tested.

PCR-RFLP using *Alu*I and *Eco*RI revealed a lack of size polymorphism of restriction fragments in all studied strains of *P. jenningsi*, which did not permit their

differentiation. Band patterns obtained by PCR-RFLP with enzyme *Tru*II showed genetic polymorphism within the 9 *P. jenningsi* strains and were subject to comparative analysis using Nei and Li's and Jaccard's similarity coefficients. Both diagrams differentiated the West-Central Asian and Japanese strains into two groups on the basis of different electrophoretic band patterns of RFLP products obtained with the *Tru*II restrictase. Probably because of PCR products used for this experiment included two or three isoforms of hsp70 the amount of length of restriction fragments was not ca 440bp. Because of the identical band patterns within the West-Central Asian and Japanese groups, the intra-group similarity coefficients had a value of 1, i.e. the strains were 100% homologous. The similarity between both of these groups was calculated as 32% and 20% depending on which coefficient was used. The difference is attributable to different mathematical formulas used to calculate each coefficient, thus these values must be considered as relative values and not absolute genetic distances.

These results are compatible with earlier studies using the RAPD method in which these two groups were also detected (Przyboś *et al.* 2003b; Skotarczak *et al.* 2004a, b). However, in contrast to the restriction analyses, RAPD showed a higher level of variation, determining lower level divisions within the West-Central Asian and Japanese groups. Congruent results from independent phylogenetic analyses strongly support the likelihood of the tree topology and the conclusion that the described phylogenetic relationships between the 9 *P. jenningsi* strains are biologically real. The results of the phylogenetic analyses performed on data from various molecular markers and mathematical models unambiguously verify the existence of two sibling species in *P. jenningsi*. However, it should be underlined that the application of molecular methods does not allow for the description of new species. The use of genetic variation only, however detailed, is not sufficient for the evaluation of new taxa. The detection of genetic polymorphism is not sufficient for the description of the basic systematic unit, i.e. the species. The only uncontested means of establishing a new species is the reproductive isolation criterion which is the essence of the biological species concept (Burma and Mayr 1949). For this reason, molecularly differentiated West-Central Asian and Japanese strains detected in this study can be considered separate species only after interpretation of inter-strain crosses carried out by Przyboś *et al.* (2003b). The investigations carried out have shown the existence of

reproductive isolation barriers between West-Central Asian and Japanese strains on the basis of the percentage of surviving clones, which confidently establishes these strains as separate, sibling species. The crosses prove that these sibling species are true biological species and therefore binomial species names can be proposed for them. According to the priority statute, the first name for these ciliates (*P. jenningsi*) should be maintained by the species with the West-Central Asian strains, including the Indian strain from Bangalore, a model strain for the species. The name for the second sibling species encompass the Japanese strains could be created following Sonneborn through analogy with sibling species from the *P. aurelia* complex by adding a latin numerical prefix before the *aurelia* root. However in order to establish a new species name some more detailed research (i.e. morphometric and ecological description) should be done.

Despite the fact that the molecular methods applied in this study cannot be used as the only means of establishing a new species, they are necessary for all research of this type because of their usefulness in detecting genetic polymorphism, critical for the formation of reproductive isolation. According to the contemporary synthetic theory of evolution, mechanisms maintaining isolation between species are by-products of genome divergence through natural selection (Gavrilets 2003), therefore the detection of these changes is important for determining the nature of reproductive isolation and should be the aim of studies of the processes of speciation and the discovery of new species.

Acknowledgements. I would like to thank Prof. Ewa Przyboś from the Institute of Systematics and Evolution of Animals, Polish Academy of Sciences, Kraków, Poland for providing *P. jenningsi* strains. This research was supported financially by the Grant No. 2P04C 01126 of the State Committee for Scientific Research, Warsaw Poland.

REFERENCES

- Allen S.L., Rushford C.L., Nerad T.A., Lau E.T. (1983) Intraspecific variability in the esterases and acid phosphatases of *Paramecium jenningsi* and *Paramecium multimicronucleatum*: assignment of unidentified paramecia: comparison with *P. aurelia* complex. *J. Protozool.* **30**: 155-163
- Barth D., Krenek S., Fokin S.I., Berendonk T. U. (2006) Intraspecific genetic variation in *Paramecium* revealed by mitochondrial cytochrome *c* oxidase I sequences. *J. Eukaryot. Microbiol.* **53**: 20-25
- Boorstein W. R., Ziegelhoffer W. R., Craig E. A. (1994) Molecular evolution of Hsp70 multigene family. *J. Mol. Evol.* **38**: 1-17
- Budin K., Philippe H. (1998) New insights into the phylogeny of Eukaryotes based on Ciliate Hsp70 sequences. *Mol. Biol. Evol.* **15**: 943-956
- Burma B. H., Mayr E. (1949) The species concept. *Evolution Int. J. Org. Evol.* **3**: 369-373

- Buruco Ch., Lhomme V., Fauchere J. L. (1999) Performance criteria of DNA fingerprinting methods for typing of *Helicobacter pylori* isolates: experimental results and meta-analysis. *J. Clin. Microbiol.* **37**: 4071-4080
- Fokin S. I., Przyboś E., Chivilev M. (2001) Nuclear reorganization variety in *Paramecium* (Ciliophora: Peniculida) and its possible evolution. *Acta Protozool.* **40**: 249-261
- Fokin S. I., Przyboś E., Chivilev M., Beyer C. L., Horn M., Skotarczak B., Wodecka B., Fujishima M. (2004) Morphological and molecular investigations of *Paramecium schewiakoffi* sp. nov. (Ciliophora, Oligohymenophorea) and current status of distribution and taxonomy of *Paramecium* species. *Europ. J. Protistol.* **40**: 225-243
- Gavrilets S. (2003) Perspective: models of speciation. What we have learned in 40 years? *Evolution* **57**: 2197-2215
- Gupta R. S., Golding G. B. (1993) Evolution of Hsp70 gene and its implications regarding relationships between Archaeobacteria, Eubacteria and Eucaryotes. *J. Mol. Evol.* **37**: 573-582
- Hori M., Tomikawa I., Przyboś E., Fujishima M. (2006) Comparison of the evolutionary distances among syngens and sibling species of *Paramecium*. *Mol. Phylogenet. Evol.* **38**: 697-704
- Jerome Ch. J., Lynn D. H. (1996) Identifying and distinguishing sibling species in the *Tetrahymena pyriformis* complex (Ciliophora, Oligohymenophorea) using PCR-RFLP analysis of nuclear ribosomal DNA. *J. Euk. Microbiol.* **43**: 492-497
- Jurand A., Przyboś E. (1984) A new method of study of chromosome numbers in *Paramecium*. *Folia biol. (Kraków)* **32**: 295-300
- Kazubski S. L. (1988) Ecologic and geographical variability of Protozoa in the light of the faunal studies. *Wiad. Parazytol.* **34**: 579-589
- Kazubski S. L. (2000) Pierwotniaki pasożytnicze. *Kosmos* **49**: 627-657 (in Polish)
- Przyboś E. (1975) Genetic studies of *Paramecium jenningsi* strains (Diller et Earl, 1958). *Folia biol. (Kraków)* **23**: 425-471
- Przyboś E. (1978) Cytological and karyological studies of *Paramecium jenningsi*. *Folia biol. (Kraków)* **26**: 25-29
- Przyboś E. (1980) The African strain of *Paramecium jenningsi*. Cytological and karyological investigations. *Folia biol. (Kraków)* **28**: 391-397
- Przyboś E. (1986a) Species structure in Ciliates. *Folia biol. (Kraków)* **34**: 103-132
- Przyboś E. (1986b) Chromosomes in *Paramecium jenningsi* (Diller & Earl, 1958): A serial section study. *Folia biol. (Kraków)* **34**: 133-160
- Przyboś E., Hori M., Fokin S. I. (2003a) Strains of *Paramecium quadecaurelia* from Namibia, Africa; genetic and molecular studies. *Acta Protozool.* **42**: 357-360
- Przyboś E., Skotarczak B., Wodecka B. (2003b) Phylogenetic relationships of *Paramecium jenningsi* strains (classical analysis and RAPD studies). *Folia biol. (Kraków)* **51**: 130-145
- Rensing S. A., Maier U. G. (1994) Phylogenetic analysis of the stress-70 protein family. *J. Mol. Evol.* **39**: 80-86
- Skotarczak B., Przyboś E., Wodecka B., Maciejewska A. (2004a) Sibling species within *Paramecium jenningsi* revealed by RAPD. *Acta Protozool.* **43**: 29-35
- Skotarczak B., Przyboś E., Wodecka B., Maciejewska A. (2004b) Random amplified polymorphic DNA fingerprinting as a marker for *Paramecium jenningsi* strains. *Folia biol. (Kraków)* **52**: 117-124
- Sonneborn T. M. (1957) Breeding systems, reproductive methods, and species problems in Protozoa. In: *The Species Problem*, (Ed. E. Mayr). AAAS, Washington, 155-324
- Sonneborn T. M. (1970) Methods in *Paramecium* research. In: *Methods in Cell Physiology*, (Ed. D. M. Prescott). Academic Press, New York, 242-339
- Sonneborn T. M. (1975) The *Paramecium aurelia* complex of 14 sibling species. *Trans. Am. Microsc. Soc.* **94**: 155-178
- Strüder-Kypke M. C., Wright A. G., Fokin S. I., Lynn D. H. (2000a) Phylogenetic relationships of the genus *Paramecium* inferred from Small Subunit rRNA gene sequences. *Mol. Phylogenet. Evol.* **14**: 122-130
- Strüder-Kypke M. C., Wright A. G., Fokin S. I., Lynn D. H. (2000b) Phylogenetic relationships of the subclass Peniculia (Oligohymenophorea, Ciliophora) inferred from Small Subunit rRNA gene sequences. *J. Eukaryot. Microbiol.* **47**: 419-429
- Yamauchi K., Tada H., Usuki I. (1995) Structure and evolution of *Paramecium* hemoglobin genes. *Biochim. Biophys. Acta* **1264**: 53-62

Received on 9th May, 2006; revised version on 21st June, 2006; accepted on 23rd August, 2006

...the ... of ... in ... of ...

REFERENCES

Wang H, ... (1998) ... J. Cell. Physiol. 175:1-10.
Kumar S, ... (1999) ... J. Cell. Physiol. 178:1-10.
Chen X, ... (2000) ... J. Cell. Physiol. 180:1-10.

Changes in the Testacean Community Structure Along Small Soil Profiles

Sofie VINCKE¹, Bart Van de VIJVER², Ivan NIJS³ and Louis BEYENS¹

¹University of Antwerp, Campus Drie Eiken, Department of Biology, Research group Polar Ecology, Limnology and Paleobiology, Wilrijk; ²National Botanic Garden of Belgium, Department of Bryophytes and Thallophytes, Domein van Bouchout, Meise; ³Research group Plant and Vegetation Ecology, Department of Biology, University of Antwerp, Wilrijk, Belgium

Summary. The testate amoebae (Protozoa, Rhizopoda) fauna was studied along several small soil profiles, which were collected in the wet valley soils of Île de la Possession (Crozet Archipelago, sub-Antarctica). All soil cores were divided into 3 zones (0-3 / 3-6 / 6-10 cm) and results were compared with an earlier soil study on the island, when soil samples were taken at a depth of 5 to 10 cm. There was no turnover of testacean taxa between the different soil layers, but the changes in the community structure of the communities along the soil horizons were remarkable. In the upper soil layers (0-3 cm) more taxa belonging to characteristic morphological soil test types were observed, test types which were rarely encountered in the soil samples taken at a depth of 5 to 10 cm. The genera *Assulina*, *Centropyxis*, *Corythion*, *Heleopera* and *Nebela* were more abundant in the upper soil horizons, which led to a reduced dominance of the genus *Trinema*. Also the living fraction of the testacean fauna was significantly higher in the upper soil zones, whereas the highest amount of cysts was observed in the lowest soil horizon (6-10 cm). Some notes are made on the different disappearance patterns of "Filose" and "Lobose" taxa along the valley soil profiles of Île de la Possession. All observed changes along the small soil profiles emphasize the importance of the soil sampling strategy.

Key words: community structure, Île de la Possession, morphological soil test types, peaty valley soils, soil sampling strategy, testate amoebae.

INTRODUCTION

A previous study on the testate amoebae diversity (Protozoa, Rhizopoda) in different soil habitats (valley soils, fellfield soils, marine influenced soils) on Île de la Possession (Crozet Archipelago, sub-Antarctica) revealed 65 testacean taxa belonging to 20 different genera (Vincke *et al.* 2004a). However, the species-

genera distribution of that study showed that more than 50% of all testate amoebae tests belonged to one genus only, i.e. *Trinema*. Tests of this genus are being classified under the morphological test type "plagiostome with a visor", a test type which is very commonly observed in all sorts of soils (Bonnet 1975). Contrary to the genus *Trinema*, testate amoebae taxa belonging to other morphological test types characteristic for soils, such as the "compressed acrostome" type (e.g. genera *Assulina*, *Heleopera*, *Nebela* and *Hyalosphenia*), the "axial pseudostome" type (genera *Cyclopyxis*, *Trigonopyxis*, *Phryganella* and *Arcella*) and the "simple cryptostome" type (e.g. genera *Plagiopyxis*, *Bullinaria* and

Address for correspondence: Sofie Vincke, University of Antwerp, Campus Drie Eiken, Department of Biology, Research group Polar Ecology, Limnology & Paleobiology, Universiteitsplein 1, B-2610 Wilrijk, Belgium; Fax: +32 3 820 2950; E-mail: sofie.vincke@ua.ac.be

Protoplagiopyxis) (Bonnet 1975), were very poorly represented or not observed at all in the studied soil samples on Île de la Possession.

It is also known that a vertical distribution of these protists, which is correlated to some extent with the test shape, can be observed in most soil habitats (Bonnet 1964). In general, larger and more spiny species are found in the upper soil horizons, whereas flatter and smaller species are observed in the lower horizons. The majority (96%) of the testate amoebae taxa found in the soils studied by Vincke *et al.* (2004a), were taxa with relatively small tests (ranging from 8 µm to 75 µm) without spines.

During the field campaign (1999-2000) on Île de la Possession, the soil samples were taken for diatom analysis at a depth varying from 5 to 10 cm (Van de Vijver *et al.* 2002). This might be below the active zone for testate amoebae and therefore it remains unclear whether other morphological test types and larger or more spiny testate amoebae taxa have been overlooked due to inappropriate sampling at that time.

The present study aims to enlarge our knowledge on the vertical distribution of testate amoebae in the wet valley soils on Île de la Possession. Therefore 21 small soil cores, all divided into three zones (see Materials and Methods), were collected during the new field campaign (2004-2005) on the island. Next to changes in the testacean diversity (taxa and test types), specific attention will be given to changes in test size, dead/living ratio, Lobose/Filose index ("Lobose" and "Filose" are referring to the shape of the pseudopodia of the testaceans) and population densities along these soil profiles. The results of the small soil cores will be compared with the observed testacean fauna in the wet valley soils in Vincke *et al.* (2004a).

MATERIALS AND METHODS

Sampling strategy and sample analysis

During the austral summer of 2004-2005 twenty-one small soil cores were collected on Île de la Possession. For each of the 7 sampling sites (Bollard / Jardin Japonais / La Pérouse / Pointe Basse / Rivière du Camp / Vallée de la Hébé / Vallée des Branloires), three soil cores were taken at a sufficiently large distance from each other (> 100m). The soil cores were taken with a cork borer (diameter 22 mm) and each core (total length 10 cm) was sub-divided into three zones: 0-3 cm (upper zone: samples "A"); 3-6 cm (middle zone: samples "B") and 6-10 cm (lower zone: samples "C"), leading to a total of 63 samples. The zero level has been determined as being the

bare soil after removal of living plant material. All samples were fixed immediately with 3% formaldehyde and stored in 25 ml PVC bottles. For each soil core, soil moisture was measured at a depth of 5 cm and 20 cm (Eijkelkamp TRIME-FM), temperature at a depth of 3 cm and 10 cm (Novo Quick®) and the dominant surrounding vegetation was noted. Appendix 1 lists the environmental data of the 21 small soil cores.

Sampling sites were chosen randomly scattered on the entire island (Fig. 1), but the soil type was fixed. Since the dry fell-field soils on the island contained little or no testate amoebae (Vincke *et al.* 2004a), all soil cores were taken exclusively in wet valley soils. This species rich soil type with high population densities allows a detailed study of the distribution patterns of the testate amoebae fauna. Testacean observations in the small soil cores of this study will be compared with the ones found in the valley soils of Vincke *et al.* (2004a).

In the laboratory, about two gram of soil of each sample was mixed with 10 tablets of *Lycopodium* spores (BATCH 483216, Lund University, Sweden) in distilled water to calculate the population density. Afterwards these soil samples were passed through a sieve with a mesh diameter of 297 µm and concentrated by centrifugation (10 min at 2000 rpm). The colour rose bengal was added to the samples to distinguish dead from living individuals (at the moment of sampling). Encysted testate amoebae were considered as being alive. In each soil sample 150 tests were counted using a Leitz Wetzlar® microscope. Morphological identifications of the testate amoebae are mainly based on works by Decloître (1962, 1978, 1979, 1981), Deflandre (1928, 1929, 1936), Grospietsch (1964), Hoogenraad and de Groot (1940), Ogden and Hedley (1980) and Ogden (1983). All samples are stored at the University of Antwerp, Unit of Polar Ecology, Limnology and Paleobiology.

Data analysis

To compare the testate amoebae faunas of the 21 small soil cores and the valley soils of Vincke *et al.* (2004), the Community Coefficient of Sørensen (1948) was calculated: $2c/(a+b+2c)$, where "a" and "b" are the number of taxa exclusively observed in one study and "c" is the number of taxa the two studies have in common.

A diversity analysis comprised the calculation of the 'Gini evenness measure' (Nijssen *et al.* 1998) and the 'Shannon Wiener diversity index' (\log_{10} -based) using the Multivariate Statistical Package (MVSP, Kovach Computing Services 2002).

Ordination analyses included a hierarchic-agglomerative cluster analysis, based on a minimum variance strategy with the Squared Euclidean Distance as a dissimilarity measure (MVSP, Kovach Computing Services 2002) and a Correspondance Analysis (CANOCO, version 4.0) (Ter Braak and Smilauer 1998) to classify the species data (ln-transformed). A Canonical Correspondance Analysis was carried out to detect possible patterns within species and environmental data (CANOCO, version 4.0) (Ter Braak and Smilauer 1998). Forward selection with unrestricted Monte Carlo tests (999 permutations, $P \leq 0.05$) was used to detect which variables significantly influenced the sample/species distribution, but unfortunately no significant variables ($P > 0.1$) were selected.

To examine the relationship between the testacean test sizes and their occurrences in the different soil layers ("A"/ "B"/ "C"), a regression analysis was carried out. Therefore 10 individuals of all encountered taxa (56) were measured (length in µm) randomly over all

soil cores. Mean test sizes together with their standard errors (SE) are shown in Appendix 2. Counting 10 individuals of each taxon was a feasible number for most testate amoebae taxa, since 40 out of 60 taxa had relative abundances <0.5% (see Results). The relatively small SE's reflected a natural variability within the test sizes of the testate amoebae taxa. For 4 taxa however (*Archerella* sp. 1, *Centropyxis platystoma* (Penard) Deflandre, *Corythion* sp. 1 and *Cyclopyxis puteus* Thomas) only one individual was observed over all soil core samples, so no mean size could be calculated and therefore these 4 taxa were left out of the regression analysis. All mean test sizes were log-transformed and divided into 10 equal size-classes. For each size-class a regression analysis was performed between the log-transformed abundance data of the taxa of that particular size-class and the soil depth ("A"/"B"/"C"). Calculated slopes of these regression analyses were then used in a final regression analysis with the mean size of the testate amoebae per size-class.

Statistical tests to compare the means of diversity, evenness, number of taxa, population densities and the living testate amoebae fraction between the different soil zones ("A"/"B"/"C"), included several One Way ANOVAs (data parametric) and, Kruskal-Wallis and Mann-Whitney tests (data non-parametric) (SPSS 12.0).

RESULTS

General observations

The analysis of the 21 soil profiles revealed a testate amoebae fauna of 60 taxa (20 genera). A detailed list of all observed taxa, together with their relative abundances (%) in each soil layer ("A"/"B"/"C"), is given in Appendix 2. Two taxa, namely *Cyclopyxis puteus* and *Centropyxis sacciformis* Hoogenraad, are reported for the first time on Île de la Possession. Forty-five taxa, including these 2 previously unreported species, had relative abundances <1% (40 taxa <0.5%). Dominant taxa were *Trinema lineare* Penard (34%), *Euglypha rotunda* Wailes (20.5%) and *Difflogiella oviformis* (Penard) Bonnet *et* Thomas (10%). Thirteen testate amoebae taxa were not observed in Vincke *et al.* (2004a) and are marked with an asterisk in Appendix 2.

The Sørensen similarity analysis (0.8) between the valley soils of Vincke *et al.* (2004a) and the small soil cores, indicates that both testate amoebae faunas are very much alike in terms of species composition. Taxa that were not observed in this study, all had relative frequencies <0.5% in Vincke *et al.* (2004a). The newly observed taxa in this study also had relative abundances <0.5%.

A cluster analysis (Fig. 2) and a Correspondance analysis (not shown) revealed that all 21 soil cores had rather similar testacean faunas, since the "Squared Euclidean" distances for clustering were relatively low

and all samples were grouped together in the middle of the CA-ordination diagram. Also the similarity in species composition between the different zones of each soil profile appeared to be very high as the "A"/"B"/"C", samples of the same profile were always grouped (close) together. A Canonical Correspondence Analysis (not shown) could not reveal any clear relationships between the testate amoebae fauna and the environmental variables, since all samples were again accumulated in the centre of the ordination diagram.

Observations along the soil profiles

Species composition, diversity and population density. Changes in the relative abundances (%) of all observed testate amoebae can be derived from Appendix 2. Since 45 taxa had relative abundances <1%, trends in occurrence of these species are hard to predict. There was no turn-over of species observed along the soil profiles. Most taxa observed in soil layers "A", were also observed in soil layers "B" and "C". Nevertheless, clear differences in the total number of tests encountered per soil layer, could be observed for several taxa (Fig. 3). A clear decrease in the total number of tests encountered from zone "A" to zone "C", can be observed for taxa as *Arcella arenaria* Greeff, *Assulina muscorum* Greeff and *Corythion dubium* Taranek, whereas the amount of tests of *Difflogia pristis* Penard, *D. sp. 3*, *Trinema enchelys* Leidy, *Difflogiella oviformis* and *Pseudodifflogia fulva* Penard increases notably with depth.

Diversity analysis of the soil cores revealed no significant (One Way ANOVA: $P > 0.05$) differences in the mean Shannon-Wiener diversity, GINI evenness or the number of taxa between the 3 soil zones. Also changes in population densities were insignificant (One Way ANOVA: $P > 0.05$) (Table 1).

Morphological test types. According to Bonnet (1975) there are 5 morphological test types of testate amoebae which are characteristic (relative frequencies >10%) in soil habitats. A schematic reproduction of these 5 morphological test types is given in Fig. 4. Table 2 compares the relative abundances (%) of several genera, between the valley soils of Vincke *et al.* (2004a) and the different zones ("A"/"B"/"C"), of the small soil cores of this study. Genera have been classified according to their morphological test type and the types are once more arranged with decreasing importance in soils.

This comparison clearly shows that the upper soil layers (zone "A": 0 to 3cm) of the small soil cores contain substantially more individuals of the genera

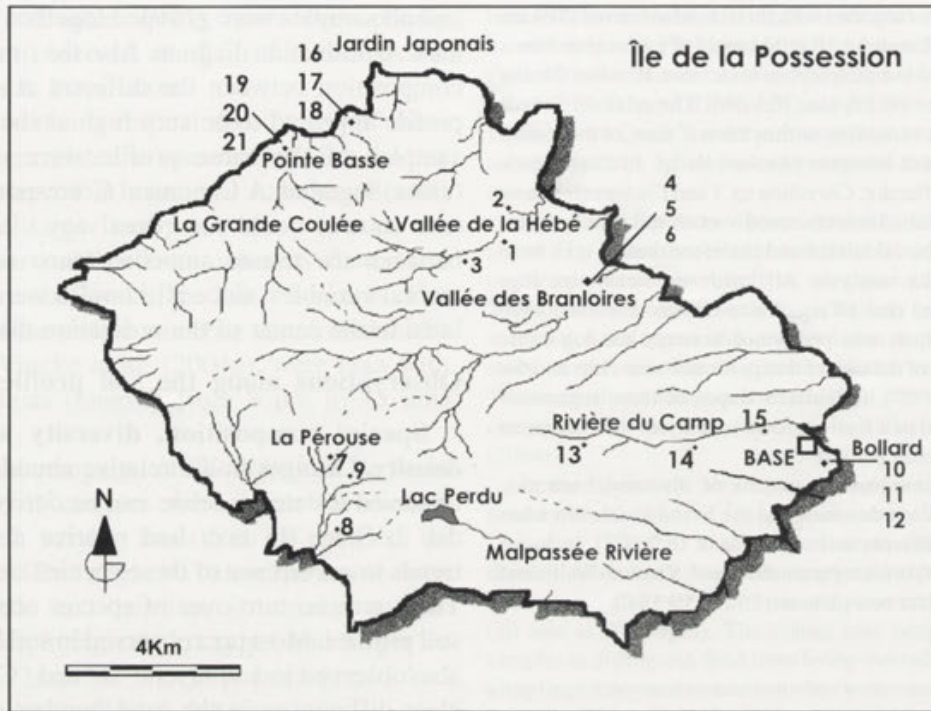


Fig. 1. Sketch map of Île de la Possession, showing the locations where the 21 small soil cores have been collected.

Assulina, *Heleopera* and *Nebela*. Also the relative abundances of the genera *Centropyxis* (especially *C. aerophila* and its varieties) and *Corythion* are higher compared to those of the other zones and of the valley soils of Vincke et al. (2004a). The detailed analysis of the soil cores (especially the upper zones "A") could not prove the presence of any species belonging to the cryptostome type. Also individuals of the axial type were again very scarce in the wet valley soils of Île de la Possession.

Test size. Smallest tests belonged to *Diffflugia* sp6 ($7.0 \pm 0.2 \mu\text{m}$) and *Difflogiella pusilla* Playfair ($9.2 \pm 0.4 \mu\text{m}$), while the largest tests belonged to *Nebela vas Certes* ($188 \pm 6 \mu\text{m}$) and *Cyclopyxis puteus* ($195 \mu\text{m}$) (see Appendix 2). The majority (66%) of all observed tests had rather small test dimensions varying between $20 \mu\text{m}$ and $40 \mu\text{m}$. This was mainly due to the high abundances of *T. lineare*, *E. rotunda* and *D. sp. 3*.

Bonnet in 1964 stated that a vertical distribution of testate amoebae can be observed in most soil habitats: larger and more spiny species are more frequently observed in the upper soil horizons, while flatter, smaller species dominate the lower horizons (Bonnet 1964). To

check if this hypothesis applied for the wet valley soils on Île de la Possession, a regression analysis was carried out between the mean sizes of the testate amoebae tests and their abundances in the different soil layers ("A"/"B"/"C"), (see Data analysis). The regression analysis revealed a very weak negative relation ($y = -0.0001x + 0.0061$, $R^2 = 0.0971$) between test sizes and their occurrences in the different soil zones. Unfortunately, this negative relation appeared not significant ($P=0.2$). Apparently, abundances of testate amoebae with large tests are too low in the soils of Île de la Possession, so a more clear relationship can not be proven.

Only 5 taxa with spines were observed, namely *Euglypha ciliata* (Ehrenberg) Penard, *E. compressa* Carter, *E. cristata* Leidy, *E. strigosa* Leidy and *Corythion* sp. 1. The 3 latter taxa had higher relative abundances in soil layer "A" (see Appendix 2), but a significant statistical trend could not be observed due to the low numbers of individuals of these spiny taxa.

Living testacean fraction. Only 3.4% of the testate amoebae fauna (including cysts) was alive at the moment of sampling. Statistical tests showed a high significant difference between the mean number of living

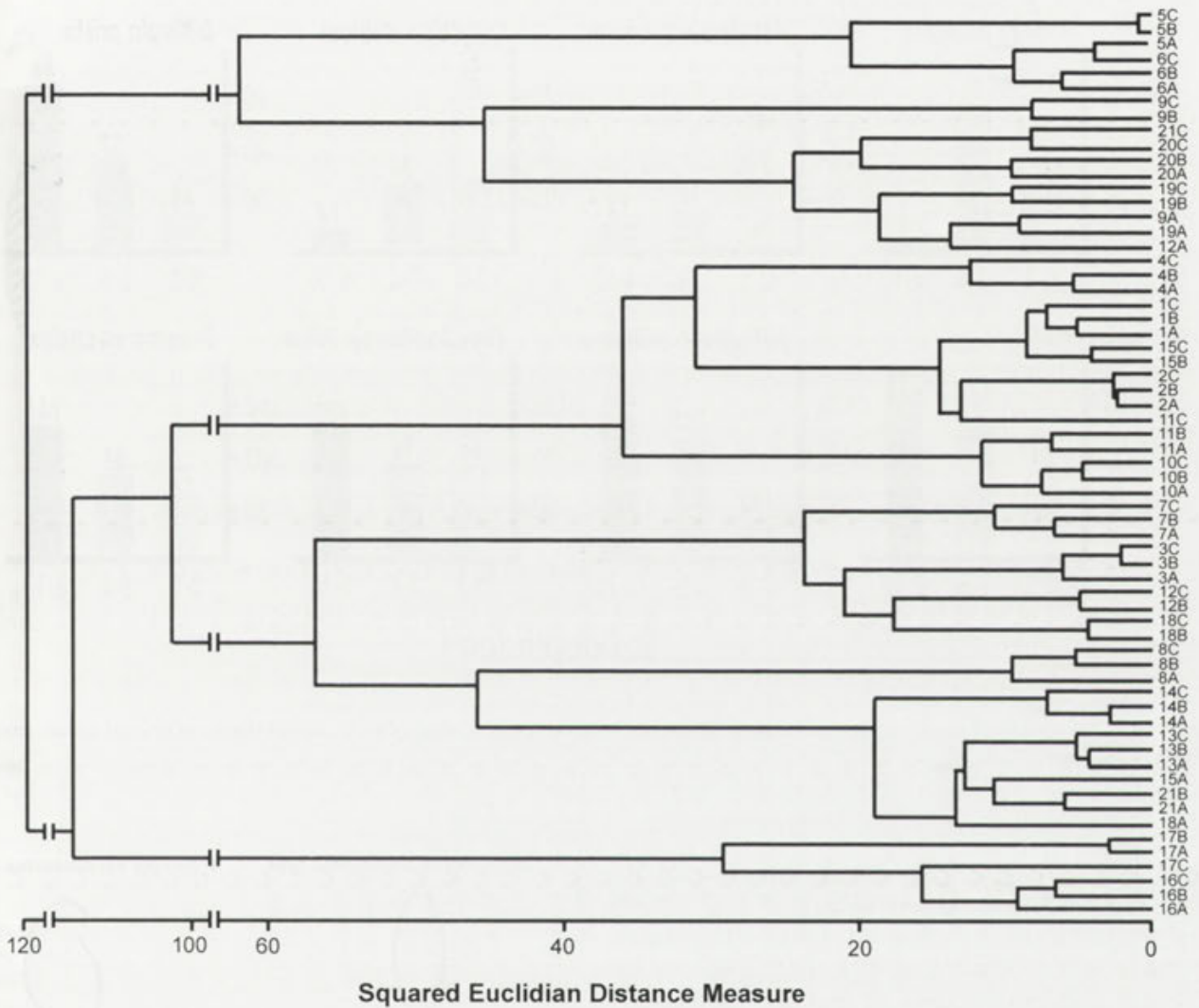


Fig. 2. Cluster dendrogram, showing the similarity between the different zones ("A"/"B"/"C") of each soil core.

individuals found in the three different soil zones ("A"/"B"/"C"), (Kruskal-Wallis test, $P < 0.001$). Three pairwise comparisons between "A"/"B", "B"/"C" and "A"/"C" layers also revealed significant differences between the layers (Mann-Whitney tests, "A"/"B": $P < 0.0001$; "B"/"C": $P < 0.01$; "A"/"C": $P < 0.0001$). The quantity of living testate amoebae was clearly the highest in the upper soil layers (zone "A": 0 to 3 cm) and decreased rapidly towards more profound soil layers (zones "B"/"C") (Fig. 5). The variation of living individuals within each layer is shown by the means and their standard deviation (zone "A": 10 ± 3 ; zone "B": 4 ± 4 ; zone "C": 2 ± 3). Individuals that were alive in the lower

soil zones ("B"/"C": 3 to 10 cm) were more frequently encysted, compared to the ones in soil zone "A" (Fig. 5). However, the observed number of cysts (0.4%) was too low to establish a statistical trend.

Lobose-Filose index. The LF-index of Bonnet (1976) was calculated for the 3 different soil layers (zone "A": -0.65; zone B: -0.59; zone C: -0.61). Genera, such as *Diffugiella* and *Cryptodiffugia*, with pseudopodia in between "Lobose" and "Filose", were left out of the calculation. All LF-values were rather similar to the one found for the wet valley soils (-0.68) in Vincke *et al.* (2004a), once again due to the overall dominance of euryvalent species of *Trinema*, *Euglypha* and *Corythion*

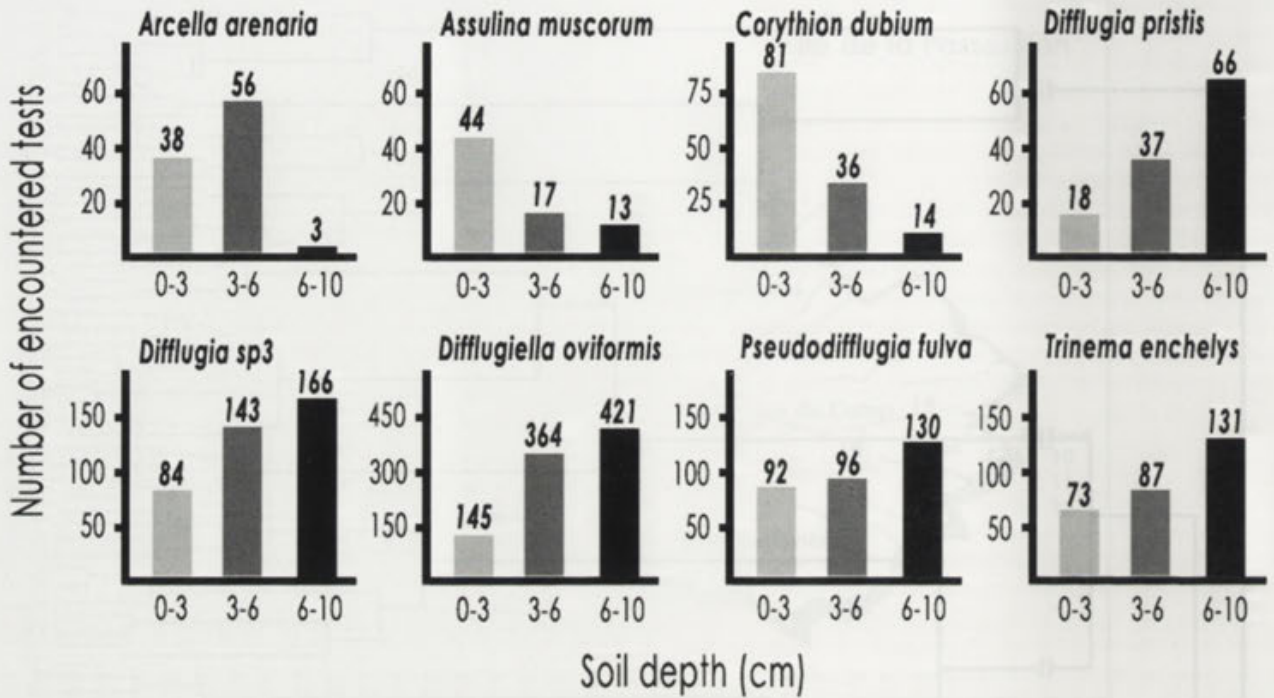


Fig. 3. The total number of tests encountered in the different soil zones (0-3 cm / 3-6 cm / 6-10 cm soil depth) of several testate amoebae species.

(Balik 1994). No remarkable changes between the LF-values of the different soil layers (“A”/“B”/“C”), could be observed (Kruskall-Wallis test, $P=0.8$). This means that the amount of tests belonging to the “Filosa” and the “Lobosa” does not decrease or increase significantly with depth.

DISCUSSION

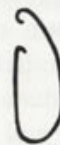
A comparison of the testacean fauna observed in the small soil cores with the one observed in the wet valley soils of Vincke *et al.* (2004a), shows that there are only small differences in species composition between both studies. Apparently, the fact that the soil samples in the previous study had been taken rather deep (5 to 10 cm), has no major influence on the species richness of the testate amoebae fauna taxa in the soil samples.

However, significant differences are observed in the community structure when comparing the relative abundances of several taxa. Genera, such as *Assulina*, *Heleopera* and *Nebela*, belonging to the most common morphological test type in soils (compressed acrostome), have remarkably higher relative abundances, especially

- 1. Compressed acrostome type
- 4. Simple cryptostome type



- 2. Plagiostome with a visor type
- 5. Simple acrostome type



- 3. Axial type



Fig. 4. A schematic reproduction of the 5 morphological test types with the highest relative frequencies in soils. The 5 test types are arranged with decreasing importance in soil habitats. Other morphological test types of Bonnet (1975) are not shown.

in soil zone “A”, compared to the ones of the valley soils of Vincke *et al.* (2004a). Also tests belonging to the

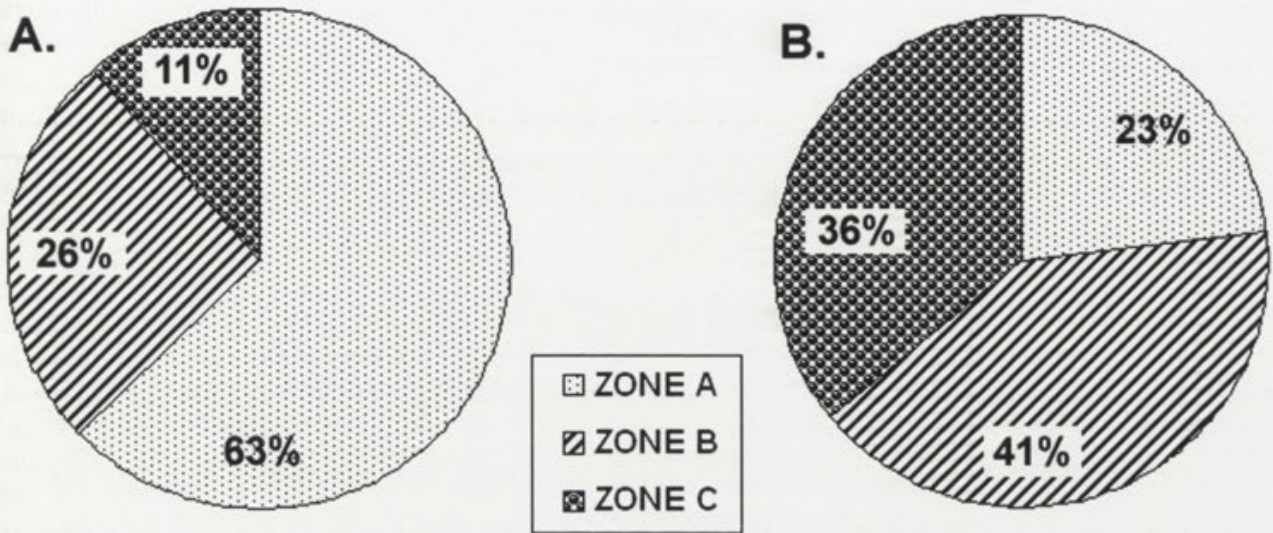


Fig. 5. Pie diagrams showing (A) the percentages of living tests encountered in each soil zone ("A"/ "B"/ "C"), and (B) the percentages of encysted individuals in each zone.

Table 1. Means with standard errors of the Shannon-Wiener Diversity Index, the GINI Evenness Measure, the total number of taxa and the testacean population densities in each soil zone ("A"/ "B"/ "C").

	Zone "A" (0-3 cm)	Zone "B" (3-6 cm)	Zone "C" (6-10 cm)
Shannon-Wiener Diversity Index	0.80 ± 0.03	0.80 ± 0.03	0.78 ± 0.03
GINI Evenness measure	0.34 ± 0.01	0.36 ± 0.02	0.33 ± 0.01
Number of taxa	15.5 ± 0.6	14.9 ± 0.8	15.0 ± 0.7
Population density per gram soil	1553050 ± 186185	2051562 ± 374040	1991323 ± 432607

genera *Centropyxis* and *Corythion* of the "plagiostome with a visor" test type, are more frequently observed in this study. Again, their abundance appears to be the highest in the upper soil layers "A", the part of the soil which was not sampled in Vincke *et al.* (2004a). The increase of the other characteristic soil test types leads to a reduced dominance of the genus *Trinema* in the soil cores (34% versus 51% in Vincke *et al.* 2004a).

Tests of *Assulina muscorum* and *Corythion dubium*, two taxa characteristic for drier habitats (Vincke *et al.* 2004c), were more frequently observed (also living individuals) in the upper soil layers "A", where moisture values were considerably lower than in soil zones 'B' and "C". Living individuals of these two taxa in soil layers "B" and "C" (3 to 10cm) were very scarce, but

when observed, they were always encysted. In contrast to this, tests of *Pseudodiffugia fulva*, *Trinema enchelys* and several *Diffugia* taxa, all characteristic taxa for moist to wetter (even aquatic) habitats, had remarkable higher abundances in the lower soil zones (6 to 10 cm). Living (not encysted) individuals of these taxa were encountered in all soil layers, but encysted tests were more frequently observed in the upper, drier soil layer "A".

Smith (1973) observed no consistent difference in the numbers of *Corythion dubium* between the three soil horizons (0-3/3-6/6-9 cm) he studied on Signy Island. Also on South Georgia (Smith and Headland 1983) a similar testacean species composition was observed in 2 soil layers (0-3/3-6 cm) and again no pattern in the

Table 2. Comparison of the relative abundances (%) of several genera, classified according to morphological test types of Bonnet (1975), between the different zones ("A"/"B"/"C") of the soil cores of this study and the valley soils of Vincke *et al.* (2004a). The morphological test types are arranged with decreasing importance in soils (Bonnet 1975).

	Valley soils 5-10 cm	Zone "A" 0-3 cm	Small soil cores Zone "B" 3-6 cm	Zone "C" 6-10 cm
1. Compressed acrostome type				
<i>Assulina</i>	0.6	1.8	1.0	1.1
<i>Heleopera</i>	0.1	0.4	0.5	0.2
<i>Hyalosphenia</i>	0.02	0.03	0.03	0.03
<i>Nebela</i>	0.2	2.6	1.7	1.5
2. Plagiostome with a visor type				
<i>Centropyxis</i>	0.02	0.4	0.3	0.06
<i>Corythion</i>	0.8	2.7	1.1	0.4
<i>Trinema</i>	51.1	39.5	35.7	35.4
3. Axial pseudostome type				
<i>Cyclopyxis</i>	1.6	0.2	0.5	0.4
<i>Phryganella</i>	0.1	-	-	-
<i>Trigonopyxis</i>	-	-	-	-
4. Cryptostome type				
<i>Bullinaria</i>	-	-	-	-
<i>Plagiopyxis</i>	-	-	-	-
<i>Protoplagiopyxis</i>	-	-	-	-
5. Simple acrostome type				
<i>Diffugia</i>	4.9	4.6	8	9.2
<i>Diffugiella</i>	7.6	6.4	13.9	16.1
<i>Tracheleuglypha</i>	1.2	0.8	0.7	0.3

vertical distribution of abundance of the testate amoebae taxa was noticed. It is possible however that change in abundances between the different soil horizons were masked by the seasonal variations of the taxa in both studies.

Although no changes in testacean diversity nor evenness were observed between the different soil horizons on Île de la Possession, the variations in the community structure (abundance and dominance of several taxa / living fraction of testaceans) are obvious. These observations clearly indicate that the soil samples of Vincke *et al.* (2004a) were taken too deep (5 to 10 cm) into the soil and below the most active zone of testate amoebae, for this observations to be made. The results of this study clearly complete the data of the studied valley soils in Vincke *et al.* (2004a). The distinction made between the three different soil types (peaty valley soils, fellfield soils and marine influenced soils) in Vincke *et al.* (2004a) remains valuable however. Most likely similar changes in the testacean community structure along soil profiles collected in fellfield soils and marine influenced soils would be observed.

It remains striking however that even in the present study, especially in upper soil layers "A", again no taxa were observed of the cryptostome and the axial test type (except for a few tests of *Cyclopyxis*), which are both very characteristic test types in soils (Bonnet 1964). In contrast to this, tests of the cryptostome and axial type are relatively frequently encountered in soils and mosses on the neighbouring sub-Antarctic islands, Îles Kerguelen (Bonnet 1981) and Marion Island (Grospletsch 1971). Only a few empty shells of *Plagiopyxis callida* Penard, *P. declivis* Thomas and *Phryganella paradoxa* Penard were observed in previous studies in moss and aquatic habitats of Île de la Possession (Vincke *et al.* 2004b,c).

Also the expected increase in the amount of larger and more spiny taxa in the upper soil layers on Île de la Possession, was not completely fulfilled. Bonnet (1975) stated that the distribution of morphological test types was closely related to the water availability. Low moisture availability will favour species with reduced test and pseudostome size (Foissner 1987). The 21 soil cores however, were collected in valley soils with mean moisture values (VOL%) of 33 ± 4 at 5 cm depth and $60 \pm$

6 at 10 cm depth in the soil. Knowing that the rainfall on Île de la Possession usually exceeds 2400 mm per year (Frenot 1986), these valley soils seem rather moist habitats. It might be possible that individuals of genera, such as *Plagiopyxis*, *Bullinaria* and *Protoplagiopyxis* (cryptostome test type), are too drought-adapted and therefore are outcompeted in those moist habitats. Evidently, the moisture content of the habitat is not the only factor determining the testacean species distribution. Besides other variables (e.g. pH, trophic state, microbial food webs), also soil structure and soil porosity may have an important influence on the testate amoebae fauna in the soils of Île de la Possession. Since the porosity of the "peaty" valley soils is rather low, the small test dimensions of taxa in the subclass Testaceafilosia will be favoured in these soil types.

Along the soil profiles no changes in the amounts of tests belonging to either the "Lobose" or the "Filose" type were observed. This is rather striking since one would expect the destruction of empty tests under less favourable conditions deeper into the soil. Lousier and Parkinson (1981) studied the disappearance of empty tests under experimental conditions and noticed that higher moisture contents stimulated the destruction of a larger number of tests. Moreover tests with platelets (idiosomes) appeared to disappear more quickly than the ones made of sediment particles (xenosomes). Apparently these findings do not apply to the real life field conditions of the valley soils of Île de la Possession, at least not for all taxa. Relative abundances of taxa with xenosomes (genera *Centropyxis*, *Cyclopyxis*, *Diffflugia* and *Pseudodiffflugia*) were indeed higher in the lower soil layers, which may indicate a more difficult destruction of these kinds of tests, despite the higher moisture contents in this soil zone. The majority of the taxa with platelets (genera *Assulina*, *Corythion*, *Euglypha*, *Tracheleuglypha*, *Trachelocorythion* and *Trinema*) had lower relative abundances towards soil layer 'C', possibly caused by a higher disappearance rate of empty shells. However, platelet tests of some *Euglypha* taxa and especially *Trinema enchelys* seem to conserve remarkably better in the lower soil layers. Also tests of the genus *Difflogiella* seem to maintain quite well in the soils on Île de la Possession. Probably the disappearance of empty tests, especially in these "peaty" valley soils, will be a complex combination of biological, physico-chemical and mechanical features which is beyond the goal of this study. Especially in studies of fossil testacean assemblages, finding out the real reason for fluctuations in test concentrations can be problematic. After all these

variations can either be caused by differences in the decay rates of the taxa (Lousier and Parkinson 1981), or by real changes in population densities due to environmental changes in the habitat (Beyens and Meisterfeld 2001). The observed changes in the community structure and the different disappearance patterns of empty tests along soil profiles should be carefully taken into account when interpreting the (sub)fossil testacean fauna in peat cores of Île de la Possession.

Most publications on the testacean fauna in soils all over the world give no indication on the depth at which the soil samples were taken. Some studies sampled the upper 5 cm of the soil (e.g. Smith 1982, 1985; Ledeganck et al 2003), while Bonnet (1976) collected samples of 100 cm³ of soil, which is actually 10 cm deep into the soil.

In general, if one wants to study the present diversity and ecology of the testacean soil fauna, it is very important to collect soil samples in the upper layers (0 to 3cm) of the soil. Even if testate amoebae are abundantly present in the upper 10 cm of the soil (Stout and Heal 1967; Foissner and Adam 1980; Meisterfeld 1980), there might be remarkable changes observed along these 10 cm. Apparently, as proven in this study, it is not the turn-over in species composition along the soil profile that matters, but the changes in the community pattern (abundances and dominances) of the testacean fauna. Especially the living testacean fraction differs significantly between the upper soil layers and just a few centimeters beneath.

Acknowledgements. The sampling was made possible by the logistic and the financial support of the French Polar Institute (IPEV) in the frame of the Terrestrial Program DIVCRO 405 (Prof. Dr. L. Beyens & Prof. Dr. I. Nijs, Universiteit Antwerpen, Belgium). Dr. Niek Gremmen is thanked for his valuable comments and advice on statistical questions.

REFERENCES

- Balik V. (1994) On the soil testate amoebae fauna (Protozoa, Rhizopoda) of the Spitsbergen Islands. *Arch. Protistenkd.* **144**: 365-372
- Beyens L., Meisterfeld R. (2001) Protozoa: Testate Amoebae. In: Tracking environmental change using lake sediments. Volume 3: Terrestrial, algal and silicious indicators (Eds. J. P. Smol, H. J. B. Birks and W. M. Last.) Kluwer Academic Publishers, Dordrecht, The Netherlands, 1-33
- Bonnet L. (1964) Le peuplement thécamoebien des sols. *Rev. Ecol. Biol. Sol.* **1**: 123-408
- Bonnet L. (1975) Types morphologiques, écologie et évolution de la thèque chez les thécamoebiens. *Protistol.* **3**: 363-378
- Bonnet L. (1976) Le peuplement thécamoebien édaphique de la cote-d'ivoire. Sols de la région de Lamto. *Protistol.* **4**: 539-554
- Bonnet L. (1981) Thécamoebiens (Rhizopoda, Testacea). *Bull. Com. Nat. Fran. Res. Antarct.* **48**: 23-32
- Declòtre L. (1962) Le genre *Euglypha* Dujardin. *Arch. Protistenkd.* **106**: 51-100

- Decloître L. (1978) Le genre *Centropyxis* I. Compléments à jour au 31 décembre 1974 de la Monographie du genre parue en 1929. *Arch. Protistenk.* **120**: 63-85
- Decloître L. (1979) Le genre *Centropyxis* II. Compléments à jour au 31 décembre 1974 de la Monographie du genre parue en 1929. *Arch. Protistenk.* **121**: 162-192
- Decloître L. (1981) Le genre *Trinema* Dujardin, 1841. Révision à jour au 31 décembre 1979. *Arch. Protistenk.* **124**: 193-218
- Deflandre G. (1928) Le genre *Arcella*. *Arch. Protistenkd.* **64**: 152-288
- Deflandre G. (1929) Le genre *Centropyxis*. *Arch. Protistenkd.* **67**: 322-375
- Deflandre G. (1936) Etude monographique sur le genre *Nebela* Leidy. *Ann. Protistol.* **5**: 201-327
- Foissner W. (1987) Soil Protozoa: Fundamental Problems, Ecological Significance, Adaptations in Ciliates and Testaceans, Bioindicators and Guide to the Literature. (Eds. J. O. Cotliss and D. J. Patterson). *Prog. Protistol.* **2**: 69-212
- Foissner W., Adam H. (1980) Vertikalverteilung und Artenzahl der terrestrischen Ciliaten und Testaceen einer Almweide und einer Schipiste auf der Schlossalm bei Bad Hofgastein. *Zool. Anz.* **205**: 181-187
- Frenot Y. (1986) Interactions entre la faune lombricienne et les systèmes édaphiques d'une île subantarctique: Île de la Possession, Archipel Crozet. Thèse de l'Université de Rennes, France
- Grospietsch T. (1964) Die gattungen *Cryptodifflugia* und *Difflugiella* (Rhizopoda, Testacea). *Zool. Anz.* **172**: 243-257
- Grospietsch T. (1971) Rhizopoda. Beitrag zur ökologie der testaceen Rhizopoden von Marion Island. Max-Planck-Institut für Limnologie, Plön **37**: 411-419
- Hoogenraad H. R., de Groot A. A. (1940) Zoetwaterhizopoden en - heliozoën. Boschma H. Fauna van Nederland IX Leiden
- Kovach Computing Services (2002) Multivariate Statistical Package Version 3.1, Users' Manual. Kovach Computing Services, Pentraeth, Wales
- Ledeganck P., Nijs L., Beyens L. (2003) Plant functional group diversity promotes soil protist diversity. *Protist* **154**: 239-249
- Lousier J. D., Parkinson D. (1981) The disappearance of empty tests of litter- and soil testate amoebae (Testacea, Rhizopoda, Protozoa). *Arch. Protistenk.* **124**: 312-336
- Meisterfeld R. (1980) Die Struktur von Testaceenzönosen (Rhizopoda, Testacea) in Böden des Sollings. *Ver. Ges. Oekol.* **8**: 435-447
- Nijssen D., Rousseau R., Van Hecke P. (1998) The Lorenz curve: a graphical representation of evenness. *Coenoses* **13**: 33-38
- Ogden C. G. (1983) Observations on the systematics of the genus *Difflugia* in Britain (Rhizopoda, Protozoa). *Bull. Br. Mus. Nat. Hist. Zool. Ser.* **44**: 1-73
- Ogden C. G., Hedley R. H. (1980) An atlas of freshwater testate amoebae. Br Mus Nat Hist, Oxford University Press, Oxford
- Smith H. G. (1973) The Signy Island terrestrial reference sites: III. Population ecology of *Corythion dubium* (Rhizopoda: Testacida) in site 1. *Br. Antarct. Surv. Bull.* **33 and 34**: 123-135
- Smith H. G. (1982) The terrestrial protozoan fauna of South Georgia. *Polar Biol.* **1**: 173-179
- Smith H. G. (1985) The colonisation of volcanic tephra on Deception Island by Protozoa: long-term trends. *Br. Antarct. Surv. Bull.* **66**: 19-33
- Smith H. G., Headland R. K. (1983) The population ecology of soil testate rhizopods on the sub-Antarctic island of South Georgia. *Rev. Ecol. Biol. Sol.* **20**: 269-286
- Sørensen T. (1948) A method of establishing groups of equal amplitude in plant sociology based on similarity of species content. Det Kongelige Danske Videnskabernes Selskabs, Biologisk Skrifter, Copenhagen, **54**: 1-34
- Stout J. D., Heal O. W. (1967) Protozoa. Academic Press, London & New York, Soil Biology, 149-195
- Ter Braak C. J., Smilauer P. (1998) CANOCO Reference Manual and User's Guide to Canoco for Windows. Software for Canonical Community Ordination (version 4.0). Centre for Biometry, Wageningen
- Van de Vijver B., Ledeganck P., Beyens L. (2002) Soil diatom communities from Île de la Possession (Crozet, sub-Antarctica). *Polar Biol.* **25**: 721-729
- Vincke S., Ledeganck P., Beyens L., Van de Vijver B. (2004a) Soil testate amoebae from sub-Antarctic Îles Crozet. *Antarct. Sci.* **16**: 165-174
- Vincke S., Beyens L., Van de Vijver B. (2004b) Freshwater testate amoebae communities from Île de la Possession, Crozet Archipelago, Subantarctica. *Arct. Antarct. Alp. Res.* **36**: 584-590
- Vincke S., Gremmen N., Beyens L., Van de Vijver B. (2004c) Moss dwelling testacean fauna of Île de la Possession. *Polar Biol.* **27**: 753-766

Received on 26th April, 2006; revised version on 12th June, 2006; accepted on 16th July, 2006

Appendix 1. Overview of the locations and environmental characteristics of the 21 small soil cores.

Soil core	Sampling site	Soil Moisture (Vol %)		Temperature (°C)		Dominant surrounding vegetation
		5 cm	20 cm	3 cm	10 cm	
1	Vallée de la Hébé	35.3	51.8	7.8	6.8	<i>Sanonia uncinata</i> and <i>Poa pratensis</i>
2	Vallée de la Hébé	40	96.4	7.3	6.5	<i>Jamesoniella grandiflora</i> , other mosses and <i>Poa pratensis</i>
3	Vallée de la Hébé	31.3	82.9	7.4	6.2	<i>Acaena magellanica</i> and mosses
4	Vallée des Branloires	49.5	100	7.9	7.4	different mosses and <i>Poa pratensis</i>
5	Vallée des Branloires	16.6	26.6	7.2	5.4	<i>Blechnum penna-marina</i> , some mosses and <i>Poa pratensis</i>
6	Vallée des Branloires	15.6	46.6	8.6	7.4	different mosses, <i>Poa pratensis</i> and <i>Lycopodium saururus</i>
7	La Pérouse	13	23.5	4.3	4.8	different mosses, <i>Azorella selago</i> and <i>Poa pratensis</i>
8	La Pérouse	76.8	73.7	6	5	<i>Breutelia</i> sp. and other mosses
9	La Pérouse	37.7	46.1	7	6	<i>Jamesoniella grandiflora</i> , other mosses and <i>Poa pratensis</i>
10	Bollard	40.1	77.7	10.3	8.9	<i>Breutelia</i> sp., <i>Juncus</i> sp. and <i>Uncinia compacta</i>
11	Bollard	30.7	82.4	11.7	8.6	<i>Jamesoniella grandiflora</i> , <i>Agrostis magellanica</i> and <i>Juncus</i> sp.
12	Bollard	8.65	31.4	11.3	7.2	<i>Blechnum penna-marina</i> and <i>Racomitrium</i> sp.
13	Rivière du Camp	30.8	32	12.8	9.6	<i>Sanonia uncinata</i> , <i>Acaena magellanica</i> and <i>Azorella selago</i>
14	Rivière du Camp	24.8	40.3	14.8	12	<i>Breutelia</i> sp and <i>Blechnum penna-marina</i>
15	Rivière du Camp	22.2	82.7	9.2	8.7	<i>Polytrichum</i> sp. and <i>Poa pratensis</i>
16	Jardin Japonais	19.8	31.5	10.1	9.2	<i>Poa annua</i> and <i>P. coockii</i>
17	Jardin Japonais	25.5	56.1	9.2	8.6	<i>Acaena magellanica</i> , <i>Ranunculus biternatus</i> and <i>Poa annua</i>
18	Jardin Japonais	37.6	64.8	9.9	8.3	<i>Cotula plumosa</i>
19	Pointe Basse	20.3	21.1	16.8	10.9	<i>Racomitrium</i> sp., <i>Juncus</i> sp. and <i>Agrostis magellanica</i>
20	Pointe Basse	48.3	94	9.2	8	<i>Hypnum cupressiforme</i> and <i>Juncus</i> sp.
21	Pointe Basse	60.6	90.2	18	13.1	<i>Ranunculus biternatus</i> , <i>Juncus</i> sp. and <i>Bryum</i> sp.

Appendix 2. List of all observed testate amoebae taxa in the small soil cores together with their mean test size (in μm) and standard error (SE). For 4 taxa the length of the only observed individual is noted. Relative abundances (%) of the taxa in each soil zone ("A"/"B"/"C") are added. Taxa which had not been encountered in Vincke et al. (2004a) are marked with *.

	Zone "A"	Zone "B"	Zone "C"	Mean test size \pm SE
<i>Arcella arenaria</i> Greeff	1.21	1.78	0.10	72 \pm 3
* <i>Arcella discoides</i> Ehrenberg	0.03	-	0.06	105 \pm 4
* <i>Archerella</i> sp1	0.03	-	-	34
<i>Assulina muscorum</i> Greeff	1.40	0.54	0.41	46 \pm 2
* <i>Assulina</i> sp1	0.41	0.44	0.67	39 \pm 2
<i>Centropyxis aerophila</i> Deflandre	0.32	0.16	0.48	61 \pm 2
* <i>Centropyxis aerophila</i> v. <i>sphagnicola</i> Deflandre	0.03	0.10	0.03	58 \pm 1
<i>Centropyxis aerophila</i> v. <i>sylvatica</i> Deflandre	-	0.03	-	80 \pm 3
* <i>Centropyxis platystoma</i> (Penard) Deflandre	0.03	-	-	60
* <i>Centropyxis sacciformis</i> Hoogenraad	-	-	0.06	85 \pm 3
<i>Corythion dubium</i> Taranek	2.57	1.14	0.44	36 \pm 2
* <i>Corythion</i> sp1	0.10	-	-	42
<i>Cryptodifflugia compressa</i> Penard	0.19	0.54	0.38	20.8 \pm 0.4
<i>Cyclopyxis</i> sp1	-	0.03	-	27.9 \pm 0.6
* <i>Cyclopyxis puteus</i> Thomas	0.22	0.44	0.38	195
<i>Cyphoderia</i> sp1	2.48	2.32	1.33	41.5 \pm 0.7
* <i>Difflugia angulostoma</i> Gauthier-Lièvre et Thomas	0.03	-	0.03	65 \pm 3
<i>Difflugia bacillifera</i> Penard	0.06	0.06	0.06	125 \pm 4
<i>Difflugia globulosa</i> Dujardin	0.03	0.03	0.06	63 \pm 2
<i>Difflugia globulus</i> Hopkinson	0.13	0.25	0.38	40 \pm 1
<i>Difflugia lucida</i> Penard	-	0.06	-	64 \pm 3
<i>Difflugia pristis</i> Penard	0.57	1.17	2.10	41 \pm 2
<i>Difflugia pulex</i> Penard	-	-	0.13	31 \pm 1
<i>Difflugia</i> sp3	2.67	4.54	5.27	31 \pm 3
<i>Difflugia</i> sp6	0.70	1.40	0.48	7.0 \pm 0.2
<i>Difflugia</i> sp7	0.03	0.19	0.19	35 \pm 2
<i>Difflugia</i> sp9	0.16	0.32	0.48	40 \pm 3
<i>Difflugia</i> sp10	0.19	-	-	40 \pm 2
<i>Difflugiella crenulata</i> Playfair	0.86	0.63	0.79	23.8 \pm 0.5
<i>Difflugiella oviformis</i> (Penard) Bonnet et Thomas	4.60	11.56	13.37	14.4 \pm 0.4
<i>Difflugiella oviformis</i> var. <i>fusca</i> (Penard) Bonnet et Thomas	-	0.13	-	13.8 \pm 0.4
* <i>Difflugiella</i> sp1	0.16	0.10	0.06	24.9 \pm 0.5
<i>Difflugiella pusilla</i> Playfair	0.76	1.52	1.87	9.2 \pm 0.4
<i>Edaphonobiotus campascoides</i> Schb., Foiss. et Meisterf.	0.86	0.76	1.40	32 \pm 2
<i>Euglypha bryophila</i> (Penard) Jung	0.22	0.19	0.16	61 \pm 2
* <i>Euglypha ciliata</i> (Ehrenberg) Penard	0.22	0.10	0.22	70 \pm 2
<i>Euglypha ciliata</i> var. <i>glabra</i> Wailes	0.38	0.16	0.19	70 \pm 2
<i>Euglypha compressa</i> Carter	0.06	-	0.03	80 \pm 2
<i>Euglypha compressa</i> var. <i>glabra</i> Cash	0.03	0.10	0.03	81 \pm 2
<i>Euglypha cristata</i> Leidy	0.48	0.32	0.22	49.5 \pm 2.6
<i>Euglypha laevis</i> Perty	0.67	0.19	0.16	24.1 \pm 0.9
<i>Euglypha polylepis</i> (Bonnet) Bonnet et Thomas	0.57	0.29	0.16	37.8 \pm 0.9
<i>Euglypha rotunda</i> Wailes	21.30	19.90	20.25	28.5 \pm 1.4
* <i>Euglypha strigosa</i> Leidy	0.13	0.06	0.03	79.3 \pm 2.7
* <i>Euglypha strigosa</i> v. <i>glabra</i> Wailes	-	0.03	-	78.3 \pm 2.7
<i>Euglypha tuberculata</i> Dujardin	-	0.06	0.03	62.2 \pm 3.3
<i>Heleopera sylvatica</i> Penard	0.44	0.54	0.22	72 \pm 3
<i>Hyalosphenia</i> sp 1	0.03	0.03	0.03	80 \pm 2
<i>Microchlamys patella</i> (Claperede et Lachmann) Cockerell	6.79	4.89	4.29	41 \pm 1
<i>Nebela dentistoma</i> Penard	2.44	1.52	1.37	85 \pm 3
<i>Nebela tubulata</i> Brown	0.06	0.10	0.10	76 \pm 3
<i>Nebela vas</i> Certes	0.06	0.03	0.03	188 \pm 6
<i>Pseudodifflugia fulva</i> Penard	2.92	3.05	4.13	17.7 \pm 0.5
<i>Pseudodifflugia gracilis</i> Schlumberger	-	-	0.10	60 \pm 2
<i>Pseudodifflugia gracilis</i> var. <i>terricola</i> Bonnet et Thomas	-	0.03	0.03	30 \pm 1
<i>Tracheleuglypha dentata</i> Vedjowsky	0.83	0.70	0.25	49 \pm 2
<i>Trachelocorythion pulchellum</i> (Penard) Bonnet	2.06	1.62	1.49	28.8 \pm 0.9
<i>Trinema complanatum</i> Penard	-	0.13	-	49 \pm 2
<i>Trinema enchelys</i> Leidy	2.32	2.76	4.16	46 \pm 2
<i>Trinema lineare</i> Penard	37.14	32.92	31.24	27.2 \pm 0.8

An Initial Account of the Terrestrial Protozoa of Ascension Island

David M. WILKINSON¹ and Humphrey G. SMITH²

¹Biological and Earth Sciences, Liverpool John Moores University, Byrom Street, Liverpool; ²Environmental Sciences, James Starley Building, Coventry University, Coventry, UK

Summary. An initial account of the terrestrial protozoan fauna of Ascension Island (7° 57' s, 14° 22' w), based on nine samples from across the range of the island's habitats, describes 52 taxa: 11 flagellates, 8 gymnamoebae, 1 helizoa, 11 ciliates and 21 testate amoebae. These tend to be cosmopolitan species with wide habitat tolerances (e.g. many are also found in polar regions). The testate amoebae are missing the larger (>150 µm) taxa, suggesting these may show dispersal limitation. There is evidence that compared to an area of continental land mass the protozoan fauna may be relatively species poor, however unlike the case with the macroscopic organisms, there is no evidence for endemic species on this island. These results are discussed in the context of microbial biogeography, especially in the context of debates over the claimed cosmopolitan nature of microbial distributions.

Key words: Ascension Island, biogeography, ciliates, flagellates, gymnamoebae, soil protozoa, testate amoebae, testate rhizopods, thecamoebians.

INTRODUCTION

From our perspective at the start of the XXI-st century, the XVIII and XIX centuries appear to have been a wonderfully romantic time to be a naturalist. The adventurous researcher could travel to scientifically unknown regions, describing not only new species but studying entire floras and faunas for the first time. While it is now very difficult to find regions where the macroscopic organisms have been completely unstud-

ied, many such locations still exist for exploration by microbiologists. Ascension Island, in the tropical South Atlantic, is one such place. As far as we are aware there have been no studies of the terrestrial protozoa, despite the fact that the island's remote location makes it potentially interesting in the context of microbial biogeography. For example, data from the island would be highly relevant to ongoing debates about the extent of cosmopolitan distributions in microbial biogeography (e.g. Foissner 1999, Wilkinson 2001, Finlay 2002, Dolan 2006, McArthur 2006). In this paper we present data on protozoa isolated from soil and bryophyte samples from nine sites on Ascension Island; ranging across the diversity of the islands' microclimates from the very wet to the extremely arid and discuss the relevance of these data to important ideas in microbial biogeography.

Address for correspondence: David M. Wilkinson, Biological and Earth Sciences, Liverpool John Moores University, Byrom Street, Liverpool L3 3AF, UK; E-mail: D.M.Wilkinson@ljmu.ac.uk

Ascension Island is a recent volcanic island approximately one million years old, covering 97 km² in the South Atlantic Ocean (7°57' S, 14°22' W) (Ashmole and Ashmole 2000, Gray *et al.* 2005). Prior to its discovery by humans at the start of the sixteenth century, it appears to have had a limited flora, comprising 25–30 vascular plant species, around 10 of which were endemic (Cronk 1980, Ashmole and Ashmole 2000). Recent data on the conservation status of the surviving native plants are provided by Gray *et al.* (2005). Much of the ecological work on the island has concentrated on either the sea birds (reviewed by Bourne and Simmons 1998, Ashmole and Ashmole 2000) or the Green Turtles *Chelonia mydas* (e.g. Broderick *et al.* 2006). The invertebrates have been shown to include a number of endemic species, including at least five endemic pseudoscorpiones (Duffey 1964, Ashmole and Ashmole 1997). From the XIX century onwards there was a programme of plant and animal introductions with the aim of making the environment more pleasant for humans (Duffey 1964, Wilkinson 2004). Before these introductions even high on the islands' mountain, where water is plentiful, the largest plants were ferns and a single species of endemic shrub *Oldenlandia adscensionis*, which was probably always rare (Cronk 1980). These introductions are of particular relevance for our study of the terrestrial protozoa as they created the cloud forest system on Green Mountain (Fig. 1a) which was included in our sampling sites and because some of these plants were imported to the island with soil (Hart-Davis 1972) which is virtually certain to have contained protozoan taxa. Most of the island is very arid with limited vegetation cover (Fig. 1b).

METHODS

Field sites

Samples were collected from nine sites (7 soil and 2 bryophyte samples) covering a range of potential habitats for soil microbes. Soil samples were collected from the soil surface after any litter layer had been removed. All samples were collected during July 2003. Details of the sites are given in Table 1 and some examples are shown in Fig. 1. After collection all samples were dried for storage (either air or oven dried, depending on the air humidity at the time of collection), it is likely that all samples were x-rayed during their passage to our laboratories in Britain.

Laboratory methods

Samples were analysed for protozoan genera and species by culturing for all taxa, and by direct observation for testate amoebae.

Bacterial food for the cultures was provided in the form of *Klebsiella aerogenes* (NCIB strain 418) grown on rich nutrient agar: Beef extract 10 g, bacteriological peptone 6 g, yeast extract 2 g, NaCl 5 g, Agar 15 g, distilled water 1 l. After 3 days' incubation at 25°C, *Klebsiella* was harvested and transferred to non-nutrient agar plates. Five replicate plates were used for each soil sample. Approximately 2 g of soil were inoculated onto each plate seeded with *Klebsiella* and flooded with Buschnell-Haas solution: CaCl₂ · 2H₂O 0.02 g, FeCl₃ · 6H₂O 0.05 g, K₂HPO₄ 1.0 g, KH₂PO₄ 1.0 g, MgSO₄ · 7H₂O 0.2 g, NH₄NO₃ 1.0 g, distilled water 1 l. Cultures were incubated at 20°C and examined by phase-contrast microscopy after 3, 6, 10, 25, 43 and 67 days' incubation. A final examination was made one year later.

Direct examination for testate amoebae was made by a modification of Couteaux' (1967) filtration method. For this 0.5 g soil was suspended in 250 ml distilled water and agitated for 1 h, 20 ml aliquots of suspension were then filtered through 0.45 grade Millipore membrane filters. Filters, bearing residue, were air-dried at room temperature. Filter segments were cleared in xylene and mounted in Canada balsam, with ten replicates for each sample. Species were identified from test characteristics, with the aid a wide range of publications and web-sites. Important sources used in the identification of testates and other protozoa included those by Sandon (1927), Curds (1969), Ogden and Hedley (1980), Page (1988), Patterson and Headley (1992), Charman *et al.* (2000), Clarke (2003), and Mitchell (2003).

Sample pH's were measured on a saturated paste (left 20 min to equilibrate) using a Pye model 292 pH-meter. Organic matter content by loss on ignition was determined through the ignition of dried samples for 4 h at 550°C (Berglund 1986). Because of limited material, loss on ignitions could only be performed on 4 of the 7 soil samples.

RESULTS

Descriptions of the sites along with the pH of the substrate and organic matter content, where available, are given in Table 1; photographs showing some of the sample sites and illustrating the range of variation in terrestrial habitats on Ascension Island are shown in Fig. 1. Occurrence of non-testate amoebae species are shown in Table 2. These comprise the flagellates, gymnaeobae, ciliates and heliozoa; all of which were identified from cultured samples. Occurrence of testate amoebae are shown in Table 3; these were the results of direct counts from samples and/or culturing of samples as indicated in this table. Although considered to be taxa most usually characteristic of damp and organic rich soils (e.g. Smith and Coupe 2002), testates were found in all our sites even very arid ones with extremely low organic matter (although at site 6 they were only represented by a single empty test). In most cases the testates were found in direct counts, suggesting that they were ecologically active in these soils and bryophytes; four



Figs 1a, b. Ascension Island habitats and sampling sites (for details of sampling sites see Table 1). **A** - *Bamboo* sp. cloud forest at the summit of Green Mountain. All the plants which can be seen in this photograph are introduced species. Prior to these introductions the dominant plants on the mountain were a number of fern species which are now either rare or extinct. Sample 1 was taken from soil at this site while sample 2 was taken from epiphytic moss growing on the Bamboos. **B** - Away from Green Mountain most of Ascension is very arid. Sample 7 was collected from just below the summit of Sisters Peak (the highest point in the photograph), while sample 8 was taken from lower down on the peak (on the opposite side of the Peak from the one shown in the photograph) in an area near the road with some invasive Mexican Thorn *Prosopis juliflora* plants.

Table 1. Sampling locations and soils data (pH and organic matter content by loss on ignition) for the protozoan sampling sites. Grid References are for the British Ordnance Survey's map of the Island (series G 892, edition 4-GSGS).

Site (Grid reference)	Location	Altitude (m)	pH	Loss on ignition (%)	Comments
1 (725 209)	Summit Green Mountain	850	4.9	36.4	Soil
2 (724 209)	Summit Green Mountain	850	4.3	no data - but pure plant material.	Epiphytic Moss
3 (725 207)	Elliot's Path, Green Mountain	750	5.2	29.2	Soil from fern rich site
4 (725 207)	Elliot's Path, Green Mountain	750	5.6	no data	Soil from under grasses, within 10 m of site 3.
5 (716 213)	Cronk's Path, Green Mountain.	660	6.3	no data	Soil from wooded habitat.
6 (743 248)	Hummock point	sea level	5.7	0.8	Soil; very arid, habitat of endemic Spurge <i>Euphorbia organoides</i>
7 694 238)	Sisters Peak, just below the summit.	420	6.4	no data	Soil; arid, limited plant cover e.g. <i>Ipomoea pescaprae</i>
8 (699 232)	Base of Sisters Peak, near the road.	240	6.1	2.2	Soil with some limited vegetation of Pine <i>Pinus</i> and Thorn <i>Prosopis juliflora</i>
9 (737 207)	Near Devils Ash Pit	520	5.8	no data - but primarily plant material.	Moss and lichen "crust."

taxa were only found after culturing. This study identified 52 taxa of protozoa from the soils and bryophyte habitats of Ascension Island. Prior to this study we could find no records of any of these groups for the island in the literature. Total species richness of protozoan taxa for each site are given at the base of Table 3.

DISCUSSION

This study provides the first data on soil protozoa from Ascension Island. Because of its remote location these data are potentially valuable in understanding the biogeography of free living microbes. Clearly our work

Table 2. Results of culturing of samples for non-testates for the 9 sites (details of sites are given in Table 1).

Taxa	1	2	3	4	5	6	7	8	9
Flagellates									
<i>Bobo saltans</i> Ehrenberg			x	x	x	x			
<i>Cercomonas crassicauda</i> Alexeieff				x					
<i>Heteromita globosa</i> Stein	x	x		x	x		x	x	x
<i>Mastigamoeba limax</i> Moroff	x		x		x				
<i>Menoidium</i> sp. Perty			x						
<i>Monosiga</i> sp. Kent									x
<i>Pseudophyllomitus apiculata</i> (Skuja) Lee						x	x		
<i>Rhynchomonas nasuta</i> Klebs	x								
<i>Spiromonas angusta</i> Dujardin							x		
<i>Spongomonas</i> sp. Stein									x
<i>Spumella elongata</i> Belcher et Swale		x		x	x	x	x		x
Gymnamoebae									
<i>Acanthamoeba astronyxis</i> Ray et Hayes		x						x	x
<i>Mayorella</i> sp. Schaeffer	x			x					x
<i>Naegleria gruberi</i> Schardinger		x							
<i>Platyamoeba</i> sp. Page							x		
<i>Thecamoeba striata</i> Penard									x
<i>Valkampfia ustiana</i> Page	x				x			x	
<i>Vanella platypodia</i> Gläser			x						
<i>Vexillifera bacillipedes</i> Page		x							x
Helizoa									
<i>Ciliophrys azurina</i> Mikrjukov et Patterson								x	x
Ciliates									
<i>Colpoda cucullus</i> Muller			x					x	x
<i>Colpoda steini</i> Maupas		x	x	x	x	x	x	x	x
<i>Colpoda</i> sp. Ehrenberg				x					
<i>Gonostomum affine</i> Stein							x		
<i>Homalozoon</i> sp. Stokes				x					
<i>Leptopharynx sphagnetorum</i> (Levander) Mermod							x	x	x
<i>Litonotus</i> sp. Wrzesniewski	x								
<i>Tachysoma pellationella</i> (Müller-Stein)								x	
<i>Pseudoglaucoma muscorum</i> Kahl									x
<i>Uroleptus</i> sp. (Ehrenberg) Stein							x		x
<i>Uronema nigricans</i> Florentin				x	x				
Total non-testate taxa	6	6	5	10	7	4	9	8	15

is an initial investigation based on the analysis of only nine small samples; however our study is comparable to the information available from several other South Atlantic islands which have been the subject of similar sized investigations (Table 4). Larger sample sizes would undoubtedly produce more extensive species lists. For example early work on Ile de la Possession, Iles Crozet (47°S), based on a similar level of sampling to our study, gave testate lists of eight (Richters 1907) and nine (Smith 1975) species. However substantially more detailed work on this island has recently raised this total to 58 taxa (Vincke *et al.* 2004).

Although based on limited samples our study provides interesting perspectives on several aspects of microbial

ecology and biogeography. The testate amoebae data are particularly relevant to biogeographical debates because testate cysts are formed inside the organisms test and so it is relatively easy to assign a size to testate taxa, when discussing its dispersal. This is not the case for many other protozoan groups, for example the cysts of the ciliate *Colpoda cucullus* (which appears in our Ascension species list: Table 2) are 35 µm in diameter while its trophozoites are 40–110 µm long (Sandon 1927). All the testate taxa identified from Ascension are widely distributed around the globe; this is consistent with the 'everything is everywhere' idea which suggests, in its strongest version, that all free living microbes have cosmopolitan distributions and are found wherever the

Table 3. Testate data for the 9 sites. D - signifies found only in direct counts; C - only found in cultures and, B - found both by direct counts and culturing.

Testate amoebae	1	2	3	4	5	6	7	8	9
<i>Arcella hemispherica</i> Perty									D
<i>Arcella arenaria</i> Greef			D						D
<i>Arcella discoidea</i> Ehrenberg					D				
<i>Arcella vulgaris</i> Ehrenberg									D
<i>Assulina muscorum</i> Greef		D							
<i>Assulina seminulum</i> Ehrenberg			C						
<i>Centropyxis aerophila</i> Deflandre		D		D			D	D	B
<i>Centropyxis cassis</i> Wallich	D								
<i>Centropyxis constricta</i> Ehrenberg									D
<i>Corythion dubium</i> Taranek		B							
<i>Cyclopyxis eurystoma</i> Deflandre							D	D	D
<i>Cyclopyxis kahli</i> Deflandre				D					D
<i>Diffugia globulosa</i> Dujardin				D	D				D
<i>Diffugia longicollis</i> Deflandre						D			
<i>Euglypha rotunda</i> Wailes									C
<i>Euglypha strigosa</i> Ehrenberg	C								
<i>Lesquereusia spiralis</i> Ehrenberg			D						
<i>Lesquereusia modesta</i> Rhumbler			D		D				
<i>Phryganella acropodia</i> Herwig <i>et</i> Lesser	D	D	D				D	D	D
<i>Trinema enchelys</i> Leidy		B	C						
<i>Trinema lineare</i> Penard		C			C				C
Total testate taxa	2	7	6	3	4	1	3	3	11
Total protozoa (testates + other groups)	8	13	11	13	11	5	12	11	26

Table 4. Comparison of our Ascension data with other initial reconnaissance type surveys of soil protozoa on mid-Atlantic islands. Data for the islands other than Ascension from the "Quest" Expedition (Sandon and Cutler 1924) which collected a similar number of samples to our on work.

	Tristan da Cunha (37°S)	Gough Island (40°S)	St. Helena (16°S)	Ascension (8°S)
Gymnamoebae	5	6	5	8
Testates	7	14	3	21
Ciliates	11	9	8	11
Flagellates	22	16	15	11

correct habitat occurs (e.g. Finlay 2002). However, it is of interest that the Ascension testate fauna is apparently missing the larger taxa. Using the same data set of testate sizes as used by Wilkinson (2001), most of the Ascension taxa have median test sizes (either length or diameter, whichever is largest) below 100 µm and only one (*Centropyxis constricta*) has a median size of 150 µm. The analysis in Wilkinson (2001) suggested that, for testates, limited geographical range becomes commoner above sizes of 100-150 µm. The absence of the larger testate species from our Ascension samples is

consistent with this idea. Certainly, using classical morphological approaches, we found no evidence for endemic taxa amongst any of the microbial groups we studied; this result is different from that found in the multicellular plants and animals of Ascension where several endemics have been described (Ashmole and Ashmole 2000).

As well as the tendency of testates to be cosmopolitan in their distribution another striking feature, which runs counter to the commonly observed patterns in macroscopic species, is the lack of specialist tropical

species. Strikingly all our testate species, with two exceptions (*Arcella vulgaris* and *Diffflugia longicollis*), are also recorded in the Arctic data set of Beyens and Chardez (1995). Indeed *A. vulgaris* has been recorded in the high arctic by other authors (Balik 1994, Hodgkinson *et al.* 2004) while *D. longicollis* was found in the sub-Antarctic (Smith and Headland 1983), so all the testate taxa described from the tropical Ascension Island are also found in polar habitats!

Although, as described above, our species lists are far from complete they are consistent with the hypothesis that Ascension has a relatively impoverished soil protozoan fauna; presumably because of a combination of its recent geological origin, remote location and predominance of arid habitats. This is suggested by a comparison of our testate data with that described by Meisterfeld and Tan (1998) in their preliminary study of the testates of the previously unstudied Mount Buffalo National Park in Australia. They sampled a similar number of sites to our Ascension study (8 compared with our 9) but found 50 taxa of testates (compared to our 21).

The ciliates show a similar pattern to the testates, with most of the species identified from Ascension exhibiting a cosmopolitan distribution (Foissner 1998). An apparent exception is *Pseudoglaucoma muscorum* which has previously only been recorded from the Holarctic (Foissner 1998). This could suggest that this taxon is more widely distributed than previously thought; as would be suggested by the 'everything is everywhere' ideas of Finlay and colleagues (e.g. Finlay and Clarke 1999, Finlay and Fenchel 1999, Finlay 2002). This interpretation is made more plausible by the taxons small size (<30 µm) and the possibility of confusion with other similar looking taxa such as *Uronema nigricans* and *Cyclidium glaucoma*. However it could have been introduced to the island by humans, as it is known that not only plants but also soil was introduced to the island from the northern hemisphere during the XIX-th century (Hart-Davis 1972). The other groups are also comprised of widespread species, often with broad habitat requirements. For example the flagellate *Rhyncomonas nasuta* has been recorded from fresh and sea water as well as soils (Cowling 1994), while several of our flagellate and gymnamoebae have been recorded in Antarctic dry valleys (Bamford *et al.* 2005).

The common pattern for macroscopic species is that islands are species poor for their size but rich in endemic species (Whittaker 1998). Although our species lists are clearly not comprehensive they do strongly suggest that only part of this pattern is seen in soil protozoa; while our

data are consistent with the soils of Ascension being relatively species poor we found no evidence for endemism based on our classical morphological approach to protozoan identification. Clearly there is the possibility that molecular methods may discover 'cryptic' species, which although genetically distinct are not recognisable by morphological methods (Dolan 2006). However, so far, molecular studies on widespread ciliate taxa (e.g. *Colpoda spp* and *Gonostomum affine*) have failed to find such cryptic species (Bowers *et al.* 1998, Foissner *et al.* 2001). A striking feature of the species identified from Ascension is that they are not specialist tropical species and in many cases have also been recorded from polar regions - again this result is counterintuitive to biologists familiar with larger organisms. The testate amoebae data are particularly interesting, being consistent with the idea that the larger testates show limited distributions and for these taxa 'everything is not everywhere'. The soil protozoa of remote islands, such as Ascension, would clearly repay more detailed study.

REFERENCES

- Ashmole N. P., Ashmole M. J. (1997) The land fauna of Ascension Island: new data from caves and lava flows, and a reconstruction of the prehistoric ecosystem. *J. Biogeogr.* **24**: 549-589
- Ashmole P., Ashmole M. (2000) St. Helena and Ascension Island: a Natural History. Anthony Nelson, Oswestry
- Balik V. (1994) On the soil Testate Amoebae fauna (Protozoa: Rhizopoda) of the Spitsbergen Islands (Svalbard). *Arch. Protistenk.* **144**: 365-372
- Bamford S. S., Wall D. H., Virginia R. A. (2005) Distribution and diversity of soil protozoa in the McMurdo Dry Valleys of Antarctica. *Polar Biol.* **28**: 756-762
- Berglund B. E. (1986) Handbook of Holocene Paleocology and Paleohydrology. John Wiley, London
- Beyens L., Chardez D. (1995) An annotated list of Testate Amoebae observed in the Arctic between the longitudes 27°E and 168°W. *Arch. Protistenk.* **146**: 219-233
- Bourne W. R. P., Simmons K. E. L. (1998) A preliminary list of the birds of Ascension Island, South Atlantic Ocean. *Sea Swallow* **47**: 42-56
- Bowers N., Kroll T. T., Pratt J. R. (1998) Diversity and geographical distribution of riboprints from three cosmopolitan species of Colpoda Müller (Ciliophora: Colpodea). *Europ. J. Protistol.* **34**: 341-347
- Broderick A. C., Frauenstein R., Glen F., Hays G. C., Jackson A. L., Pelembe T., Ruxton G. D., Godley B. J. (2006) Are Green turtles globally endangered? *Global Ecol Biogeogr.* **15**: 21-26
- Charman D. J., Hendon D., Woodland W. A. (2000) The Identification of Testate Amoebae in Peats. Quaternary Research Association Technical Guide No. 9. London
- Clarke K. J. (2003) Guide to the Identification of Soil Protozoa - Testate Amoebae. Soil Biodiversity Programme Research Report No.4, FBA Special Publication, Ambleside
- Couteaux M.-M. (1967) Une technique d'observations thecamoebiens du sol pour l'estimation de leur desite absolue. *Rev. Ecol. Biol. Sol.* **4**: 593-596
- Cowling A. J. (1994) Protozoan distribution and adaptation. In: Soil Protozoa. (Ed. J. F. Darbyshire) CAB International, Wallingford, 5-42

- Cronk Q. C. B. (1980) Extinction and survival in the endemic vascular flora of Ascension Island. *Biol. Conserv.* **17**: 207-219
- Curds C. R. (1969) An Illustrated Key to the British Freshwater Ciliated Protozoa Community Found in Activated Sludge. Water Pollution Research Technical Paper No.12, HMSO
- Dolan J. R. (2006) Microbial Biogeography? *J. Biogeogr.* **33**: 199-200
- Duffey E. (1964) The terrestrial ecology of Ascension Island. *J. Appl. Ecol.* **1**: 219-251
- Finlay B. J. (2002) Global dispersal of free-living microbial eukaryote species. *Science* **296**: 1061-1063
- Finlay B. J., Clarke K. J. (1999) Ubiquitous dispersal of microbial species. *Nature* **400**: 828
- Finlay B. J., Fenchel T. (1999) Divergent perspectives on protist species richness. *Protist* **150**: 229-233
- Foissner W. (1998) An updated compilation of world soil ciliates (Protozoa, Ciliophora), with ecological notes, new records, and descriptions of new species. *Europ. J. Protistol.* **34**: 195-235
- Foissner W. (1999) Protist diversity: estimates of the near-imponderable. *Protist* **150**: 363-368
- Foissner W., Stoeck T., Schmidt H., Berger H. (2001) Biogeographical differences in a common soil ciliate, *Gonostomum affine* (Stein), as revealed by morphological and RAPID-Fingerprint analysis. *Acta Protozool.* **40**: 83-97
- Gray A., Pelembe T., Stroud S. (2005) The conservation of the endemic vascular flora of Ascension Island and threats from alien species. *Oryx* **39**: 449-453
- Hart-Davis D. (1972) Ascension; the Story of a South Atlantic Island. Constable, London
- Hodkinson I. D., Coulson S. J., Webb N. R. (2004) Invertebrate community assembly along proglacial chronosequences in the high Arctic. *J. Anim. Ecol.* **73**: 556-568
- McArthur J. V. (2006) Microbial Ecology; an Evolutionary Approach. Academic Press, Burlington USA
- Meisterfeld R., Tan L.-W. (1998) First records of Testate Amoebae (Protozoa: Rhizopoda) from Mount Buffalo National Park, Victoria: preliminary notes. *Victorian Nat.* **115**: 231-238
- Mitchell E. A. D. (2003) Identification keys for testate amoebae. http://wslar.epfl.ch/mitchell/edward/Identification_keys/Keys.htm
- Ogden C. G., Hedley R. H. (1980) An Atlas of Freshwater Testate Amoebae. British Museum (Natural History), London
- Page F. C. (1988) A New Key to Freshwater and Soil Gymnamoebae. CCAP and FBA, Ambleside
- Patterson D. J., Headley S. (1992) Free-living Freshwater Protozoa - A Colour Guide. Wolfe Publishers, London
- Richters F. (1907) Die Faune de Moosrasen des Gaussbergs under einiger Sudlicher Inseln. Deutsch Sudpolar Expedition 1901-1903, **9**: *Zoologie I*, 259-302
- Sandon H. (1927) The Composition and Distribution of the Protozoan Fauna of the Soil. Oliver & Boyd, Edinburgh & London
- Sandon H., Cutler D. W. (1924) Some protozoa from the soils collected by the "Quest" expedition (1921-22). *J. Linn. Soc. Zool.* **36**: 1-16
- Smith H. G. (1975) Protozoaires terricoles de l'île de la Possession. *Rev. Ecol. Biol. Sol.* **12**: 523-530
- Smith H., Coupe S. (2002) Testate amoebae - past, present and future. *Europ. J. Protistol.* **37**: 367-369
- Smith H. G., Headland R. K. (1983) The population ecology of soil testate rhizopods on the sub-Antarctic island of South Georgia. *Rev. Ecol. Biol. Sol.* **20**: 269-286
- Vincke S., Gremmen N., Beyens L., Van Der Vijver B. (2004) The moss-dwelling testacean fauna of Ile de la Possession. *Polar Biology* **27**: 753-766
- Whittaker R. J. (1998) Island Biogeography: Ecology, Evolution and Conservation. Oxford University Press, Oxford
- Wilkinson D. M. (2001) What is the upper size limit for cosmopolitan distribution in free-living microorganisms? *J. Biogeogr.* **28**: 285-291
- Wilkinson D. M. (2004) The parable of Green Mountain: Ascension Island, ecosystem construction and ecological fitting. *J. Biogeogr.* **31**: 1-4

Received on 8th May, 2006; revised version on 6th June, 2006; accepted on 16th July, 2006

Cryptic Species in a Morphospecies Complex of Heterotrophic Flagellates: the Case Study of *Caecitellus* spp.

Klaus HAUSMANN¹, Petra SELCHOW¹, Frank SCHECKENBACH², Markus WEITERE² and Hartmut ARNDT²

¹Division of Protozoology, Institute of Biology / Zoology, Free University of Berlin, Berlin, Germany; ²Department of General Ecology and Limnology, Zoological Institute, University of Cologne, Cologne, Germany

Summary. Recent molecular studies have revealed quite different genotypes within morphospecies of heterotrophic nanoflagellates (HNF) as identified by light microscopy, e.g. for *Caecitellus parvulus*, known as one of the 20 most common heterotrophic flagellates worldwide. We combined molecular and morphological analyses to clarify if the morphospecies *Caecitellus parvulus* includes genetically as well as ultrastructurally and behaviourally distinguishable species with or without a different geographical distribution. Therefore we compared the ultrastructure, the small subunit of the ribosomal DNA (SSU rDNA), the growth rates as well as the locomotion patterns of two strains of *C. cf. parvulus* isolated from deep sea sediments and from the surface water of the oligotrophic Angola Basin, South Atlantic. The reconstruction of the kinetid architecture of two strains of *C. cf. parvulus* revealed differences in the number of microtubules in flagellar root 3, which surrounds the oral region and forms the cytoskeleton of the feeding basket. The number of microtubules in this region is also different from the description given earlier in the literature for *Caecitellus parvulus*. Additionally, there are significant differences between the two studied strains in the length of their posterior flagellum, their locomotion velocity and their moving pattern as well as in their growth rates. These observations, together with the results of the molecular comparison of the SSU rDNA of 11 different strains of *Caecitellus*, suggest the existence of at least three distinguishable species. Our results indicate cryptic speciation within the morphospecies *Caecitellus parvulus*. We describe two new *Caecitellus* species, i.e. *Caecitellus paraparvulus* and *Caecitellus pseudoparvulus*, which have been newly established within a *Caecitellus*-complex.

Keywords: *Caecitellus paraparvulus* n. sp., *C. pseudoparvulus* n. sp., cryptic species, heterotrophic flagellates, species complex.

INTRODUCTION

Heterotrophic flagellates are major consumers of bacteria, cyanobacteria and microalgae in a large variety of aquatic ecosystems. Consequently, they play an

important role as nutrient remineralizers and are mainly responsible for the carbon transfer to higher trophic levels in both pelagic and benthic environments of the oceans (e.g. Fenchel 1982a, Azam *et al.* 1983, Gasol and Vaqué 1993). In natural planktonic assemblages, the abundances of heterotrophic flagellates range from 10² to 10⁵ cells per ml (Berninger *et al.* 1991). Despite their high abundance and their importance in aquatic ecosystems, little is known about the biogeography and species-level diversity of many heterotrophic nanoflagellates (Preisig *et al.* 1991, Lee and Patterson 1998, Arndt *et al.*

Address for correspondence: Klaus Hausmann, Division of Protozoology, Institute of Biology / Zoology, Free University of Berlin, Königin-Luise-Str. 1-3, D-14195 Berlin, Germany; FAX (+49) 30 83 85 64 77; E-mail: hausmann@zedat.fu-berlin.de

2000). The question of the biodiversity and distribution of global free-living protists in general is still being intensively discussed (e.g. Foissner 1999, Finlay 2002). Some studies have been carried out to clarify the question of ubiquitous dispersal or endemism of protozoan species by investigating extreme habitats such as the deep sea or even hydrothermal vents (Atkins *et al.* 2000, Hausmann *et al.* 2002, Arndt *et al.* 2003, Scheckenbach *et al.* 2005). The deep sea is an extreme habitat (high pressure, absence of light, poor nutrients concentration, low temperature) which covers more than 60 % of the earth's surface. Despite the vastness of this biotope, knowledge on deep sea organisms, especially on protists, is still very limited (Finlay 2002, Turley 2002).

Numerous protists found in the deep sea sediments are also known from surface waters, but others which have been found in the deep sea have not been reported from shallow waters (Hausmann *et al.* 2002, Arndt *et al.* 2003). There are several known mechanisms which could account for genetic exchange between protist populations from different habitats; the high probability of dispersal of small organisms through e.g. global oceanic circulation, the formation of resting stages or the formation and sinking of marine snow (Finlay 2002, Turley 2002) are examples of such mechanisms. Small sinking aggregates are micro-environments for many heterotrophic flagellates within the water column (Caron 1991, Turley 2002, Kjørboe *et al.* 2004), e.g. for *Caecitellus parvulus*.

The different views of the biodiversity of protists are tightly connected with the differences in understanding of what a species is (Schlegel and Meisterfeld 2003). According to Mayden (1997), there are over twenty different species concepts.

The alpha taxonomy of heterotrophic flagellates is based mostly on a morphospecies concept (Patterson and Lee 2000). Because of the small size of flagellates, electron microscopy has to be used for morphological taxonomic characterisation and to prove restricted distribution (Foissner 1999), but it is still not used for most field studies and species descriptions.

The application of molecular criteria suggests that behind traditional morphospecies a much greater number of physiological or molecular species is hidden (Patterson and Lee 2000).

The heterotrophic nanoflagellate *Caecitellus parvulus* (Griessmann 1913) Patterson *et al.* (1993) is one of the 20 most common heterotrophic flagellates worldwide (Patterson and Lee 2000) and has always been regarded as a single species (Larsen and Patterson 1990, Ekeboom

et al. 1995/1996, Patterson and Simpson 1996, Atkins *et al.* 2000, Al-Qassab *et al.* 2002, Lee *et al.* 2003). The small, biflagellated gliding cells inhabit sediments and particle surfaces. Their anterior flagellum beats stiffly from side to side as cells glide with the posterior flagellum trailing behind. The species was first assigned to the genus *Bodo* as *B. parvulus* (Griessmann 1913), but Patterson *et al.* (1993) revealed ultrastructural features which are not compatible with a bodonid flagellate and placed it in the new genus *Caecitellus*, which they regarded as "a genus of uncertain affinities". O'Kelly and Nerad (1998) reconstructed the kinetid architecture of this species and found a high similarity to the Bicosoecida. The new term Hamatores (Al-Qassab *et al.* 2002) groups *Caecitellus* together with the pseudodendromonads. Both taxa lack three partite mastigonemes but share ultrastructural characteristics with the bicosoecids. Therefore they are related to the stramenopiles (Al-Qassab *et al.* 2002).

However, molecular studies from Scheckenbach *et al.* (2005) revealed quite different genotypes within morphospecies of heterotrophic nanoflagellates, so far identified by light microscopy as a single species. Therefore the studied strains of *Caecitellus parvulus* which were collected during an expedition with the German RV METEOR (cruise 48/1, DIVA I, year 2000) from deep sea sediments and surface water of the oligotrophic South Atlantic, Angola Basin, are designated as *C. cf. parvulus*.

The goal of the present study was to clarify whether the morphospecies *Caecitellus parvulus* includes genetically as well as morphologically and behaviourally distinguishable species and whether or not these species have different geographical distributions. Therefore we compared their morphology and ultrastructural architecture, their locomotion behaviour and growth characteristics as well as the genotype of two strains of *C. cf. parvulus*, i.e. an isolate from the deep sea with a strain from the surface water. This approach opens a new way to study biodiversity in protists.

MATERIAL AND METHODS

Sampling and cultivation of organisms

The *Caecitellus cf. parvulus* strains examined in this study were collected in July 2000 during the METEOR cruise 48/1 (DIVA I) in the oligotrophic South Atlantic and the Angola Abyssal Plain (the coordinates of the sampling locations are given in Table 1). Clonal

cultures were established and kept in culture as described in detail in Scheckenbach *et al.* (2005).

For the ultrastructural studies, the strains *Caecitellus cf. parvulus* DQ220712 (deep sea) and DQ220713 (surface water) were cultured at 19°C in artificial seawater (23‰ salinity). Sterilised wheat grains were added as a polysaccharide supply.

Pseudobodo tremulans strain DQ220718 was isolated by A.P. Mylnikov from brackish water of the Baltic Sea. The *Caecitellus* strain with the GenBANK accession number DQ230538 has been retrieved from the "American Type Culture Collection" (ATCC50091) and was the subject of a previous analysis by O'Kelly and Nerad (1998). All strains sequenced in this study and all sequences retrieved from GenBANK are referred to by their GenBANK accession numbers.

Light microscopy

Observations were made using an inverted microscope (ZEISS Axiovert 200, equipped with differential interference contrast optics). Micrographs were taken with an OLYMPUS OM-2N camera. For applied morphological nomenclature see Fig. 7.

Scanning electron microscopy

Cells were fixed for 15 min at room temperature on 0.1% Poly-L-Lysine coated cover slips with the Parducz fixative (Parducz 1967). Fixed cells were washed 5 × 5 min in artificial seawater (23‰ salinity) and dehydrated in a graded series of ethanol. Cells were dried in a BAL-TEC CPD 030 apparatus. After coating with gold in a BALZERS UNION SCD 040 sputter device, cells were examined with a FEI Quanta 200 ESEM.

Transmission electron microscopy

Cells were concentrated by centrifugation (200 rpm) and fixed for 30 min at room temperature in a fixative basically described by O'Kelly and Nerad (1998).

After fixation the cells were transferred into agar blocks for better handling, dehydrated in a graded ethanol series, and embedded in araldit epoxy resin. Sections were made with a diamond knife, mounted on formvar-coated grids or slots and stained with uranyl acetate and lead citrate. They were examined with a PHILIPS EM 208 or a PHILIPS 120 BIO TWIN.

Table 1. Strain identifiers, sources of isolation and lengths of 18S rDNA of *Caecitellus cf. parvulus* strains sequenced in this study. Strain identifiers correspond to GenBANK accession numbers.

Accession number	Source	Sequence length
DQ220712	19°17.4'S 3°52.2'E, - 5424 m Angola Abyssal Plain, South Atlantic Ocean	1631
DQ220713	17°04.9'S 4°40.8'E, - 1 m South Atlantic Ocean	1646
DQ220714	19°17.4'S 3°52.2'E, - 5424 m Angola Abyssal Plain, South Atlantic Ocean	1669
DQ220715	19°19.8'S 3°55.6'E, - 5425 m Angola Abyssal Plain, South Atlantic Ocean	1681
DQ220716	16°23.1'S 5°27.0'E - 5388 m Angola Abyssal Plain, South Atlantic Ocean	1684
DQ220717	18°25.3'S 4°44.0'E, - 5392 m Angola Abyssal Plain, South Atlantic Ocean	1676
DQ230538	Sargasso Sea, - 100 m North Atlantic Ocean	1696

Table 2. *P*-distances of *Caecitellus parvulus* in percent (pairwise-deletion option set). Strain identifiers refer to GenBANK accession numbers. Strains sequenced in this study are in bold.

	(1)	(2)	(3)	(4)	(5)	(6)	(7)	(8)	(9)	(10)	(11)
AF174368 (1)											
AF174367 (2)	0.00										
DQ220715 (3)	4.55	4.44									
DQ220716 (4)	4.60	4.49	0.00								
DQ220713 (5)	4.39	4.39	0.00	0.00							
AY827847 (6)	4.54	4.55	0.00	0.00	0.00						
AY827848 (7)	4.65	4.66	0.12	0.12	0.13	0.12					
DQ220717 (8)	4.48	4.49	0.06	0.12	0.00	0.06	0.12				
DQ220714 (9)	4.38	4.39	0.00	0.00	0.00	0.00	0.12	0.00			
DQ220712 (10)	5.96	5.96	5.28	5.28	5.30	5.28	5.50	5.28	5.28		
DQ230538 (11)	5.85	5.86	5.55	5.60	5.24	5.54	5.46	5.20	5.17	0.00	

Locomotion analysis

Gliding cells of the *Caecitellus* strains DQ220712 and DQ220713, both grown at 19°C, were documented using an S-VHS video unit (JVC TK-1085E video camera, JVC TM-1500PS monitor, JVC BR-S600E video recorder). The velocity of gliding cells was measured by means of frame-by-frame analysis over the time cells needed to glide 10 µm straight forward. The movement of the anterior flagellum was studied in detail by measuring angles and times of the flagellar stroke. The angle was measured from the assumed median line of the cell (0°) to the outermost right (A) and left (B) point of the stroke (Fig. 1).

Growth experiments

The food provided for the *Caecitellus* strains DQ220712, DQ220713 and DQ230538 in these experiments was the heterotrophic bacterium *Halomonas halodurans*, grown in artificial seawater (23 ‰ salinity) with 0.1 % yeast extract added. Bacterial cultures were grown on a shaker at room temperature. After three days they were heat-killed to prevent overgrowth, harvested by centrifugation and resuspended three times in fresh artificial seawater.

All strains of *Caecitellus* were grown in sterile 50 ml tissue culture flasks (Sarsted, Newton, USA) with the addition of 10⁸ heat-killed bacteria ml⁻¹. This abundance is far above a threshold concentration for food limitation (Boenigk and Arndt 2002) and provides optimal growth conditions. In order to estimate the number of bacteria in the cultures, 50 µl subsamples were taken. The samples were fixed with 1% glutaraldehyde, stained with 0.1 mg ml⁻¹ DAPI (Porter and Feig 1980), retained on a black 0.2 µm polycarbonate filter and counted using a ZEISS Axioskop equipped with epifluorescence facilities.

The cultures were grown continuously at 19°C. Two independent replicates were considered for each of the three stains. The growth rates (r , d⁻¹) were calculated with the help of the abundances determined during the exponential growth phase: $r = \ln(N_1) - \ln(N_0)$. N_0 is the abundance at the start of the experiment and N_1 the abundance after one day. The doubling time (DT, h) was then calculated with the help of the growth rate: $DT = (\ln(2)/r) * 24$.

DNA extraction, SSU rDNA amplification and sequencing

DNA was extracted using a modified CTAB procedure (Clark 1992). The small subunit rDNA was amplified and sequenced as described in detail in Scheckenbach *et al.* (2005).

DNA sequence analysis

Determined sequence fragments were assembled manually and unambiguously aligned together with other sequences retrieved from GenBank using the ClustalX multiple alignment program version 1.83 (Thompson *et al.* 1994). Uncorrected genetic distances (p -distances) were calculated using MEGA version 3.0 (Kumar *et al.* 2004) with pairwise-deletion option set. Phylogenetic analyses were performed by using the maximum likelihood (ML) (Felsenstein 1981), maximum parsimony (MP) (Swofford and Olsen 1990) and minimum evolution (ME) (Rzhetsky and Nei 1992) methods. The precision of the internal nodes was assessed by bootstrapping (Felsenstein 1985). For ML analysis the transition/transversion ratio was set to 1.24. The model of nucleotide substitution used for ME analysis was LogDet (Lockhart *et al.* 1994, Steel 1994). For ML and MP analysis,

PHYLIP version 3.63 was used (Felsenstein 2004); MEGA version 3.0 was used for ME analysis.

RESULTS

Overall structure

Caecitellus cf. *parvulus* from the deep sea (DQ220712) and from the surface water (DQ220713) is a biflagellate cell with a slightly rounded triangular profile. The body shape appears angular because of a large feeding basket protruding on the ventral-apical side (Figs 2, 3). The basket is internally supported by a horseshoe-shaped cytoskeletal structure of numerous microtubules; these microtubules are also mainly responsible for the characteristic form of the mouth region. The large ingestion apparatus is easily observable even under a light microscope (Figs 2, 3). SEM micrographs clearly show that a lip surrounds the rim of the oral apparatus (Figs 4-6). The cell length varies from 2.0 to 4.5 µm. Two flagella of unequal length originate from the apical-ventral side of the cell (Figs 2-6). The anterior flagellum projects forward and beats laterally in a stiff manner. It is about 1.5 × the length of the cell body in both strains of *Caecitellus* (Figs 4-6). The cell usually glides smoothly

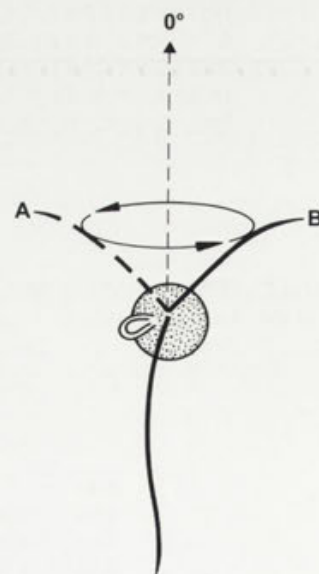


Fig. 1. Scheme depicting the rotating movement of the anterior flagellum. The time needed for a complete flagellar stroke was measured as well as the maximum angles of deflection to the outermost left (A) and right point (B) from an assumed median line of the cell (0°).



Figs 2-6. Light and scanning electron micrographs of *Caecitellus*. **2, 3** - differential interference contrast light micrographs, ventral view of living cells (**2** - deep sea strain DQ220712; **3** - surface water strain DQ220713), arrow - ingestion apparatus; **4-6** - scanning electron micrographs showing a lip surrounding the rim of the oral apparatus (arrow); **4** - cell of strain DQ220712 with adjacent bacterium (B); **5, 6** - lateral views of strain DQ220713 cells; **7** - clay model of *Caecitellus* illustrating the in this study applied nomenclature: a - anterior flagellum, p - posterior flagellum, d - dorsal, v - ventral, l - left, r - right, arrow - direction of locomotion. Scale bars: 5 μm (2, 3); 2 μm (4-6).

forward along its fully extended posterior flagellum, which trails underneath the cell body and shows significant differences in length between the two strains DQ220712 and DQ220713 (Fig. 8).

TEM micrographs (Figs 9-12) show that cells from both *Caecitellus* strains generally follow a similar basic structural plan. For example, three microtubular roots originate from the two basal bodies: one compactly structured root (R3) and two less complex roots (R1 and R4) (Figs 9, 10) (nomenclature according to O'Kelly and Nerad 1998).

The cells are uninucleate and contain mitochondria with tubular cristae. One mitochondrion is always located close to the nucleus at its ventral side and is associated with the compact root (R3) at the right side of the cell, next to so-called electron lucent bodies (Fig. 11). There is only one dictyosome per cell, which is located close to the nucleus and dorsal to the flagellar basal bodies (Fig. 12).

The glycocalyx of the DQ220712 strain appears as a relatively thick electron dense layer (Figs 9, 11) compared to the glycocalyx of the DQ220713 strain which is hardly recognisable at all (Figs 10, 12). The thick glycocalyx layer covers the complete cell surface includ-

ing flagellar pocket, cytostome as well as the two flagella.

The flagellar apparatus

The kinetid contains two basal bodies (1 and 2), one broad and complex microtubular root (R3) and two simple ones (R1 and R4) (Figs 9, 10), a striated band (Figs 16-18) and a connecting fibre (Fig. 19).

The two basal bodies are linked together by a connecting fibre and to R3 by a striated band. The latter leads from the right hand side of basal body 2 as far away as the point of separation of R3 (Figs 18, 19). It runs slightly anterior to R3 (Fig. 14) and has a connection to basal body 1. The connecting fibre extends between the bases of the two basal bodies from the left hand side of basal body 2 towards the base of basal body 1 (Fig. 19).

The basal bodies of the posterior (1) and anterior flagellum (2) are each approximately 0.5 μm long and oriented to each other in an L-shaped manner. Their longitudinal axes do not run coplanar, but are shifted approx. 0.15 μm to each other and are slightly laterally tilted. Electron-dense material is located in the proximal lumen of the basal bodies (Fig. 12, arrow). Cross

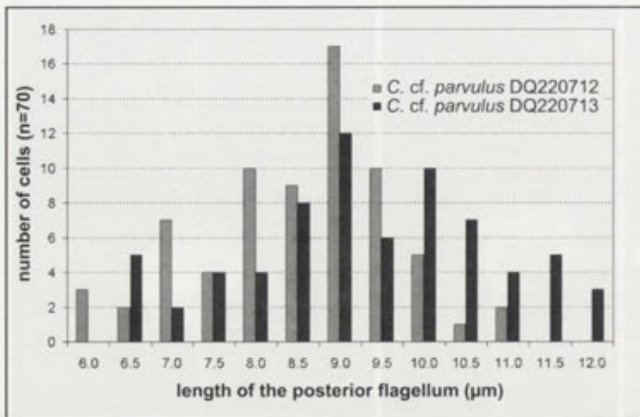


Fig. 8. Diagram showing significant ($p < 0.001$; $z = -3.311$; U-test) differences in the length of the posterior flagellum of *Caecitellus* cf. *parvulus* strain DQ220712 (deep sea) and strain DQ220713 (surface water).

sections of this region clearly show the kinetosomal $9 \times 3 + 0$ structure (Fig. 13). There is a basal axonemal plate at the level of the plasmalemma (Fig. 12, arrowhead).

R1, composed of two microtubules, originates in an electron-dense material on the right side of basal body 2 (Figs 9, 19) at its midregion and extends to the dorsal surface to the left side of the cell (Fig. 12). R3 consists of three subunits: the abc subunit, the 8-35 subunit [(in strain DQ220713; named 8-29 subunit in strain DQ220712) and the x subunit (Figs 9, 10)].

At the origin of R3, which lies at the ventral side of the proximal end of basal body 2, the root consists initially of eight microtubules (Fig. 13). After a short distance three more microtubules are added, which appear in cross section as an L-shaped structure with a typical $8 + 3$ pattern (Fig. 14). The three added microtubules are the abc subunit of R3. The subunit separates from the root (Figs 15, 16) and turns slightly to the left, forming a tight loop around the posterior flagellar insertion (Figs 19, 22).

The broadest subunit of R3, initially consisting of eight microtubules, increases in number up to 35 (Fig. 28) and passes to the right side of the ventral region, forming a loop that supports the peristome (Fig. 20). It then passes left and back to make contact with the abc subunit (Figs 9, 19). At the point of separation, R3 is associated with electron-dense material subtending the eight-microtubule subunit (Fig. 22). In the ascending root (Figs 11, 32), which is the broader subunit of R3, the number of

microtubules increases. In the deep sea strain (DQ220712) 35 microtubules (Fig. 28) and in the surface strain (DQ220713) as many as 29 microtubules (Fig. 29) have been detected. The highest number of microtubules is reached just before the turning point of the loop (Fig. 32). Figures 23-27 are serial sections through an oral apparatus. The section plane of these micrographs is indicated in Fig. 11 by a dotted line. The microtubules of the ascending side of the loop increase in number compared to the descending side of the loop (Figs 23-27).

These extra microtubules have no obvious connection to the basal bodies, whereas the junction of the large loop and the abc loop are visible in Figs 18, 19. Most microtubules of the descending root terminate before the two parts of the loop join. In Fig. 23 there are only five microtubules left in the descending root.

An individual microtubule called x runs parallel to the large loop (Figs 12, 20, 23-31). This microtubule has its origin close to the separation of R3 and extends to the outside of the loop in the lip at approximately the same level as the second microtubule from the 8-35 loop. In the area of the turning point of the x-microtubule, one additional microtubule is detectable directly underneath it (Figs 30, 31).

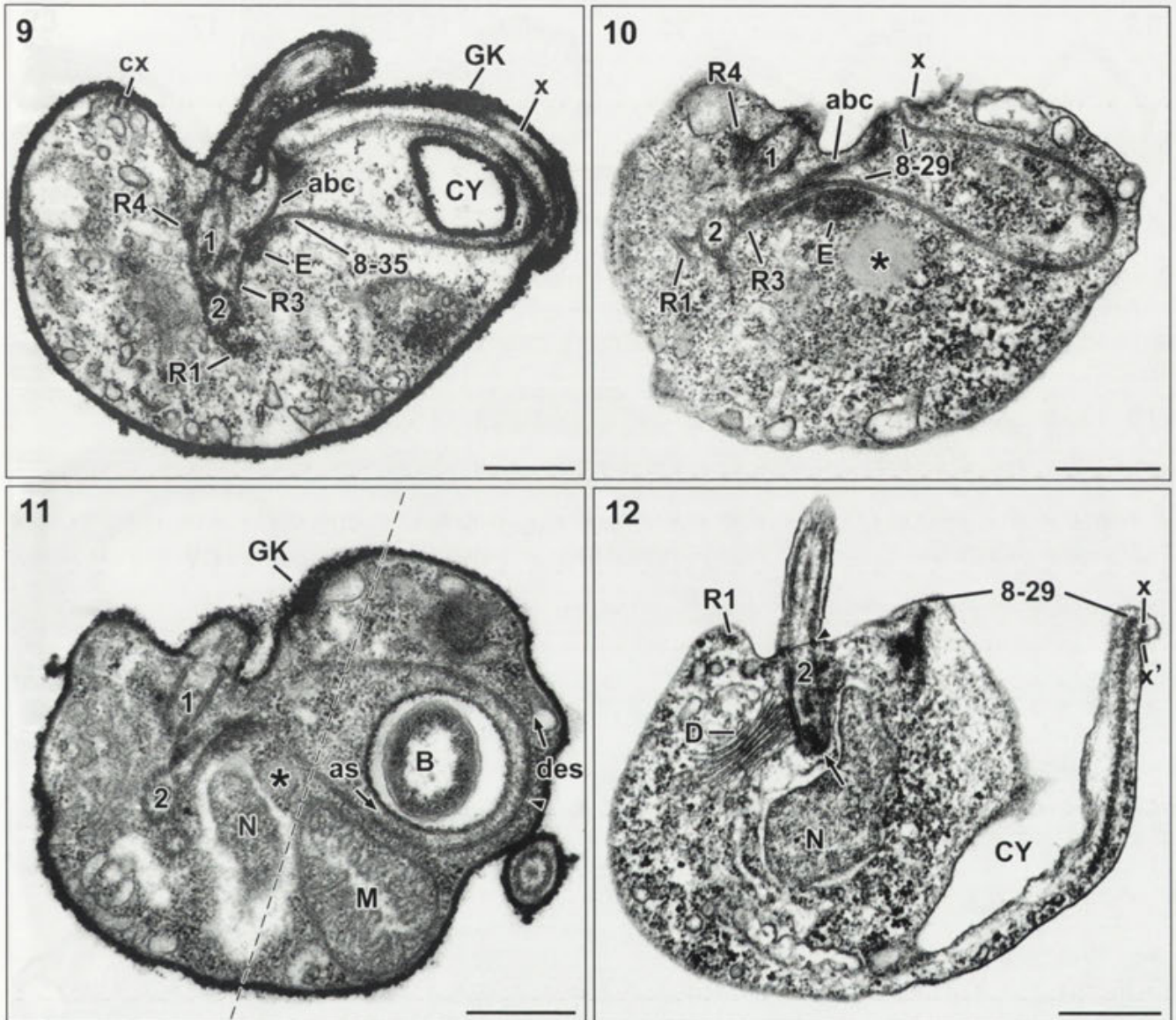
The end of R3 is made of the microtubules c and x (Fig. 32), which combine the small and the large loops at the left side of the cell and run around the insertion region of the posterior flagellum towards the dorsal apical cell side (Figs 18, 20).

R4 consists of only two microtubules which arise from the basal body of the anterior flagellum (Figs 9, 18, 22). It leads from the dorsally oriented part of the correspondent basal body to the left ventral side of the cell and terminates near the end part of R3.

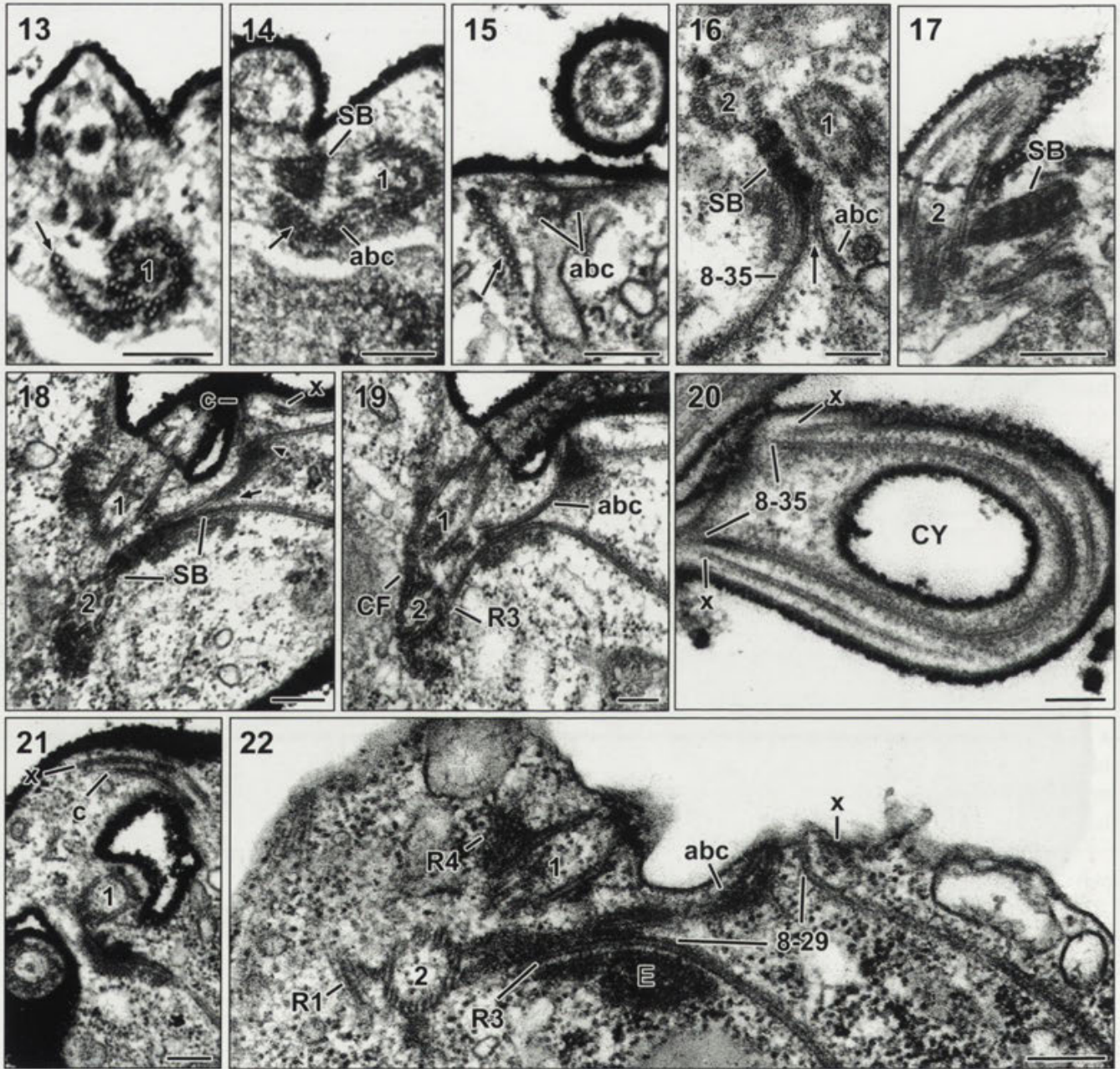
Summarizing the structural and ultrastructural features, the strains DQ220712 and DQ220713 show significant differences in the length of the posterior flagellum, the appearance of the glycocalyx and the maximal number of microtubules in R3.

Locomotion pattern

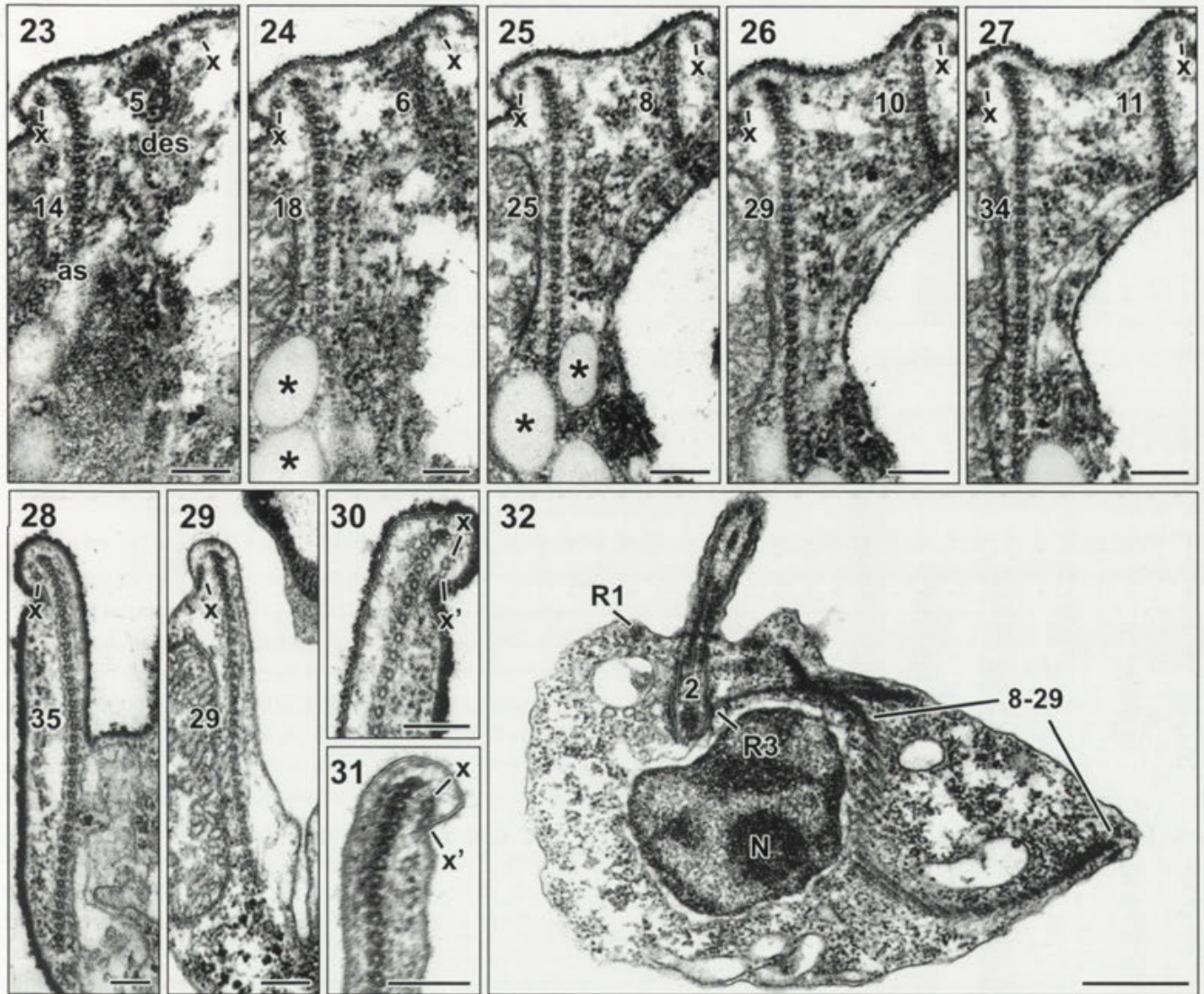
Both studied *Caecitellus* strains have a moving anterior and a trailing posterior flagellum; their locomotion patterns look therefore very similar. Nevertheless, Fig. 33 shows that significant differences in the velocity of the gliding cells were measurable (Fig. 33a), as well as in the angle the anterior flagellum describes when it moves (Fig. 33b) and in the time it needs for one circle (Fig. 33c). Cells of the surface water strain (DQ220713)



Figs 9-12. Transmission electron micrographs showing the general cellular organisation of the two examined *Caecitellus* strains [DQ220712, deep sea (9, 11) and DQ220713, surface water (10, 12)]; 9, 10 - horizontal sections, viewed from anterior/dorsal showing microtubular root 1 (R1) and root 3 (R3) originating from basal body of anterior flagellum (2); R3 splitting into a short loop (abc), a large loop (8-35, resp. 8-29) and a single microtubule (x); electron-dense material (E) at separation point of abc loop and 8-35 loop, x-microtubule leading at the right side of the cell around the cytotome (CY); microtubular root 4 (R4) originating at basal body of posterior flagellum (1); 9 - microtubules c and x at the anterior/left side of the cell; GK - glycocalyx. 10 - electron-lucent body (asterisk) in close vicinity to ascending part of 8-29-loop; after turning point (arrowhead) large loop turning left, its descending part (des) passing along ventral side of the cell; bacterium (B) inside oral apparatus; dotted line indicates approximate section plane of Figs 23-27; 12 - longitudinal section of basal body 2 with electron-dense material in its proximal end (arrow) and with basal plate at level of the plasmalemma (arrowhead); dictyosom (D) close to the left of basal body 2 and the nucleus (N); prominent cytopharynx (CP) surrounded by basket of 8-29 microtubules; in the lip microtubule x' underneath microtubule x; root 1 (R1) directly underneath the anterior surface at the left side of the cell. Scale bars: 0.5 μ m.



Figs 13-22. Kinetid architecture of *Caecitellus* (13-21: strain DQ220712, deep sea; 22: strain DQ220713, surface water). 13 - cross section of the proximal end of basal body 1 (1) and R3 (arrow); 14 - cross section of L-shaped part of R3, basal body 1 and striated band (SB) at a point slightly distal to that of Fig. 10; R3 depicted as L-shaped structure with typical 8, 3 pattern, showing the start of separation of abc and 8 subunit of R3 (arrow); 15 - cross section of 8 subunit (arrow) and abc microtubules at a level distal to R3-separation; 16 - cross section of basal body 2 and oblique section of basal body 1, showing position of striated band (SB) and separation of R3 in abc subunit and 8-35 loop (arrow) 17 - oblique section of basal body 2 illustrating its association with striated band (arrow); 18, 19 - consecutive sections of the connecting structures of basal bodies 1 and 2: i) striated band (SB) and connecting fibre (CF), ii) proximal end of R3 with its point of separation (arrow) as well as junction of the descending 8-35 loop, iii) abc loop (arrowhead), iii) continuation of microtubules c and x at left side of the cell; 20 - longitudinal section of microtubule x and 8-35 loop leading around the cytostome (CY); 21 - distal end of R3 consisting of microtubules c and x leading around the insertion of the posterior flagellum (1). 22 - kinetid of *Caecitellus* cell strain DQ220713 (surface water), section through the dorsal anterior side of the cell showing i) basal bodies 1 and 2, ii) the origin of microtubular roots R1, R3 and R4, iii) parts of the subunits of R3 (8-29, abc, x). Scale bars: 0.2 μ m.



Figs 23-32. Microtubular structure of the feeding basket of *Caecitellus*. **23-27** - serial sections of a feeding basket of a cell of strain DQ220712 (section plane - dotted line in Fig. 11) showing i) increasing number of microtubules in ascending (as) and descending (des) part of 8-35 subunit of R3, ii) location of electron lucent bodies (asterisks), iii) position of microtubule x; **28** - ascending root with max. 35 microtubules (strain DQ220712) and in **29** with max. 29 microtubules in strain DQ220713; **30** - cell of strain DQ220712; **31** - cell of strain DQ220713 showing microtubule x' in the lip immediately underneath microtubule x in the area of the turning point of the loop; **32** - cell of strain DQ220713 in dorsal view illustrating basket structure of 8-29 loop (ascending subunit), origin of root 3 (R3) at basal body 2 anteriorly to the nucleus (N) and location of R1 at the left anterior side of the cell. Scale bars: 0.2 μm (23-27, 30, 31); 0.5 μm (28, 29, 32).

move faster forward and have an anterior flagellum which describes a smaller angle in less time than most cells of the studied deep sea strain (DQ220712).

Growth rates

The growth rates of the surface water strain (DQ220713) and deep sea strain (DQ220712) differed

distinctly with mean (\pm range) maximal growth rates of $3.13 \pm 0.48 \text{ d}^{-1}$ for the surface water isolate and $4.47 \pm 0.25 \text{ d}^{-1}$ for the deep sea isolate (Fig. 34). These growth rates mean doubling times of 5.4 and 3.7 h, respectively. With a mean (\pm range) maximal growth rate for the ATCC50091 strain of $5.34 \pm 0.04 \text{ d}^{-1}$ (mean doubling time: 3.1 h), this strain was more similar to the deep sea strain than to the surface water strain.

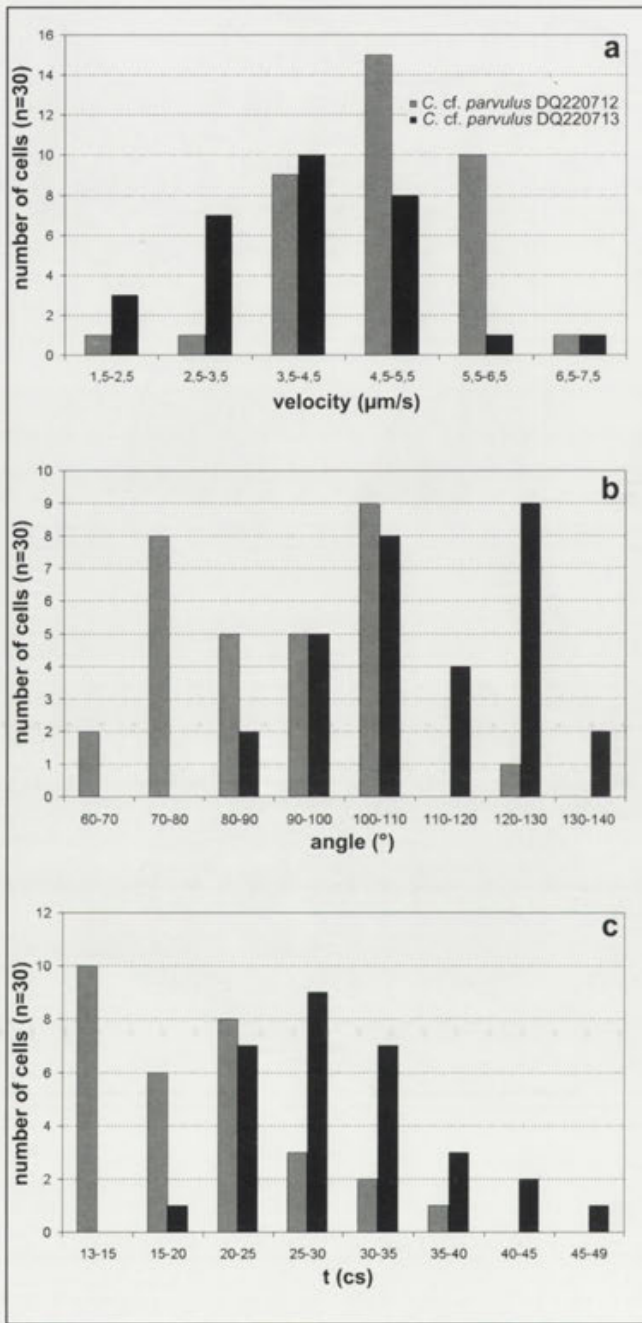


Fig. 33. The locomotion velocity of the two studied *Caecitellus* strains differs significantly (a) as well as the angle which the anterior flagellum describes during its activity (b). Also the time which is needed to complete one cycle of the anterior flagellum differs significantly (c).

Molecular data

All sequences of *Caecitellus parvulus* obtained in this study have nearly the same length as those reported

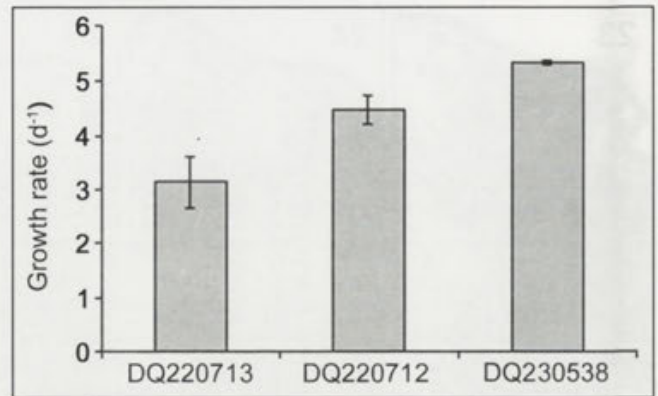


Fig. 34. Mean (± range) maximal growth rates of the *Caecitellus* strains DQ220713 (from the surface water of the South Atlantic), DQ220712 (from the deep sea of the South Atlantic) and DQ230538 (ATCC).

from previous studies (Table 1). After an initial phylogenetic analysis comprising a broad range of heterokont taxa, the labyrinthulid *Ulkenia profunda* has been chosen to root the tree. This initial analysis supported the placement of *Pseudobodo tremulans* as basal bicosoecid taxon (Karpov *et al.* 2001), although its placement at the root of the bicosoecids varies depending on the taxa and the numbers of sequences included in phylogenetic analysis. An unstable branching pattern has been observed regarding the bicosoecid *Symbiomonas scintillans*. This taxon has therefore been excluded from phylogenetic analysis. With the exception of *Cafeteria*, all phylogenetic methods recovered the same optimal tree topology, with each node supported by high bootstrap values (Fig. 35). In ML and MP analysis, *Cafeteria* branches at the root of the *Caecitellus* clade with moderate bootstrap support (ML: 65; MP: 52), in ME analysis at the root of the *Adriamonas/Siluania* clade (bootstrap value: 64).

The clade composed of both *Pseudobodo* strains (DQ220718: isolated by A.P. Mylnikov from brackish water of the Baltic Sea near Hiddensee, Germany; AF315604: isolated by A. P. Mylnikov from brackish water of the White Sea) branches first, followed by the clade composed of *Siluania*, *Adriamonas* and *Cafeteria* and finally the clade comprising the different strains of *Caecitellus*. The tree shows a paraphyletic family Siluniidae (*Siluania*, *Adriamonas* and *Caecitellus*; Karpov *et al.* 2001) and Cafeteriidae (*Cafeteria* and *Pseudobodo*; Moestrup 1995), but discrepancies between morphological and molecular data concerning this

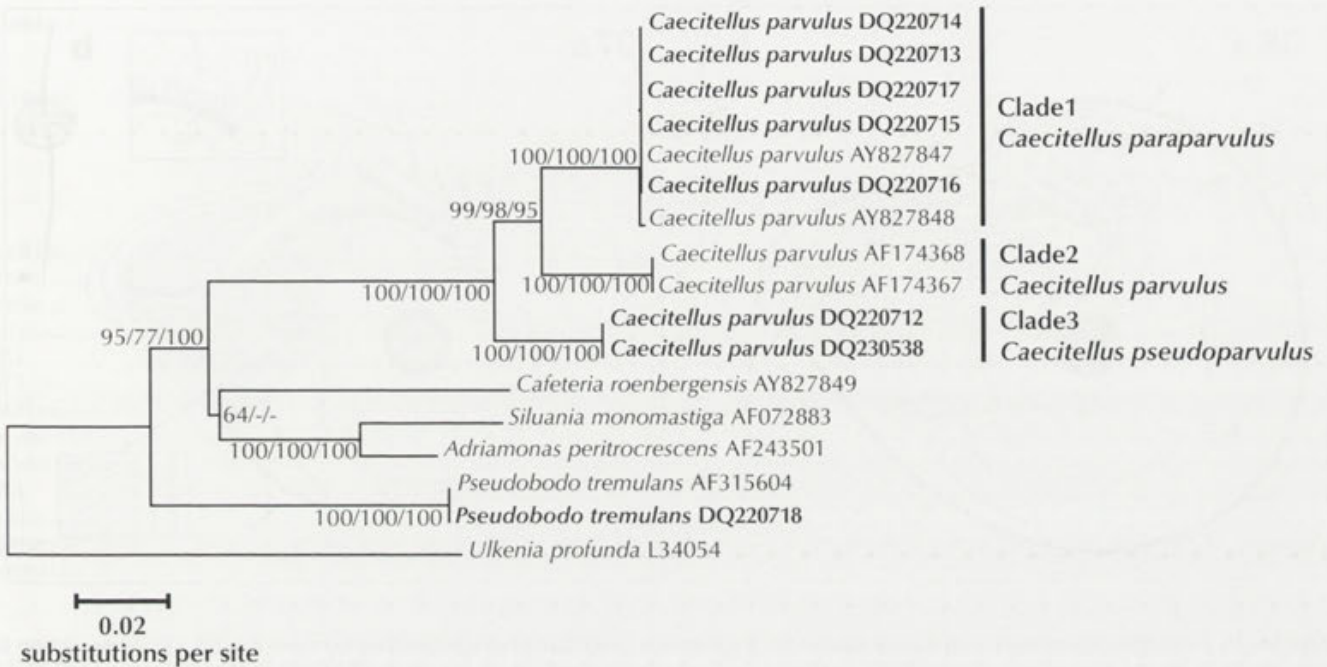


Fig. 35. Rooted minimum evolution bootstrap consensus tree of the order Bicosoecida (Grassé), Karpov 1998, using 1533 positions (nucleotide substitution model: LogDet; complete-deletion option set). The tree was rooted using *Ulkenia profunda* as outgroup. Numbers at the nodes are bootstrap support percentages from 250 replicates using the minimum evolution method (left) and from 100 replicates for both the maximum likelihood (middle) and maximum parsimony (right) methods. Strain identifiers refer to the GenBank accession numbers. Strains sequenced in this study are in bold.

families are well known and have already been addressed in detail by Karpov *et al.* (2001).

In all trees obtained, *Caecitellus* forms a monophyletic group with three distinct clades and with very high bootstrap support values. The first clade (Clade 1) is composed of strains which were all isolated in 2000 from sediments of the Angola Abyssal Plain, with the exception of one strain (DQ220713), the ultrastructure of which is also subject of this study, taken from the surface water of the South Atlantic Ocean. The second clade (Clade 2) is composed of both strains sequenced by Atkins *et al.* (2000) isolated in 1995 from mussel beds of deep sea hydrothermal vents of the Eastern Pacific Rise (AF174367), respectively in 1996 from New Bedford Harbor, Massachusetts (AF174368). The third clade (Clade 3) is composed of the strain DQ230538 isolated in 1981 by P. G. Davis, the ultrastructure of which has been studied by O'Kelly and Nerad (1998) and of the strain DQ220712 isolated in 2000 from deep sea sediments of the Angola Abyssal Plain, the ultrastructure of which is subject to this study.

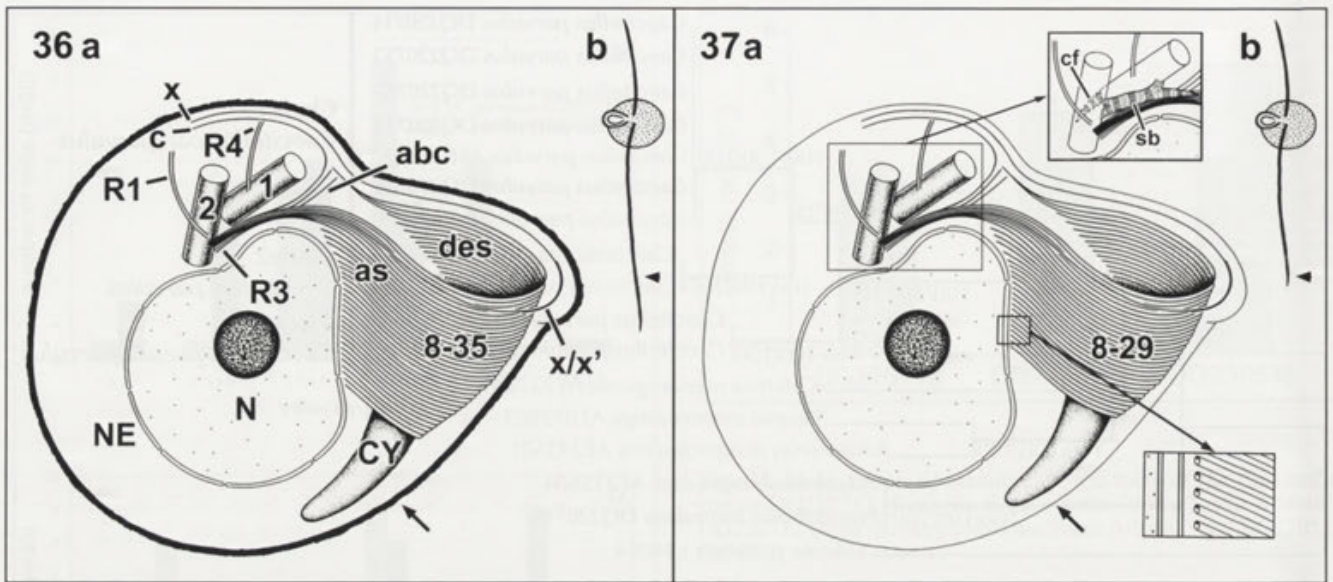
Uncorrected distances (*p*-distances) have been calculated for all strains of *Caecitellus* (Table 2) and show

very high ribosomal sequence divergences within this group, as well as for both *Pseudobodo* strains (0.20%). Mean *p*-distances and their standard deviations have been calculated between the three major clades of *Caecitellus* as well as within these clades. Mean distances within all three clades are equally low with minimal variances (Clade1: 0.05 ± 0.03 %; Clade2: 0.00%; Clade3: 0.00%). On the other hand, very high mean distances with at the same time low variances can be observed in all three cases between these clades (Clade1/Clade2: 4.50 ± 0.50 %; Clade1/Clade3: 5.35 ± 0.52 %; Clade2/Clade3: 5.91 ± 0.54 %).

DISCUSSION

Morphological Data

At the level of light-microscopy there are no obvious structural differences visible between the two investigated *Caecitellus cf. parvulus* strains DQ220712 (from the deep sea) and DQ220713 (from the surface water). Their cell shape and way of movement seems to be in



Figs 36, 37. Schematic reconstruction of the position of the basal bodies 1 and 2, the paths of the flagellar roots R1, R3 and R4 in relation to the contour of the cell, the nucleus (N) and the cytopharynx (CY) in *Caecitellus cf. parvulus*, strain DQ220712 (**36a**) and strain DQ220713 (**37a**), dorsal view; feeding basket built of 8-35 (**36a**) or 8-29 (**37b**) microtubules with ascending (as) and descending (des) parts; separation of R3 into subunits abc, 8 and x; turning point with additional microtubule x' directly underneath x; microtubules c and x representing end of R3 at left/ventral side of the cell; differences in the appearance of the glycocalyx of both strains are indicated by an arrow; **36b** and **37b** contour of a complete cell of *C. cf. parvulus*, strain DQ220712 (**36b**) and strain DQ220713 (**37b**) seen ventrally; arrowhead pointing to the differences in length of the posterior flagellum. Insets in **37** (the depicted features are identical in the two investigated strains): above: path of connecting fiber (cf) and striated band (sb); below: microtubules of feeding basket without intimate contact with nuclear envelop (NE).

conformity with almost all previous light-microscopical descriptions (e.g. Patterson *et al.* 1993, Tong 1997a, O'Kelly and Nerad 1998, Lee and Patterson 2000, Al-Qassab *et al.* 2002, Lee *et al.* 2003). An additional thread trailing from the outer margin of the mouth, noted only by Tong (1997b) and Tong *et al.* (1998), was not seen in the present study.

However, biometric analysis showed significant differences in the length of the posterior flagellum of the two studied strains of *C. cf. parvulus*. But the average length of the posterior flagellum in both strains is within the size range reported in the literature for *C. parvulus* (e.g. O'Kelly and Nerad 1998, Atkins *et al.* 2000, Al-Qassab *et al.* 2002, Lee *et al.* 2003).

The ultrastructural comparison of *Caecitellus cf. parvulus* strains DQ220712 and DQ220713 shows that in general both strains follow a similar basic structural plan, but there are differences in the appearance of the glycocalyx and in the maximal number of microtubules in the flagellar root 3 (R3).

Only in strain DQ220712 is the glycocalyx visible as a relatively thick, electron-dense layer. It is hardly

recognisable at all in strain DQ220713 and in all published TEM micrographs of *Caecitellus parvulus* (Patterson *et al.* 1993, O'Kelly and Nerad 1998). Differences in the morphological appearance of the glycocalyx are useful tools to differentiate e.g. between the amoeba genera *Vanella* and *Platyamoeba* at the ultrastructural level (Page and Blakey 1979). On the other hand, molecular studies have revealed that glycocalyx appearance is not necessarily also a reliable phylogenetic marker to distinguish between the genera in this case (Sims *et al.* 2002).

The kinetids of both ultrastructurally investigated *C. cf. parvulus* strains also differ from the kinetid of the described *Caecitellus parvulus* in the maximal number of microtubules found in R3, which forms the cytoskeletal fundament of the feeding basket. O'Kelly and Nerad (1998) counted a maximum of approximately 24 microtubules for *C. parvulus* (strain DQ230538 from the Pacific Ocean). With eleven microtubules more, strain *C. cf. parvulus* DQ220712 (from the South Atlantic deep sea) has a much larger feeding basket. Nevertheless, the feeding basket of *C. cf. parvulus* strain

Table 3. Summary of differences between the species of the *Caecitellus* complex.

Criteria	<i>Caecitellus</i> complex				
	<i>C. parvulus</i> Patterson <i>et al.</i> 1993	<i>C. pseudoparvulus</i> O'Kelly and Nerad 1998	Atkins <i>et al.</i> 2000	<i>C. paraparvulus</i> this study	<i>C. paraparvulus</i> this study
cell length	4-7 µm	3-7 µm	3-10 µm	2-4 µm	2.5-4.5 µm
ratio: anterior flagellum/cell length	?	1.5-2.5	1	1-2	1-2
ratio: posterior flagellum/cell length	?	2.5-3.5	3-4	2.5-4.5	2-4.5
glycocalyx	thin	thin	?	thick	thin
R1	?	2 mt	?	2 mt	2 mt
R3 (proximal)	?	8+3	?	8+3	8+3
R3 (maximal)	?	24 mt	?	35 mt	29 mt
x -mt (R3)	?	+	?	+	+
x' -mt (R3)	?	-	?	+	+
R4	?	2 mt	?	2 mt	2 mt
genetical distance to <i>C. parvulus</i>	?	?		5.91%	4.5%
genetical distance to <i>C. pseudoparvulus</i>	?	?	5.91%		5.35%
genetical distance to <i>C. paraparvulus</i>	?	?	4.5%	5.35%	

? - not reported; R1, R3, R4 - root 1, 3, 4; mt - microtubule

DQ220713 (from the South Atlantic surface water) with its 29 microtubules is smaller than that of strain DQ220712, but includes still more microtubules than described for *C. parvulus* (O'Kelly and Nerad 1998).

The differences of the glycocalyx and the feeding basket could be indicative for a different ecological niche and/or geographic distribution, but the molecular data show that the three resulting morphological and genetically distinctive clades include strains from different habitats and locations. Whether or not the differences in the feeding basket size are coupled with differences in the size of their food (bacteria) is thus far unknown, but not unlikely.

Locomotion pattern

The difference between the gliding velocities of the two studied strains is significant, as are the dynamics of their anterior flagellum. This might attest differences in the size of the preferred food particles (mainly bacteria). Further investigations are in progress to clarify this point by using inert, artificial food particles of different sizes to determine both the optimal dimensions of the food and the time needed for the ingestion process, as has been studied extensively in species of other heterotrophic flagellate groups e.g. by Boenigk *et al.* (2001a-c, 2002).

Growth rates

The maximal growth rates measured for the three *Caecitellus* strains, i.e. the deep sea strain DQ220712, the surface water strain DQ220713 and the strain DQ230538, were within the range reported for other heterotrophic flagellates (Fenchel 1982b, Sherr *et al.* 1984, Eccleston-Parry and Leadbeater 1994). The ranges of the measured growth rates showed no overlap between the strains, indicating distinct differences. The deep sea strain showed a higher growth rate compared to the surface water strain, even though the growth experiments were conducted under surface water conditions (19 °C, atmospheric pressure). This was not surprising, as it has been repeatedly demonstrated that deep sea heterotrophic flagellates show high growth rates under surface water conditions (Patterson *et al.* 1993, Atkins *et al.* 1998, Arndt *et al.* 2003). The growth rates of the deep sea strain (DQ220712) are closer (though not identical) to those of the DQ230538 strain than to those of the surface water strain from the same region. This finding matches the molecular data which shows that the deep sea and the DQ230538 strain are closely related (both cluster within Clade 1), whereas the surface water strain (DQ220713) clusters within Clade 3. Furthermore, the lower growth rates of the *C. cf.*

Table 4. SSU rDNA signature sequences of *Caecitellus parvulus*, *C. pseudoparvulus* and *C. paraparvulus*.

Species	Sequence signature (5'-3')	Position ¹	Environmental sequences considered
A			
<i>Caecitellus parvulus</i> ²	tacttgatagcttttctactc	118	
	caattctagagctaagacgcgctat	152	
	gtgctcgtagtcggtc	601	AY046666
	ggctggcgcgtgtgct	625	
	ccgctttggcggcc	645	
	cttg	735	AY046666
	gaactgctcgaaagcg	840	AY046666
	tagaccctggttcagggtgcta	1261	AY046666
	cgcgagtcacatctcgca	1500	AY046666
	agcgcagctccgctcgcgcgagaagtggtt	1596	AY046666
B			
<i>Caecitellus pseudoparvulus</i> ⁴	atttattagatacaaccacacca	187	
	tgactctacg	446	
	atgccactcccgcca ⁵	601	
	tggcgatgtggagttc ⁵	625	
	cgattgtt ⁵	964	
	cgggctctgttttcagggtgccg ⁵	1261	
	cgaagaccccgcgctcgcgcgagaactggcta ⁵	1596	
	C		
<i>Caecitellus paraparvulus</i> ³	cacttgatagctctctactt	118	AY789784
	gtttccggcgcctccccttc	601	AY789784, AM041117
	cggggacacggggacc	625	AJ965041, AJ965066, AJ965067, AY789784
	tacg	735	AJ965041, AJ965066, AJ965067, AM041117, AY789784
	gata	761	AJ965041, AJ965066, AJ965067, AM041117
	cctggcccctgcggc	1596	

¹Position in *Caecitellus pseudoparvulus* DQ230538 used as reference.

²Signature sequences always matching *Caecitellus* AF174367 and AF174368.

³Signature sequences always matching *Caecitellus* AY827847, AY827848, and DQ220713-DQ220716.

⁴Signature sequences always matching *Caecitellus* AY520455, DQ220712, and DQ230538.

⁵Signature sequences also matching *Caecitellus* AY520456.

parvulus strain DQ220713 (from the South Atlantic surface water) coincided with a smaller feeding basket compared to strain DQ220712. This might reflect a strategy of high exploration of resources in the latter, which results in high growth rate under optimal food conditions. However, such conclusions on the link between molecular data, ultrastructure and growth rate need to be taken with caution unless further strains are investigated.

Molecular Data

The high level of genetic divergence within the morphospecies *Caecitellus parvulus* and the high boot-

strap support for the three clades suggest that this species complex represents an assemblage of microscopically similar morphotypes united by morphological traits visible on the level of light-microscopy: one trailing flagellum, one stiffly and slowly moving anterior flagellum, flattened and often triangular in profile (Patterson *et al.* 1993, O'Kelly and Nerad 1998, Lee *et al.* 2000). The present molecular data alone proposes that the morphospecies *C. parvulus* is no longer maintainable as such and that it will need to be divided into three different species. They do not cluster together based on their geographical origins or habitats; strains from the South Atlantic Ocean and the North Atlantic Ocean as well as

strains from the Eastern Pacific Ocean and the North Atlantic Ocean are identical. Besides the molecular data, the only way to reliably distinguish at least two (Clade 1 and Clade 3) of the three lineages is the ultrastructural data including the behavioural observations presented in this study.

Conclusions

The ultrastructural distinction and the large genetic differences between the three clades of the morphospecies *Caecitellus parvulus* as well as the high degree of the genetic similarity within each genotype demonstrate the existence of at least three species within a *Caecitellus* complex.

Recent molecular studies indicate that several cryptic species might exist among protists (e.g. Nanney *et al.* 1998, Darling *et al.* 2004, Scheckenbach *et al.* 2005). At least in some cases, detailed comparisons of morphological and non-morphological features showed that also pseudo-cryptic species exist and that slight morphological differences may separate species (Huber *et al.* 1997, Darling *et al.* 1999, de Vargas *et al.* 1999, Sáez *et al.* 2003, Sáez and Lozano 2005). Therefore the results of the present study led to descriptions of two new *Caecitellus* species. One called *Caecitellus paraparvulus* includes the strains of Clade 1 of this study; the other new species, named *Caecitellus pseudoparvulus*, includes both strains of Clade 3 (Fig. 35). O'Kelly and Nerad (1998) presented only light microscopical photographs of the now newly designated strain *Caecitellus pseudoparvulus* DQ230538, isolated from the Sargasso Sea. For the ultrastructural description of *Caecitellus parvulus* they used the strain ATCC50712, which was isolated from the North Pacific Ocean. Unfortunately this strain is no longer available from the American Type Culture Collection, were it was deposited (O'Kelly and Nerad 1998). Therefore it does not seem to be possible to investigate the genotype of this strain at present. Clade 2 includes two strains of *C. parvulus* which were sequenced and described by Atkins *et al.* (2000) using light microscopy.

As pointed out by de Vargas *et al.* (1999) for planktonic foraminifers, our results (including the results of Scheckenbach *et al.* 2005) indicate that the worldwide species diversity of *Caecitellus parvulus* - as a case study of heterotrophic nanoflagellates - might be greatly underestimated if a morphospecies concept is exclusively applied. Different strains of the three species of the genus *Caecitellus* were found in different loca-

tions or habitats. Consequently it seems there is no evidence for endemism of the *Caecitellus* species, but special micro-environment and behavioural conditions might exist.

Finally, our results show the potential of combined DNA, ultrastructural and behavioural analyses for detection of species complexes within morphospecies of heterotrophic flagellates.

Taxonomic Diagnosis (Table 3)

Genus *Caecitellus* (Patterson *et al.* 1993)

Distinguishable at the level of light microscopy among gliding flagellates by a conspicuous ventral mouth, the orientation of the two flagella and the beat pattern of the anterior flagellum (Al-Qassab *et al.* 2002). Cell sizes from 2-10 μm have been reported. The small heterotrophic nanoflagellates have somewhat rounded or triangular profiles and feed on bacteria. The anterior flagellum inserts apically, is about 1-2.5 times the cell length and beats anteriorly and stiffly. The measurements for the length of the posterior trailing flagellum range from 2 to 4.5 times the cell length (e.g. Griessmann 1913, Larsen and Patterson 1990, Patterson *et al.* 1993, O'Kelly and Nerad 1998, Tong *et al.* 1998, Lee and Patterson 2000, Al-Qassab *et al.* 2002, Lee *et al.* 2003, present study).

Caecitellus parvulus (Basionym: *Bodo parvulus*, Griessmann 1913) Patterson *et al.* (1993). For detailed ultrastructural description see O'Kelly and Nerad (1998). Sequence signature see Table 4 A.

Caecitellus pseudoparvulus n. sp.

The kinetid of *Caecitellus pseudoparvulus* is basically similar to the kinetid of *C. parvulus* as described by O'Kelly and Nerad (1998). Different is the maximal number of microtubules of the large loop of R3. 35 microtubules were counted in the cytostome for *C. pseudoparvulus*. An additional microtubule x' is located in the area of the turning point of the large loop directly underneath microtubule x, first described in this study for *C. pseudoparvulus* and *C. paraparvulus*. Within the *Caecitellus*-complex only *C. pseudoparvulus* shows a relatively thick electron-dense glycocalyx. *C. pseudoparvulus* has on the average a longer posterior flagellum than *Caecitellus paraparvulus*. Sequence signature see Table 4 B.

Caecitellus paraparvulus n. sp.

The first-described *Caecitellus* species, *C. paraparvulus*, has basically the same ultrastructure as described by O'Kelly and Nerad (1998) for

C. parvulus. Different is the maximal number of microtubules of the large loop of R3. With approximately 29 microtubules, *C. paraparvulus* has five microtubules more than *C. parvulus* and six microtubules fewer than *C. pseudoparvulus* in its feeding basket. As described for *C. pseudoparvulus*, there is an x'-microtubule underneath the x-microtubule. The glycocalyx of *C. paraparvulus* is thin or hardly visible without special staining procedures. Compared to *C. pseudoparvulus*, this species usually has a shorter posterior flagellum. Sequence signature see Table 4 C.

Acknowledgements. This study was funded by the German Research Foundation (DFG; Ar 288/5-1 and HA 818/18-1). We would like to thank Prof. Diethard Tautz (University of Cologne, Institute of Genetics, Cologne, Germany) for helpful comments and discussions. We also thank the scientific illustrator Peter Adam (Free University of Berlin, Institute of Biology / Zoology, Berlin, Germany) for preparing Figs 36 and 37.

REFERENCES

- Al-Qassab S., Lee W. J., Murray S., Simoson A. G. B., Patterson D. J. (2002) Flagellates from stromatolites and surrounding sediments in Shark Bay, Western Australia. *Acta Protozool.* **41**: 91-144
- Arndt H., Dietrich D., Auer B., Cleven E.-J., Gräfenhan T., Weitere M., Mylnikov A. P. (2000) Functional diversity of heterotrophic flagellates in aquatic ecosystems. In: *The Flagellates*, (Eds. B. S. C. Leadbeater., J. C. Green). Systematics Association Special Publications. Taylor & Francis, London, 240-268
- Arndt H., Hausmann K., Wolf M. (2003) Deep sea heterotrophic nanoflagellates of the Eastern Mediterranean Sea: qualitative and quantitative aspects of their pelagic and benthic occurrence. *Mar. Ecol. Prog. Ser.* **256**: 45-56
- Atkins M. S., Anderson O. R., Wirsén C. O. (1998) Effects of hydrostatic pressure on the growth rates and encystment of flagellated protozoa isolated from a deep-sea hydrothermal vent and a deep shelf region. *Mar. Ecol. Prog. Ser.* **171**: 85-95
- Atkins M. S., Teske A. P., Anderson O. R. (2000) A survey of flagellate diversity at four deep-sea hydrothermal vents in the Eastern Pacific Ocean using structural and molecular approaches. *J. Euk. Microbiol.* **47**: 400-411
- Azam F., Fenchel T., Field J.G., Gray J. S., Meyer-Reil L. A., Thingstad F. (1983) The ecological role of water-column microbes in the sea. *Mar. Ecol. Prog. Ser.* **10**: 257-263
- Berninger U.-G., Finlay B. J., Kuuppo-Leinikki P. (1991) Protozoan control of bacterial abundances in freshwater. *Limnol. Oceanogr.* **36**: 139-147
- Boenigk J., Arndt H. (2002) Bacterivory by heterotrophic flagellates: community structure and feeding strategies. *Antonie van Leeuwenhoek* **81**: 465-480.
- Boenigk J., Arndt H., Cleven E. J. (2001a) The problematic nature of fluorescently labeled bacteria (FLB) in *Spumella* feeding experiments - an explanation by using video microscopy. *Arch. Hydrobiol.* **152**: 329-338
- Boenigk J., Matz C., Jürgens K., Arndt H. (2001b) The influence of preculture conditions and food quality on the ingestion and digestion process of three species of heterotrophic nanoflagellates. *Microbiol. Ecol.* **42**: 168-176
- Boenigk J., Matz C., Jürgens K., Arndt H. (2001c) Confusing selective feeding with differential digestion in bacterivorous nanoflagellates. *J. Euk. Microbiol.* **48**: 425-432
- Boenigk J., Matz C., Jürgens K., Arndt H. (2002) Food concentration dependent regulation of food selectivity of interception feeding bacterivorous nanoflagellates. *Aquatic Microbiol. Ecol.* **27**: 195-202
- Caron D. A. (1991) Heterotrophic flagellates associated with sedimenting detritus. In: *The Biology of Free-living Heterotrophic Flagellates*, (Eds. D. J. Patterson, J. Larsen). Clarendon Press, Oxford, 77-92
- Clark G. C. (1992) Riboprinting: a molecular approach to the identification and taxonomy of protozoa. In: *Protocols in Protozoology*, (Eds. J. J. Lee, A. T. Soldo). Allen, Lawrence, Kansas, D4.1-D4.4
- Darling K. F., Wade C. M., Kroon D., Leigh Brown A. J., Bijam J., (1999) The diversity and distribution of modern planktonic foraminiferal small subunit ribosomal RNA genotypes and their potential as tracers of present and past ocean circulations. *Paleoceanography* **14**: 3-12
- Darling K. F., Kucera M., Pudsey C. J., Wade C.M. (2004) Molecular evidence links cryptic diversification in polar planktonic protists to quaternary climate dynamics. *Proc. Natl. Acad. Sci. USA* **101**: 7657-7662
- de Vargas C., Norris R., Zaninetti L., Pawlowski J. (1999) Molecular evidence of cryptic speciation in planktonic foraminifers and their relation to oceanic provinces. *Proc. Natl. Acad. Sci. USA* **96**: 2864-2868
- Eccleston-Parry J. D., Leadbeater B. S. C. (1994) The effect of long-term low bacterial density on the growth kinetics of three marine heterotrophic microflagellates. *J. Exp. Mar. Biol. Ecol.* **117**: 219-233
- Ekeboom J., Patterson D. J., Vørs N. (1995/1996) Heterotrophic flagellates from coral reef sediments (Great Barrier Reef, Australia). *Arch. Protistenkd.* **146**: 251-272
- Felsenstein J. (1981) Evolutionary trees from gene frequencies and quantitative characters: finding maximum likelihood estimates. *Evolution* **35**: 1229-1242
- Felsenstein J. (1985) Confidence limits on phylogenies: an approach using the bootstrap. *Evolution* **39**: 783-791
- Felsenstein J. (2004) PHYLIP (Phylogeny Inference Package) version 3.63. Distributed by the author. Department of Genome Sciences, University of Washington, Seattle
- Fenchel T. (1982a) Ecology of heterotrophic microflagellates. I. Some important forms and their functional morphology. *Mar. Ecol. Prog. Ser.* **8**: 211-223
- Fenchel T. (1982b) Ecology of heterotrophic flagellates. II. Bioenergetics and growth. *Mar. Ecol. Prog. Ser.* **8**: 225-231
- Finlay B. J. (2002) Global dispersal of free-living microbial eukaryote species. *Science* **296**: 1061-1063
- Foissner W. (1999) Protist diversity: estimates of the near-imponderable. *Protist* **150**: 363-368
- Gasol J. M., Vaqué D. (1993) Lack of coupling between heterotrophic nanoflagellates and bacteria: a general phenomenon across aquatic systems? *Limnol. Oceanogr.* **38**: 657-665
- Griessmann K. (1913) Über marine Flagellaten. *Arch. Protistenkd.* **32**: 1-78
- Hausmann K., Weitere M., Wolf M., Arndt H. (2002) *Meteora sporadica* gen. et sp. nov. (Protista incertae sedis) - an extraordinary free-living protist from the Mediterranean deep sea. *Europ. J. Protistol.* **38**: 171-177
- Huber B., Bijama J., Darling K. (1997) Cryptic speciation in the living planktonic foraminifer *Globigerinella siphonifera* (d'Orbigny). *Paleobiology* **23**: 33-62
- Karpov S. A., Sogin M. L., Silberman J. D. (2001) Rootlet homology, taxonomy, and phylogeny of bicosoecids based on 18S rRNA gene sequences. *Protistology* **2**: 34-47
- Kjørboe T., Grossart H.-P., Ploug H., Tang K., Auer B. (2004) Particle-associated flagellates: swimming patterns, colonizing rates, and grazing on attached bacteria. *Aquat. Microb. Ecol.* **35**: 141-152
- Kumar S., Tamura K., Nei M. (2004) MEGA3: Integrated software for Molecular Evolutionary Genetics Analysis and sequence alignment. *Briefings in Bioinformatics* **5**: 2

- Larsen J., Patterson D. J. (1990) Some flagellates (Protista) from tropical marine sediments. *J. Nat. Hist.* **24**: 801-937
- Lee J. J., Leedale G. F., Bradbury P. (Eds.) (2000) An Illustrated Guide to the Protozoa, 2nd ed. Allen Press Inc., Lawrence, KS, USA
- Lee W. J., Patterson D. J. (1998) Diversity and geographic distribution of free-living heterotrophic flagellates - analysis by PRIMER. *Protist* **149**: 229-244
- Lee W. J., Patterson D. J. (2000) Heterotrophic flagellates (Protista) from marine sediments of Botany Bay, Australia. *J. Nat. Hist.* **34**: 483-562
- Lee W. J., Brandt S. M., Vørs N., Patterson D. J. (2003) Darwin's heterotrophic flagellates. *Ophelia* **57**: 63-98
- Lockhart F. J., Steel M. A., Hendy M. D., Penny D. (1994) Recovering evolutionary trees under a more realistic model of sequence evolution. *Mol. Biol. Evol.* **11**: 605-612
- Mayden R. L. (1997) A hierarchy of species concepts: the denouement in the saga of species problem. In: Species: the Units of Biodiversity, (Eds. M. F. Claridge, H. A. Dawah., M. R. Wilson). London, Chapman and Hall, 381-424
- Moestrup Ø. (1995) Current status of chrysophyte "splinter groups": synurophytes, pedinellids, silicoflagellates. In: Chrysophyte Algae: Ecology, Phylogeny, Development, (Eds. C. Sangren, J. P. Smol, J. Kristiansen). Cambridge University Press, Cambridge, UK, 75-91
- Nanney D. L., Park C., Preparata R., Simon E. M. (1998) Comparison of sequence differences in a variable 23S rRNA domain among sets of cryptic species of ciliated protozoa. *J. Euk. Microbiol.* **45**: 91-100
- O'Kelly C. J., Nerad T. A. (1998) Kinetid architecture and bicosoecid affinities of the marine heterotrophic nanoflagellate *Caecitellus parvulus* (Griessmann 1913) Patterson *et al.* (1993). *Europ. J. Protistol.* **34**: 369-375
- Page F. C., Blakey S. M. (1979) Cell surface structure as a taxonomic character in the Thecamoebidae (Protozoa: Gymnamoebia). *Zool. J. Linn. Soc.* **66**: 113-135
- Parducz B. (1967) Ciliary movement and coordination in ciliates. *Int. Rev. Cytol.* **21**: 91-128
- Patterson D. J., Simpson A. G. B. (1996) Heterotrophic flagellates from coastal marine and hypersaline sediments in Western Australia. *Europ. J. Protistol.* **32**: 423-448
- Patterson D. J., Lee W. J. (2000) Geographic distribution and diversity of free-living heterotrophic flagellates. In: The Flagellates, (Eds. B. S. C. Leadbeater, J. C. Green). Systematics Association Special Publications, Taylor & Francis, London, 269-287
- Patterson D. J., Nygaard K., Steinberg G., Turley C. M. (1993) Heterotrophic flagellates and other protists associated with oceanic detritus throughout the water column in the North Atlantic. *J. Mar. Biol. Assoc. UK* **73**: 67-95
- Porter K. G., Feig Y. S. (1980) The use of DAPI for identifying and counting aquatic microflora. *Limnol. Oceanogr.* **25**: 943-948
- Preisig H. R., Vørs N., Hällfors G. (1991) Diversity of heterotrophic heterokont flagellates. In: The Biology of Free-living Heterotrophic Flagellates, (Eds. D. J. Patterson, J. Larsen). Clarendon Press, Oxford, 361-400
- Rzhetsky A., Nei M. (1992) A simple method for estimating and testing minimum-evolution trees. *Mol. Biol. Evol.* **9**: 945-967
- Sáez A. G., Lozano E. (2005) Body doubles. Cryptic species: as we discover more examples of species that are morphologically indistinguishable, we need to ask why and how they exist. *Nature* **433**: 111
- Sáez A. G., Probert I., Geisen M., Quinn P., Young J. R., Medlin L. K. (2003) Pseudo-cryptic speciation in coccolithophores. *Proc. Natl. Acad. Sci. USA* **100**: 7163-7168
- Scheckenbach F., Wylezich C., Weitere M., Hausmann K., Arndt H. (2005) Molecular identity of strains of heterotrophic flagellates isolated from surface waters and deep sea sediments of the South Atlantic based on SSU rDNA. *Aquat. Microb. Ecol.* **38**: 239-247
- Schlegel M., Meisterfeld R. (2003) The species problem in protozoa revisited. *Europ. J. Protistol.* **39**: 349-355
- Sherr B. F., Sherr E. B., Newell S. Y. (1984) Abundance and productivity of heterotrophic nanoplankton in Georgia coastal waters. *J. Plankt. Res.* **6**: 195-202
- Sims G. P., Aitken R., Rogerson A. (2002) Identification and phylogenetic analysis of morphologically similar naked amoebae using small subunit ribosomal RNA. *J. Euk. Microbiol.* **49**: 478-484
- Steel M. A. (1994) Recovering a tree from the leaf colourations it generates under a Markov model. *Appl. Math. Lett.* **7**: 19-24
- Swofford D. L., Olsen G. J. (1990) Phylogeny reconstruction. In: Molecular Systematics, (Eds. D. M. Hillis, C. Moritz). Sinauer Associates, Sunderland, 411-501
- Thompson J. D., Higgins D. G., Gibson T. J. (1994) CLUSTAL W: improving the sensitivity of progressive multiple alignment through sequence weighting, positions-specific gap penalties and weight matrix choice. *Nucleic Acids Res.* **22**: 4673-4680
- Tong S. M. (1997a) Heterotrophic flagellates from the water column in Shark Bay, Western Australia. *Mar. Biol.* **128**: 517-536
- Tong S. M. (1997b) Heterotrophic flagellates and other protists from Southampton water. *Ophelia* **47**: 71-131
- Tong S. M., Nygaard K., Bernard C., Vørs N., Patterson D. J. (1998) Heterotrophic flagellates from the water column in Port Jackson, Sydney, Australia. *Europ. J. Protistol.* **34**: 162-194
- Turley C. (2002) The importance of "marine snow". *Microbiol. Today* **29**: 177-179

Received on 25th April, 2006; revised version on 10th July, 2006; accepted on 13th September, 2006

On Two Marine Oligotrich Ciliates, *Spirostrombidium agathae* n. sp. and *S. schizostomum* (Kahl, 1932) n. comb. from China, with a Key to the Identification of Seven Well-Characterized *Spirostrombidium* spp. (Ciliophora: Oligotrichida)

Dapeng XU¹, Weibo SONG^{1, 2}, Xiaofeng LIN² and Alan WARREN³

¹Laboratory of Protozoology, KLM, Ocean University of China, Qingdao, P. R. China; ²Laboratory of Protozoa, College of Life Science, South China Normal University, Guangzhou, P. R. China; ³Department of Zoology, Natural History Museum, Cromwell Road, London, UK

Summary. Two marine oligotrich ciliates, *Spirostrombidium agathae* n. sp. and *S. schizostomum* (Kahl, 1932) n. comb. (basonym: *Strombidium schizostomum* Kahl, 1932), were isolated from the littoral zone of coastal waters near Qingdao (Tsingtao), northern China. The morphology and infraciliature of each was studied from live and protargol-stained specimens. The new species *S. agathae* is distinguished from its congeners by the following combination of characters: small size, distribution of extrusomes, presence of two prolonged thigmotactic membranelles, number of anterior and ventral membranelles, and number of dikinetids in girdle and ventral kineties. The ciliary pattern of the poorly known *Strombidium schizostomum* Kahl, 1932, which has never been studied using modern methods since it was originally reported, indicates that it should be a member of the genus *Spirostrombidium*. Thus a new combination, *Spirostrombidium schizostomum* (Kahl, 1932) n. comb., is proposed. Based on the present studies and data published previously, a key to the identification of seven well-characterized *Spirostrombidium* spp. is provided.

Key words: infraciliature, morphology, *Spirostrombidium agathae* n. sp., *S. schizostomum* n. comb., Strombidiidae, taxonomy.

INTRODUCTION

The genus *Spirostrombidium* Jankowski, 1978 was established by Jankowski (1978) on the basis of the spiraled "cytoskeleton", which Agatha (2004) considered to be a misinterpretation of the distribution of extrusomes, as the main distinguishing feature. Petz

et al. (1995) improved the diagnosis mainly by including the arrangement of the ventral and girdle kineties, which are parallel to one another in the posterior portion of the cell. Agatha (2004), however, noted that this arrangement of somatic kineties can be achieved in one of two ways and that these can be distinguished by the ciliation of the dikinetids that comprise the kineties, i.e. either the anterior or posterior basal bodies can be ciliated (but not both). Based on this character, Agatha (2004) split the genus into two: *Spirostrombidium (sensu stricto)* in which the ventral kinety and posterior portion of the

Address for correspondences: Weibo Song, Laboratory of Protozoology, KLM, Ocean University of China, Qingdao, 266003, P. R. China; Fax +86-532-82032283; E-mail address: wsong@ouc.edu.cn

girdle kinety are inversely orientated, i.e. anterior basal bodies are ciliated in the ventral kinety vs. posterior basal bodies ciliated in the girdle kinety, and *Parallelostrombidium* in which the ventral kinety and posterior portion of the girdle kinety have the same orientation, i.e. the anterior basal bodies are ciliated in both cases. Consequently Agatha (2004) supplied a further improved diagnosis of *Spirostrombidium*: girdle kinety dextrally spiraled, posterior portion inversely orientated and parallel to longitudinal ventral kinety.

During surveys of the ciliate fauna in the costal regions near Qingdao, China, two oligotrich ciliates were collected. After comparison with similar taxa, one of them is believed to be a new form of *Spirostrombidium*, *S. agathae* n. sp., and the other is conspecific with *Strombidium schizostomum* Kahl, 1932. Based on its pattern of somatic ciliature, the latter is transferred to the genus *Spirostrombidium* as a new combination.

MATERIALS AND METHODS

Spirostrombidium agathae. Organisms were sampled from coastal waters near Qingdao (Tsingtao, 36°08'N; 120°43'E) on 1 March 2005. The upper 10 cm layer of sand was collected with seawater *in situ*. The samples were then transferred to Petri dishes and maintained in the laboratory for several days at room temperature (ca 22°C) as a raw culture for further studies.

Spirostrombidium schizostomum. Samples were collected on 5 August 2002 from shrimp-farming ponds near Qingdao, China. Glass slides fixed in a slide frame served as artificial substrates and were immersed in the water until a biofilm was formed (~10 days). Then the slides were retrieved out and transferred to Petri dishes with marine water from the sampling site.

The locomotion of the organisms was studied in Petri dishes under a dissecting microscope. The morphology was investigated using bright field and differential interference contrast microscopy. The infraciliature was revealed by protargol impregnation (Wilbert 1975). Drawings of live cells were based on free-hand sketches and photomicrographs, while those of silver-impregnated cells were made using a camera lucida.

Terminology is mainly according to Agatha *et al.* (2005).

RESULTS

Order Oligotrichida Bütschli, 1889

Family Strombidiidae Fauré-Fremiet, 1970

Genus *Spirostrombidium* Jankowski, 1978

Spirostrombidium agathae n. sp. (Figs 1, 2; Table 1)

Diagnosis: Small marine *Spirostrombidium*, approximately 35 × 25 µm *in vivo*, and 30 × 23 µm after

protargol staining; dorsoventrally flattened ca 2:3; body oblong (length: width ratio ~2:1) with apical protrusion at right anterior end; transparent hemitheca which covers posterior half of cell composed of two parts; buccal cavity extends posteriorly to about one-third of cell length; on average 14 anterior and 7 ventral membranelles; two posteriorly directed thigmotactic membranelles; one ellipsoidal macronucleus; extrusomes prominent, composed of three parts: (1) on ventral side, the extrusomes evenly arranged along the girdle kinety, (2) an extra extrusomes group arranged along shoulder area on dorsal side, and (3) the extrusomes arranged along the margin of hemitheca on dorsal side; girdle and ventral kineties consist of approximately 37 and 16 dikinetids respectively.

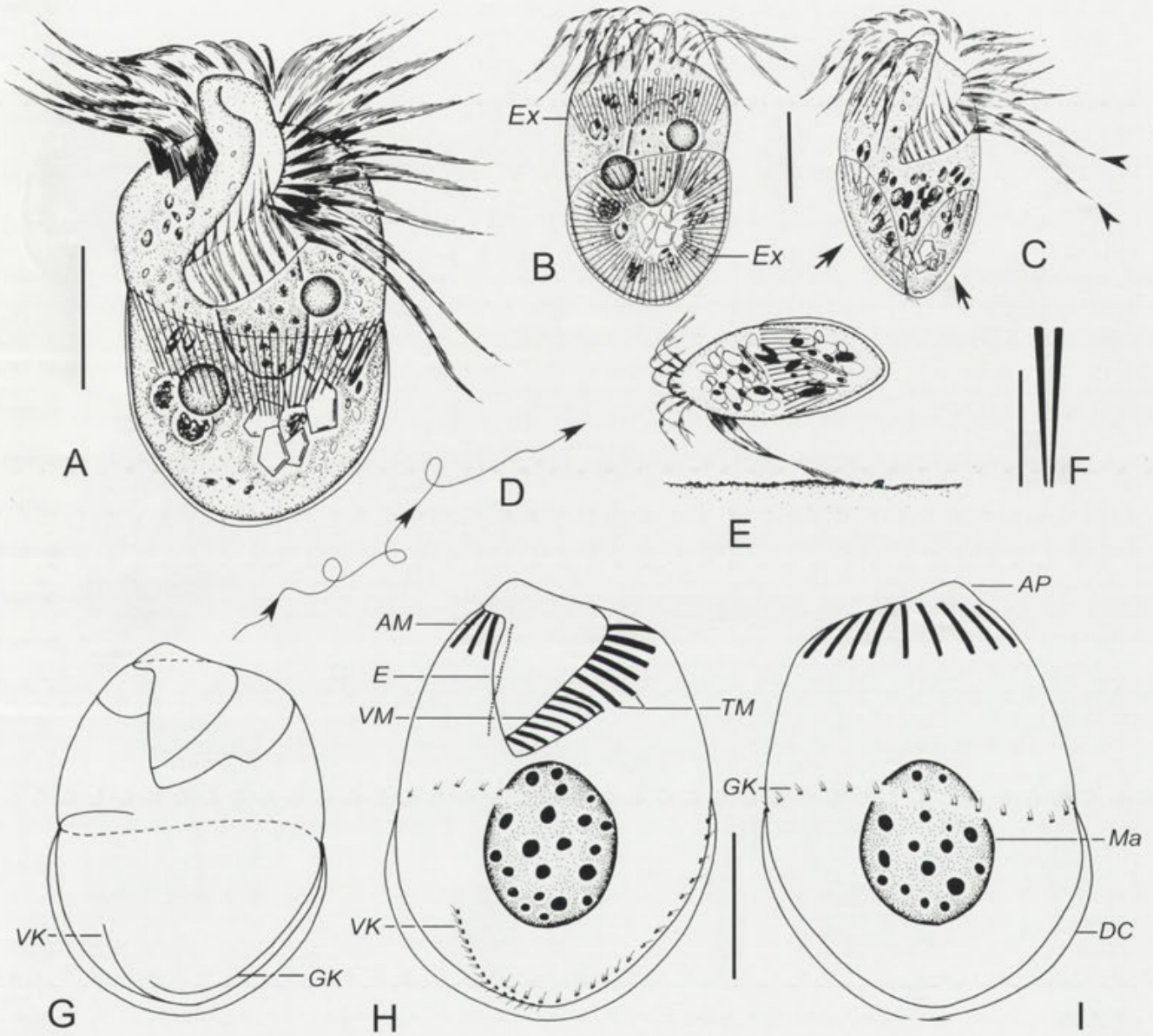
Type locality and ecological features: Marine sand in coastal area near Qingdao (Tsingtao, 36°08'N; 120°43'E), China; water temperature ca 6°C, salinity ca 32 ‰, and pH ca 7.9.

Deposition of slides: Two permanent slides of protargol-impregnated specimens are deposited as a holotype and a paratype in the Laboratory of Protozoology, OUC, China with registration numbers 2005:03:01:01 and 2005:03:01:02, respectively.

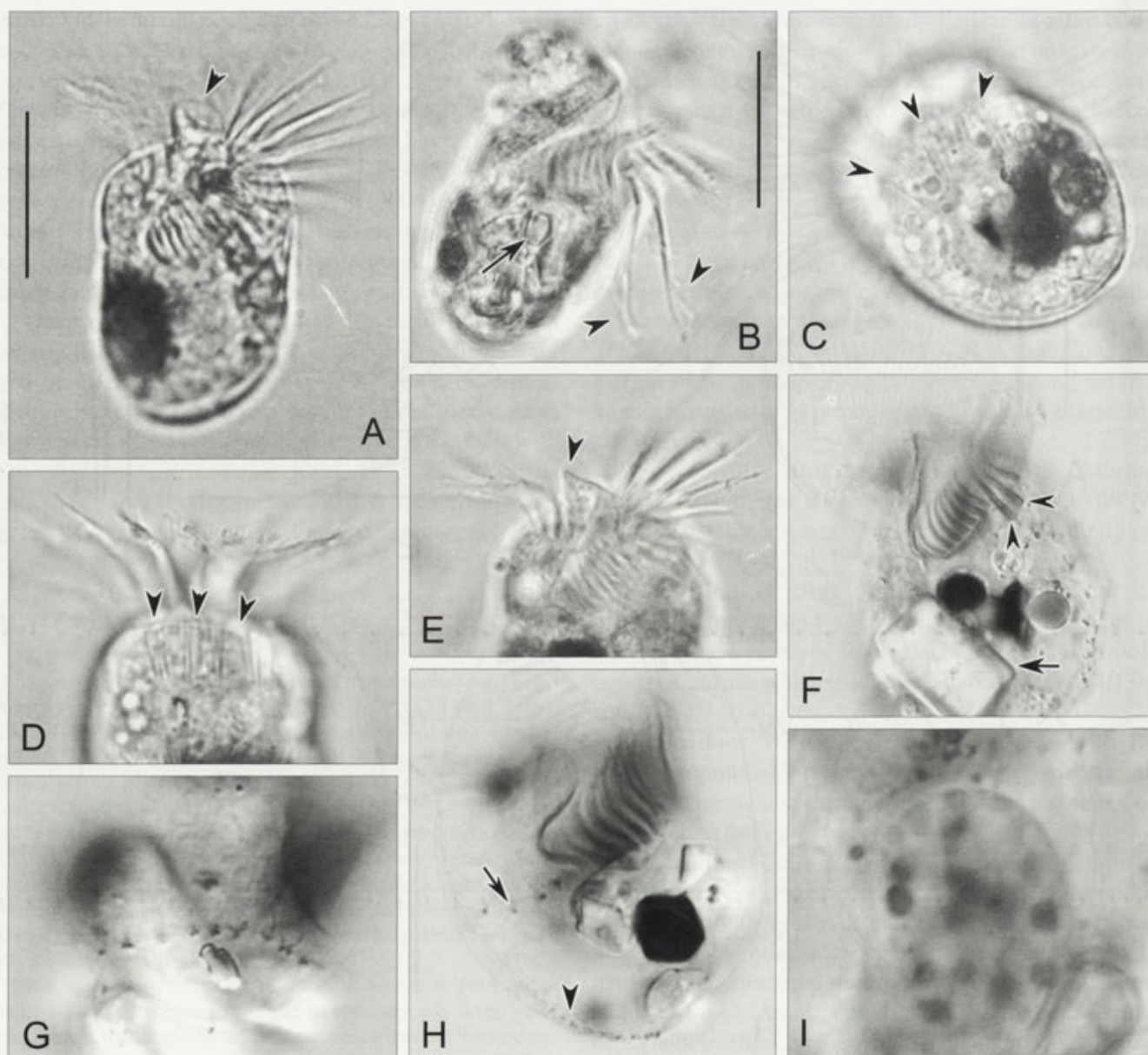
Dedication: We dedicate this new species to Dr Sabine Agatha, University of Salzburg, Austria, in acknowledgement of her contribution to the taxonomy of marine planktonic ciliates.

Description: Cells *in vivo* 30–35 × 25–30 µm, mostly 35 × 25 µm. Cell shape constant, oblong (length: width ratio ~2:1) with posterior end bluntly rounded; when viewed from ventral side, usually broadest at the “shoulder” region, equatorial area always slightly constricted (Figs 1A; 2A). Anterior end of cell transversely truncated with hyaline, ca 5 µm high, apical protrusion (also known as the peristomial collar) at right side of peristome that can be recognized *in vivo* but usually disappears or becomes undetectable after protargol impregnation (Figs 1A; 2A, arrowhead). Cell dorsoventrally flattened with thickness:width ratio approximately 2:3 (Fig. 1C).

Cell fragile, sensitive to presence of coverslip and easily bursts when water temperature increases or on contact with the water surface. Pellicle delicate with thin, transparent hemitheca that covers posterior half of cell (Figs 1A, B, C arrows). Hemitheca obliquely oriented and composed of two parts: one ventral, which is comparatively small, and one dorsal which is larger (Figs 1B, C). No cortical platelets recognizable either *in vivo* or in silvered specimens. Cytoplasm colourless, contains



Figs 1A-I. *Spirostrombidium agathae* n. sp. from life (A-F) and after protargol impregnation (G-I). **A** - ventral view of a representative specimen; **B, C** - dorsal (B) and right lateral (C) views, arrows indicate the transparent hemitheca, arrowheads mark the two prolonged membranelles; **D** - swimming trace; **E** - to show the creeping state, note the cell attached to the substrate by its two thigmotactic membranelles; **F** - extrusomes; **G** - pattern of somatic ciliature; **H, I** - ventral (H) and dorsal (I) views of ciliary pattern. AM - anterior membranelles; AP - apical protrusion; DC - distended cell surface; E - endoral membrane; Ex - extrusomes; GK - girdle kinety; Ma - macronucleus; TM - thigmotactic membranelles; VK - ventral kinety; VM - ventral membranelles. Scale bars: 10 μ m (A, H, I); 5 μ m (F).



Figs 2A-I. Photomicrographs of *Spirostrombidium agathae* n. sp. from life (A-E) and after protargol impregnation (F-I). **A** - resting specimen showing typical body shape, arrowhead marks the apical protrusion; **B** - left lateral view, arrow indicates refractive particles in cytoplasm and arrowheads mark two thigmotactic membranelles; **C** - posterior view to show extrusomes (arrowheads); **D** - dorsal view, arrowheads demonstrate extrusomes; **E** - arrowhead to show apical protrusion; **F** - ventral view, arrowheads indicate thigmotactic membranelles and arrow marks the large refractive particle in cytoplasm; **G** - to show dikinetics in girdle kinety; **H** - ventral view, arrow indicates girdle kinety while arrowhead marks ventral kinety; **I** - to demonstrate macronucleus. Scale bars: 20 μ m (A, B).

green inclusions 1-2 μ m across and quartz particles 3-10 μ m in size (Figs 2B, F, arrow). Extrusomes prominent, acicular, 6-8 μ m long, composed of three parts: (1) on ventral side, the extrusomes evenly arranged along the girdle kinety (Fig. 1A), (2) an extra extrusomes group

arranged along shoulder area on dorsal side (Figs 1B; 2D, arrowheads), and (3) the extrusomes arranged along the margin of hemitheca on dorsal side (Figs 1B; 2C, arrowheads). Neither contractile vacuole nor cytophyge detected. Single macronucleus broadly ellipsoidal in shape

Table 1. Morphometric characterization of *Spirostrombidium agathae* n. sp. (upper line) and *S. schizostomum* (Kahl, 1932) n. comb. (lower line). Data based on protargol-impregnated specimens. All measurements in μm . Abbreviations: M - median, Max - maximum, Mean - arithmetic mean, Min - minimum, n - number of specimens, SD - standard deviation.

Characters	Min	Max	Mean	M	SD	n
Cell length	26	34	29.4	28	2.6	15
Cell width	40	60	45.3	45	4.8	20
Apex to cytostome, distance*	20	28	23.1	24	2.2	15
Apex to the macronucleus	24	32	28.2	28	3.6	20
Apex to anterior end of girdle kinety, distance	14	16	14.8	15	0.9	15
Posterior cell end to posterior end of girdle kinety, distance	16	26	20.9	20	2.9	20
Anterior membranelles, number	11	13	11.9	12	1.0	15
Ventral membranelles, number	8	14	11.0	10	1.5	20
Thigmotactic membranelles, number	12	16	14.1	14	1.3	14
Macronucleus length	8	13	10.5	10	1.4	16
Macronucleus width	3	6	4.4	4.5	1.0	14
Girdle kinety, number of dikinetids	3	6	4.4	4.0	0.9	16
Ventral kinety, number of dikinetids	13	16	14.1	14	0.8	11
Thigmotactic membranelles, number	16	19	17.3	17	1.1	18
Macronucleus length	7	8	7.4	7	0.5	11
Macronucleus width	10	12	10.5	10	0.7	18
Girdle kinety, number of dikinetids	2	2	2	2	0.0	18
Ventral kinety, number of dikinetids	0	0	0	0	0	20
Thigmotactic membranelles, number	10	14	12.6	13	1.7	16
Macronucleus length	14	28	21.6	22	3.8	18
Macronucleus width	9	11	9.8	10	0.6	16
Girdle kinety, number of dikinetids	10	13	11.9	12	1.4	18
Ventral kinety, number of dikinetids	34	42	36.9	36	2.8	14
Thigmotactic membranelles, number	46	67	56.3	56	5.9	16
Macronucleus length	14	17	15.5	16	0.8	14
Macronucleus width	12	18	14.7	14	2.1	16
Girdle kinety, number of dikinetids	10	13	11.2	10.5	1.4	14
Ventral kinety, number of dikinetids	16	20	17.3	18	1.6	16

* Measured from anteriormost point of cell to the posterior end of buccal zone of membranelles (= ventral membranelles);

and centrally located, containing many small nucleoli each $\sim 3 \mu\text{m}$ across (Figs 1I, 2I). No micronucleus detected possibly due to its poor uptake of silver.

Locomotion by one of two mechanisms: moderately fast when crawling on debris with its ventral side facing down and two thigmotactic membranelles in contact with substrate (Fig. 1E), or swimming smoothly while rotating about longitudinal body axis (Fig. 1D).

Somatic ciliature composed exclusively of dikinetids (Figs 1H, I; 2G, H). Girdle kinety consists of approximately 37 (34-42) dikinetids, each having a cilium (*ca* $1.5 \mu\text{m}$ in length) associated with the left basal body and a relatively shorter fibre (?) with the right basal body. Girdle kinety extends from mid-ventral side transversely across ventral and dorsal sides, curves posteriad along left margin, across posterior pole and terminates subterminally on right ventrolateral area (Figs 1G, H, I; 2G, H, arrow). Thus, the girdle kinety spirals approxi-

mately once around cell. Ventral kinety, which is composed of approximately 16 (14-17) densely arranged dikinetids, each having a cilium associated with the anterior basal body (*ca* $1.5 \mu\text{m}$ in length) and a relatively shorter fibre (?) with the posterior one. Ventral kinety extends antieriad from posterior pole, parallel to distal end of girdle kinety and terminates in sub-equatorial region (Figs 1G, H; 2H, arrowhead). Girdle and ventral kineties have inverse orientation in terms of their basal body ciliation. No fragment-like "extra" kinety observed.

Oral apparatus occupies anterior end of cell (Figs 1H, I; 2F, H). Buccal cavity extending obliquely to the right and terminating about 1/3 of the way down the cell (Figs 1A, 2A). Adoral zone of membranelles divided into anterior and ventral portions separated by the two thigmotactic membranelles. Anterior portion with about 14 (13-16) membranelles, ventral portion with about

7 (7-8) membranelles, all of which are composed of three rows of basal bodies. Cilia of anterior membranelles *ca* 15 μm in length, stretching laterally or slightly anteriorly when swimming (Fig. 1A). Two thigmotactic membranelles distinct *in vivo* due to their longer cilia (about 20 μm long) and always directed posteriorly like two tails (Figs 1A, C; 2B, arrowheads), but less conspicuous in protargol impregnations where the bases (about 5 μm long) are only slightly longer than those of the anterior membranelles. Bases of ventral membranelles 2-3 μm long and bases of anterior membranelles about 4 μm long. Endoral membrane on inner wall of buccal lip on right side of oral cavity, rarely recognizable either in protargol-stained specimens or *in vivo*, probably composed of a single row of monokinetids. Pharyngeal fibres not observed.

Remarks: There are only two congeners with thigmotactic membranelles, i.e., *Spirostrombidium cinctum* and *Spirostrombidium urceolare* (Table 2). Unlike the genus *Strombidium*, the hemitheca of which is composed of polygonal cortical plates (Song *et al.* 2000, Agatha *et al.* 2005, Xu *et al.* 2005), no cortical platelets are recognizable in either of the *Spirostrombidium* spp. species studied here, either *in vivo* or in silvered specimens. Furthermore the hemitheca of both species is obliquely orientated and appears to be composed of two parts whereas the hemitheca of most other strombidiids is usually cup-like. However, it is unknown whether it is a species-specific feature or merely depends on the nutritional state (hungry/well fed) or the nutrition type (mixotrophy/heterotrophy) of the species. According, such a difference should not be overinterpreted.

Spirostrombidium agathae can be separated from *S. urceolare* (Stein, 1867) Lei, Xu *et al.* Song, 1999 by its smaller cell size (30-35 \times 25-30 vs. 70-80 \times 35-50 μm *in vivo*), different course of the girdle kinety (originates from mid-ventral cell vs. originates from dorsal side of cell), and in having fewer: thigmotactic membranelles (2 vs. 3); anterior membranelles (13-16 vs. 20-22); ventral membranelles (7-8 vs. 13-16); dikinetids in the girdle kinety (34-42 vs. 87-21) and ventral kinety (14-17 vs. 38-48) (Lei *et al.* 1999).

Spirostrombidium cinctum (Kahl, 1932) Petz, Song *et al.* Wilbert, 1995 has a similar cell shape to *S. agathae* and is also a marine species. It can be differentiated from *S. agathae* by presence of extra kinety (vs. absence in *S. agathae*) and having more: anterior membranelles (23-28 vs. 13-16); ventral membranelles (12-15 vs. 7-8); thigmotactic membranelles (3-4 vs. 2);

dikinetids in the girdle kinety (51-77 vs. 34-42) and ventral kinety (18-29 vs. 14-17) (Xu and Song 2006).

Spirostrombidium sauerbreyae (Kahl, 1932) Petz, Song *et al.* Wilbert, 1995 is the type species of the genus although its infraciliature remains unknown. It can be separated from *S. agathae* by its much larger cell size (100-55 vs. 30-35 μm) and its lack of thigmotactic membranelles (vs. 2 thigmotactic membranelles in *S. agathae*) (Sauerbrey 1928, Kahl 1932).

Considering their morphology of live specimens, three marine *Strombidium* spp. (the infraciliature of which remain unknown), which also have thigmotactic membranelles, should be compared with our new species, namely: *S. fourneleti* (Dragesco, 1960) Maeda *et al.* Carey, 1985, *S. faurei* Dragesco, 1960, and *S. clavellinae* von Buddenbrock, 1922.

Strombidium faurei was found in fine sand at Roscoff and also has two thigmotactic membranelles. It can be distinguished from *S. agathae*, however, by its much larger cell size (75 vs. 30-35 μm), position of thigmotactic membranelles (separating from the adoral membranelles vs. locating in the adoral membranelles) and absence of a hemitheca (vs. present in *S. agathae*) (Dragesco 1960).

Although it has two thigmotactic membranelles, *Strombidium fourneleti* can be separated from our new species by its cell shape (globular vs. elongated barrel-shaped), presence of polygonal cortical platelets (vs. absent), position of thigmotactic membranelles (separating from the adoral membranelles vs. locating in the adoral membranelles), and larger cell size (50-65 vs. 30-35 μm) (Dragesco 1960).

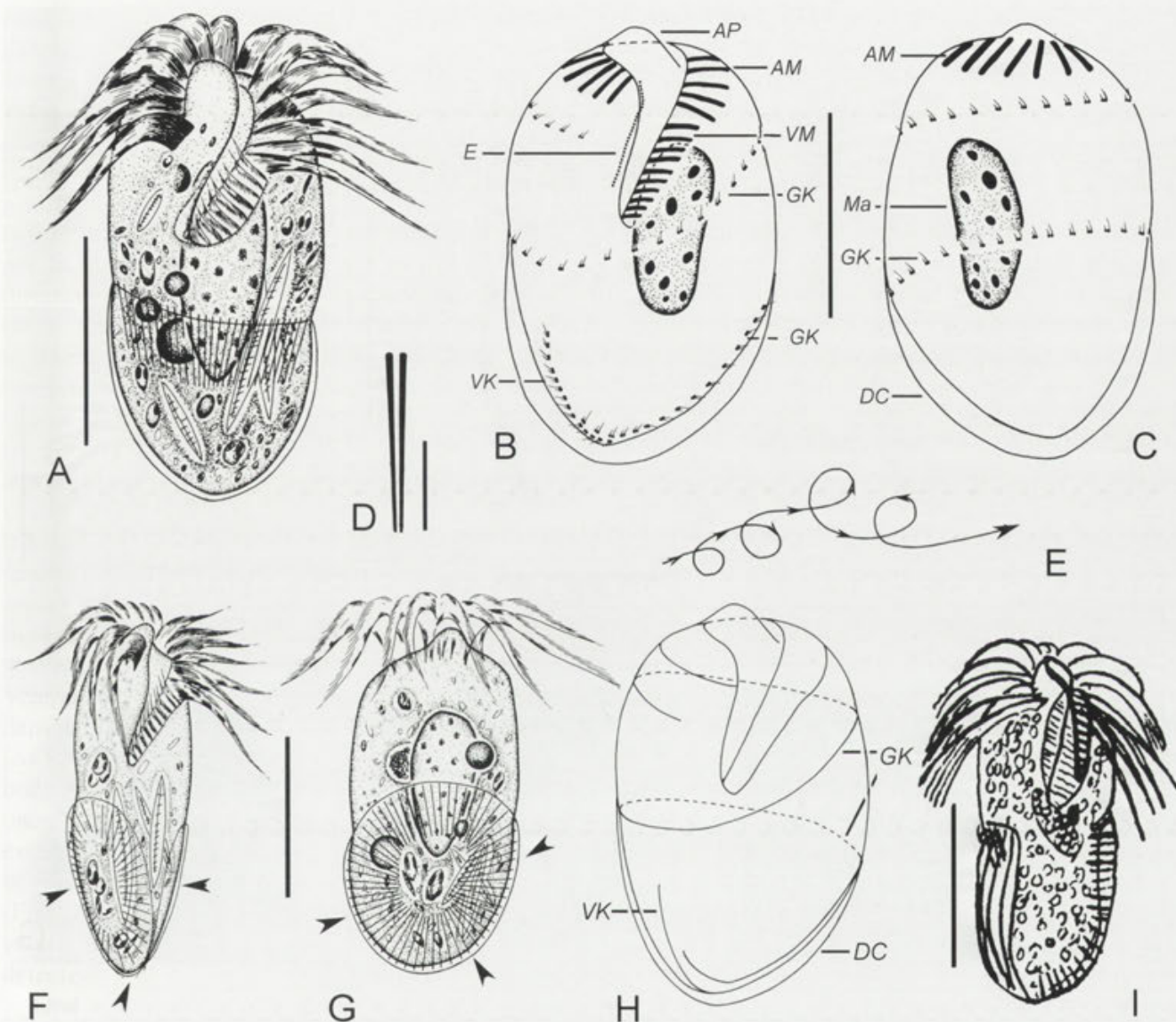
Strombidium clavellinae is similar to *Spirostrombidium agathae* in terms of its general appearance (Buddenbrock 1922). It differs from the latter, however, by its much larger cell size (70-80 vs. 30-35 μm) and having 4 thigmotactic membranelles (vs. only 2 in *S. agathae*).

***Spirostrombidium schizostomum* (Kahl, 1932) n. comb. (Figs 3, 4; Table1)**

Basionym: *Strombidium schizostomum* Kahl, 1932

The infraciliature of *Spirostrombidium schizostomum* has never been described, hence we here supply an improved diagnosis based on previous as well as present data.

Improved diagnosis: Medium-sized marine *Spirostrombidium*, approximately 50-70 \times 25-30 μm *in vivo*, and 45 \times 28 after protargol staining; dorsoventrally flattened *ca* 2:3; body asymmetric barrel-shaped with

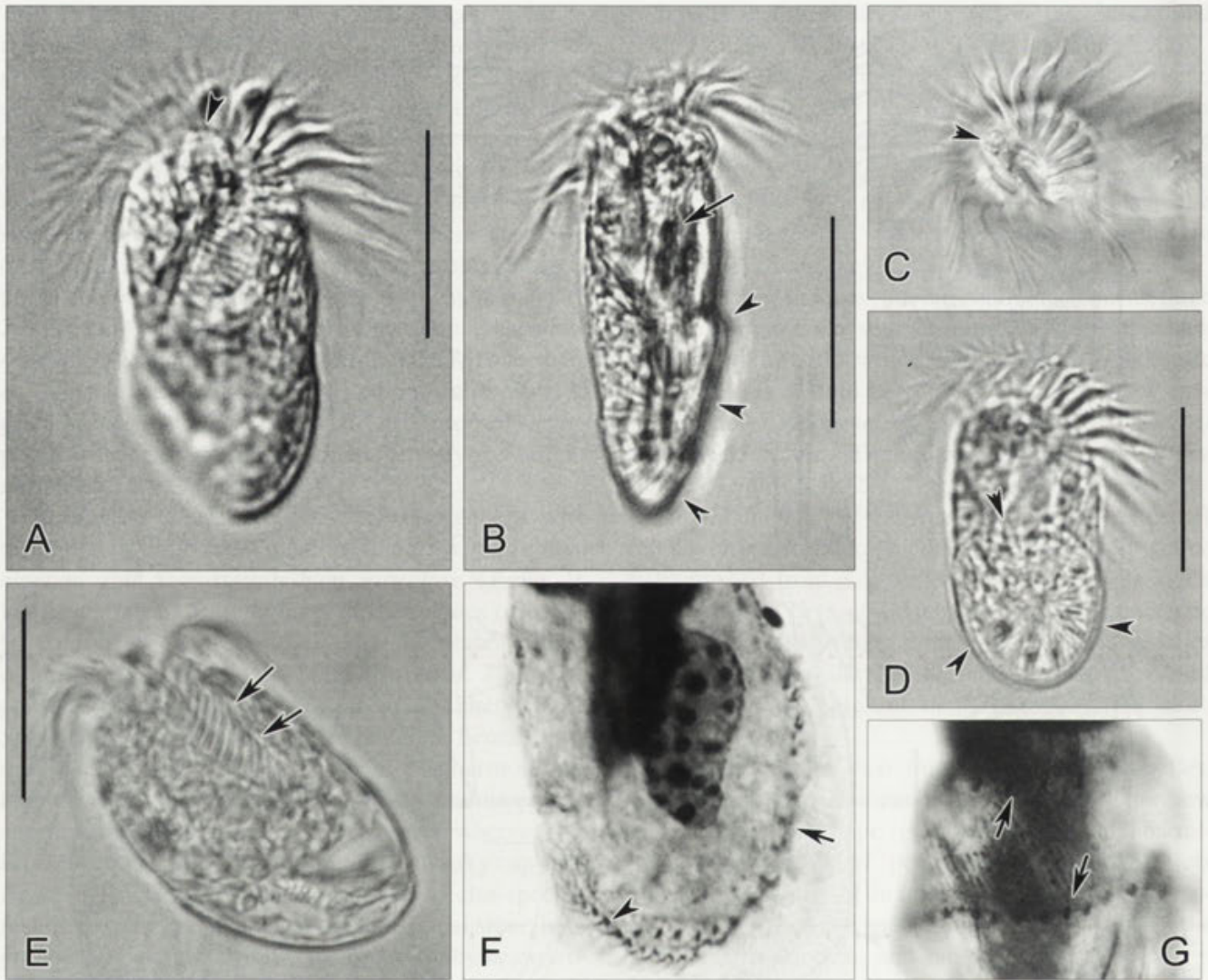


Figs 3A-I. *Spirostrombidium schizostomum* from life (A, D, E-G, I) and after protargol impregnation (B, C, H). **A** - ventral view of a typical specimen; **B, C** - ventral (B) and dorsal (C) views of ciliary pattern; **D** - extrusomes; **E** - pattern of locomotion; **F, G** - right lateral (F) and dorsal (G) views, arrowheads mark the hemitheca; **H** - pattern of somatic ciliature; **I** - ventral view of specimen (from Kahl, 1932). AM - anterior membranelles; AP - apical protrusion; DC - distended cell surface; E - endoral membrane; GK - girdle kinety; Ma - macronucleus; VK - ventral kinety; VM - ventral membranelles. Scale bars: 25 μm (A, C, G); 5 μm (D); 40 μm (I).

apical protrusion; on average 17 anterior and 11 ventral membranelles; one ellipsoidal macronucleus; extrusomes prominent, arranged along equatorial area on ventral of cell and along the margin of hemitheca on dorsal side; girdle and ventral kineties consist of about 56 and 14 dikinetids respectively.

Deposition of slide: One voucher slide (registration number 2002:08:05) with protargol-impregnated specimens is deposited in the Laboratory of Protozoology, Ocean University of China.

Description of the Qingdao population: Cells *in vivo* mostly about 55-65 \times 25-30 μm . Cell shape gener-



Figs 4A-G. Photomicrographs of *Spirostrombidium schizostomum* from life (A-E) and after protargol impregnation (F, G). **A** - ventral view of a typical specimen; **B** - right lateral view, to show the hemitheca (arrowheads) and diatoms in cytoplasm (arrow); **C** - top view, to show the apical protrusion (peristomial collar, arrowhead); **D** - dorsal view, arrowheads indicate hemitheca; **E** - ventral view of a slightly compressed individual, arrows mark ventral membranellae; **F** - ventral view, to show the macronucleus, girdle kinety (arrow) and ventral kinety (arrowhead); **G** - dorsal view, arrows mark the girdle kinety. Scale bars: 30 μ m (A, B, D).

ally constant, slightly asymmetric and elongated barrel-shaped with posterior end bluntly pointed; when viewed from ventral side equatorial area always slightly narrowed (Figs 3A, 4A). Cell dorsoventrally flattened, thickness: width ratio about 2:3 (Figs 3F, 4B). Collar region domed to form a conspicuous apical protrusion (also known as the peristomial collar), *ca* 5 μ m high, which may disappear or become undetectable after protargol impregnation (Figs 3A; 4A, C, arrowhead). No thigmotactic membranellae detected.

Pellicle relatively rigid with thin and transparent hemitheca covering the posterior 1/2 of cell. Hemitheca obliquely oriented and composed of two parts: a ventral part, which is comparatively small, and a dorsal part which is larger (Figs 3F, G). No cortical platelets recognizable either *in vivo* or in silvered specimens. Cell surface distinctly distended posterior to equatorial area in fixed cells. Cytoplasm colourless to grayish, sometimes yellow-green due to ingested algae including large diatoms (Figs 3A, 4B), which often render cell dark or

even opaque when observed at low magnifications. Extrusomes prominent, acicular, *ca* 8-10 μm long, evenly arranged along equatorial area of cell on ventral side and along margin of hemitheca on dorsal side, not in bundles (Figs 3A, F, G). Neither a contractile vacuole nor a cypocyte were detected. Macronucleus ovoid to ellipsoid, centrally located, containing numerous small globular nucleoli about 2 μm across (Fig. 4F). Micronucleus not found. Moving fast in wild spirals and changing direction frequently, never observed to stop swimming (Fig. 3E).

Somatic ciliature as shown in Figs 3B, C, H; 4F, G and composed exclusively of dikinetids. Girdle kinety consists of 56 (range 46-67) dikinetids, each having a cilium (*ca* 1.5 μm in length) associated with the left basal body and a relatively shorter fibre (?) with the right one. Girdle kinety starts in shoulder area on right ventral side, follows an almost complete circle across dorsal and ventral sides, then curves posteriad along left margin, across posterior pole and terminates subterminally in right ventrolateral area (Figs 3B, C, H; 4F, G). Thus, the girdle kinety spirals approximately twice around cell. Ventral kinety composed of approximately 14 (12-18) densely arranged dikinetids, each having a cilium (*ca* 1.5 μm in length) associated with the anterior basal body and a relatively shorter fibre (?) with the posterior one. Ventral kinety located to right of girdle kinety, extends anteriad from posterior pole parallel to distal end of girdle kinety and terminates at subequatorial level (Figs 3B, H; 4F, arrowhead). The girdle kinety and ventral kinety have inverse orientation. No "extra" kinety detected.

Oral apparatus consists of an endoral membrane on inner wall of buccal lip and a membranellar zone (Figs 3B, C). Buccal cavity deep and prominent, extending obliquely to the right and terminates about 1/3 of the way down the body (Figs 3A; 4A, E, arrows). Membranellar zone bipartite with anterior and ventral portions comprising about 17 (16-19) and 10 (10-12) membranelles respectively, all of which are composed of three rows of basal bodies (Figs 3A, B; 4A). Cilia of anterior membranelles about 20-25 μm long, stretching laterally or even slightly posteriorly as shown in Figs 3A, 4A. Endoral membrane (E) on inner wall of buccal lip on right side of oral cavity, probably composed of a single row of monokinetids but rarely recognizable either in protargol preparations or *in vivo*, probably due to being covered by perilemma (Fig. 3B). Pharyngeal fibres not found.

Remarks: *Spirostrombidium schizostomum* was originally reported by Kahl (1932) under the name *Strombidium schizostomum*. Its infraciliature, however, remained undescribed until the present study. Consequently we identify our organism mainly on its basic morphology *in vivo* and habitat, *viz.* the cell shape and size, the shape of the macronucleus, the number of anterior membranelles, and its marine biotope. Kahl (1932) mentioned the presence of 4 "pointed" membranelles in his organism. We also found several anterior membranelles that appear somewhat pointed in some, though not all, specimens during live observation. We do not, however, consider this to be a significant character for species circumscription. Furthermore, the buccal cavity of Kahl's population is narrow, almost entirely covered with the buccal lip, and extends almost longitudinally. We surmise these differences could be population-dependent and should not be exaggerated. Given the strong similarities between the Qingdao population and that described by Kahl (1932), we are confident that the two are conspecific.

Spirostrombidium pseudocinctum (Wang, 1934) Petz, Song *et* Wilbert, 1995 resembles *S. schizostomum* in having similar cell size after staining, a similar number of dikinetids in the girdle kinety and in lacking thigmotactic membranelles. The former can nevertheless be clearly separated from *S. schizostomum* by: (1) the girdle kinety spirals only once around the cell (*vs.* girdle kinety spirals almost twice in *S. schizostomum*); (2) the horizontal arrangement of the ventral membranelles (*vs.* ventral membranelles almost longitudinally positioned in *S. schizostomum*); (3) the greater number of anterior membranelles (26-29 *vs.* 16-19 in *S. schizostomum*) and ventral membranelles (14-17 *vs.* 10-12 in *S. schizostomum*); (4) the number of dikinetids in the ventral kinety (*ca* 6 *vs.* 12-18 in *S. schizostomum*) (Petz *et al.* 1995).

Spirostrombidium cinctum (Kahl, 1932) Petz, Song *et* Wilbert, 1995 differs from *S. schizostomum* in having extra kinety (*vs.* absence), more anterior membranelles (23-28 *vs.* 16-19), more dikinetids in the ventral kinety (18-29 *vs.* 12-18), and 3-4 thigmotactic membranelles (*vs.* absent) (Xu and Song 2006).

Based on both morphology of live specimens and infraciliature (Petz *et al.* 1995, Song and Packroff 1997, Lei *et al.* 1999, Song *et al.* 1999, Xu and Song 2006, present study), a key to the identification of the seven *Spirostrombidium* spp. that have been examined following silver impregnation is supplied:

- 1 Thigmotactic membranelles present.....2
 1' Thigmotactic membranelles absent.....4
 2 Extra kinety present.....3
 2' Extra kinety absent.....*S. cinctum*
 3 Girdle kinety originates from mid-ventral cell.....
*S. agathae*
 3' Girdle kinety originates from dorsal side of
 cell.....*S. urceolare*
 4 Girdle kinety spirals approximately twice around
 cell.....*S. schizostomum*
 4' Girdle kinety spirals approximately once around
 cell.....5
 5 Free living.....6
 5' Endocommusal in sea urchin.....*S. echini*
 6 >25 anterior membranelles.....*S. pseudocinctum*
 6' <25 anterior membranelles.....*S. platum*

Acknowledgements. This work was supported by "The National Science Foundation of China" (Project Nos. 30430090, 40376045) and Darwin Initiative Programme (Project No. 14-015) which is funded by the UK Department for Environment, Food and Rural Affairs.

REFERENCES

- Agatha S. (2004) Evolution of ciliary patterns in the Oligotrichida (Ciliophora, Spirotricha) and its taxonomic implications. *Zoology* **107**: 153-168
- Agatha S., Strüder-Kypke M. C., Beran A., Lynn D. H. (2005) *Pelagostrombidium neptuni* (Montagnes and Taylor, 1994) and *Strombidium biarmatum* nov. spec. (Ciliophora, Oligotrichida): phylogenetic position inferred from morphology, ontogenesis, and gene sequence data. *Europ. J. Protistol.* **41**: 65-83
- Buddenbrock W. v. (1922) Über eine neue *Strombidium*-Art aus Helgoland (*Str. clavellinae*). *Arch. Protistenk.* **45**: 129-132
- Dragesco J. (1960) Cilié mésopsammiques littoraux. Systématique, morphologie, écologie. *Trav. Stn biol. Roscoff* **12**: 1-356
- Jankowski A. W. (1978) Revision of a system of class Polyhymenophora (Spirotricha). *Tezisky Dokl. Zool. Inst. Akad. Nauk SSSR*, 39-40 (in Russian)
- Kahl A. (1932) Urtiere oder Protozoa I: Wimpertiere oder Ciliata (Infusoria) 3. Spirotricha. *Tierwelt Dtl.* **25**: 399-650
- Lei Y., Xu K., Song W. (1999) Free-living ciliates from marine farming ponds. In: *Progress in Protozoology* (Eds. W. Song, K. Xu, X. Shi, X. Hu, Y. Lei, J. Wei, Z. Chen, X. Shi, M. Wang). Qingdao Ocean Univ. Press, Qingdao, 269-295 (in Chinese)
- Petz W., Song W., Wilbert N. (1995) Taxonomy and ecology of the ciliate fauna (Protozoa, Ciliophora) in the endopagial and pelagial of the Weddell Sea, Antarctica. *Stapfia* **40**: 1-223
- Saurebrey E. (1928) Beobachtungen über einige neue oder wenig bekannte marine Ciliaten. *Arch. Protistenk.* **62**: 355-407
- Song W., Packroff G. (1997) Taxonomische Untersuchungen an marinen Ciliaten aus China mit Beschreibungen von zwei neuen Arten, *Strombidium globosaneum* nov. spec. und *Strombidium platum* nov. spec. (Protozoa, Ciliophora). *Arch. Protistenk.* **147**: 331-360
- Song W., Wilbert N., Warren A. (1999) Three new entocommusal ciliates from digestive tract of sea urchins of the Weddell Sea, Antarctica (Protozoa, Ciliophora). *Polar Biol.* **22**: 232-240
- Song W., Wang, M., Warren A. (2000) Redescriptions of three marine ciliates, *Strombidium elegans* Florentin, 1901, *Strombidium sulcatum* Claparède & Lachmann, 1859 and *Heterostrombidium paracalkinsi* Lei, Xu & Song, 1999 (Ciliophora, Oligotrichida). *Europ. J. Protistol.* **36**: 327-342
- Wilbert N. (1975) Eine verbesserte Technik der Protargolimprägation für Ciliaten. *Mikrokosmos* **64**: 171-179
- Xu D., Song W. (2006) Hapantotypification and morphological redescription of the marine planktonic ciliate, *Spirostrombidium cinctum* (Kahl, 1932) Petz, Song et Wilbert, 1995 (Ciliophora: Oligotrichida). *Acta Protozool.* **45**: 17-25
- Xu D., Song W., Hu X. (2005) Notes on two marine ciliates from the Yellow Sea, China: *Placus salinus* and *Strombidium apolatum* (Protozoa, Ciliophora). *J. Ocean Univ. China* **4**: 137-144

Received on 22nd June, 2006; revised version on 1st September, 2006; accepted on 13th October, 2006

Eimeria terraepokotorum n. sp. (Apicomplexa: Eimeriidae) from *Hoplobatrachus occipitalis* (Anura: Ranidae) from Kenya

Miloslav JIRKŮ¹ and David MODRÝ^{1,2}

¹Department of Parasitology, University of Veterinary & Pharmaceutical Sciences, Brno; ²Institute of Parasitology of Academy of Sciences of the Czech Republic, České Budějovice, Czech Republic

Summary. *Eimeria terraepokotorum* n. sp. (Apicomplexa: Eimeriidae) is described from *Hoplobatrachus occipitalis* from Kenya. Endogenous stages develop extranuclearly, in the cytoplasm of epithelial cells of the small intestine. Oocysts ovoidal to broadly elliptical, 20.2 (18.0-24.5) × 16.0 (13.5-18.5) μm; lacking micropyle and polar granule. Oocyst residuum present. Sporocysts dizoic, 9.8 (8.5-11.5) × 7.2 (6.0-8.0) μm, possessing a prominent Stieda body.

Key words: Africa, Anura, Apicomplexa, Coccidia, *Eimeria terraepokotorum* n. sp., *Hoplobatrachus occipitalis*, Kenya.

INTRODUCTION

During a long-term study of parasites of African vertebrates we examined fecal samples from numerous anurans from Kenya, and recently described 2 new *Eimeria* species (Jirků and Modrý 2005).

Here, we provide a summary of all anurans, examined during 3 field trips to Kenya in 2003 and 2004, together with the description of a new species of *Eimeria*. The type host of this new *Eimeria*, *Hoplobatrachus occipitalis* (Günther, 1858), the Afri-

can Tigrine Frog (Anura: Ranidae), is one of the most widely distributed anuran species of Afro-tropical zoogeographic realm. It inhabits a wide range of habitats from wells and seasonal water courses in arid areas to permanent water bodies, swamps and rivers in tropical savanna (Schleich *et al.* 1996, Rödel 2000, Channing and Howell 2006).

MATERIALS AND METHODS

Animals were collected during 3 field trips to Kenya in 2003 and 2004. Fecal samples of all animals (Table 1) were examined coprologically using a flotation method (see below). Most dissected animals were preserved in 70% alcohol and voucher specimens are deposited in the Herpetological Collection of the National Museums of Kenya, Nairobi.

Address for correspondence: Miloslav Jirků, Department of Parasitology, University of Veterinary & Pharmaceutical Sciences, Palackého 1-3, CZ-612 42 Brno, Czech Republic; E-mail: miloslav.jirku@seznam.cz

Five specimens (1 juvenile, 2 subadults, 2 adults) of *H. occipitalis* were collected at the beginning of the rainy season on the end of September 2004. The frogs were caught in temporary pools and seasonal water course near Nginyang village in west-central Kenya. Frogs were identified according to Channing and Howell (2006). Animals were placed for several hours into plastic boxes until they defecated, than euthanized by overdosing them with barbiturates (Thiopental® Spofa), dissected and processed for the following protocol.

Pieces of liver, kidney, muscle and equidistantly spaced portions of the gastrointestinal tract were fixed in 10% buffered formalin, processed routinely for histology, stained with haematoxylin and eosin, and examined for the presence of endogenous stages of coccidia.

Fecal samples were placed (and suspended) immediately in 2.5% aqueous solution of potassium dichromate ($K_2Cr_2O_7$) in vials containing enough air, stored at room temperature for 2 weeks, transported to the laboratory in the Czech Republic, and examined for the presence of coccidian oocysts. Oocysts were concentrated by flotation method, using modified Sheather's sugar solution (specific gravity 1.3), and examined using Nomarski interference contrast optics (NIC).

Measurements were made on 10-15 individuals of each endogenous developmental stage, and on 30 oocysts, using an Olympus AX 70 microscope equipped with a calibrated ocular micrometer and

are reported in micrometers (μm), usually as the means, followed by ranges in parentheses.

RESULTS

In total, 209 specimens of 16 anuran taxa were examined coprologically (Table 1). Of all the frogs examined, 5 (2.4%) possessed coccidian oocysts in their feces. Samples from 3 host species from 3 localities provided material suitable for further taxonomic work. As a result, 3 new species *Eimeria* were characterized morphologically, based both on endogenous and exogenous developmental stages, and described as a new species. Two of these species were described previously (Jirků and Modrý 2005). Additionally, unsporulated oocysts of undetermined coccidium, were found in feces of a single specimen of *Ptychadena* sp. 1 from Cheptongei village (Southern Cherangani Hills).

One juvenile and one subadult of *Hoplobatrachus occipitalis* from Nginyang shed oocysts of a previously

Table 1. Summary of anurans examined coprologically during the 3 field trips to Kenya in 2003 - 2004. Footnotes: a - samples collected in August 2003; b - samples collected in January 2004; c - samples collected in September 2004. Abbreviations: R - results of coprological examination (n examined / n infected with *Eimeria* sp.); UC - unsporulated coccidian oocysts observed in feces; RV - Rift Valley province; C - Coast province; E - East province; W - West province.

Taxon	Locality	R	coccidia found
<i>Afrana</i> sp. 1	Morijo ^a RV	4/0	-
<i>Afrana</i> sp. 2	E slope of Mt. Wargese ^c RV	1/0	-
<i>Afrana</i> sp. 2	Wamba ^a RV	3/0	-
<i>Bufo</i> cf. <i>garmani</i>	Wamba ^a RV	2/0	-
<i>Bufo</i> cf. <i>garmani</i>	South Horr ^c RV	4/0	-
<i>Bufo gutturalis</i>	Witu ^c C	2/0	-
<i>Bufo</i> sp. 1	Loyangalani ^c E	2/0	-
<i>Bufo</i> sp. 2	Nginyang ^c RV	4/0	-
<i>Chiromantis petersii kelleri</i>	Kula Mawe ^b E, Mt. Forole ^c E	1/1 ^b , 1/0 ^c	<i>Eimeria fragilis</i>
<i>Hoplobatrachus occipitalis</i>	Nginyang ^c RV	5/2	<i>Eimeria terraepokotorum</i>
<i>Hyperolius viridiflavus</i>	Kakamega ^a W, Wamba ^a RV	40/0 ^a , 6/1 ^c	<i>Eimeria wambaensis</i>
<i>Hyperolius kivuensis</i>	Kakamega ^a W	20/0	-
<i>Kassina senegalensis</i>	South Horr ^c RV	20/0	-
<i>Tomopterna</i> sp.	Nginyang ^c RV	15/0	-
<i>Tomopterna</i> sp.	South Horr ^c RV	10/0	-
<i>Ptychadena</i> sp. 1	Cheptongei ^b RV	2/1	UC
<i>Ptychadena</i> sp. 2	E slope of Mt. Wargese ^c RV	4/0	-
<i>Ptychadena</i> sp. 3	Kakamega ^b W	3/0	-
<i>Ptychadena</i> sp. 2	Wamba ^a RV	2/0	-
<i>Xenopus</i> sp.	Cheptongei ^b RV	15/0	-
<i>Xenopus</i> sp.	Kakamega ^b W	15/0	-
<i>Xenopus</i> sp.	Loita Hills ^a and Nguruman Esc. ^c RV	25/0	-
<i>Xenopus</i> sp.	Marsabit ^a E	10/0	-
Total of 16 taxa	14 localities	209/5 (2.4%)	3 spp. in total

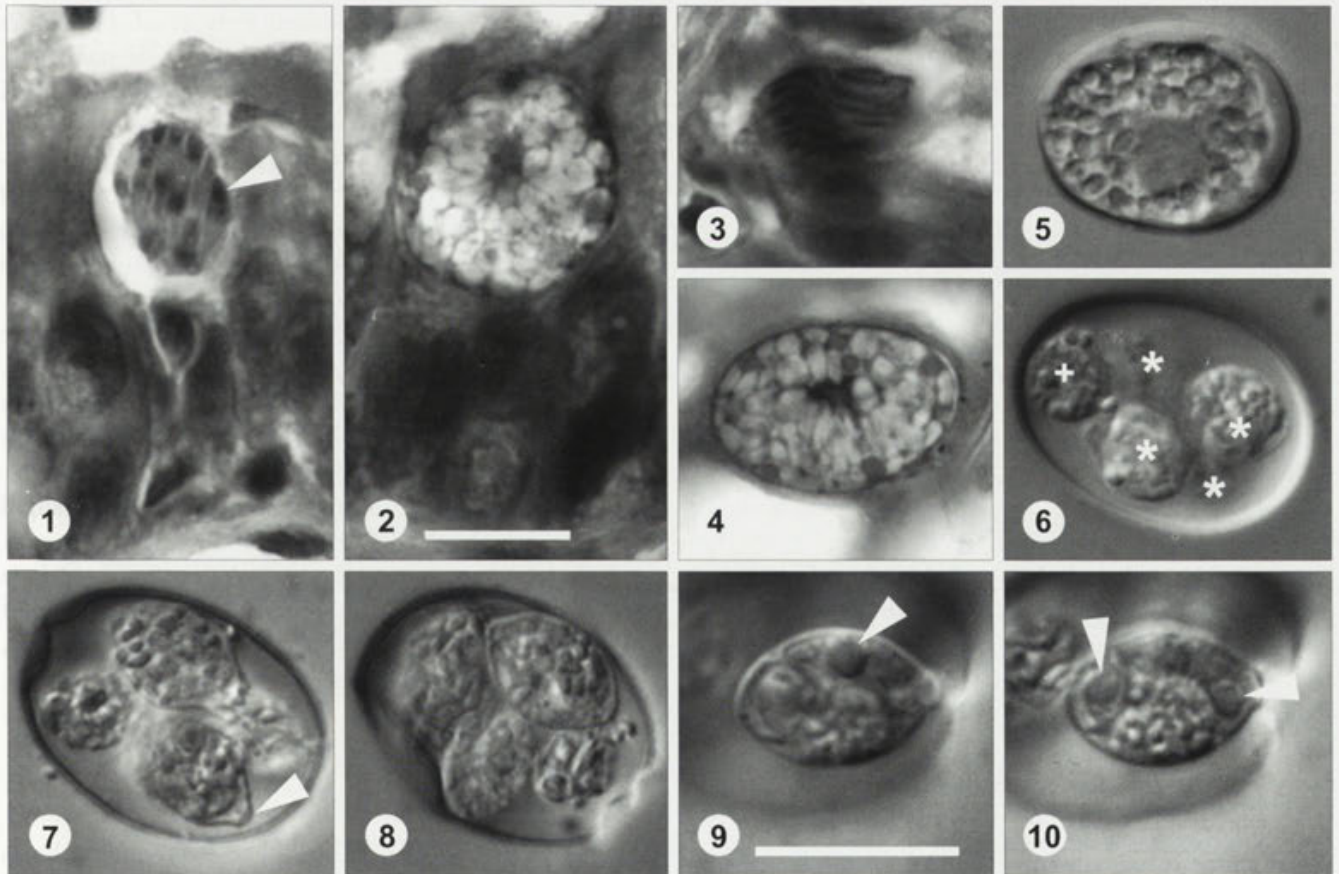
undescribed coccidium, evidently belonging to the genus *Eimeria* s. str. Neither coccidian oocysts nor endogenous stages were detected in another juvenile and two adult *H. occipitalis* from the same locality.

***Eimeria terraepokotorum* n. sp.**

Endogenous stages: All endogenous stages, putatively identified as those belonging to this species develop in the cytoplasm of epithelial cells of the small intestine. Mature meronts (Fig. 1) are spherical to broadly elliptical, $8-12 \times 5-8$, containing approximately 20, somewhat spirally arranged merozoites. In haematoxylin & eosin stained sections, one end of each merozoite (probably apical complex) is usually more

intensely stained (Fig. 1, arrowhead). Mature macrogamonts (Fig. 2), $16-19 \times 13-17$, are spherical or elliptical, containing a few distinct wall forming bodies (1.5-2 in diameter). Mature microgamonts elliptical, $10-12 \times 6-9$, containing numerous relatively thick-bodied microgametes (Fig. 3). In histological sections, unsporulated oocysts (Fig. 4), measuring $18-20 \times 11.5-15$, were found in the posterior part of the small intestine, either still attached to the intestinal mucosa, or freely in the intestine lumen. In most cases, oocysts were easily distinguishable from macrogamonts by the presence of thin, but clearly visible oocyst wall.

Exogenous stages, oocysts: Unsporulated oocysts isolated from preserved feces (Fig. 5) contain sporont,



Figs 1-4. Micrographs of endogenous stages of *Eimeria terraepokotorum* in histological sections stained with haematoxylin and eosin. **1** - mature meront possessing numerous merozoites with one end intensely stained (arrowhead); **2** - mature macrogamont with a few wall forming bodies on its periphery; **3** - mature microgamont showing relatively rough bodied microgametes; **4** - unsporulated oocyst within intestinal lumen. Note that fine oocyst wall is already clearly visible on its surface.

Figs 5-10. Nomarski interference micrographs of oocysts isolated from feces. **5** - unsporulated oocyst showing vacuolated area within sporont; **6** - oocyst in process of sporulation, showing 4 sporocysts (stars) and oocyst residuum (cross). Note that granules of the oocyst residuum resemble those forming sporocyst residua. **7** - fully sporulated oocyst with a sporocyst showing typical shape of Stieda body (arrowhead); **8** - fully sporulated oocyst; **9** - sporocyst possessing fully developed sporozoite with distinct nucleus (arrowhead); **10** - same sporocyst as on Fig. 9., focused to show 2 refractile bodies (one on each end) of the sporozoite (arrowheads). Scale bars: 5 μ m. Magnification of Figs 1-8, refer to scale bar of Fig. 2, and Figs 9, 10 to scale bar of Fig. 9.

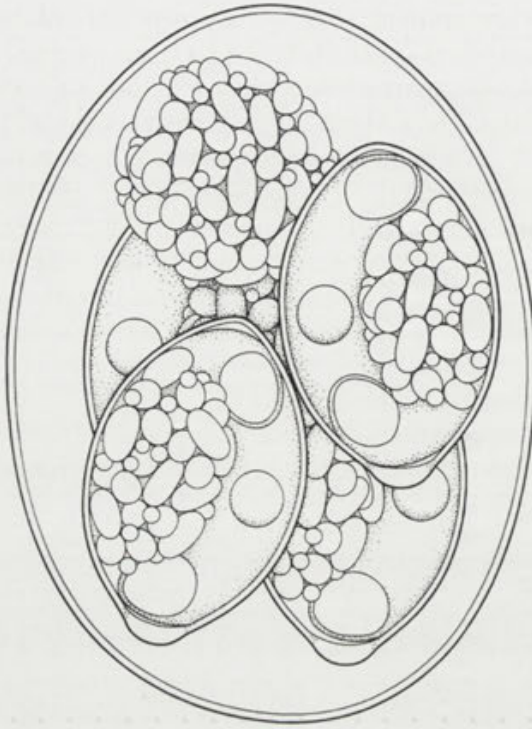


Fig. 11. Composite line drawing of sporulated oocyst of *Eimeria terraepokotorum* n. sp. Scale bar: 5 µm.

composed of rough, elongate granules (2×1.5). Spherical halo (nucleus), up to 8 in diameter, is visible within sporont. Fully sporulated oocysts (Figs 7-11), relatively variable both in size and shape (compare Figs 5-8), are ovoidal to broadly elliptical, 20.2 ($18.0-24.5$) \times 16.0 ($13.5-18.5$), shape index (length: width ratio, SI) 1.3 ($1.1-1.4$). Oocyst residuum (7-11 in diameter) present, composed of spherical to subspherical mass of granules resembling those forming sporocyst residua (see below). Micropyle and polar granule absent. Oocyst wall colorless, smooth, approximately 0.6 thick, unilayered in light microscopy. Sporocysts dizoic, 9.8 ($8.5-11.5$) \times 7.2 ($6.0-8.0$), possessing prominent Stieda body ($1.5-2 \times 0.5-0.7$) (Fig. 7). Sporocyst pole, opposite to Stieda body is usually slightly pointed. Finely granulated sporozoites without visible striation, contain probably 2 (one on each end) refractile bodies ($2-3 \times 1.5-2$), and centrally located nucleus (2 in diameter). Sporocyst residuum composed by the mass of granules completely filling space between sporozoites (Figs 7, 8) or forming subspherical mass (Figs 9, 10). Granules of the sporocyst residuum are of two types: elongated ones ($2-2.5 \times 1-1.5$) accompanied by distinctly finer spherical granules ($0.5-1$ in diameter).

Generally, the size and shape of granules, forming both sporocyst and oocyst residua is quite variable. Such variability may be associated with the process of sporulation, since granules of sporont are considerably coarser, than those forming residua of mature oocysts and sporocysts (compare Fig. 5 with Figs 6-10).

Type host: *Hoplobatrachus occipitalis* (Günther, 1858), (Anura: Ranidae), African Tigrine Frog.

Type material: Photosyntypes of oocysts in various stages of sporulation and hematoxylin and eosin stained paraffin sections with endogenous stages, together with piece of type-hosts' liver (for eventual DNA isolation) are deposited in the collection of the Department of Parasitology, University of Veterinary and Pharmaceutical Sciences Brno, Czech Republic under the collection number R 113/05. Voucher specimen of *Hoplobatrachus occipitalis* [a symbiotype sensu Frey *et al.* (1992)] is deposited in herpetological collection of National Museums of Kenya, Nairobi, under collection number: NMK A/4246.

Type locality: Kenya, Nginyang (Rift Valley province, $01^{\circ}09'33''$ N, $37^{\circ}15'47''$ E). All examined *H. occipitalis* were collected in temporary pools in riverside sand sediments along the river flowing through the Nginyang village.

Prevalence: 2/5 (40 %) frogs from Nginyang were infected.

Sporulation and sporulation time: Exogenous, only unsporulated oocysts were observed in intestine in histological sections.

Site of infection: Epithelial cells of the entire small intestine, extranuclear.

Etymology: Specific name *terraepokotorum* is a genitive case of Latin term Terra Pokotorum (= Land of Pokots); it reflects the location of the type locality, situated in the hearth of territory of Pokot tribe.

DISCUSSION

Of all 18 *Eimeria* spp. described from anuran hosts to date, only 3 species are similar enough to be compared to *E. terraepokotorum* n. sp. *Eimeria cyanophlyctis* Chakravarty et Kar, 1944 from India differs in having distinctly narrower ($11.0 \times 4.4-6.6$. vs. $8.5-11.5 \times 7.2$ $6.0-8.0$ in *E. terraepokotorum* n. sp.), spindle-shaped sporocysts lacking sporocyst residuum (Chakravarty and Kar 1952). *Eimeria leptodactyli* Carini, 1931 from S America, most closely resembling *E. terraepokotorum* n. sp. by oocysts and sporocyst size, differs in general

appearance of oocyst residuum (granules arranged in rosettes) and presence of only scanty sporocyst residuum (Carini 1931). *Eimeria streckeri* Upton et McAllister, 1988 from North America differs in oocyst shape (spherical), presence of distinct vacuole within oocyst residuum (absent in *E. terraepokotorum* n. sp.), and presence of indistinct Stieda body (distinct in *E. terraepokotorum* n. sp.) (Upton and McAllister 1988). Additionally, *E. terraepokotorum* n. sp. differs clearly from both congeners (*Eimeria fragilis* and *Eimeria wambaensis*) recently described from African amphibians (Jirků and Modrý 2005) by oocyst and sporocyst size and shape, by the presence of oocyst residuum, and by the presence of distinct Stieda body. Moreover, the localization of endogenous stages of *E. terraepokotorum* n. sp. is different, as both *E. fragilis* and *E. wambaensis* are strictly intranuclear.

Although Table 1 is self explanatory two aspects of coccidian infections in anurans obtained during our study are worth to note. Both infected *H. occipitalis* were immature. This result is in contradiction to suggestions of other authors (Upton and McAllister 1988, Bolek et al. 2003) that coccidian infections in frogs may be restricted mainly to breeding animals. This might be true in case of terrestrial species, but our data show that, at least in semiaquatic species, infections can be common also in immature, non-breeding individuals. On the other hand, we examined 65 individuals of African claved frogs (*Xenopus* spp.) of various age from 4 localities, without any positive record of coccidian infection. All *Xenopus* spp. are strictly aquatic anurans with extraordinarily diverse parasitofauna (Tinsley 1996). Despite the fact that high numbers of *Xenopus* spp. were imported to Europe and USA as laboratory animals, no coccidia have ever been reported from these hosts. The apparent absence of coccidia in *Xenopus* spp. is surprising, since aquatic life-style in dense populations might normally favor infection by coccidian parasites with direct life-cycle.

Acknowledgements. The research on diversity of parasites of East African vertebrates was facilitated by Biota East Africa; we are deeply indebted to Wolfgang Böhme, Jörn Koehler and Stefan Lötters for generous help. We thank Richard Bagine (Kenyan Wildlife Service), Patrick Malonza and Damaris Rotich (both from National Museums of Kenya) for help with organization of the research. Asad Anwar friendly offered the accommodation in Nairobi and organized logistics of expeditions to N Kenya. We thank members of the expedition team, namely Jana Kopečná, Jan Votýpka, Martin Kamler, Eva Hasiková, David Čálek and Petr Nečas for help with the field work. We are indebted to Olympus C&S for generous technical support. This study was supported by grants Nos. 206/03/1544 and 524/03/H133 from the Grant Agency of the Czech Republic.

REFERENCES

- Bolek M. G., Janovy J., Irizarry-Rovira A. R. (2003) Observations on the life history and descriptions of coccidia (apicomplexa) from the western chorus frog, *Pseudacris triseriata triseriata*, from eastern Nebraska. *J. Parasitol.* **89**: 522-528
- Carini A. (1931) *Eimeria leptodactyli* n. sp., rencontrée dans l'intestin du *Leptodactylus ocellatus*. *C. R. Seances Soc. Biol. Ses Fil.* **106**: 1019
- Chakravarty M., Kar A. B. (1952) The life history and affinities of two salientian Coccidia, *Isoispora stomaticae* and *Eimeria cyanophlyctis*, with a note on *Isoispora wenyoni*. *Proc. Zool. Soc. Bengal.* **5**: 11-18
- Channing A., Howell K. M. (2006) Amphibians of East Africa. Cornell University and Edition Chimaira, Ithaca, London and Frankfurt, NY, UK and Germany
- Frey J. K., Yates T. L., Duszynski D. W., Gannon W. L., Gardner S. L. (1992) Designation and curatorial management of type host specimens (symbiotypes) for new parasite species. *J. Parasitol.* **78**: 930-932
- Jirků M., Modrý D. (2005) *Eimeria fragilis* and *E. wambaensis*, two new species of *Eimeria* Schneider (Apicomplexa: Eimeriidae) from African anurans. *Acta Protozool.* **44**: 167-173
- Rödel M. (2000) Herpetofauna of West Africa, Vol. I Amphibians of the West African Savanna. Edition Chimaira, Frankfurt am Main, Germany
- Schleich H. H., Kästle W., Kabisch K. (1996) Amphibians and Reptiles of North Africa. Koeltz Scientific Publishers, Koenigstein, Germany
- Tinsley R. C. (1996) Parasites of *Xenopus*. In: The Biology of *Xenopus*, (Eds. R. C. Tinsley, H. R. Kobel). The Zoological Society of London, 233-261
- Upton S. J., McAllister C. T. (1988) The coccidia (Apicomplexa: Eimeriidae) of Anura, with descriptions of four new species. *Can. J. Zool.* **66**: 1822-1830

Received on 14th February, 2006; revised version on 11th June, 2006; accepted on 16th July, 2006

Cofilin-like Protein Influences the Motility of *Amoeba proteus*

Wanda KŁOPOCKA¹, Katarzyna WIERZBICKA¹, Paweł POMORSKI¹, Patryk KRZEMIŃSKI¹ and Anna WASIK²

¹Department of Molecular and Cellular Neurobiology, ²Department of Cell Biology, Nencki Institute of Experimental Biology, Warszawa, Poland

Summary. The organization of *Amoeba proteus* cortical layer is highly associated with cofilin-like protein activity. This protein is involved in actin dynamics in the middle-anterior region of migrating cells, but does not take place in processes of the cortical network disorganization that occurred in the uroid. Cofilin homologue and actin co-localized at the leading edge, in the cortical and perinuclear cytoskeleton, in the area of cellular adhesion and in streaming endoplasm. Actin dynamics induced by cofilin-like protein are important for normal morphology and motility of *A. proteus*.

Key words: actin dynamic, *Amoeba proteus*, cofilin-like protein.

INTRODUCTION

Actin filaments in nonmuscle cells are highly dynamic and play an essential role in numerous cellular processes, including cell migration, endocytosis and cytokinesis. Organization of the contractile network in tissue cells as well as in amoebae is highly associated with activity of actin-binding proteins, including capping, severing, depolymerizing ones, as well as the motor proteins - myosins. Their function depends on the

activating signals, and it is regulated by different signal pathways.

The ADF/cofilins (ACs) are a family of small (15-20 kDa) proteins, expressed in all so far examined eukaryotic cells, that severs and depolymerizes ADP-filaments. ADF/cofilin was first discovered and purified in 1980 from embryonic chick brain extracts by Bamburg *et al.* (1980). Since then, the family was grown to include a number of related proteins, e. g. *Acanthamoeba* actophorin (Quirk *et al.* 1993) and *Dictyostelium discoideum* coactosin (de Hostas *et al.* 1993).

Phosphorylation is a principle regulator of ACs function. The activity of ACs is inhibited by phosphorylation at Ser-3 near the N terminus (Agnew *et al.* 1995) or Ser-2 in *Acanthamoeba castellanii* actophorin with the exception of related proteins from yeast and

Address for correspondence: Anna Wasik, Department of Cell Biology, Nencki Institute of Experimental Biology, Polish Academy of Sciences, Pasteur St. 3, 02-093 Warszawa, Poland; E-mail: a.wasik@nencki.gov.pl

Dictyostelium discoideum (Blanchoin *et al.* 2000). Phosphorylation blocks ACs interaction with ADP-actin filaments and monomers. LIM kinase (Yang *et al.* 1998, Arber *et al.* 1998) controls the activity of most ACs by phosphorylation. A specific phosphatase called slingshot activates ACs by removing the inhibitory phosphate (Niwa *et al.* 2002).

The main activity of ACs has been found from *in vitro* studies to be to increase actin filament turnover (Carlier *et al.* 1997, Maciver 1998, McGough *et al.* 2001). ACs accomplish this by depolymerizing filaments at their pointed ends, thereby providing a pool of actin monomers for a filament assembly, and severing actin filaments and consequently increase the number of filaments ends for polymerization (Bamburg *et al.* 1999, Carlier *et al.* 1999, Maciver and Hussey 2002). Together with profilin (and thymosin- β 4 in higher eukaryotes), ADF/cofilin (AC) and capping of barbed ends allow cells to maintain a high concentration of unpolymerized actin far from equilibrium (Pollard and Borisy 2003).

In the highly motile *A. proteus* the cortical cytoskeleton undergoes dynamic reorganization. During migration in the uroidal region contraction accompanied by solation leads to disorganization of the cortical system. Cytoskeletal proteins, including actin oligomers and monomers, are released into the endoplasmic streaming and flow to the top of advancing pseudopodia where, just beneath the plasma membrane, actin polymerization and cross-linking of microfilaments occur. Differences in the cortical system organization and aggregation are tightly related to the mechanism of the actin cytoskeleton assembly and contraction. RhoA- and Rac1-like proteins are involved in the regulation of these processes (Kłopocka and Rędowicz 2003, 2004; Kłopocka *et al.* 2005). Recently, we revealed that organization of the cortical layer in *A. proteus* is associated with the Arp2/3 complex activity (Pomorski *et al.* in press). In migrating amoeba actin polymerizes in Arp2/3 complex-dependent manner under the plasma membrane around the cell except distal parts: uroidal pole, retracting pseudopodia and tips of advancing ones. We also showed that the maximal content of filamentous actin in migrating amoeba is in the middle-posterior region, what was interpreted as an effect of the strong isometric contraction and aggregation of actin filaments in this region.

Here, we are focused on the localization and the effect of cofilin-like protein on *A. proteus*, including the role of endogenous cofilin in the morphology and motility of this amoeba *in vivo*.

MATERIALS AND METHODS

Cell culture. *Amoeba proteus* (strain Princeton) was cultured at room temperature in the standard Pringsheim medium. Amoebae were fed on *Tetrahymena pyriformis* twice a week, and used for experiments on the third day after feeding.

Immunoblotting. *A. proteus* cells were homogenised in a solution containing 10% sucrose, 20 mM imidazole (pH 7.0), 1 mM dithiothreitol, 50 mM NaCl, 10 mM sodium pyrophosphate, and 1 "Complete" tablet (Roche) per 25 ml of the solution.

Jurkat cells were centrifuged at 2500 g for 5 min, washed in PBS, and resuspended in lysis buffer containing: 1% Nonidet P-40, 120 mM NaCl, 50 mM Tris/HCl, pH 7.5, and freshly added proteinase inhibitors.

Immunoblotting procedure with the antisera against: α -actin (Sigma) and cofilin (Sigma) was carried out according to Kłopocka and Rędowicz (2004).

Immunolocalization studies. The distribution of cofilin-like protein was examined by indirect immunocytochemistry in migrating amoebae. Migrating cells were fixed and permeabilized according to Kłopocka and Rędowicz (2004). They were incubated overnight at 4°C with polyclonal antibody against human cofilin at a dilution of 1:20. This was followed by incubation with Alexa Fluor 488-conjugated anti-mouse secondary antibody (Invitrogen) at a dilution of 1:200 for 60 min at 37°C and then washing in PBS solution. For simultaneous assessment of F-actin distribution, cells were additionally stained by Alexa Fluor 546-phalloidin (Invitrogen). The stain was visualized with the confocal laser-scanning microscope (CLSM) Zeiss LSM 510. For co-localization measurements double laser and double excitation was used. No cross excitation or fluorescence bleed-through were observed (data not shown).

Locomotion studies. The effect of the inhibition of endogenous cofilin on *A. proteus* was examined by observation of living amoebae after microinjecting them with polyclonal antibody against human cofilin (final concentration 25 μ g/ml) diluted in Pringsheim medium. Controlled cells were microinjected with Pringsheim medium and the solution in which antibody was supplied (50% glycerol, 20 mM sodium phosphate pH 7.5, 150 mM NaCl, 1.5 mM NaN_3 , 1 mg/ml BSA (data not shown).

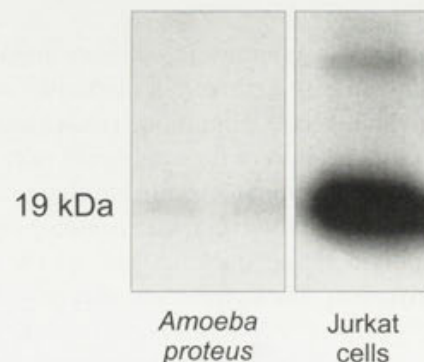


Fig. 1. Detection of cofilin-like protein. After separation of sodium dodecyl sulfate-polyacrylamide gel electrophoresis 25 μ g of *Amoeba proteus* homogenate proteins as well as 25 μ g of Jurkat cells lysate were probed with antibody against human cofilin, followed by detection with HRP-conjugated secondary antibody.

Micronjections were carried out according to Kłopocka and Rędowicz (2004).

RESULTS

Detection and localization of the cofilin-like protein

The cofilin-like protein from *Amoeba proteus* with apparent mass of about 19 kDa (Fig. 1), similar to the mass of cofilin from Jurkat cells, was identified by immunoblot analysis with specific polyclonal antibody raised against human cofilin. Jurkat cells express cofilin, so lysate of these cells was used as a positive control to confirm specificity of the signal detected in *A. proteus* homogenate.

Figure 2 presents CLSM optical sections through migrating amoebae which show the intracellular distribution of amoeba cofilin homologue. Figures 2A, B, C are optically sectioned images at 7.6 μm above the glass substrate. They show the cofilin-like protein (Fig. 2A), F-actin (Fig. 2B) distribution and their co-localization (Fig. 2C) on the ventral side of the migrating amoeba. Amoeba actin and cofilin are accumulated at the close contact site with substratum in the area where adhesive structures are formed. Optical sectioned images recorded at 15.2 μm from the glass substrate (Figs 2D, E, F) show the distribution of cofilin homologue (Fig. 2D), F-actin (Fig. 2E) and their co-localization (Fig. 2F) in the middle part of the cell sectioned along the longitudinal axis.

Cofilin-like protein localized in the middle-anterior region. It was concentrated in three different cell areas

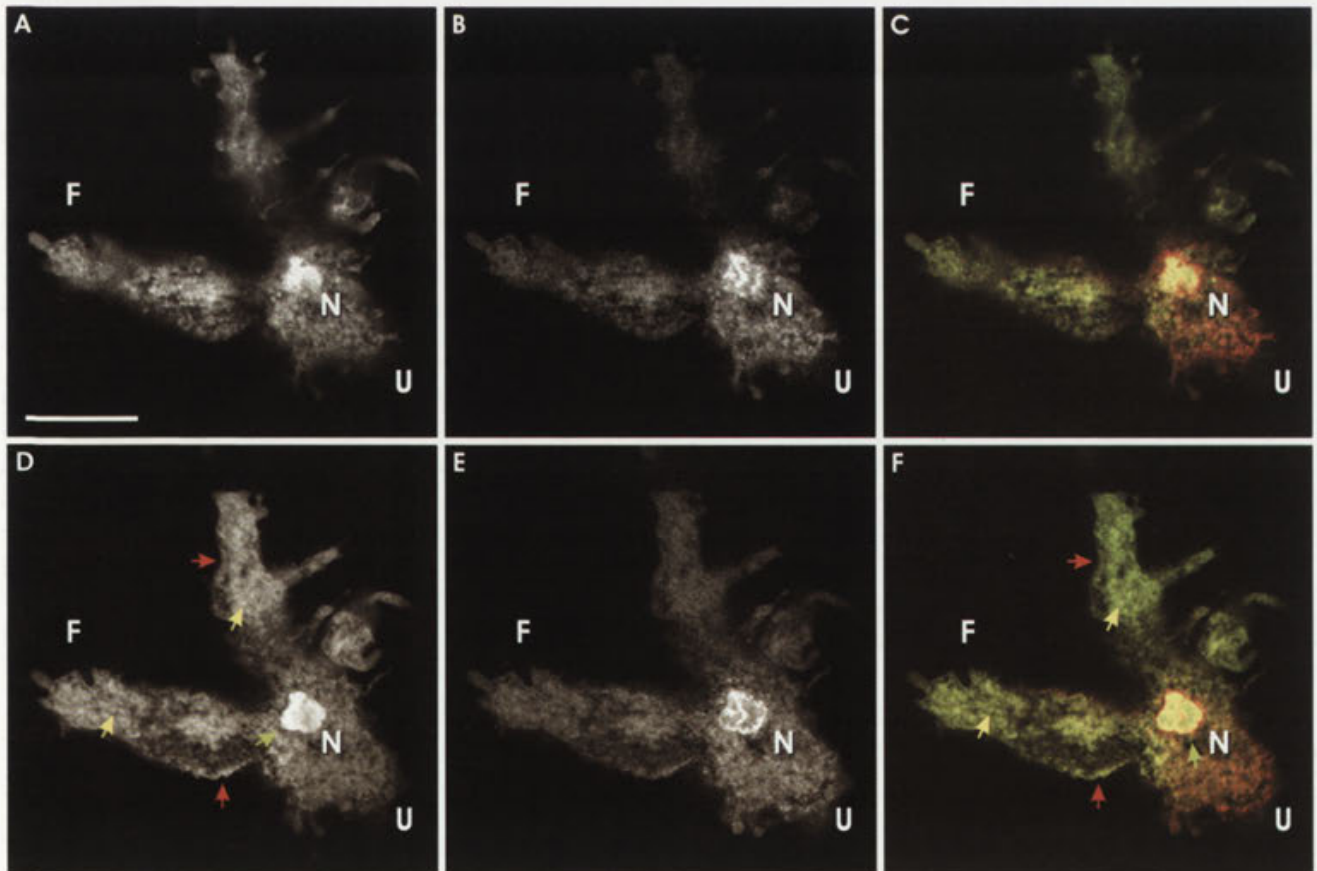


Fig. 2. Localization of cofilin homologue in migrating *Amoeba proteus*. Optically sectioned images of fluorescein and rhodamine staining at 7.6 μm (A-C) and 15.2 μm (D-F) from the glass substrate. Immunofluorescence using polyclonal antibody against human cofilin (A, D). Arrows point to areas where cofilin-like protein is recruited. Alexa Fluor 546-labelled phalloidin for F-actin (B, E). Co-localization of amoeba cofilin and F-actin (C, F). Red, green and yellow arrows show cortical layer, perinuclear area and adhesive region, respectively. F - front, N - nucleus, U - uroid. Scale bar: 50 μm .

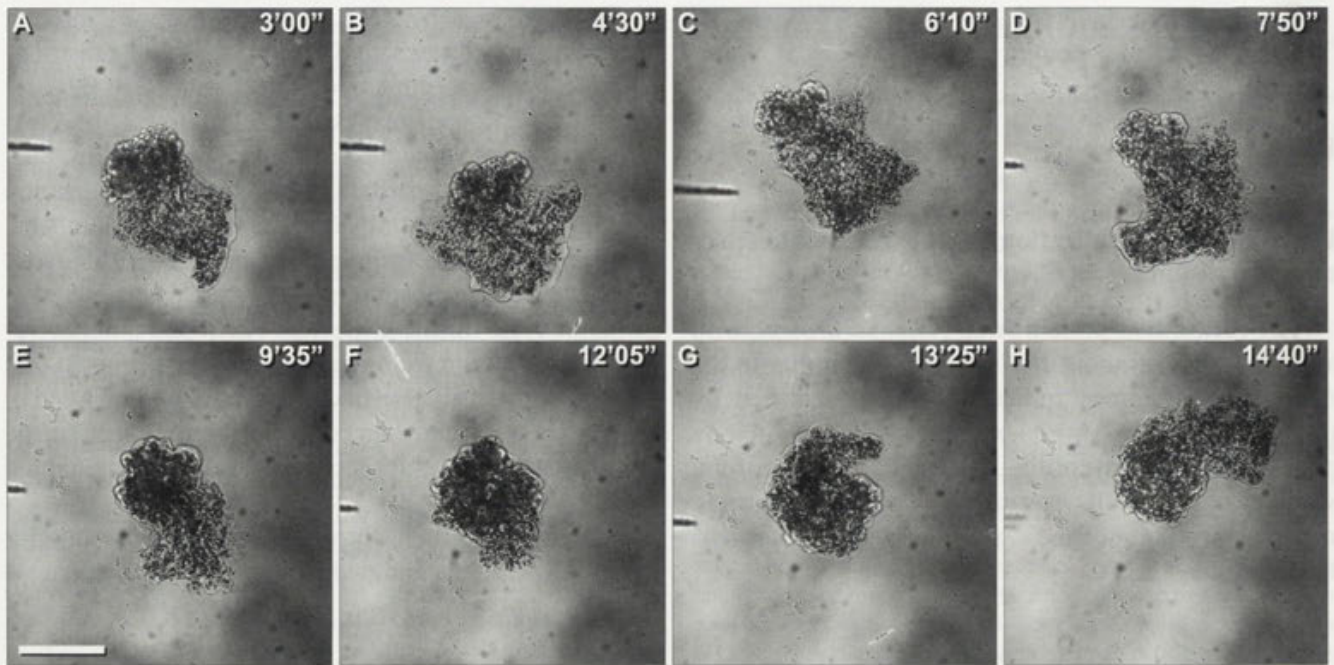


Fig. 3. Behavior of *Amoeba proteus* after microinjection of polyclonal antibody against human cofilin. Note the atypical mode of migration. Scale bar: 100 μ m.

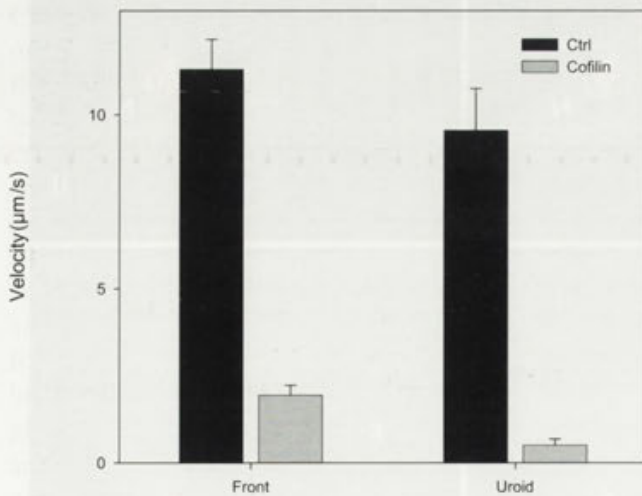


Fig. 4. The effect of blocking endogenous cofilin on the rate of frontal progression and uroidal retraction during migration of *Amoeba proteus*. Cofilin-like protein was blocked by microinjection of amoebae with polyclonal antibody against human cofilin.

and accompanied by F-actin: in the cortical network (Figs 2D and 2F, red arrows), in the perinuclear cytoskeleton (Figs 2D and 2F, green arrow) and in the area

where adhesive structures are developed (Figs 2D and 2F, yellow arrows).

Effect of inhibition of endogenous cofilin on locomotion of *A. proteus*

The effect of blocking the amoeba endogenous cofilin on the morphology and migration of amoebae was examined by microinjection of migrating cells with polyclonal antibody against human cofilin. Control cells were injected with the Pringsheim medium and with the solution in which antibody was supplied. They resumed their locomotion within 1 min. The mode and the velocity of migration were not changed (data not shown). Control experiments were consistent with data observed by Kłopocka and Rędownicz (2003, 2004).

Figure 3 demonstrates the results of blocking the endogenous cofilin-like protein by microinjecting migrating amoeba with the polyclonal anti-cofilin antibody. Observed, drastic changes in the morphology and rate of migration seem to be irreversible - each experiment was recorded for 60 min and the behaviour of amoebae was not changed. Amoebae started to migrate within 2-3 min after treatment. The cells were strongly contracted with inhibited formation of new fronts and disordered polar-

ization. They were also strongly attached to the substratum compared to control. A quantification of the effect of cofilin-like protein blocking on amoeba locomotion is presented in Fig. 4. Treatment of amoebae with antibody led to an inhibition of the frontal edge progression (above 90%) as well as the uroid retraction (about 80%), when compared with control amoebae.

DISCUSSION

Cell motility bases on actin assembly and disassembly, formation and disorganization of special cytoskeletal structures and contraction of the acto-myosin system. These processes are involved in creating and maintenance of cellular polarization, frontal protrusion, cell adhesion and tail region contraction connected with de-adhesion. Cell motility relies on the correct spatial and temporal reorganization of actin cytoskeleton that is regulated by numerous actin-binding proteins.

ADF/cofilins have been recognized as a family of essential, conserved, widespread acting-binding proteins important *in vivo* for the acceleration of actin filaments turnover during cell motility (Pantaloni *et al.* 2001) and cytokinesis (Gunsalus *et al.* 1995, Nagaoka *et al.* 1995).

Actin filament disassembly is necessary for polarized protrusion during cells migration. ACs localize to sites of intense actin filaments turnover (Bamburg and Bray 1987, Svitkina and Borisy 1999) including lamellipodium of crawling fibroblasts (Dawe *et al.* 2003), lamellipodium of keratocytes (Pollard and Borisy 2003), leading edge of *Acanthamoeba* (Quirk *et al.* 1993). A significant accumulation of cofilin was also observed at the leading edges of protruding pseudopodia in flattened cells of *D. discoideum* (Aizawa *et al.* 1995, 1997). In migrating tissue cells intense actin polymerization in the front of lamellipodia forms so-called dendritic brush (Svitkina and Borisy 1999), and is responsible for membrane displacement. Actin polymerization at the leading edge of migrating *A. proteus* seems to be rather insufficient in providing the driving force for a membrane displacement (Pomorski *et al.* in press). Microfilaments in fronts of advancing pseudopodia run mostly parallel to the plasma membrane (Wehland *et al.* 1979), and their formation is independent on the Arp2/3 complex. However, the reconstruction of the cortical layer in advancing fronts is necessary for maintenance of polarized migration. Actin filaments turnover in cortical cytoplasm, except tips of protruding pseudopodia is necessary for the formation of three dimensional contractile network

that activity generates force necessary for endoplasmic streaming, fronts protrusion, de-adhesion and retraction of the uroidal region.

Our results show that organization of the cortical layer in *A. proteus* is highly associated with cofilin-like protein activity. This protein is involved in actin dynamics in the middle-anterior region of migrating cells, but does not take place in processes of the cortical network disorganization occurring in the uroid. Observations on amoebae microinjected with the fluorescence G-actin (Gawlitta *et al.* 1980, Stockem *et al.* 1983) indicated a rather high rate of actin exchange between cytoplasmic matrix and the cell cortex in the middle-anterior region. Optical sectioning observation clearly indicated that cofilin homologue and actin co-localized at the leading edge, in the cortical and perinuclear cytoskeleton, in the area of cellular adhesion and in streaming endoplasm of this amoeba (Fig. 2). We suggest that cofilin-like protein is engaged in the regulation of actin filament turnover at regions of dramatically reorganizing actin cytoskeleton: at leading edge where the reconstruction of the cortical layer starts from elements of actin cytoskeleton bringing here by endoplasmic streaming (Grębecki 1982), in the cortical and perinuclear network where the processes of Arp2/3 complex-dependent actin polymerization occur, in the formation of adhesive structures, and in actin depolymerizing and severing in endoplasmic streaming.

In vivo experiments with inhibition of cofilin-like protein have revealed that this protein is a key player in the regulation of actin dynamics in *A. proteus*, and it is necessary for the proper cell migration. Cells lacking cofilin or over-expressing constitutively active LIM kinase have impaired locomotion (Arber *et al.* 1998, Chen *et al.* 2001), and those over-expressing cofilins are more motile (Aizawa *et al.* 1996).

Blocking endogenous cofilin by microinjecting amoebae with antibody against human cofilin caused the distinct and irreversible changes in the locomotive shape of the examined amoeba (Fig. 3) and significant (about 90%) inhibition of their migration (Fig. 4). Slowing down of actin filaments turnover leads to the strong contraction and the adhesion, inhibition of new fronts formation and polarization disorders. These changes seem to be related to disturbances in the reconstruction of the cortical layer at the leading edge, reorganization of the contractile network in the middle-anterior region and formation of adhesive structures.

It may be concluding that actin dynamics induced by cofilin-like protein are important for normal morphology and motility of *Amoeba proteus*.

Further studies are needed to clarify the function of cofilin-like protein during amoeba migration and the role of its activation and inactivation.

Acknowledgments. This work was supported by a statutory grant to the Nencki Institute of Experimental Biology from the State Committee for Scientific Research.

REFERENCES

- Agnaew B. J., Minamide L. S., Bamburg J. R. (1995) Reactivation of phosphorylated actin depolymerizing factor and identification of the regulatory site. *J. Biol. Chem.* **270**: 17582-17587
- Aizawa H., Sutoh K., Tsubuki S., Kawashima S., Ishii A., Yahara I. (1995) Identification, characterization, and intracellular distribution of cofilin in *Dictyostelium discoideum*. *J. Biol. Chem.* **270**: 10923-10932
- Aizawa H., Sutoh K., Yahara I. (1996) Overexpression of cofilin stimulates bundling of actin filaments, membrane ruffling and cell movement in *Dictyostelium*. *J. Cell Biol.* **132**: 335-344
- Aizawa H., Fukui Y., Yahara I. (1997) Live dynamics of *Dictyostelium* cofilin suggests a role in remodeling actin latticework into bundles. *J. Cell Sci.* **110**: 2333-2344
- Arber S., Barbayannis F. A., Hanser H., Schneider C., Stanyon C. A., Bernard O., Caroni P. (1998) Regulation of actin dynamics through phosphorylation of cofilin by LIM-kinase. *Nature* **393**: 805-809
- Bamburg J. R., Bray D. (1987) Distribution and cellular localization of actin depolymerizing factor. *J. Cell Biol.* **105**: 2817-2815
- Bamburg J. R., Harris H. E., Weeds A. G. (1980) Partial purification and characterization of an actin depolymerizing factor from brain. *FEBS Lett.* **121**: 178-182
- Bamburg J. R., McGough A., Ono S. (1999) Putting a new twist on actin. ADF/cofilins modulate actin dynamics. *Trends Cell Biol.* **9**: 364-370
- Blanchoin L., Robinson R. C., Choe S., Pollard T. D. (2000) Phosphorylation of *Acanthamoeba* actophorin (ADF/cofilin) blocks interaction with actin without a change in atomic structure. *J. Mol. Biol.* **295**: 203-211
- Carlier M. F., Laurent V., Santolini J., Melki R., Didry D., Xia G.-X., Hong Y., Chua N.-H., Pantaloni D. (1997) Actin depolymerizing factor (ADF/Cofilin) enhances the rate of filament turnover; implication in actin based-motility. *J. Cell Biol.* **136**: 1307-1323
- Carlier M. F., Ressad F., Pantaloni D. (1999) Control of actin dynamics in cell motility. Role of ADF/cofilin. *J. Biol. Chem.* **274**: 33827-33830
- de Hostas E. L., Bradtke B., Lottspeich F., Gerisch G. (1993) Coactosin, a 17 kDa F-actin binding protein from *Dictyostelium discoideum*. *Cell Motil. Cytoskeleton* **26**: 181-191
- Chen J., Godt D., Gunsalus K., Kiss I., Goldberg M., Laski F. A. (2001) Cofilin/ADF is required for cell motility during *Drosophila* ovary development and oogenesis. *Nat. Cell Biol.* **3**: 204-209
- Dawe H. R., Minamide L. S., Bamburg J. R., Cramer L. P. (2003) ADF/cofilin controls cell polarity during fibroblast migration. *Curr. Biol.* **13**: 252-257
- Gawlińska W., Stockem W., Wehland J., Weber K. (1980) Organization and spatial arrangement of fluorescein-labeled native actin microinjected into normal locomoting and experimentally influenced *Amoeba proteus*. *Cell Tissue Res.* **206**: 181-191
- Grębecki A. (1982) Supramolecular aspects of amoeboid movement. *Acta Protozool.* **21**: 117-130
- Gunsalus K. C., Banaccors S., William E., Vern F., Gatt M., Goldberg M. L. (1995) Mutation in twinstar, a *Drosophila* gene encoding a cofilin/ADF homologue, result in defect in centrosome migration and cytokinesis. *J. Cell Biol.* **131**: 1243-1259
- Kłopocka W., Rędowicz M. J. (2003) Effect of Rho family GTP-binding proteins on *Amoeba proteus*. *Protoplasma* **220**: 163-172
- Kłopocka W., Rędowicz M. J. (2004) Rho/Rho-dependent kinase affects locomotion and actin-myosin II activity of *Amoeba proteus*. *Protoplasma* **224**: 113-121
- Kłopocka W., Moraczewska J., Rędowicz M. J. (2005) Characterisation of the Rac/PAK pathway in *Amoeba proteus*. *Protoplasma* **225**: 77-84
- Maciver S. K. (1998) How ADF/cofilin depolymerizes actin filaments. *Curr. Opin. Cell Biol.* **10**: 140-144
- Maciver S. K., Hussey P. J. (2002) The ADF/cofilin family: actin-remodeling proteins. *Genome Biol.* **3**: 3007.1-3007.12
- McGough A., Pope B., Weeds A. (2001) The ADF/Cofilin family: accelerators of actin reorganization. *Results Probl. Cell Differ.* **32**: 135-154
- Nagaoka R., Abe H., Kusano K., Obinata T. (1995) Concentration of cofilin, a small actin-binding protein, at a cleavage furrow during cytokinesis. *Cell Motil. Cytoskeleton* **30**: 1-7
- Niwa R., Nagata-Ohashi K., Takeichi M., Mizuno K., Uemura T. (2002) Control of actin reorganization by Slingshot, a family of phosphatases that dephosphorylate ADF/cofilin. *Cell* **108**: 233-246
- Pantaloni D., Le Clairche C., Carlier M.-F. (2001) Mechanism of actin-based motility. *Science* **292**: 1502-1506
- Pollard T. D., Borisy G. G. (2003) Cellular motility driven by assembly and disassembly of actin filaments. *Cell* **112**: 453-465
- Pomorski P., Krzeminski P., Wasik A., Wierzbicka K., Baranska J., Kłopocka W. Actin dynamics in *Ameba proteus* motility. *Protoplasma* (in press)
- Quirk S., Maciver S. K., Ampe C., Doberstein S. K., Kaiser D.A., VanDamme J., Vandekerckhove J. S., Pollard T. D. (1993) Primary structure of and studies on *Acanthamoeba* actophorin. *Biochemistry* **32**: 8525-8533
- Stockem W., Hoffman H. U., Gruber B. (1983) Dynamics of the cytoskeleton in *Amoeba proteus*. I. Redistribution of microinjected fluorescein-labeled actin during locomotion, immobilization and phagocytosis. *Cell Tissue Res.* **232**: 79-96
- Svitkina T. M., Borisy G. G. (1999) Arp2/3 Complex and ADF/cofilin in dendritic organization and treadmilling of actin filament array in lamellipodia. *J. Cell Biol.* **145**: 1009-1026
- Wehland J., Weber K., Gawlińska W., Stockem W. (1979) Effects of the actin-binding protein DNAase I on cytoplasmic streaming and ultrastructure of *Amoeba proteus*. An attempt to explain amoeboid movement. *Cell Tissue Res.* **199**: 353-72
- Yang N., Higuchi O., Nagata K., Wada A., Kangawa K., Nishida E., Mizuno K. (1998) Cofilin phosphorylation by LIM-kinase 1 and its role in Rac-mediated actin reorganization. *Nature* **393**: 809-812

Received on 12th September, 2006; accepted on 27th September, 2006

Comparison of the Amount and Demonstrability of Endogeneous Hormones and Bound Insulin After Paraformaldehyde and Edac Fixation in *Tetrahymena*

György CSABA¹, Péter KOVÁCS¹ and Éva PÁLLINGER²

¹Department of Genetics, Cell and Immunobiology, Semmelweis University; ²Immunogenomic Research Group, Hungarian Academy of Sciences, Budapest, Hungary

Summary. The amount of three endogeneous hormones (insulin, β -endorphin, and triiodothyronine) and FITC-insulin binding were studied in *Tetrahymena* using confocal microscopy and flow cytometry after paraformaldehyde (Pf) or carbodiimide (EDAC) fixation. After EDAC fixation the measurable hormone content was 2.5 \times , 4 \times , 6 \times more, respectively, related to Pf fixation (significance: $p < 0.001$). This means that EDAC, which causes crosslinking between COOH and amino groups inside a molecule and between molecules could inhibit the escape of hormones during the procedure. However, FITC-insulin binding was also threefold after EDAC fixation which means that some other effects must be considered. The results show that 1) EDAC fixation is more suitable to watch the whole hormone content in a cell (in *Tetrahymena*, at present); 2) more vertebrate-like hormone is present in *Tetrahymena*, than it was believed before and 3) triiodothyronine is also present in *Tetrahymena* (first observation).

INTRODUCTION

In the early seventies of the last century was demonstrated at first that protozoa (exactly *Tetrahymena*) can react (sometimes specifically) to the hormones of higher ranked animals and can select between closely related hormone molecules (Csaba and Lantos 1973, 1975; Csaba 1980, 2000). After that, many hormone-

like molecules were found in *Tetrahymena* which were immunologically similar to that of phylogenetically higher animals and could mimic the effects of these hormones (LeRoith *et al.* 1980, 1982, 1983; Lenard 1992). Later the signal transduction mechanisms were studied (Kovács and Csaba 1987, 1990, 1992) as well as the structure of *Tetrahymena* insulin receptor (Christopher and Sundermann 1995, Leick *et al.* 2001, Christensen *et al.* 2003) and both showed similarities to the mammalian ones.

For localization of hormones immunocytochemistry and confocal microscopy are very suitable and up to date methods, while the amount of hormones can be determined by flow cytometry. Nevertheless, the loss of

Address for correspondence: György Csaba, Department of Genetics, Cell and Immunobiology, Semmelweis University, Nagyvárad tér 4, 1445 Budapest, Hungary; E-mail: csagyor@dgci.sote.hu

hormones during the procedure of preparation seems to be high. For inhibiting the loss, EDAC fixation was recommended by Finnish authors (Panula *et al.* 1988, 1995) in case of the nervous system and biogenic amines, as EDAC causes cross-linking of COOH and amino-groups inside a molecule and between molecules, hindering the escape of small molecules (Handbook 2005). In *Tetrahymena* we also found that more serotonin and histamine can be measured after EDAC fixation related to the traditional paraformaldehyde (Csaba *et al.* 2006). In the present experiments the measurable amount and the localization of three non-biogenic-amine hormone, with different molecular weights, are studied as well as the binding of insulin, comparing the effect of paraformaldehyde and EDAC fixation.

MATERIALS AND METHODS

Cells and culturing. *Tetrahymena pyriformis* GL strain was used in the logarithmic phase of growth. The cells were cultured at 28°C in tryptone medium (Sigma, St.Louis, USA) containing 0.1% yeast extract, for 48 h. The density of *Tetrahymena* cultures studied was 10⁴ cell/ml.

Flow cytometric analysis. Samples of cells were fixed with 4% paraformaldehyde solution [dissolved in pH 7.2 phosphate buffered saline (PBS)] or with freshly prepared 4% N-(3-Dimethylaminopropyl)-N'-ethylcarbodiimide hydrochloride (EDAC, Sigma, St.Louis, USA) solution for 5 min, and then washed twice in wash buffer (0.1% bovin serum albumin [BSA]; 20 mM Tris-HCl; 0.9% NaCl; 0.05% Nonidet NP-40; pH 8.2). To block nonspecific binding of antibodies the cells were treated with blocking buffer (1% BSA in PBS) for 30 min at room temperature. Aliquots from cell suspensions (50 µl) were transferred into tubes, and 50 µl primary antibody [diluted 1:200 in antibody buffer (1% BSA in wash buffer)] was added for 30 min at room temperature. The 1st antibody

were anti-endorphin, anti-T3 and anti insulin purchased from Sigma. FITC-insulin (Sigma) was used for studying insulin binding. Negative controls were carried out with 50 µl PBS containing 10 mg/ml BSA, instead of primary antibody. After washing four times with wash buffer to remove excess primary antibody the 1st antibody treated cells were incubated with FITC-labelled secondary antibody (anti-rabbit IgG for anti-endorphin and anti-T3; or anti-mouse IgG for anti-insulin; both purchased from Sigma; in dilution 1:50 with antibody buffer) for 30 min at room temperature.

For controlling the specificity, autofluorescence of the cells and aspecificity of the secondary antibodies were detected. This latter means that the fluorescence of cells treated only with the secondary antibody (without the specific first antibody) was also measured in each series. The measurement was done in a FACSCalibur flow cytometer (Becton Dickinson, San Jose, USA), using 5.000 cells for each measurement. In the cell populations the hormone content (concentration) had been compared. For the measurement and analysis CellQuest Pro program was used. The numerical comparison of detected values was done by the comparison of percentual changes of geometric mean channel values (Geo-mean) to the appropriate control groups by using Origin program and Student t-test. The experiments were done thrice with similar results and Table 1 demonstrates one of these experiments.

Confocal microscopic analysis. After the flow cytometric analysis the cells were subjected to confocal microscopic analysis in a BioRad MRC 1024 confocal laser scanning microscope, equipped with krypton-argon mixed gas-laser as a light source, at an excitation wavelength of 480 nm line.

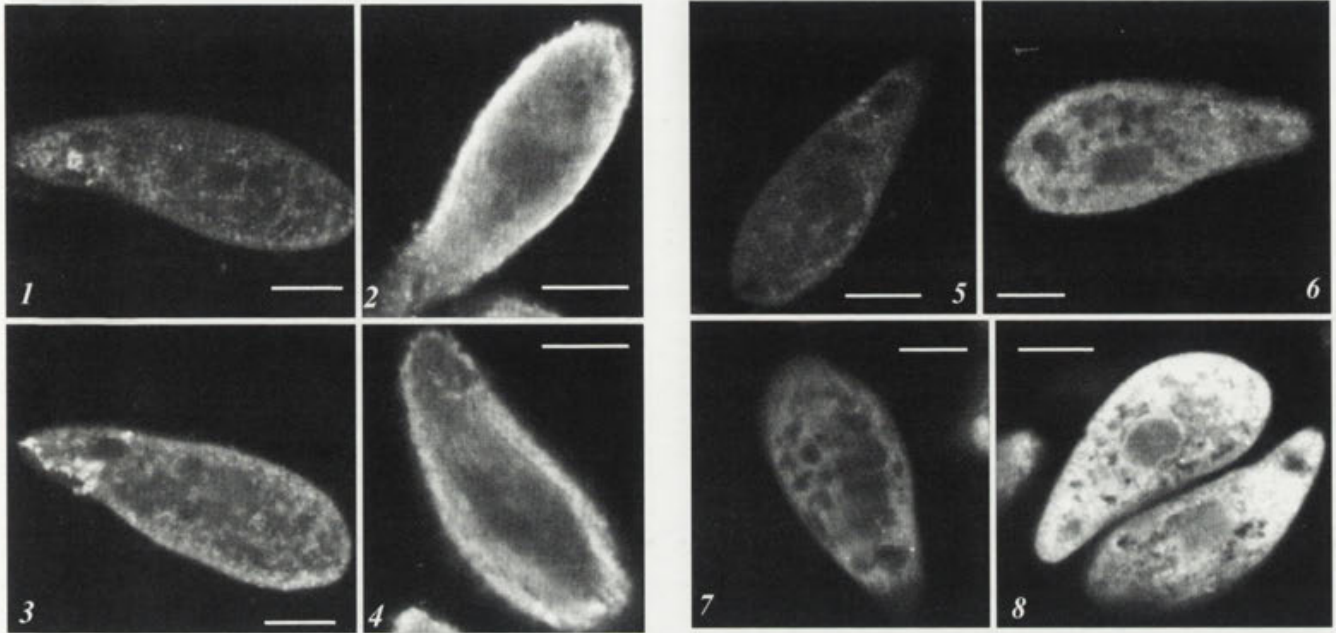
RESULTS

Considering the data of the flow cytometric analysis each hormone was measured at a higher level after EDAC fixation. The significance between the values of the two different fixation was very high ($p < 0.001$). The difference between the values in the case of endorphin was almost fourfold, in case of insulin 2 and a half-fold,

Table 1. Measurable hormone concentrations after different fixations.

Fixative	Hormone	Geo-mean +/- s.d.	Significance to Pf*
Paraformaldehyde	endorphin	16.85 +/- 2.21	
	insulin	6.17 +/- 0.37	
	triiodothyronine	15.27 +/- 1.0	
	FITC-insulin	386.58 +/- 36.8	
EDAC	endorphin	59.39 +/- 4.51	p < 0.001
	insulin	15.15 +/- 0.66	p < 0.001
	triiodothyronine	93.79 +/- 6.48	p < 0.001
	FITC-insulin	1201.1 +/- 31.78	p < 0.001

* Pf - paraformaldehyde



Figs 1-8. 1 - Formaldehyde fixed *Tetrahymena*. Anti-endorphin treatment. 2 - EDAC-fixed *Tetrahymena*. Anti-endorphin treatment. 3 - Formaldehyde fixed *Tetrahymena*. Anti-T₃ treatment. 4 - EDAC-fixed *Tetrahymena*. Anti-T₃ treatment.

5 - Formaldehyde fixed *Tetrahymena*. Anti-insulin treatment. 6 - EDAC-fixed *Tetrahymena*. Anti-insulin treatment. 7 - Formaldehyde fixed *Tetrahymena*. FITC-insulin treatment. 8 - EDAC-fixed *Tetrahymena*. FITC-insulin treatment. Scale bars: 10 μm.

in case of T₃ -this was the highest- more than six-fold. More than threefold FITC-insulin was bound by the cells after EDAC fixation than after paraformaldehyde fixation (Table 1). This means that EDAC fixation is more advantageous in the study of amino acid and polypeptide hormones, in addition to the previously demonstrated biogenic amines (Csaba *et al.* 2006).

The confocal microscopic analysis supports the flow cytometric data. In each EDAC-fixed cell more hormone is visible, than after paraformaldehyde fixation (Figs 1-8). In addition EDAC-fixation shows clearer the localization of hormones. In case of endorphin it is localized first of all under the surface of the cell membrane (Fig 2) and diffusely inside the cell. There is a similar situation in case of T₃ however, the localization of the hormone on the oral field is better seen after paraformaldehyde fixation (Figs 3, 4). Insulin is localized inside the cell diffusely, in a much higher amount after EDAC-fixation (Figs 5, 6). FITC-insulin is also localized diffusely and the structures on the surface of which insulin is bound are rather visible after EDAC fixation (Figs 7, 8).

DISCUSSION

Four molecules were chosen for studying the differences between the two fixatives. A small amino acid hormone, T₃, a small and a large polypeptide hormone, endorphin and insulin; and FITC-insulin which can be bound by the insulin receptors present in *Tetrahymena*. The hormones studied can be found in *Tetrahymena*. Insulin was demonstrated at first (LeRoith *et al.* 1980) after its binding sites (Csaba and Lantos 1975), and before the detailed determination of its receptors (Christopher and Sundermann 1995, Christensen *et al.* 2003, Leick *et al.* 2001). Later endorphin and endorphin-binding were also found (LeRoith *et al.* 1980, O'Neill *et al.* 1988, Zipser *et al.* 1988, Chiesa *et al.* 1993, Renaud *et al.* 1995, Csaba and Kovács, 1999, Rodriguez *et al.* 2004). T₃ was not determined previously in *Tetrahymena*, so this is the first exact observation on its presence. In earlier experiments we tried to demonstrate T₃, but the method was not sensitive enough for proving it (Csaba and Nagy 1987). However the binding sites of T₃ on the cell membrane and in the nucleus were shown

also in earlier experiments (Csaba *et al.* 1977, Csaba and Sudár 1978) The use of the present very sensitive methods allowed the enrichment of our knowledge on the hormone-pool of *Tetrahymena*.

The water-soluble EDAC intermolecularly crosslinks amino- and carboxylic acid- groups and also forms intramolecular crosslinks (Handbook 2005). This crosslinking which can be found not only in hormones but in the surrounding molecules (membranes included) inhibits the free movement of the small hormones out of the cell (Ma *et al.* 2004, Bakos *et al.* 2000). Considering these data it is understandable, why EDAC fixation elevated the measurable level of the hormones. However, further explanation is needed if we observe the size of the hormones studied.

T_3 is a small molecule, an amino-acid-type hormone with very high mobility across the membranes, similar to the biogenic amines, for the fixation of which EDAC was recommended at first (Panula *et al.* 1988, 1995). This explains why was so expressed the difference between the two fixations. Endorphin is a small polypeptide and insulin is a large one. The difference between this two peptides can explain the difference - fourfold and two and a half-fold - in the effect of EDAC. However, it can be supposed that insulin - being a large protein - can not escape from the cell also in case of paraformaldehyde fixation. In addition, significantly more exogenously given FITC-insulin was bound by the cells, which can not be explained by the escape-theory. This means that the cross-linking caused by EDAC develops more changes than simply the condensation of molecules and membranes.

Summarizing the results: the experiments call attention to the priority of EDAC fixation if the amount of some biologically active molecules are studied immunocytochemically, and shows that more amount of hormones can be present than it was believed before. However, support by chemical and/or physiological measurements are needed for the exact statement. As a first observation the T_3 content of *Tetrahymena* can be mentioned.

Acknowledgements. This work was supported by the National Research Fund (OTKA T-037303), Hungary. The authors thank Mss. Katy Kallay, Angela Kozak and Marianna Kincses for their expert technical assistance.

REFERENCES

- Bakos D., Jorge-Herrero E., Koller J. (2000) Resorption and calcification of chemically modified collagen/hyaluronan hybrid membranes. *Polim. Med.* **30**: 57-64
- Chiesa R., Silva W. I., Renaud F. L. (1993) Pharmacological characterization of an opioid receptor in the ciliate *Tetrahymena*. *J. Eukaryot. Microbiol.* **40**: 800-804
- Christensen S. T., Guerra C. F., Awan A., Wheatley D. N., Satir P. (2003) Insulin receptor-like proteins in *Tetrahymena thermophila* ciliary membranes. *Curr. Biol.* **13**: R50-52
- Christopher G., Sundermann C. H. (1995) Isolation and partial characterisation of the insulin binding site of *Tetrahymena pyriformis*. *Biochem. Biophys. Res. Com.* **212**: 515-523
- Csaba G. (1980) Phylogeny and ontogeny of hormone receptors: the selection theory of receptor formation and hormonal imprinting. *Biol. Rev.* **55**: 47-63
- Csaba G. (2000) Hormonal imprinting: its role during the evolution and development of hormones and receptors. *Cell Biol. Int.* **24**: 407-414
- Csaba G., Lantos T. (1973) Effect of hormones on protozoa. Studies on the phagocytotic effect of histamine, 5-hydroxytryptamine and indoleacetic acid in *Tetrahymena pyriformis*. *Cytophysiol. Cytobiologie* **7**: 361-365
- Csaba G., Lantos T. (1975) Effect of insulin on the glucose uptake of protozoa. *Experientia* **31**: 107-109
- Csaba G., Sudár F. (1978) Demonstration of triiodothyronine binding sites of *Tetrahymena* by a new scanning autoradiography method. *Acta Biol. Med. Germ.* **37**: 1381-1386
- Csaba G., Nagy S. U. (1987) Presence (hPL, prostaglandin) and absence (triiodothyronine, thyroxine) of hormones in *Tetrahymena*: experimental facts and open questions. *Acta Physiol. Hung.* **70**: 105-110
- Csaba G., Kovács P. (1999) Localization of beta-endorphin in *Tetrahymena* by confocal microscopy. Induction of the prolonged production of the hormone by hormonal imprinting. *Cell Biol. Int.* **23**: 695-702
- Csaba G., Sudár F., Nagy S. U., Dobozy O. (1977) Localization of hormone receptors in *Tetrahymena*. *Protoplasma* **91**: 179-189
- Csaba G., Kovács P., Pállinger É. (2006) EDAC-fixation increases the demonstrability of biogenic amines in the unicellular *Tetrahymena*. A flow cytometric and confocal microscopic comparative analysis. *Cell Biol. Int.* **30**: 412-415
- Handbook (2005) A guide to fluorescent probes and labeling technologies. <http://probes.invitrogen.com/handbook/sections/0502.html> 10th ed.
- Kovács P., Csaba G. (1987) The role of Ca^{2+} in hormonal imprinting of the *Tetrahymena*. *Acta Physiol. Hung.* **69**: 167-169
- Kovács P., Csaba G. (1990) Influence of the phosphoinositol (PI) system in the mechanism of hormonal imprinting. *Biochem Biophys Res Commun* **170**: 119-126
- Kovács P., Csaba G. (1992) Effect of inhibition and activation of tyrosin kinase on insulin imprinting in *Tetrahymena*. *Cell Biochem. Funct.* **10**: 267-271
- Leick V., Bog-Hansen T. C., Juhl H. A. (2001) Insulin/FGF-binding ciliary membrane glycoprotein from *Tetrahymena*. *J. Membr. Biol.* **181**: 47-53
- Lenard J. (1992) Mammalian hormones in microbial cells. *Trends Biochem. Sci.* **17**: 147-150.
- LeRoith D., Schiloach J., Roth J., Lesniak M. A. (1980) Evolutionary origins of vertebrate hormones: substances similar to mammalian insulin are native to unicellular eukaryotes. *Proc. Natl. Acad. Sci. USA* **77**: 6184-6186
- LeRoith D., Liotta A.H., Roth J., Schiloach J., Lewis M. E., Pert C.B., Krieger D. T. (1982) ACTH and beta endorphin like materials are native to unicellular organisms. *Proc. Natl. Acad. Sci. USA* **79**: 2086-2090
- LeRoith D., Schiloach J., Berelowitz M., Frohman L. A., Liotta A. S., Krieger B. T., Roth J. (1983) Are messenger molecules in microbes the ancestors of the vertebrate hormones and tissue factors? *Fed. Proc.* **42**: 2602-2607
- Ma L., Gao C., Mao Z., Zhou J., Shen J. (2004) Biodegradability and cell mediated contraction of porous collagen scaffolds: the effect of lysine as a novel crosslinking bridge. *J Biomed Mater Res A* **71**: 334-342
- O'Neill J. B., Pert C. B., Ruff M. R., Smith C. C., Higgins W. J., Zipser B. (1988) Identification and characterization of the opiate

- receptor in the ciliated protozoan, *Tetrahymena*. *Brain Res.* **450**: 303-315
- Panula P., Happola O., Airaksinen M. S., Auvinen S., Virkamaki A. (1988) Carbodiimide as a tissue fixative in histamine immunocytochemistry and its application in developmental neurobiology. *J. Histochem. Cytochem.* **36**: 259-269
- Panula P., Eriksson K., Gustafsson M., Reuter M. (1995) An immunocytochemical method for histamine: application to the planarians. *Hydrobiologia* **305**: 291-295
- Renaud F. L., Colon I., Lebron J., Ortiz N., Rodriguez F., Cadilla C. (1995) A novel opioid mechanism seems to modulate phagocytosis in *Tetrahymena*. *J. Eukaryot. Microbiol.* **42**: 205-207
- Rodriguez E., Lazaro M. I., Renaud F. L., Matino M. (2004) Opioid activity of beta-endorphin-like proteins from *Tetrahymena*. *J. Eukaryot. Microbiol.* **51**: 60-65.
- Zipser B., Ruff M. R., O'Neill J. B., Smith C. C., Higgins W. J., Pert C. B. (1988) The opiate receptor: a single 110 kDa recognition molecule appears to be conserved in *Tetrahymena*, leech and rat. *Brain Res.* **463**: 296-304

Received on 7th February, 2006; revised version on 10th July, 2006; accepted on 23rd August, 2006

Ultrastructural Events in the Predator-induced Defence Response of *Colpidium kleini* (Ciliophora: Hymenostomatia)

Janusz FYDA¹, Gabrielle KENNAWAY², Katarzyna ADAMUS¹ and Alan WARREN²

¹Department of Hydrobiology, Institute of Environmental Sciences, Jagiellonian University, Kraków, Poland; ²Department of Zoology, Natural History Museum, London, UK

Summary. The hymenostome ciliate *Colpidium kleini* undergoes a morphological defence response when in the presence of the predatory ciliate *Lembadion bullinum*, with cells of *C. kleini* becoming shorter and wider and thus more difficult for *L. bullinum* to ingest. The ultrastructural events associated with this morphological transformation were investigated by transmission electron microscopy. A number of differences between defended and undefended *C. kleini* cells were observed with defended cells showing: an increased localization of mitochondria in the peripheral regions of the cell cortex; a mobilization of mucocysts; a change in the appearance of the plasmalemma. Possible explanations for these ultrastructural events are discussed.

Key words: ciliate, *Lembadion bullinum*, morphological transformation, mucocyst, TEM.

INTRODUCTION

Predator-induced defence responses in ciliates have been the subject of several studies since the phenomenon was first reported by Kuhlmann and Heckmann (1985). While most of these studies have dealt primarily with morphological responses, others have focused on changes in life history, behaviour, trophic strategy and growth kinetics (for reviews see Wicklow 1997, Kuhlmann *et al.* 1999). Predator-induced responses have only been reported in three classes of ciliates:

Hypotrichia, Stichotrichia and Hymenostomia. A recent investigation failed to extend the range of ciliate groups with a capacity for predator-induced change (Fyda *et al.* 2005).

Only two genera of hymenostomes are known to exhibit predator-induced defence responses: *Lambornella* and *Colpidium*. In the case of *Lambornella* the response takes the form of a trophic shift from free-living trophonts to parasitic theronts (Washburn *et al.* 1988). By contrast, cells of *Colpidium kleini* and *C. colpoda* increase in volume and become more spherical in shape in the presence of the predatory peniculine ciliate *Lembadion bullinum* (Fyda 1998).

Ultrastructural investigations have rarely been carried out on defended ciliate morphotypes so the changes

Address for correspondence: Janusz Fyda, Department of Hydrobiology, Institute of Environmental Sciences, Jagiellonian University, Gronostajowa 7, 30-387 Kraków, Poland; Fax: +48 (0)12 664 6912; E-mail: fyda@eko.uj.edu.pl

that occur at the subcellular level are poorly understood. Notable exceptions are the studies by Jerka-Dziadosz *et al.* (1987) and by Wicklow (1997) on the hypotrich *Euplotes octocarinatus* and the stichotrich *Onychodromus quadricornutus* respectively. Hitherto there have been no ultrastructural studies of defended morphotypes among the hymenostomes. In this paper we present preliminary observations on ultrastructural differences between defended and undefended cells of *Colpidium kleini*.

MATERIALS AND METHODS

Stock cultures of *Colpidium kleini* and *Lembadion bullinum* from the Department of Hydrobiology, Jagiellonian University, Kraków were used as the primary source of experimental organisms. Clonal cultures of each were established for use in the present study. All *C. kleini* cells examined during the present study, both defended and undefended, were derived from the same clone. Defended cells of *C. kleini* were obtained according to Fyda (1998). Predator and prey were combined in the same Petri dish and incubated for 48 h. Undefended *C. kleini* were obtained by incubating in the absence of *Lembadion*. Cells were harvested by micropipette and prepared for examination by transmission electron microscopy (TEM) according to the method of Kennaway and Lewis (2004). All cells were treated identically, the only variable being whether or not they had been exposed to the predator *Lembadion*. Ultrathin sections of at least three defended and three undefended cells of *C. kleini* were examined using a Hitachi H7100 TEM.

RESULTS AND DISCUSSION

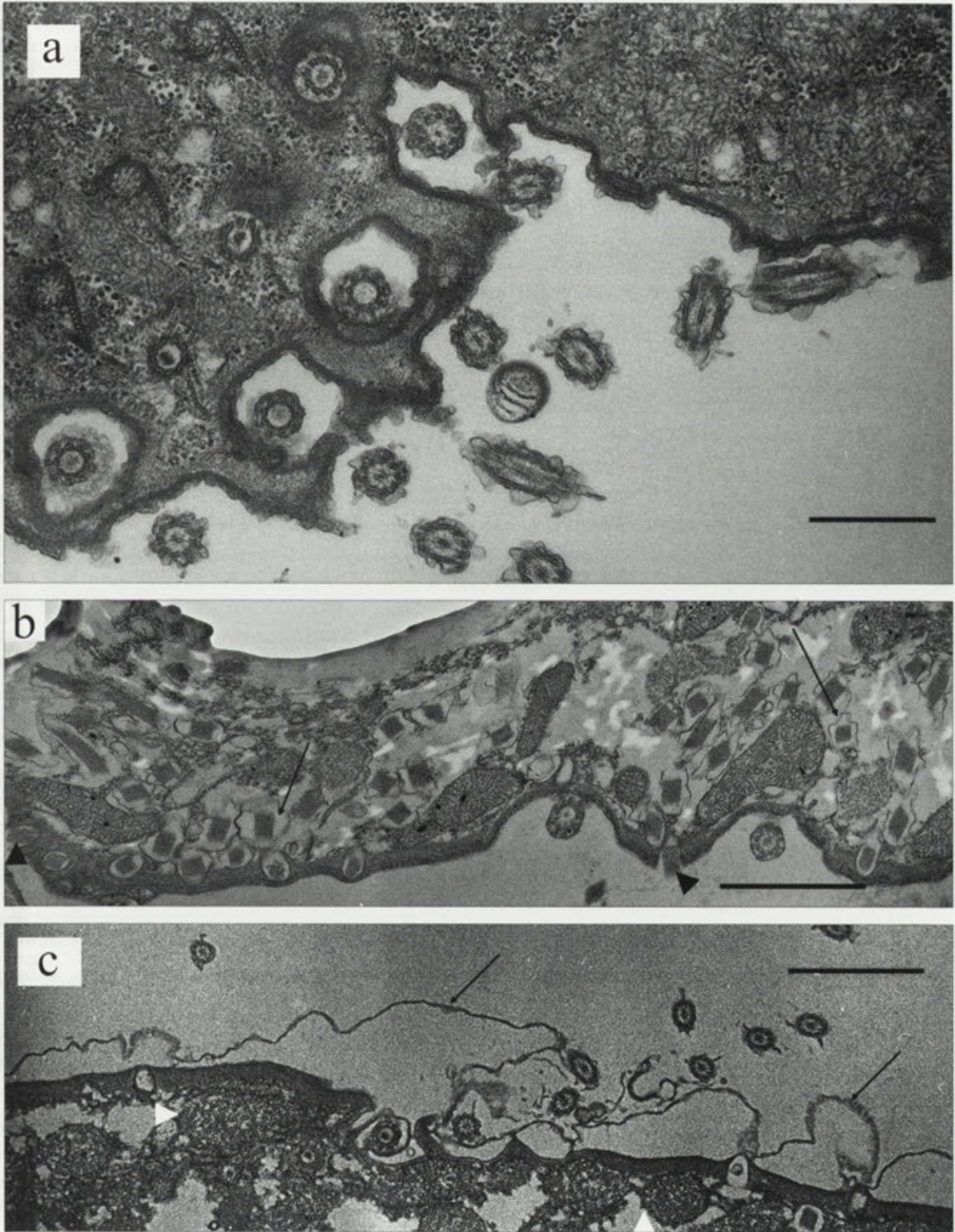
The ultrastructure of the cortical regions of typical defended and undefended *Colpidium kleini* cells are shown in Figures 1a-c. From these it can be seen that a number of changes occur at the ultrastructural level during the defence response, specifically with respect to the distribution of mitochondria, the appearance of the plasmalemma (plasma membrane) and the number and activity of the mucocysts. Although the three micrographs do not necessarily show the same region of the cell, examination of whole-cell sections reveal the same ultrastructural differences in the cortex of defended vs undefended cells throughout the organism.

In defended morphotypes the mitochondria appear to be localized in the cortical region (Fig. 1c). It has long been known that many mitochondria in ciliates localize underneath the pellicle (Fauré-Fremiet 1910, Horning 1927) and some are closely associated with the epiplasm (Aufderheide 1983). It has been postulated that the

cortical mitochondria are involved in active interchange processes in protozoa (Doyle 1935). The expansion of the cortex which gives rise to the cell enlargement during the defence response in *C. kleini* presumably entails increased activity in this region of the cell and might thus account for the cortical localization of the mitochondria.

The second ultrastructural feature that characterises transformed *Colpidium kleini* is the presence of large numbers of mucocysts in the cortical and sub-cortical regions of the cell. Mucocysts are a type of extrusome, the main function of which is to export material to the cell surface. They comprise a paracrystalline contents bounded by a membrane. Mucocysts are produced in the endoplasm and migrate to the cell periphery where they dock with the cell membrane. The mucocyst membrane then fuses with the cell membrane releasing its contents to the outside (Paulin 1996). Figure 1b shows examples of these mucocysts in the cortex of a partly defended *C. kleini* cell. Some appear to be fusing with the plasmalemma thus discharging their contents to the outside (Fig. 1b, arrowheads). Enhanced uptake of Alcian Blue in defended cells provides further support for the presence of higher numbers of mucocysts (data not shown). By contrast, mucocysts were not observed in the control (undefended) cell (Fig. 1a). A variety of functions have been suggested for mucocysts in different ciliates some of which, e.g. defence against predators, are still at the hypothesis level while others, e.g. secretion of material for cyst wall production, are supported by compelling evidence (for reviews, see Hausmann 1978, Rosati and Modeo 2003). It is noteworthy that increased rates of encystment have recently been reported in the hypotrich *Euplotes muscorum* when in the presence of certain predators (Fyda *et al.* 2005). This suggests that the mobilization of mucocysts is indeed involved during the predator-induced response in *E. muscorum*. For *C. kleini*, however, there is no evidence of predator-induced cyst formation so the fate of the contents of the mucocysts once it has been exported from the cell, and its role in the defence response, are unknown. One possibility is that once secreted, the mucocyst contents may coat the cell thereby blocking chemical receptor sites on the cell surface thus compromising the *Lembadion* prey recognition system.

A third feature that distinguishes defended cells of *Colpidium kleini* from undefended cells is the expansion of the plasmalemma. In undefended cells the plasmalemma lies in close proximity to the outer and inner alveolar membranes forming the typical three-mem-



Figs 1a-c. *Colpidium kleini*, transmission electron micrographs of cortical regions of defended and undefended cells. **a** - undefended cell. **b** - cell undergoing induced morphological change. Note the mucocysts (arrows) some of which appear to have fused with the cell membrane thus discharging their contents to the outside (arrowheads). **c** - defended cell. Note the expanded plasmalemma (arrows) and localization of mitochondria beneath the pellicle (arrowheads). Scale bars: 1 μm (a); 750 nm (b, c).

brane structure that bounds the ciliate pellicle (Fig. 1a). In transformed cells the plasma membrane is expanded to such an extent that large spaces are formed between it and the outer alveolar membrane (Fig. 1c).

In addition to their assumed protective function, the mucocysts may also play a role in facilitating the shape change that characterizes the defence response in *Colpidium kleini* which involves an increase in cell diameter and therefore an expansion of the cell surface area (Fyda 1998). One mechanism by which this may occur would be if, following fusion of the mucocyst membrane with the plasmalemma, the vacuolar membrane is retained at the cell surface rather than being immediately recycled within the cell. In this way, the mucocysts may provide at least part of the additional membranous material required for the cell expansion to occur. The same process may also allow for the expansion of the plasmalemma shown in Fig. 1c. In his review of protist extrusomes, Hausmann (1978) notes that the fate of the mucocyst membrane following discharge is unknown.

Previous ultrastructural studies of predator-induced defensive morphotypes in ciliates have been restricted to the lateral wings and the dorsal spines that develop in transformed cells of *Euplotes octocarinatus* and *Onychodromus quadricornutus* respectively (Jerka-Dziadosz *et al.* 1987, Wicklow 1997). Both these studies report the appearance of additional microtubules in the sub-pellicular region of the cell, the function of which is thought to be that of supporting the expanding cell cortex. In the case of *Euplotes octocarinatus* there is an increase in the number of microtubular triads on both the dorsal and ventral surfaces of the lateral wings and extra single microtubules between the dorsal triads (Jerka-Dziadosz *et al.* 1987), while in *Onychodromus quadricornutus* bundles of microtubules develop along the axis of the defensive spines (Wicklow 1997). Although no change in the number of cortical microtubules was observed in the present study, unpublished investigations of defended *C. colpoda* cells, i.e. using an antibody directed against acetylated tubulin (TELU 348), have shown that elongation of both the transverse and postciliary microtubules occurs (Iftode, pers. comm.).

Acknowledgements. We would like to thank Lawrence Bannister and John Hopkins (Guy's, King's and St Thomas' School of Biomedical Science, London, UK) for their valuable advice in interpreting the results. This work was funded by the NATO Collaborative Linkage Programme (grant no. CLG 976627).

REFERENCES

- Aufderheide K. J. (1983) Mitochondrial associations with specific components of the cortex of *Tetrahymena thermophila* Nanney & McCoy, 1976: microtubules and epiplasm. *J. Protozool.* **30**: 457-460
- Doyle W. L. (1935) Distribution of mitochondria in the foraminiferan, *Iridia diaphana*. *Science* **81**: 387
- Fauré-Fremiet E. (1910) Étude sur les mitochondries des protozoaires et des cellules sexuelles. *Arch. Anat. Microsc.* **11**: 457-648
- Fyda J. (1998) Predator induced morphological changes in the ciliate *Colpidium* (Protozoa, Ciliophora). *Europ. J. Protistol.* **34**: 111-117
- Fyda J., Warren A., Wolinska J. (2005) An investigation of predator-induced defense responses in ciliated protozoa. *J. Nat. Hist.* **39**: 1431-1442
- Hausmann K. (1978) Extrusive organelles in Protists. *Int. Rev. Cytol.* **52**: 197-276
- Horning E. S. (1927) On the orientation of mitochondria in the surface cytoplasm of infusorians. *Aus. J. Exp. Biol. Med. Sci.* **4**: 187-190
- Jerka-Dziadosz M., Dosche C., Kuhlmann H-W., Heckmann K. (1987) Signal-induced reorganization of the microtubular cytoskeleton in the ciliated protozoan *Euplotes octocarinatus*. *J. Cell. Sci.* **87**: 555-564
- Kennaway G. M., Lewis J. M. (2004) An ultrastructural study of hypnozygotes of *Alexandrium* species (Dinophyceae). *Phycologia* **43**: 353-363
- Kuhlmann H. W., Heckmann K. (1985) Interspecific morphogens regulating prey-predator relationships in Protozoa. *Science* **227**: 1347-1349
- Kuhlmann H. W., Kusch J., Heckmann K. (1999) Predator induced defenses in ciliated protozoa. In: *The Ecology and Evolution of Inducible Defenses*, (Eds. R. Tollrian, C. D. Harvell). Princeton University Press, New Jersey, USA, 142-155
- Paulin J. J. (1996) Morphology and cytology of ciliates. In: *Ciliates: Cells as Organisms*, (Eds K. Hausmann, P. C. Bradbury). Gustav Fischer, Stuttgart, Germany, 1-40
- Rosati G., Modeo L. (2003) Extrusomes in ciliates: diversification, distribution, and phylogenetic implications. *J. Euk. Microbiol.* **50**: 383-402
- Washburn J. O., Gross M. E., Mercer D. R., Anderson J. R. (1988) Predator-induced trophic shift of a free-living ciliate: parasitism of mosquito larvae by their prey. *Science* **240**: 1193-1195
- Wicklow B. J. (1997) Signal-induced defensive phenotypic changes in ciliated protists: morphological and ecological implications for predator and prey. *J. Euk. Microbiol.* **44**: 176-188

Received on 13th September, 2006; revised version on 19th September, 2006; accepted on 26th September, 2006

The Sphagnum Ponds of Simmelried in Germany: A biodiversity Hot-Spot for Microscopic Organisms. Martin Kreutz and Wilhelm Foissner
Protozoological Monographs, Vol. 3, 1-267 2006 © Shaker-Publishers; ISBN 3-8322-2544-7; price 30€

Anyone interested in microscopic organisms, specialist or amateur, will be delighted with this work. The paper by M. Kreutz and W. Foissner is actually an unprecedented album (or "field guide") of microscopic organisms from bacteria through the smallest Metazoa. Of course, protists make up the bulk of the list. Altogether 656 species are presented on 229 beautifully arranged plates of breath-taking micrographs. Apart from the indisputably great aesthetic value, the pictures are very informative. Most images were taken from living specimens using differential interference contrast. Thus the organisms can be seen in their natural shape and colour without any distortion usually caused by fixatives. All possible morphological aspects visible by means of light-microscopy, such as: cilia, surface sculpture, loricas, mucus envelopes, extrusomes and so on, are shown with astonishing precision. In several instances even parasites are presented. Very well reproduced natural colours add to the beauty and to the scientific value of the pictures. The characteristic colour of cytoplasm, symbionts, and food vacuoles, rarely shown in ciliate literature, are all important aspects of taxonomic description. Those who have ever tried to photograph living ciliates or fast moving flagellates will certainly appreciate these pictures. Such astonishing images of moving protozoans could be obtained by using an electronic flash integrated with a special collector providing Köhler illumination. Pictures of living organisms are often accompanied with three-dimensional SEM views. Some plates with ciliates contain in addition bright-field micrographs of silver-impregnated specimens to demonstrate their complex ciliary patterns. The text, except for a short introduction, is reduced to very instructive figure legends. A well organized index makes it easy to find any species by genus or species name.

All the organisms presented in this monograph were found in Simmelried, a three-hectare wetland with six small ponds, located in southern Germany. The ponds were investigated for microscopic organisms from 1994 to 2005. The species documented in the monograph are actually only about two thirds of species recorded at the site. Interestingly, among about 800 protistan species found, the authors recorded at least 100 undescribed species. This monograph is certainly an important contribution to the knowledge on protistan biodiversity, however, it leaves the main controversy unresolved. The astonishing diversity of species recorded at such a restricted area seems to support the "everything is everywhere" hypothesis. On the other hand, the surprisingly large number of undescribed species, even among relatively well known euglenids and chrysophytes, suggests that the total number of protistan species may be vastly underestimated. Also, the apparent absence of some common species in Simmelried ponds, in spite of intense research, indicates that we are far from understanding the mechanisms that control structure of microbial communities.

Krzysztof Wiąckowski
 Kraków

1. Nazwa i adres
2. Data

The following text is a scan of a document, likely a protocol or report, with some text appearing to be mirrored or bleed-through from the reverse side. The text is mostly illegible due to the quality of the scan and the orientation of the page.

Acknowledgement of *Acta Protozoologica* Reviewers, Volume 45

The editors wish to acknowledge the assistance of the following colleagues listed below, who have served as reviewers for one or more manuscripts submitted to be published in Volume 45 of *Acta Protozoologica* in 2006.

Erna Aeschet	Hans J. Lipps
Sabine Agatha	Anna Lundén
Khaled A. S. AL-Rasheid	Pierangelo Luporini
O. Roger Anderson	Denis H. Lynn
Christian C. F. Bardele	Thomas E. E. McQuistion
Linda Basson	Tadeusz Michałowski
Louis Beyens	Edward A. Mitchell
Damer Blake	David J. S. Montagnes
Hubert Blatterer	Alexander P. Mylnikov
Helmut Berger	Celso Vataru Nakamura
Robert Booth	Yasuo Nakaoka
Marta Helena Branquinha de Sá	Charls James Newbold
Reynolds K. Brobey	Hung Nguyen-Viet
Guy Brugerolle	Barbara F. Nowak
Zigui Chen	Jan Pawlowski
Søren Tvorup Christensen	Wolfgang Petz
John C. Clamp	Ewa Przyboś
Annette W. Coleman	Renate Radek
John O. Corliss	Dave Roberts
Angela J. Davis	Sergio Rosati
Johannes F. De Jonckheere	Andre L. Santos
José Fernando Díaz	Peter Satir
Donald W. Duszynski	Martin Schlegel
Florence Dzierszinski	Ariadna Sitja-Bobadilla
Slava S. Epstein	Sergei O. Skarlato
Genoveva F. Esteban	Michael Sleigh
Tom Fenchel	Humphrey Smith
Jeff L. Firkins	André Louis Souza dos Santos
Wilhelm Foissner	Thorsten Stoeck
Sergei I. Fokin	Michaela Strüder-Kypke
Peter Frenzel	Mihoko Takahashi
Jacek Gaertig	Richard G. Titus
Juan Carlos Gutiérrez	Steve J. Upton
Johannes H. P. Hackstein	David Walliker
Klaus Hausmann	Manfred Wanner
Manabu Hori	Bhusita Wannissorn
Kwang W. Jeon	Alan Warren
Svetlana Kisidayova	Rudolf Wegensteiner
Alicja Kurnatowska	Louis M. Weiss
J. I. Ronny Larsson	Krzysztof Wiąckowski
Brian S. Leander	Irena Wita
Won Je Lee	Andre Denis Wright
Vagn Leick	Kuidong Xu

Author Index: Acta Protozoologica 45 (1-4) 2006

- Abdel-Baki A.-A.** see **Ali M. et al.** 97
- Adamus K.** see **Fyda J. et al.** 461
- Agatha S. and Riedel-Lorjé J. C.:** Redescription of *Tintinnopsis cylindrica* Daday, 1887 (Ciliophora: Spirotricha) and unification of tintinnid terminology. 137
- Alen T. A. van** see **Hoek A. H. A. M. van et al.** 215
- Ali M., Abdel-Baki A.-A. and Sakran T.:** *Myxidium elmatboului* n. sp. and *Ceratomyxa ghaffari* n. sp. (Myxozoa: Myxosporae) parasitic in the gallbladder of the Red Sea houndfish *Tylosurus choram* (Rüppell, 1837) (Teleostei: Belonidae) from the Red Sea, Egypt. 97
- AL-Rasheid K.** see **Foissner W.** 1
- AL-Rasheid K.** see **Foissner W. et al.** 323
- Amogan H. P., Martinez J. P., Ciuffetti L. M., Field K. G. and Reno P. W.:** Karyotype and genome size of *Nadelspora canceri* determined by pulsed field gel electrophoresis. 249
- Arndt H.** see **Hausmann K. et al.** 415
- Badewitz H.-J.** see **Meisterfeld R.** 167
- Bandyopadhyay P. K.** see **Mitra A. K.** 289
- Benedikt V.** see **Hauptmanová K. et al.** 105
- Beyens L.** see **Vincke S. et al.** 65, 395
- Borgohain P.** see **Naqvi I. et al.** 53
- Brugerolle G.:** Description of a new freshwater heterotrophic flagellate *Sulcomonas lacustris* affiliated to the collodictyonids. 175
- Cebrián J. A.** see **de la Fuente G. et al.** 225
- Cicarelli R. M. B.** see **Manzine L. R. et al.** 367
- Ciuffetti L. M.** see **Amogan H. P. et al.** 249
- Cortez D. A. G.** see **Pedroso R. B. et al.** 231
- Cortez L. E. R.** see **Pedroso R. B. et al.** 231
- Csaba G.** see **Kovács P.** 205
- Csaba G., Kovács P. and Pállinger É.:** Comparison of the amount and demonstrability of endogeneous hormones and bound insulin after paraformaldehyde and EDAC fixation in *Tetrahymena*. 455
- Da Silva M. T. A.** see **Manzine L. R. et al.** 367
- De Jonckheere J. F.:** Isolation and molecular identification of Vahlkampfiid amoebae from an Island (Tenerife, Spain). 91
- De la Fuente G., Pérez-Quintana M., Cebrián J. A. and Fondevila M.:** Preliminary study on the effect of exposure to low temperature on the viability of both mixed and monocultures of rumen protozoa. 225
- Dias Filho B. P.** see **Pedroso R. B. et al.** 231
- Esteban G. F.:** Book review "Antarctic marine protists" edited by Fiona J. Scott and Harvey J. Marchant 211
- Field K. G.** see **Amogan H. P. et al.** 249
- Foissner W. and AL-Rasheid K.:** A unified organization of the Stichotrichine oral apparatus, including a description of the buccal seal (Ciliophora: Spirotrichea). 1
- Foissner W.:** Biogeography and dispersal of microorganisms: A review emphasizing protists. 111
- Foissner W., Pichler M., AL-Rasheid K. and Weisse T.:** The unusual, lepidosome-coated resting cyst of *Meseres corlissi* (Ciliophora: Oligotrichea): encystment and genesis and release of the lepidosomes. 323
- Foissner W. and Pichler M.:** The unusual, lepidosome-coated resting cyst of *Meseres corlissi* (Ciliophora: Oligotrichea): genesis of four complex types of wall precursors and assemblage of the cyst wall. 339
- Fondevila M.** see **de la Fuente G. et al.** 225
- Fyda J., Kennaway G., Adamus K. and Warren A.:** Ultrastructural events in the predator-induced defence response of *Colpidium kleini* (Ciliophora: Hymenostomatia). 461
- Golemansky V. and Todorov M.:** New data to the shell ultrastructure and the biometry of the marine interstitial testate amoebae (Rhizopoda: Testaceafilosia). 301
- Gong J. and Song W.:** Redescriptions of three cyrtophorid ciliates from marine biofilm, with estab-

- lishment of a new genus, *Wilbertella* nov. gen. (Ciliophora: Cytrophorida: Lynchellidae). 153
- Greczek-Stachura M.** see **Tarcz S. et al.** 255
- Gremmen N.** see **Vincke S. et al.** 65
- Gupta R.** see **Naqvi I. et al.** 53
- Hackstein J. H. P.** see **Hoek A. H. A. M. van et al.** 215
- Hájek M.** see **Opravilová V.** 191
- Hauptmanová K., Benedikt V. and Literák I.:** Blood parasites in passerine birds in Slovakian East Carpathians. 105
- Hausmann K., Selchow P., Scheckenbach F., Weitere M. and Arndt H.:** Cryptic species in a morphospecies complex of heterotrophic flagellates: the case study of *Caecitellus* spp. 415
- Hayashi S.** see **Hoshina R. et al.** 377
- Hoek A. H. A. M. van, Alen T. A. van, Vogels G. D. and Hackstein J. H. P.:** Contribution by the methanogenic endosymbionts of anaerobic ciliates to methane production in Dutch freshwater sediments. 215
- Hoshina R., Hayashi S. and Imamura N.:** Intraspecific genetic divergence of *Paramecium bursaria* and re-construction of the paramecian phylogenetic tree. 377
- Hu X. and Suzuki T.:** Observation on a Japanese population of *Pseudoamphisiella alveolata* (Kahl, 1932) Song et Warren, 2000 (Ciliophora: Hypotrichida): morphology and morphogenesis. 41
- Hu X.** see **Song W. et al.** 271
- Imamura N.** see **Hoshina R. et al.** 377
- Ji D., Song W. and Warren A.:** Redescriptions of three marine peritrichous ciliates, *Zoothamnium alternans* Claparède et Lachmann, 1859, *Z. sinense* Song, 1991 and *Z. commune* Kahl, 1933 (Ciliophora: Peritrichia), from North China. 27
- Jin L.-P.** see **Liu X.-Y. et al.** 241
- Jirků M. and Modrý D.:** *Eimeria terraepokotorum* n. sp. (Apicomplexa: Eimeriidae) from *Hoplobatrachus occipitalis* (Anura: Ranidae) from Kenya. 443
- Kennaway G.** see **Fyda J. et al.** 461
- Kłopocka W., Wierzbicka K., Pomorski P., Krzemiński P. and Wasik A.:** Cofilin-like protein influences the motility of *Amoeba proteus*. 449
- Kocik E., Sobczak M. and Rędownicz M. J.:** Codon usage in *Amoeba proteus* significantly differs from *Entamoeba histolytica* and *Acanthamoeba castellanii*. 313
- Kovács P. and Csaba G.:** Tubulin is not posttranslationally modified (acetylated or polyglutamylated) in *Tetrahymena* macronucleus. 205
- Kovács P.** see **Csaba G. et al.** 455
- Krzemiński P.** see **Kłopocka W. et al.** 449
- Kuźnicki L.** see **Sikora J.** 317
- Kuźnicki L.** see **Sikora J.** 319
- Lahr D. J. G. and Lopes S. G. B. C.:** Morphology, biometry, ecology and biogeography of five species of *Diffugia* Leclerc, 1815 (Arcellinida: Diffugiidae), from Tiete River, Brazil. 77
- Lee K.-L. D.** see **Liu X.-Y. et al.** 241
- Li L. and Song W.:** Phylogenetic positions of two cryptophorid ciliates, *Dysteria procera* and *Hartmannula derouxii* (Ciliophora: Phyllopharyngea: Dysteriida) inferred from the complete small subunit ribosomal RNA gene sequences. 265
- Li L.** see **Song W. et al.** 271
- Lin X.** see **Xu D. et al.** 433
- Literák I.** see **Hauptmanová K. et al.** 105
- Liu X.-Y., Lee K.-L. D., Mao Y.-Z., Jin L.-P.:** Isolation, characterization and phylogenetic analysis of the cytochrome *b* gene (*Cyb*) from the hypotrichous ciliate *Pseudourostyla cristata*. 241
- Lopes S. G. B. C.** see **Lahr D. J. G.** 77
- Ma H.** see **Song W. et al.** 271
- Maciejewska A.:** Sibling species within *Paramecium jenningsi* revealed by PCR-RFLP. 387
- Manzine L. R., Da Silva M. T. A., Thiemann O. H. and Cicarelli R. M. B.:** Molecular characterization of *Blastocrithidia culicis* L17 ribosomal protein. 367
- Mao Y.-Z.** see **Liu X.-Y. et al.** 241
- Martinez J. P.** see **Amogan H. P. et al.** 249

- Meisterfeld R. and Badewitz H.-J.:** A redescription of *Amphizonella violacea* (Amoebozoa: Arcellinida). 167
- Mitra A. K. and Bandyopadhyay P. K.:** *Trichodina haldari* n. sp. and *Paratrachodina bassonae* n. sp. (Ciliophora: Peritrichida) from Indian fresh water fishes. 289
- Modrý D.** see Šíroký P. 183
- Modrý D.** see Jirků M. 443
- Morgado-Díaz J. A.** see Pedroso R. B. *et al.* 231
- Nakamura C. V.** see Pedroso R. B. *et al.* 231
- Naqvi I., Gupta R., Borgohain P. and Sapra G. R.:** Morphology and morphogenesis of *Rubrioxystrixa indica* n. sp. (Ciliophora: Hypotrichida). 53
- Nicholls K. H.:** *Cryptodifflugia leachi* n. sp., a minute new testate rhizopod species (Rhizopoda: Phryganellina). 295
- Nijs I.** see Vincke S. *et al.* 395
- Opravilová V. and Hájek M.:** The variation of testacean assemblages (Rhizopoda) along the complete base-richness gradient in fens: A case study from the Western Carpathians. 191
- Pállinger É.** see Csaba G. *et al.* 455
- Pedroso R. B., Ueda-Nakamura T., Dias Filho B. P., Cortez D. A. G., Cortez L. E. R., Morgado-Díaz J. A. and Nakamura C. V.:** Biological activities of essential oil obtained from *Cymbopogon citratus* on *Crithidia deanei*. 231
- Pérez-Quintana M.** see de la Fuente G. *et al.* 225
- Pichler M.** see Foissner W. 339
- Pichler M.** see Foissner W. *et al.* 323
- Pomorski P.** see Kłopotka W. *et al.* 449
- Prajer M.** see Tarcz S. *et al.* 255
- Przyboś E.** see Tarcz S. *et al.* 255
- Rędowicz M. J.** see Kocik E. *et al.* 313
- Reno P. W.** see Amogan H. P. *et al.* 249
- Riedel-Lorjé J. C.** see Agatha S. 137
- Roberts D.** see Song W. *et al.* 271
- Sakran T.** see Ali M. *et al.* 97
- Sapra G. R.** see Naqvi I. *et al.* 53
- Scheckenbach F.** see Hausmann K. *et al.* 415
- Selchow P.** see Hausmann K. *et al.* 415
- Sikora J. and Kuźnicki L.:** Book received „Festschrift 25 Jahre Deutsche Gesellschaft für Protozoologie” by Klaus Hausmann and Renate Radek. 317
- Sikora J. and Kuźnicki L.:** Acta Protozoologica 1963-2006. 319
- Šíroký P. and Modrý D.:** Two eimerian coccidia (Apicomplexa: Eimeriidae) from the critically endangered Arakan Forest Turtle *Heosemys depressa* (Testudines: Geoemydidae), with description of *Eimeria arakanensis* n. sp. 183
- Smith H. G.** see Wilkinson D. M. 407
- Sobczak M.** see Kocik E. *et al.* 313
- Song W.** see Xu D. 17
- Song W.** see Ji D. *et al.* 27
- Song W.** see Gong J. 153
- Song W.** see Li L. 265
- Song W., Warren A., Roberts D., Wilbert N., Li L., Sun P., Hu X. and Ma H.:** Comparison and redefinition of four marine, coloured *Pseudokeronopsis* spp. (Ciliophora: Hypotrichida), with emphasis on their living morphology. 271
- Song W.** see Xu D. *et al.* 433
- Sun P.** see Song W. *et al.* 271
- Suzuki T.** see Hu X. 41
- Tarcz S., Przyboś E., Prajer M. and Greczek-Stachura M.:** Intraspecific variation of diagnostic rDNA genes in *Paramecium dodecaurelia*, *P. tredecaurelia* and *P. quadecaurelia* (Ciliophora: Oligohymenophorea). 255
- Thiemann O. H.** see Manzine L. R. *et al.* 367
- Todorov M.** see Golemansky V. 301
- Ueda-Nakamura T.** see Pedroso R. B. *et al.* 231
- Van De Vijver B.** see Vincke S. *et al.* 65, 395
- Vincke S., Van de Vijver B., Gremmen N. and Beyens L.:** The moss dwelling testacean fauna of the Strømness Bay (South Georgia). 65

- Vincke S., Van De Vijver B., Nijs I. and Beyens L.:** Changes in the testacean community structure along small soil profiles. 395
- Vogels G. D. see Hoek A. H. A. M. van et al.** 215
- Warren A.:** see **Ji D. et al.** 27
- Warren A. see Song W. et al.** 271
- Warren A. see Xu D. et al.** 433
- Warren A. see Fyda J. et al.** 461
- Wasik A. see Kłopocka W. et al.** 449
- Weisse T. see Foissner W. et al.** 323
- Weitere M. see Hausmann K. et al.** 415
- Wiąckowski K.:** Book review of "The sphagnum ponds of Simmelried in Germany: A biodiversity hot-spot for microscopic organisms" by Martin Kreutz and Wilhelm Foissner. 465
- Wierzbicka K. see Kłopocka W. et al.** 449
- Wilbert N. see Song W. et al.** 271
- Wilkinson D. M. and Smith H. G.:** An initial account of the terrestrial Protozoa of Ascension Island. 407
- Xu D. and Song W.:** Hapantotypification and morphological redescription of the marine planktonic ciliate, *Spirostrombidium cinctum* (Kahl, 1932) Petz, Song et Wilbert, 1995 (Ciliophora: Oligotrichida). 17
- Xu D., Song W., Lin X. and Warren A.:** On two marine oligotrich ciliates, *Spirostrombidium agathae* n. sp. and *S. schizostomum* (Kahl, 1932) n. comb. from China, with a key to the identification of seven well-characterized *Spirostrombidium* spp. (Ciliophora: Oligotrichida). 433

Subject Index: Acta Protozoologica 45 (1-4) 2006

Acta Protozoologica 1963-2006 319

Amoeba proteus

- codon usage analysis 313
- cofilin-like protein 449

Amphibia parasite - *Eimeria terraepokotorum* n. sp. 443

Amphizonella violacea

- ecology 167
- morphology 167
- redescription 167

Anaerobic ciliates

- methanogenic endosymbiont 215
- phylogenetic relationship 215
- seasonal variations 215

Apicomplexa 105, 183, 231, 367, 443

Bacteria

- biogeography 111
- dispersal 111

Biogeography of

- bacteria 111
- chrysophytes 111
- ciliates 111
- dinoflagellates 111
- microfungi 111
- testate amoebae 65, 77, 111, 191

- *Tintinnopsis cylindrica* 137

Bird (East Carpathian) blood parasite

- *Haemoproteus* spp. 105
- *Leucocytozoon* spp. 105
- list of species 105
- *Plasmodium* spp. 105
- *Trypanosoma* spp. 105

Blastocrithidia culicis L17 ribosomal protein

- molecular characterization 367
 - phylogenetic analysis 367
- Book review 211, 317, 465

Caecitellus

- complex 415
- *paraparvulus* n. sp.
 - morphology 415
 - ultrastructure 415
- SSU rDNA 415
- *pseudoparvulus* n. sp.
 - morphology 415
 - ultrastructure 415
 - SSU rDNA 415
- taxonomic diagnosis 415

Ceratomyxa ghaffari n. sp.

- fish parasite 97
- morphology 97

Chardezia caudata

- morphology 301
- morphometry 301

Chlamydonella

- *derouxi*
 - infraciliature 153
 - morphology 153
 - morphometry 153
 - redescription 153
- *pseudochilodon*
 - infraciliature 153
 - morphology 153
 - morphometry 153

- redescription 153
- Chlamydonellopsis calkinsi*
- infraciliature 153
- morphology 153
- morphometry 153
- redescription 153
- Chromosome-size polymorphism in *Nadelspora canceri* 249
- Chrysophytes
- biogeography 111
- dispersal 111
- Ciliates
- anaerobic see Anaerobic ciliates
- biogeography 111
- dispersal 111
- Ciliophora 1, 17, 27, 41, 53, 111, 137, 153, 205, 241, 255, 265, 271, 289, 323, 339, 377, 387, 433, 461
- Cladistic analysis see Methods
- Codon usage analysis in *Amoeba proteus* 313
- Cofilin-like protein of *Amoeba proteus* 449
- Colpidium kleini*
- morphological transformation 461
- mucocys 461
- ultrastructure 461
- Community analysis of testate amoebae 67, 191, 395
- Cortex reorganization *Meseres corlissi* 339
- Corythionella*
- *minima*
- morphology 301
- morphometry 301
- *pontica*
- morphology 301
- morphometry 301
- Crithidia deanei* - insect parasite
- effect of oil from *Cymbopogon citratus* 231
- ultrastructure 231
- viability 231
- Crustacean parasite *Nadelspora canceri* 249
- Cryptodifflugia leachi* n. sp. morphology 295
- Cymbopogon citratus* oil - antiprotozoan activity 231
- Cyst of
- *Meseres corlissi*
- wall precursors genesis 339
- lepidosomes 323, 339
- phylogenetic analysis 339
- *Naegleria*
- *canariensis* n. sp. 91
- *tenerifensis* n. sp. 91
- *Vahlkampfia*
- *ciguana* n. sp. 91
- *orchilla* n. sp. 91
- Cytochrome B gene (*Cyb*) of *Pseudourostyla cristata*
- amino acid sequence 241
- phylogenetic analysis 241
- Difflugia*
- *claviformis*
- biogeography 77
- ecology 77
- morphology 77
- morphometry 77
- *corona*
- biogeography 77
- ecology 77
- morphology 77
- morphometry 77
- *gigantea*
- biogeography 77
- ecology 77
- morphology 77

- morphometry 77
- *gramen*
- biogeography 77
- morphometry 77
- ecology 77
- morphology 77
- *lanceolata*
- biogeography 77
- ecology 77
- morphology 77
- morphometry 77
- Dinoflagellates
- biogeography 111
- dispersal 111
- Dispersal of
- bacteria 111
- ciliates 111
- chrysophytes 111
- dinoflagellates 111
- microfungi 111
- testate amoebae 111
- Dysteria procera* - SSU rRNA nucleotide sequence 265
- Ecology of
- testate amoebae 65, 77, 167, 191
- *Tintinnopsis cylindrica* 137
- Effect of
- low temperature on rumen protozoa viability 225
- oil from *Cymbopogon citratus* on *Crithidia deanei* 231
- Eimeria*
- *arakanensis* n. sp. - reptiles parasite 183
- cf. *mitraria*
- list of hosts 183
- reptiles parasite 183
- *terraepokotorum* n. sp. - amphibia parasite 443
- Endocytosis of *Meseres corlissi* 339
- Exocytosis of *Meseres corlissi* 323, 339
- Fish parasite
- *Ceratomyxa ghaffari* n. sp. 97
- *Myxidium elmatboulii* n. sp. 97
- *Paratrichodina bassonae* n. sp. 289
- *Trichodina haldari* n. sp. 289
- Genetic divergence of *Paramecium bursaria* 377
- Genesis of *Meseres corlissi* cyst
- lepidosomes 323
- cyst wall precursors 339
- Haemoproteus* spp. bird blood parasite 105
- Hartmannula derouxi* - SSU rRNA nucleotide sequence 265
- Hormones in *Tetrahymena pyriformis* 455
- Infraciliature of
- *Chlamydonella*
- *pseudochilodon* 153
- *derouxi* 153
- *Chlamydonellopsis calkinsi* 153
- *Pseudoamphisiella alveolata* 41
- *Pseudokeronopsis*
- *carnea* 271
- *flava* 271
- *flavicans* 271
- *rubra* 271
- *Rubrioxytricha indica* n. sp. 53
- Spirostrombidium*
- *cinctum* 17

- *agathae* n. sp. 433
- *schizostomum* n. comb. 433
- *Tintinnopsis cylindrica* 137
- *Zoothamnium*
 - *alternans* 27
 - *commune* 27
 - *sinense* 27
- Insect parasite *Crithidia deanei* 231
- Isolation of cytochrome B gene (*Cyb*) from *Pseudourostyla cristata* 241
- Karyotype of *Nadelspora canceri*** 249
- Key of**
 - *Pseudokeronopsis* spp. 271
 - *Spirostrombidium* spp. 433
- L17 ribosomal protein from *Blastocrithidia culicis***
 - molecular characterization 367
 - phylogenetic analysis 367
- Lepidosomes of *Meseres corlissi* 323, 339
- Leucocytozoon* spp. bird blood parasite 105
- Light microscope see Methods
- List of
 - East Carpathian bird's blood parasites 105
 - hosts of
 - blood parasites 105
 - *Eimeria mitraria* 183
 - testate amoebae species 65, 191
- Low temperature effect on rumen protozoa 225
- LSU rRNA gene sequences
 - intraspecific polymorphism of *Paramecium*
 - *dodecaurelia* 255
 - *tredecaurelia* 255
 - *quadecaurelia* 255
 - phylogenetic analysis of *Paramecium*
 - *dodecaurelia* 255
 - *tredecaurelia* 255
 - *quadecaurelia* 255
- Macronucleus tubulin in *Tetrahymena pyriformis*** 205
- Mastigophora 105, 175, 415
- Meseres corlissi*
 - cortex reorganization 339
 - cyst
 - wall precursors genesis 339
 - phylogenetic analysis 339
 - endocytosis 339
 - exocytosis 323, 339
 - lepidosomes 323, 339
- Methanogenic endosymbiont of
 - anaerobic ciliates 215
 - methanogenesis 215
 - phylogenetic relationship 215
- Methods**
 - cladistic analysis 65, 111, 215, 241, 255, 265, 367
 - fluorescence microscope 205, 215, 449, 455
 - light microscope 17, 27, 41, 53, 77, 91, 97, 137, 153, 167, 175, 183, 215, 225, 231, 271, 289, 295, 301, 415
 - PCR analysis 91, 215, 241, 255, 265, 271, 367, 387, 415
 - protargol impregnation 1, 17, 27, 41, 53, 137, 153, 271, 323, 339, 433
 - scanning electron microscope 1, 77, 137, 167, 301, 415
 - silver nitrate method 27, 153
 - transmission electron microscope 175, 231, 323, 339, 415, 461
- Micramphora pontica*
 - morphology 301
 - morphometry 301
- Microfungi**
 - biogeography 111
 - dispersal 111

Microsporidia 249

Morphogenesis of

- *Pseudoamphisiella alveolata* 41
- *Rubrioxytricha indica* n. sp. 53

Morphology of

- *Amphizonella violacea* 167
- *Caecitellus*
 - *paraparvulus* n. sp. 415
 - *pseudoparvulus* n. sp. 415
- *Ceratomyxa ghaffari* n. sp. 97
- *Chlamydonella*
 - *pseudochilodon* 153
 - *derouxi* 153
- *Chlamydonellopsis calkinsi* 153
- *Colpidium kleini* 461
- *Cryptodifflugia leachi* n. sp. 295
- cyst of
 - *Naegleria canariensis* n. sp. 91
 - *Naegleria tenerifensis* n. sp. 91
 - *Vahlkampfia ciguana* n. sp. 91
 - *Vahlkampfia orchilla* n. sp. 91
- *Eimeria*
 - *arakanensis* n. sp. 183
 - cf. *mitraria* 183
 - *terraepokotorum* n. sp. 443
- *Myxidium elmatboului* n. sp. 97
- *Paratrachodina bassonae* n. sp. 289
- *Pseudoamphisiella alveolata* 41
- *Pseudokeronopsis*
 - *carnea* 271
 - *flava* 271
 - *flavicans* 271
 - *rubra* 271
- *Rubrioxytricha indica* n. sp. 53
- *Spirostrombidium*

-- *cinctum* 17-- *agathae* n. sp. 433-- *schizostomum* n. comb 433

- stichotrichine oral apparatus 1

- *Sulcomonas lacustris* n. sp. 175

- testate amoebae 77, 295, 301

- *Tintinnopsis cylindrica* 137- *Trichodina haldari* n. sp. 289- *Zoothamnium*-- *alternans* 27-- *commune* 27-- *sinense* 27

Morphometry of

- *Chlamydonella*-- *pseudochilodon* 153-- *derouxi* 153- *Chlamydonellopsis calkinsi* 153- *Paratrachodina bassonae* n. sp. 289- *Pseudoamphisiella alveolata* 41- *Pseudokeronopsis*-- *carnea* 271-- *flava* 271-- *flavicans* 271-- *rubra* 271- *Rubrioxytricha indica* n. sp. 53- *Spirostrombidium cinctum* 17

- testate amoebae 77, 301

- *Tintinnopsis cylindrica* 137- *Trichodina haldari* n. sp. 289- *Zoothamnium*-- *alternans* 27-- *commune* 27-- *sinense* 27Mucocyst of *Colpidium kleini* 461*Myxidium elmatboului* n. sp.

- fish parasite 97
- morphology 97
- Myxozoa 97
- Nadelspora cancri* - crustacean parasite
- chromosome-size polymorphism 249
- karyotype 249
- Naegleria*
- *canariensis* n. sp.
- cyst morphology 91
- rDNA sequences 91
- *tenerifensis* n. sp.
- cyst morphology 91
- rDNA sequences 91
- New combination *Spirostrombidium schizostomum* 433
- New genus
- *Sulcomonas* 175
- *Wilbertella* 153
- New species
- *Caecitellus*
- *paraparvulus* 415
- *pseudoparvulus* 415
- *Ceratomyxa ghaffari* 97
- *Cryptodifflugia leachi* 295
- *Eimeria*
- *arakanensis* 183
- *terraepokotorum* 443
- *Myxidium elmatboulia* 97
- *Naegleria*
- *canariensis* 91
- *tenerifensis* 91
- *Paratrichodina bassonae* 289
- *Rubrioxytricha indica* 53
- *Spirostrombidium agathae* 433
- *Sulcomonas lacustris* 175
- *Trichodina haldari* 289
- *Vahlkampfia*
- *ciguana* 91
- *orchilla* 91
- Ontogenesis of *Tintinnopsis cylindrica* 137
- Oral apparatus morphology of stichotrichine 1
- Paramecium**
- *bursaria*
- genetic divergence 377
- phylogenetic analysis 377
- *jenningsi* sibling species 387
- LSU rRNA intraspecific polymorphism
- *dodecaurelia* - phylogenetic analysis 255
- *quadecaurelia* - phylogenetic analysis 255
- *tredecaurelia* - phylogenetic analysis 255
- SSU rRNA intraspecific polymorphism
- *dodecaurelia* - phylogenetic analysis 255
- *quadecaurelia* - phylogenetic analysis 255
- *tredecaurelia* - phylogenetic analysis 255
- Parasite of
- amphibia see Amphibia parasite
- bird blood see Bird blood parasite
- crustacea see Crustacea parasite
- fish see Fish parasite
- insect see Insect parasite
- reptiles see Reptiles parasite
- Paratrichodina bassonae* n. sp. - fish parasite
- morphology 289
- morphometry 289
- PCR analysis see Methods
- Phylogenetic analysis of
- anaerobic ciliates 215
- base on cytochrome B gene sequence 241

- halteriine spirotrichs 339
- L17 ribosomal protein of Trypanosomatidae 367
- methanogenic endosymbiont 215
- paramecian 255, 377
- phyllopharyngean ciliates 265
- vahlkampfiid amoebae 91
- Plasmodium* spp. bird blood parasite 105
- Polymorphism
 - LSU rRNA in *Paramecium* species 255
 - of chromosome size of *Nadelspora canceri* 249
 - SSU rRNA in *Paramecium* species 255
- Protargol impregnation see Methods
- Psammonobiotus*
 - *balticus*
 - morphology 301
 - morphometry 301
 - *golemanskyi*
 - morphology 301
 - morphometry 301
- Pseudoamphisiella alveolata*
 - infraciliature 41
 - morphogenesis 41
 - morphology 41
 - morphometry 41
- Pseudokeronopsis*
 - *carnea*
 - infraciliature 271
 - morphology 271
 - morphometry 271
 - *flava*
 - infraciliature 271
 - morphology 271
 - morphometry 271
 - *flavicans*
 - infraciliature 271
 - morphology 271
 - morphometry 271
 - *rubra*
 - morphology 271
 - morphometry 271
 - key 271
 - *rubra*
 - infraciliature 271
 - morphology 271
 - morphometry 271
 - Pseudourostyla cristata* cytochrome B gene (*Cyb*)
 - amino acid sequence 241
 - phylogenetic analysis 241
- rDNA sequences analysis of
 - *Caecitellus*
 - *paraparvulus* n. sp. 415
 - *pseudoparvulus* n. sp. 415
 - *Naegleria*
 - *canariensis* n. sp. 91
 - *tenerifensis* n. sp. 91
 - *Paramecium bursaria* 377
 - *Vahlkampfia*
 - *ciguana* n. sp. 91
 - *orchilla* n. sp. 91
- Redefinition of *Pseudokeronopsis* species 271
- Redescription of
 - *Amphizonella violacea* 167
 - *Chlamydonella*
 - *pseudochilodon* 153
 - *derouxi* 153
 - *Chlamydonellopsis calkinsi* 153
 - *Spirostrombidium cinctum* 17
 - *Tintinnopsis cylindrica* 137
 - *Zoothamnium*
 - *alternans* 27
 - *commune* 27
 - *sinense* 27

- Reptiles parasite
- *Eimeria*
 - *arakanensis* n. sp. 183
 - cf. *mitraria* 183
- Rhizopoda 65, 77, 91, 111, 167, 191, 295, 301, 313, 395, 449
- Ribosomal protein, L17 from *Blastocrithidia culicis*
- molecular characterization 367
 - phylogenetic analysis 367
- Rubrioxysticha indica* n. sp.
- infraciliature 53
 - morphogenesis 53
 - morphology 53
 - morphometry 53
- Rumen protozoa - effect of low temperature on viability 225
- Seasonal variations in anaerobic ciliates 215
- Scanning electron microscope see Methods
- Sibling species of *Paramecium jenningsi* 387
- Silver nitrate method see Methods
- Spirostrombidium*
- *agathae* n. sp.
 - infraciliature 433
 - morphology 433
 - *cinctum*
 - infraciliature 17
 - morphology 17
 - morphometry 17
 - redescription 17
 - *schizostomum* n. comb.
 - infraciliature 433
 - morphology 433
- SSU rRNA gene sequences
- intraspecific polymorphism of *Paramecium*
 - *dodecaurelia* 255
 - *tredecaurelia* 255
 - *quadecaurelia* 255
 - phylogenetic analysis of *Paramecium*
 - *dodecaurelia* 255
 - *tredecaurelia* 255
 - *quadecaurelia* 255
- Stichotrichine oral apparatus morphology 1
- Sulcomonas* n. gen. 175
- Sulcomonas lacustris* n. sp.
- morphology 175
 - ultrastructure 175
- Taxonomic diagnosis of
- *Caecitellus*
 - *paraparvulus* n. sp. 415
 - *pseudoparvulus* n. sp. 415
 - Strombidiidae 433
- Terrestrial protozoa of Ascension Island 407
- Testate amoebae
- *Amphizonella violacea* redescription 167
 - biogeography 65, 77, 111, 191
 - community analysis 67, 191, 395
 - *Cryptodifflugia leachi* n. sp. 295
 - ecology
 - *Amphizonella violacea* 167
 - Antarctic 65, 395
 - Brazilian 77
 - West Carpathian 191
 - dispersal 111
 - list of species 65, 191
 - morphology 77, 167, 295, 301
 - morphometry 77, 301
- Tetrahymena pyriformis*
- macronucleus tubulin 205

- endogeneous hormones 455
- Tintinnopsis cylindrica*
- biogeography 137
- ecology 137
- morphology 137
- morphometry 137
- ontogenesis 137
- redescription 137
- Transmission electron microscope see Methods
- Trichodina haldari* n. sp. - fish parasite
- morphology 289
- morphometry 289
- Trypanosoma* spp. bird blood parasite 105
- Tubulin in *Tetrahymena pyriformis* macronucleus 205

- Ultrastructure of
- *Caecitellus*
- *paraparvulus* n. sp. 415
- *pseudoparvulus* n. sp. 415
- *Colpidium kleini* 461
- *Crithidia deanei* 231
- *Meseres corlissi* 323, 339
- *Sulcomonas lacustris* n. sp. 175

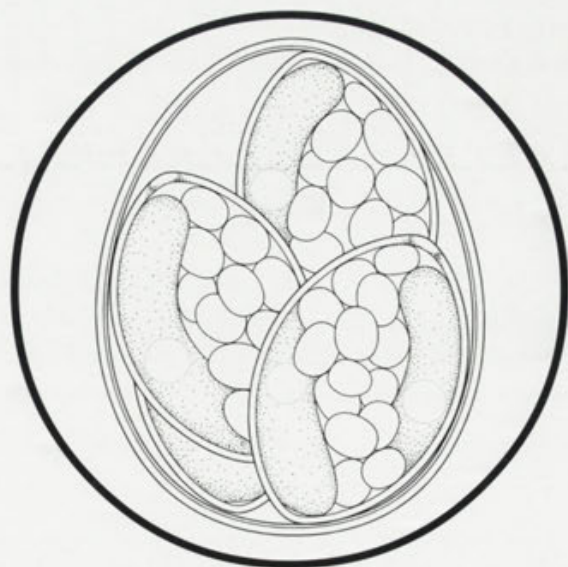
- Vahlkampfia*
- *ciguana* n. sp.
- cyst morphology 91
- rDNA sequences 91
- *orchilla* n. sp.
- cyst morphology 91
- rDNA sequences 91
- Vahlkampfiid amoebae phylogenetic analysis 91
- Viability of
- *Crithidia deanei* - oil effect 231
- rumen protozoa low - temperature effect 225

- Wilbertella* n. gen. 153

- Zoothamnium*
- *alternans*
- infraciliature 27
- morphology 27
- morphometry 27
- redescription 27
- *commune*
- infraciliature 27
- morphology 27
- morphometry 27
- redescription 27
- *sinense*
- infraciliature 27
- morphology 27
- morphometry 27
- redescription 27

ACTA

PROTOZOOLOGICA



NENCKI INSTITUTE OF EXPERIMENTAL BIOLOGY

WARSAW, POLAND

<http://rcin.org.pl>

2006

VOLUME 45

ISSN 0065-1583

Polish Academy of Sciences
Nencki Institute of Experimental Biology
and
Polish Society of Cell Biology

ACTA PROTOZOOLOGICA
International Journal on Protistology

Editor in Chief Jerzy SIKORA

Editors Hanna FABCZAK and Anna WASIK

Managing Editor Małgorzata WORONOWICZ-RYMASZEWSKA

Editorial Board

Christian F. BARDELE, Tübingen

Linda BASSON, Bloemfontein

Louis BEYENS, Antwerpen

Helmut BERGER, Salzburg

Jean COHEN, Gif-Sur-Yvette

John O. CORLISS, Bala Cynwyd

György CSABA, Budapest

Johan F. De JONCKHEERE, Brussels

Isabelle DESPORTES-LIVAGE, Paris

Genoveva F. ESTEBAN, Dorset

Tom FENCHEL, Helsingør

Wilhelm FOISSNER, Salzburg

Jacek GAERTIG, Athens (USA)

Vassil GOLEMANSKY, Sofia

Andrzej GRĘBECKI, Warszawa, *Vice-Chairman*

Lucyna GRĘBECKA, Warszawa

Donat-Peter HÄDER, Erlangen

Janina KACZANOWSKA, Warszawa

Stanisław L. KAZUBSKI, Warszawa

Leszek KUŹNICKI, Warszawa, *Chairman*

J. I. Ronny LARSSON, Lund

John J. LEE, New York

Jiří LOM, České Budějovice

Pierangelo LUPORINI, Camerino

Kálmán MOLNÁR, Budapest

David J. S. MONTAGNES, Liverpool

Jytte R. NILSSON, Copenhagen

Eduardo ORIAS, Santa Barbara

Sarah L. POYNTON, Baltimore, Berlin

Sergei O. SKARLATO, St. Petersburg

Michael SLEIGH, Southampton

Jiří VÁVRA, Praha

ACTA PROTOZOOLOGICA appears quarterly.

The price (including Air Mail postage) of subscription to *Acta Protozoologica* at 2007 is: 200.- € by institutions and 120.- € by individual subscribers. For the matters regarding subscription of the *Acta Protozoologica*, please contact Editor Elect Dr Krzysztof WIACKOWSKI, Institute of Environmental Sciences, Jagiellonian University, Gronostajowa7, 30-387 Kraków, Poland; E-mail: wiacko@eko.uj.edu.pl; phone: +48 12 664 51 21

Front cover: Jirků M. and Modrý D. (2005) *Eimeria fragilis* and *E. wambaensis*, two new species of *Eimeria* Schneider (Apicomplexa: Eimeriidae) from African anurans. *Acta Protozool.* **44**: 167-173

©Nencki Institute of Experimental Biology
Polish Academy of Sciences
This publication is supported by the Ministry of Science and
Higher Education

Desktop processing: Justyna Osmulka, Information Technology
Unit of the Nencki Institute
Printed at the MARBIS, ul. Poniatowskiego 1
05-070 Sulejówek, Poland

<http://rcin.org.pl>

Contents of Volume 45 (1-4) 2006

Number 1

W. Foissner and K. AL-Rasheid: A unified organization of the Stichotrichine oral apparatus, including a description of the buccal seal (Ciliophora: Spirotrichea). 1

D. Xu and W. Song: Hapantotypification and morphological redescription of the marine planktonic ciliate, *Spirostrombidium cinctum* (Kahl, 1932) Petz, Song *et* Wilbert, 1995 (Ciliophora: Oligotrichida). 17

D. Ji, W. Song and A. Warren: Redescriptions of three marine peritrichous ciliates, *Zoothamnium alternans* Claparède *et* Lachmann, 1859, *Z. sinense* Song, 1991 and *Z. commune* Kahl, 1933 (Ciliophora: Peritrichia), from North China. 27

X. Hu and T. Suzuki: Observation on a Japanese population of *Pseudoamphisiella alveolata* (Kahl, 1932) Song *et* Warren, 2000 (Ciliophora: Hypotrichida): morphology and morphogenesis. 41

I. Naqvi, R. Gupta, P. Borgohain and G. R. Sapra: Morphology and morphogenesis of *Rubrioxytiricha indica* n. sp. (Ciliophora: Hypotrichida). 53

S. Vincke, B. Van De Vijver, N. Gremmen and L. Beyens: The moss dwelling testacean fauna of the Strømness Bay (South Georgia). 65

D. J. G. Lahr and S. G. B. C. Lopes: Morphology, biometry, ecology and biogeography of five species of *Diffflugia* Leclerc, 1815 (Arcellinida: Difflogiidae), from Tiete River, Brazil. 77

J. F. De Jonckheere: Isolation and molecular identification of Vahlkampfiid amoebae from an Island (Tenerife, Spain). 91

M. Ali, A.-A. Abdel-Baki and T. Sakran: *Myxidium elmatboulii* n. sp. and *Ceratomyxa ghaffari* n. sp. (Myxozoa: Myxosporae) parasitic in the gallbladder of the Red Sea houndfish *Tylosurus choram* (Rüppell, 1837) (Teleostei: Belonidae) from the Red Sea, Egypt. 97

K. Hauptmanová, V. Benedikt and I. Literák: Blood parasites in passerine birds in Slovakian East Carpathians. 105

Number 2

W. Foissner: Biogeography and dispersal of micro-organisms: A review emphasizing protists. 111

S. Agatha and J. C. Riedel-Lorjé: Redescription of *Tintinnopsis cylindrica* Daday, 1887 (Ciliophora: Spirotricha) and unification of tintinnid terminology. 137

J. Gong and W. Song: Redescriptions of three cyrtophorid ciliates from marine biofilm, with establishment of a new genus, *Wilbertella* nov. gen. (Ciliophora: Cyrtophorida: Lynchellidae). 153

R. Meisterfeld and H.-J. Badewitz: A redescription of *Amphizonella violacea* (Amoebozoa: Arcellinida). 167

G. Brugerolle: Description of a new freshwater heterotrophic flagellate *Sulcomonas lacustris* affiliated to the colpodictyonids. 175

P. Široký and D. Modrý: Two eimerian coccidia (Apicomplexa: Eimeriidae) from the critically endangered Arakan Forest Turtle *Heosemys depressa* (Testudines: Geoemydidae), with description of *Eimeria arakanensis* n. sp. 183

V. Opravilová and M. Hájek: The variation of testacean assemblages (Rhizopoda) along the complete base-richness gradient in fens: A case study from the Western Carpathians. 191

P. Kovács and G. Csaba: Tubulin is not posttranslationally modified (acetylated or polyglutamylated) in *Tetrahyena macronucleus*. 205

G. F. Esteban: Book review "Antarctic marine protists" edited by Fiona J. Scott and Harvey J. Marchant 211

Number 3

A. H. A. M. van Hoek, T. A. van Alen, G. D. Vogels and J. H. P. Hackstein: Contribution by the methanogenic endosymbionts of anaerobic ciliates to methane production in Dutch freshwater sediments. 215

G. de la Fuente, M. Pérez-Quintana, J. A. Cebrián and M. Fondevila: Preliminary study on the effect of exposure to low temperature on the viability of both mixed and monocultures of rumen protozoa. 225

R. B. Pedroso, T. Ueda-Nakamura, B. P. Dias Filho, D. A. G. Cortez, L. E. R. Cortez, J. A. Morgado-Díaz and C. V. Nakamura: Biological activities of essential oil obtained from *Cymbopogon citratus* on *Crithidia deanei*. 231

X.-Y. Liu, K.-L. D. Lee, Y.-Z. Mao, L.-P. Jin: Isolation, characterization and phylogenetic analysis of the cytochrome *b* gene (*Cyb*) from the hypotrichous ciliate *Pseudourostyla cristata*. 241

H. P. Amogan, J. P. Martinez, L. M. Ciuffetti, K. G. Field and P. W. Reno: Karyotype and genome size of *Nadelspora canceri* determined by pulsed field gel electrophoresis. 249

S. Tarcz, E. Przyboś, M. Prajer and M. Greczek-Stachura: Intraspecific variation of diagnostic rDNA genes in *Paramecium dodecaurelia*, *P. tredecaurelia* and *P. quadecaurelia* (Ciliophora: Oligohymenophorea). 255

L. Li and W. Song: Phylogenetic positions of two cryptophorid ciliates, *Dysteria procera* and *Hartmannula derouxi* (Ciliophora: Phyllopharyngea: Dysteriida) inferred from the complete small subunit ribosomal RNA gene sequences. 265

W. Song, A. Warren, D. Roberts, N. Wilbert, L. Li, P. Sun, X. Hu and H. Ma: Comparison and redefinition of four marine, coloured *Pseudokeronopsis* spp. (Ciliophora: Hypotrichida), with emphasis on their living morphology. 271

A. K. Mitra and P. K. Bandyopadhyay: *Trichodina haldari* n. sp. and *Paratrichodina bassonae* n. sp. (Ciliophora: Peritrichida) from Indian fresh water fishes. 289

K. H. Nicholls: *Cryptodifflugia leachi* n. sp., a minute new testate rhizopod species (Rhizopoda: Phryganellina). 295

V. Golemansky and M. Todorov: New data to the shell ultrastructure and the biometry of the marine interstitial testate amoebae (Rhizopoda: Testaceafilosia). 301

E. Kocik, M. Sobczak and M. J. Rędowicz: Codon usage in *Amoeba proteus* significantly differs from *Entamoeba histolytica* and *Acanthamoeba castellanii*. 313

J. Sikora and L. Kuźnicki: Book received „Festschrift 25 Jahre Deutsche Gesellschaft für Protozoologie” by Klaus Hausmann and Renate Radek. 317

Number 4

J. Sikora and L. Kuźnicki: Acta Protozoologica 1963-2006. 319

W. Foissner, M. Pichler, K. Al-Rasheid and T. Weisse: The unusual, lepidosome-coated resting cyst of *Meseres corlissi* (Ciliophora: Oligotrichea): encystment and genesis and release of the lepidosomes. 323

W. Foissner and M. Pichler: The unusual, lepidosome-coated resting cyst of *Meseres corlissi* (Ciliophora: Oligotrichea): genesis of four complex types of wall precursors and assemblage of the cyst wall. 339

- L. R. Manzine, M. T. A. Da Silva, O. H. Thiemann and R. M. B. Cicarelli:** Molecular characterization of *Blastocrithidia culicis* L17 ribosomal protein. 367
- R. Hoshina, S. Hayashi and N. Imamura:** Intraspecific genetic divergence of *Paramecium bursaria* and reconstruction of the paramecian phylogenetic tree. 377
- A. Maciejewska:** Sibling species within *Paramecium jenningsi* revealed by PCR-RFLP. 387
- S. Vincke, B. Van De Vijver, I. Nijs and L. Beyens:** Changes in the testacean community structure along small soil profiles. 395
- D. M. Wilkinson and H. G. Smith:** An initial account of the terrestrial Protozoa of Ascension Island. 407
- K. Hausmann, P. Selchow, F. Scheckenbach, M. Weitere and H. Arndt:** Cryptic species in a morphospecies complex of heterotrophic flagellates: the case study of *Caecitellus* spp. 415
- D. Xu, W. Song, X. Lin and A. Warren:** On two marine oligotrich ciliates, *Spirostrombidium agathae* n. sp. and *S. schizostomum* (Kahl, 1932) n. comb. from China, with a key to the identification of seven well-characterized *Spirostrombidium* spp. (Ciliophora: Oligotrichida). 433
- M. Jirků and D. Modrý:** *Eimeria terraepokotorum* n. sp. (Apicomplexa: Eimeriidae) from *Hoplobatrachus occipitalis* (Anura: Ranidae) from Kenya. 443
- W. Klopocka, K. Wierzbicka, P. Pomorski, P. Krzemiński and A. Wasik:** Cofilin-like protein influences the motility of *Amoeba proteus*. 449
- G. Csaba, P. Kovács and É. Pállinger:** Comparison of the amount and demonstrability of endogeneous hormones and bound insulin after paraformaldehyde and EDAC fixation in *Tetrahymena*. 455
- J. Fyda, G. Kennaway, K. Adamus and A. Warren:** Ultrastructural events in the predator-induced defence response of *Colpidium kleini* (Ciliophora: Hymenostomatia). 461
- K. Wiąckowski:** Book review of "The sphagnum ponds of Simmelried in Germany: A biodiversity hot-spot for microscopic organisms" by Martin Kreutz and Wilhelm Foissner. 465

INSTRUCTIONS FOR AUTHORS

Acta Protozoologica is a quarterly journal that publishes current and comprehensive, experimental, and theoretical contributions across the breadth of protistology, and cell biology of lower Eukaryote including: behaviour, biochemistry and molecular biology, development, ecology, genetics, parasitology, physiology, photobiology, systematics and phylogeny, and ultrastructure. It publishes original research reports, critical reviews of current research written by invited experts in the field, short communications, book reviews, and letters to the Editor. Faunistic notices of local character, minor descriptions, or descriptions of taxa not based on new, (original) data, and purely clinical reports, fall outside the remit of *Acta Protozoologica*.

Contributions should be written in grammatically correct English. Either British or American spelling is permitted, but one must be used consistently within a manuscript. Authors are advised to follow styles outlined in The CBE Manual for Authors, Editors, and Publishers (6th Ed., Cambridge University Press). Poorly written manuscripts will be returned to authors without further consideration.

Research, performed by "authors whose papers have been accepted to be published in *Acta Protozoologica* using mammals, shall have been conducted in accordance with accepted ethical practice, and shall have been approved by the pertinent institutional and/or governmental oversight group(s)"; this is Journal policy, authors must certify in writing that their research conforms to this policy.

Nomenclature of genera and species names must agree with the International Code of Zoological Nomenclature (ICZN), International Trust for Zoological Nomenclature, London, 1999; or the International Code of Botanical Nomenclature, adopted by XIV International Botanical Congress, Berlin, 1987. Biochemical nomenclature should agree with "Biochemical Nomenclature and Related Documents" (A Compendium, 2nd edition, 1992), International Union of Biochemistry and Molecular Biology, published by Portland Press, London and Chapel Hill, UK.

Except for cases where tradition dictates, SI units are to be used. New nucleic acid or amino acid sequences will be published only if they are also deposited with an appropriate data bank (e.g. EMBL, GeneBank, DDBJ).

All manuscripts that conform to the Instructions for Authors will be fully peer-reviewed by members of Editorial Board and expert reviewers. The Author will be requested to return a revised version of the reviewed manuscript within four (4) months of receiving the reviews. If a revised manuscript is received later, it will be considered to be a new submission. There are no page charges, but Authors must cover the reproduction cost of colour illustrations.

The Author(s) of a manuscript, accepted for publication, must transfer copyrights to the publisher. Copyrights include mechanical, electronic, and visual reproduction and distribution. Use of previously published figures, tables, or brief quotations requires the appropriate copyright holder's permission, at the time of manuscript submission; acknowledgement of the contribution must also be included in the manuscript. Submission of a manuscript to *Acta Protozoologica* implies that the contents are original, have not been published previously, and are not under consideration or accepted for publication elsewhere.

SUBMISSION

Authors should submit manuscript to: Dr Jerzy Sikora, Nencki Institute of Experimental Biology, ul. Pasteura 3, 02-093 Warszawa, Poland, Fax: (4822) 8225342; E-mail: jurek@nencki.gov.pl or j.sikora@nencki.gov.pl.

At the time of submission, authors are encouraged to provide names, E-mails, and postal addresses of four persons who might act as reviewers. Extensive information on *Acta Protozoologica* is available at the website: <http://www.nencki.gov.pl/ap.htm>; however, please do not hesitate to contact the Editor.

Hard copy submission: Please submit three (3) high quality sets of text and illustrations (figures, line drawing, and photograph). When photographs are submitted, arranged these in the form of plate. A copy of the text on a disk or CD should also be enclosed, in PC formats, preferably Word for Windows version 6.0 or higher (IBM, IBM compatible, or MacIntosh). If they do not adhere to the standards of the journal the manuscript will be returned to the corresponding author without further consideration.

E-mail submission: Electronic submission of manuscripts by e-mail is acceptable in PDF format only. Illustrations must be prepared according to journal requirement and saved in PDF format. The accepted manuscript should be submitted as a hard copy with illustrations (two copies, one with lettering + one copy without lettering) in accordance with the standards of the journal.

Indexed in: Current Contents, Biosis, Elsevier Biobase, Chemical Abstracts Service, Protozoological Abstracts, Science Citation Index, Librex-Agen, Polish Scientific Journals Contents - Agric. & Biol. Sci. Data Base at: <http://psjc.icm.edu.pl>, Microbes.info "Spotlight" at <http://www.microbes.info>, and electronic version at Nencki Institute of Experimental Biology website in *.PDF format at <http://www.nencki.gov.pl/ap.htm> now free of charge.

ORGANIZATION OF MANUSCRIPTS

Text: Manuscripts must be typewritten, double-spaced, with numbered pages (12 pt, Times Roman). The manuscript should be organized into the following sections: Title, Summary, Key words, Abbreviations, Introduction, Materials and Methods, Results, Discussion, Acknowledgements, References, Tables, and Figure legends. Figure legends must contain explanations of all symbols and abbreviations used. The Title Page should include the title of the manuscript, first name(s) in full and surname(s) of author(s), the institutional address(es) where the work was carried out, and page heading of up to 40 characters (including spaces). The postal address for correspondence, Fax and E-mail should also be given. Footnotes should be avoided.

Citations in the text should be ordered by name and date but not by number, e.g. (Foissner and Korganova 2000). In the case of more than two authors, the name of the first author and *et al.* should be used, e.g. (Botes *et al.* 2001). Different articles by the same author(s) published in the same year must be marked by the letters a, b, c, etc. (Kpatcha *et al.* 1996a, b). Multiple citations presented in the text must be arranged by date, e.g. (Small 1967, Didier and Detcheva 1974, Jones 1974). If one author is cited more than once, semicolons should separate the other citations, e.g. (Lousier and Parkinson 1984; Foissner 1987, 1991, 1994; Darbyshire *et al.* 1989).

Please observe the following instructions when preparing the electronic copy: (1) label the disk with your name; (2) ensure that the written text is identical to the electronic copy; (3) arrange the text as a single file; do not split it into smaller files; (4) arrange illustrations as separate files; do not use Word files; *.TIF, *.PSD, or *.CDR graphic formats are accepted; (5) when necessary, use only italic, bold, subscript, and superscript formats; do not use other electronic formatting facilities such as multiple font styles, ruler changes, or graphics inserted into the text; (6) do not right-justify the text or use of the hyphen function at the end of lines; (7) avoid the use of footnotes; (8) distinguish the numbers 0 and 1 from the letters O and I; (9) avoid repetition of illustrations and data in the text and tables.

References: References must be listed alphabetically. Examples for bibliographic arrangement:

Journals: Flint J. A., Dobson P. J., Robinson B. S. (2003) Genetic analysis of forty isolates of *Acanthamoeba* group III by multilocus isoenzyme electrophoresis. *Acta Protozool.* 42: 317-324

Books: Swofford D. L. (1998) PAUP* Phylogenetic Analysis Using Parsimony (*and Other Methods). Ver. 4.0b3. Sinauer Associates, Sunderland, MA

Articles from books: Neto E. D., Steindel M., Passos L. K. F. (1993) The use of RAPD's for the study of the genetic diversity of *Schistosoma mansoni* and *Trypanosoma cruzi*. In: DNA Fingerprinting: State of Science, (Eds. S. D. J. Pena, R. Chakraborty, J. T. Epplen, A. J. Jeffreys). Birkhäuser-Verlag, Basel, 339-345

Illustrations and tables: After acceptance of the paper, drawings and photographs (two copies one with lettering + one copy without) must be submitted. Each table and figure must be on a separate page. Figure legends must be placed, in order, at the end of the manuscript, before the figures. Figure legends must contain explanations of all symbols and abbreviations used. All line drawings and photographs must be labelled, with the first Author's name written on the back. The figures should be numbered in the text using Arabic numerals (e.g. Fig. 1).

Illustrations must fit within either a single column width (86 mm) or the full-page width (177 mm); the maximum length of figures is 231 mm, including the legend. Figures grouped as plates must be mounted on a firm board, trimmed at right angles, accurately mounted, and have edges touching. The engraver will then cut a fine line of separation between figures.

Line drawings should be suitable for reproduction, with well-defined lines and a white background. Avoid fine stippling or shading. Prints are accepted only in *.TIF, *.PSD, and *.CDR graphic formats (Grayscale and Colour - 600 dpi, Art line - 1200 dpi) on CD. Do not use Microsoft Word for figure formatting.

Photographs should be sharp, glossy finish, bromide prints. Magnification should be indicated by a scale bar where appropriate. Pictures of gels should have a lane width of no more than 5 mm, and should preferably fit into a single column.

PROOF SHEETS

After a manuscript has been accepted, Authors will receive proofs for correction and will be asked to return these to the Editor within 48-hours. Authors will be expected to check the proofs and are fully responsible for any undetected errors. Only spelling errors and small mistakes will be corrected.

ACTA PROTOZOLOGICA

J. Sikora and L. Kuźnicki: Acta Protozoologica 1963-200	319
W. Foissner, M. Pichler, K. AL-Rasheid and T. Weisse: The unusual, lepidosome-coated resting cyst of <i>Meseres corlissi</i> (Ciliophora: Oligotrichea): encystment and genesis and release of the lepidosomes	323
W. Foissner and M. Pichler: The unusual, lepidosome-coated resting cyst of <i>Meseres corlissi</i> (Ciliophora: Oligotrichea): genesis of four complex types of wall precursors and assemblage of the cyst wall	339
L. R. Manzine, M. T. A. Da Silva, O. H. Thiemann and R. M. B. Cicarelli: Molecular characterization of <i>Blastocrithidia culicis</i> L17 ribosomal protein	367
R. Hoshina, S. Hayashi and N. Imamura: Intraspecific genetic divergence of <i>Paramecium bursaria</i> and reconstruction of the Paramecian phylogenetic tree	377
A. Maciejewska: Sibling species within <i>Paramecium jenningsi</i> revealed by PCR-RFLP	387
S. Vincke, B. Van de Vijver, I. Nijs and L. Beyens: Changes in the testacean community structure along small soil profiles	395
D. M. Wilkinson and H. G. Smith: An initial account of the terrestrial Protozoa of Ascension Island	407
K. Hausmann, P. Selchow, F. Scheckenbach, M. Weitere and H. Arndt: Cryptic species in a morphospecies complex of heterotrophic flagellates: the case study of <i>Caecitellus</i> spp.	415
D. Xu, W. Song, X. Lin and A. Warren: On two marine oligotrich ciliates, <i>Spirostrombidium agathae</i> n. sp. and <i>S. schizostomum</i> (Kahl, 1932) n. comb. from China, with a key to the identification of seven well-characterized <i>Spirostrombidium</i> spp. (Ciliophora: Oligotrichida)	433
M. Jirků and D. Modrý: <i>Eimeria terraepokotorum</i> n. sp. (Apicomplexa: Eimeriidae) from <i>Hoplobatrachus occipitalis</i> (Anura: Ranidae) from Kenya	443
W. Kłopocka, K. Wierzbicka, P. Pomorski, P. Krzemiński and A. Wasik: Cofilin-like protein influences the motility of <i>Amoeba proteus</i>	449
G. Csaba, P. Kovács and É. Pállinger: Comparison of the amount and demonstrability of endogenous hormones and bound insulin after paraformaldehyde and EDAC fixation in <i>Tetrahymena</i>	455
J. Fyda, G. Kennaway, K. Adamus and A. Warren: Ultrastructural events in the predator-induced defence response of <i>Colpidium kleini</i> (Ciliophora: Hymenostomatia)	461
K. Wiąckowski: Book review of "The sphagnum ponds of Simmelried in Germany: A biodiversity hot-spot for microscopic organisms" by Martin and Wilhelm Foissner	465

2006 NOVEMBER

VOLUME 45 NUMBER 4